The Redshifts of Quasars

Arthur Stewart Trew

Doctor of Philosophy

University of Edinburgh

1983

This thesis has been composed by me and consists entirely of my own work, except where specifically indicated in the text.

January, 1983

Man was not born to solve the problems of the universe, but to put his finger on the problem and then to keep within the bounds of the comprehensible.

Goethe

TABLE OF CONTENTS

CHAPTER III AN ASSESSMENT OF THE SIGNIFICANCE OF QUASAR ALIGNMENTS

CHAPTER IV OBSERVATIONS OF A CLOSE PAIR OF QUASARS

CHAPTER V NON - COSMOLOGICAL REDSHIFTS

ABSTRACT

It has been shown that no correlation exists between the inferred ejection velocities of quasar absorption lines and the intrinsic continuum flux. In the absence of a net force on the absorbing clouds this disproves intrinsic models which rely on radiative acceleration for the production of these lines.

It has also been shown that there is a statistically significant excess of quasar alignments over that expected at a specific deviation (four arc - seconds) of the central object from the line defined by the outlying members. The narrowness of this peak makes it difficult to explain as the product of simple quasar clustering.

Observation at high spectral resolution om two quasars lying in such alignments has shown no significant deviations of the absorption line distribution from the norm. Assuming that this is true for all such objects and that a significant proportion of the quasar redshift is gravitational then the observed upper limits on the rate of change of absorption line redshifts has enabled lower bounds to be placed upon the central mass. The derived masses are very large and apparently in conflict with galactic stability arguments.

Number/ magnitude distributions have been determined for two samples of quasar candidates which were previously uncalibrated.

CHAPTER I

LITERATURE SURVEY AND SUMMARY

1.1 INTRODUCTION

Considerable advances in our knowledge of the quasar phenomenon have been made over the past few years thanks mainly to availability of larger samples of quasars on which better statistical investigations can be carried out. In this thesis it is hoped to follow this trend and apply objective statistical tests to those extended and, hopefully, more homogeneous data sets.

It is fundamental to current thinking that quasar emission line redshifts are cosmological. Although alternatives are in principle possible, none is properly worked out in theory and the main - line approach is to test for consistency of this assumption with observation. Explanations are demanded for a variety of phenomena, most importantly, perhaps, for the origin of the narrow absorption lines and the spatial distribution and evolution of quasars.

The former problem has been discussed in terms of two conflicting models. In one the absorption is caused by gas clouds situated in, for example, galactic haloes and thus unconnected with the quasar. The second model examined is one in which the absorbing clouds are intrinsic to the quasar and are expelled from the central source by radiation pressure. As yet there has been no convincing proof of either theory, although the consensus favours

an extrinsic origin.

The problems of the spatial distribution and evolution of quasars are observationally linked. They are normally divided into two parts because of the differing methods used to study the distribution of objects on the sky and in redshift. Due to a lack of quantitative data little is known about the true clustering of quasars although the discovery of aligned quasar triplets raises the possibility of some new process for producing the redshift. The importance of this result is its amenability to objective statistical testing. Regarding the redshift distribution of quasars, the explanation must be in terms of some evolutionary picture as the number of distant quasars exceeds that at low redshifts. Because of the ambiguity between luminosity and density evolution, however, this problem will not be resolved until a better physical understanding of quasars is achieved. Thus while this problem is not addressed directly hereafter the magnitude calibration of quasar samples is of the utmost importance for this work and this is discussed later.

This literature review will therefore concentrate upon those two areas of research most important to this thesis, namely quasar absorption lines and the possibility of significant non - cosmological redshifts, as a summary of the entire body of current literature would be much too long and be, for the present purpose of placing the succeeding chapters in context, unnecessary.

1.2 LITERATURE REVIEW

1.2.1 Absorption Lines

Over the past few years, largely as a result of two papers (Weymann et al. 1979; Sargent et al. 1980) opinion has shifted strongly from the view that the narrow absorption lines are produced within the quasar to an extrinsic model. Whether this represents a real increase in understanding or simply a change in prejudice is still open to question. It is probably more accurate to state that the real gain has been the build - up of large, homogeneous data sets on which proper statistical analyses can be made. It is common when discussing the distribution of the absorption lines to use the concept of ejection or expulsion velocity as a measure of the redshift difference between the emission and absorption lines. This, however, does not necessarily presuppose an intrinsic origin for these systems.

The simple classification scheme for quasar absorption systems devised by Bahcall (1971) in which there were only two types, the narrow and the broad lines, has been extended in recent years to separate those systems containing metal lines and those without (Weymann 1980). This new convention is designed to reflect the supposed difference between the origins of those types of systems. There are now four classifications as follows -

a/ Those systems consisting of very broad troughs with inferred ejection velocities of the absorbing material of ~ 0.1c. Not all these absorptions have smooth profiles as in the prototype, PHL 5200 (cf. Smith 1978), but may consist of a set of partially resolved components.

b/ These are defined to be sharp absorption systems in which the expulsion velocities are less than 3,000 km/s. Such lines are most commonly seen in CIV.

c/ and d/ These classes comprise the sharp absorption lines which are displaced, invariably to the blueward, by more than 3,000 km/s from the emission line. Type c are the metal line systems while type d are the large number of hydrogen only systems seen shortward of Lyα emission, the so called Lyα forest.

It is still open to debate whether the division into types c and d is contrived or is phenomenomological because with the exception of possible differences between the redshift distributions the evidence for two distinct classes is not strong. Nevertheless, for consistency with previous work the two types of line will be discussed separately hereafter.

1.2.1.1 The Metal Line Systems

In their sample of 17 quasars with redshifts > 1.2 Weymann et al. (loc cit.) discovered a total of 34 CIV absorption line systems. These had a non - uniform distribution in velocity space, being strongly peaked about the quasar emission redshift (cf. Figure 1.1). This result was interpreted by the authors as evidence for a multi - component model in which the majority of lines in this peak were produced by gas clouds associated with the cluster of galaxies surrounding the quasar. Most of the remaining systems, which had a flatter distribution in velocity space, were then postulated to arise in haloes of galaxies lying along the line of sight to the quasar. A few lines with expulsion velocities < 0.07c were further proposed to be expelled by, for example, radiation pressure from the quasar continuum source.

The first two of these components were rediscovered in a later analysis of data culled from the literature by Weymann et al.

(1981), though no sign was found of the excess caused by the so called, ejected systems. This is not surprising as in the earlier survey these were predominantly concentrated in a couple of objects.

More recently, Young et al. (1982a) have carried out a similar study on 33 quasars, this new data having also been assembled in a homogeneous manner by observation with the same telescope and at the same resolution. Thirteen objects were common to this sample and to the Weymann ones, though principally to that of Weymann et al. (1981).

The new data, however, showed decreased evidence for the peak in the line distribution about the emission redshift. No satisfactory explanation for this disagreement has been put forward, although Young et al. (loc cit.) have criticised the method of analysis and acquisation (on photographic plates) of the Weymann et al. (1979) data. As most of the overlaps occurred with the Weymann et al. (1981) spectra this comment may be of limited importance.

While errors in the Weymann data or its reduction are a possibility this has not been substantiated by direct tests. In fact comparisons of the absorption line distributions in 1101-264 as derived by Young et al. (loc cit.) and Carswell et al. (1982a) from spectra of similar, though not identical, resolution differ significantly. The former has considerably fewer absorption systems in the wings of the emission line than the latter. This is, probably, an illustration of the difficulty of setting the continuum level in regions where it is rapidly varying. (For the study of the absorption line distribution the emission lines are regarded as continuum as well.) If there are problems in determining the correct continuum level in the emission lines then these could serve to produce or remove the peak in the distribution of absorption systems because the Equivalent Widths

of these lines are crucially dependent upon the correct setting of the zero level.

It is not clear, therefore, whether the peak exists or not. The line finding technique used by Carswell et al. (loc cit.) has been tested by comparing the derived Equivalent Widths from low resolution data with those from a later study at higher resolution (Carswell et al. 1982b). Cross checking shows that the results are in good agreement, though naturally the higher resolution data have more lines than the lower. This may be taken as evidence for the existence of the peak, though much more work will be required before it is confirmed.

What other evidence, if any, directly implies an extrinsic origin for the absorption lines? At present, only three quasars - 3C232 (Boksenberg and Sargent 1978), PKS 2020-370 (Boksenberg et al. 1980) and 0446-208 (Blades et al. 1981) have been observed to have absorption lines directly indentifiable as having arisen in galactic haloes. In each case the galaxies are so close to us that CaII H, K are the only strong lines which lie in the visual passband. The mean separation of the quasar - galaxy associations is ~ 20kpc. This distance is rather less than the halo size required to explain the observed numbers of CIV systems. The halo radii implied by such considerations depend upon the surface covering factor of the gas, the galaxy luminosity function and the cosmology adopted, but are ~ 100kpc (Burbidge et al. 1977; Weymann et al. 1979).

Although Stockton (1978) has found low redshift galaxies apparently clustering around nearby quasars a study by Weymann et al. (1978) searching for galaxies around quasars, which showed low to moderate redshift absorptions, has produced a null result. This is a considerable problem because it is not possible to postulate that these clouds are primordial and hence unrelated to galaxies

as they must have acquired their metal content from somewhere, presumably from past star formation. It may be, however, that the non - detection of these implied galaxies is due to their faintness. While further studies are in progress using CCD arrays (eg. Impey 1982) to detect fainter images these are less satisfactory because accurate redshifts will then not be attainable. Consistency arguments based upon the galaxy colours and its size must then be invoked to justify any possible physical connection between the galaxy and the absorbing gas.

For these reasons the problem may best be resolved by probing nearby galaxies and thence determining the extent and covering factor of the halo gas, as in the three objects above. This will then show whether the observed halo properties are consistent with those inferred from the absorption line statistics. Although only the low ionization lines are then observable in the visual it does not take an absorption cloud long to cool from a temperature of 100,000K (typical of the high and medium ionization systems) to 10,000K (typical of the low ionization ones). This time is inversely proportional to the cloud density but for one with 1 particle per cc. the cooling time is ~ 5,000 yr in the absence of heating (cf. Songaila 1981). These densities are implied by the non - detection of excited fine structure lines in absorption systems (cf. Bahcall and Wolf 1968). Had the densities been much higher then the upper levels would have been populated by collisions.

This means that with the typical dispersion velocities within haloes of several hundred km/s (Savage and Jeske 1981) the two scale heights are very similar. Observation of low ionization systems does, therefore, give direct insights into the formation of the CIV and Lyα lines more common in high redshift quasars. A programme to do precisely this has been proposed to PATT by Drs. Brand and Carswell and myself, though it has, as yet, not been

awarded time.

An associated test which has been used to decide between the models for the production of these lines has been to search for common absorptions in close pairs of physically separate quasars. The observations of matching absorptions in the doulble and triple quasars 0957+561 (Walsh et al. 1979) and 1115+08 (Weymann et al. 1980) respectively are not proper discriminators as the absorptions occurred before the images were lensed. Unfortunately, few suitable associations of objects exist. To date two close pairs of quasars have been studied, 1548+114 (Wampler et al. 1973) separation ~ 40 kpc, and 0029+003 (Shaver et al. 1982), separation ~ 520 kpc. In each case both members have disparate redshifts and absorption has been observed in the higher redshift quasar at the emission line redshift of the other. Corresponding absorption is not seen in the spectra of the lower redshift objects. In a second two pairs of quasars PKS 0254-334 (Wright et al. 1982), separation ~ 400kpc and 1130+106, separation ~ 1Mpc (cf. Chapter IV), common absorptions have been sought but with only dubious success.

Much has also been made of two results which, if correct, would mean that significant numbers of absorption systems were intrinsic to the quasar and expelled from the central regions by radiation pressure. The first of these was the observation, noted especially by Burbidge and Burbidge (1975), of a large number of systems which were "line locked".

Line locking is a process by which the matter distribution is controlled in velocity space by a radiation field, in this case from the quasar continuum source. Basically the idea is that if the clouds are driven away from the centre by line absorption of continuum radiation then this acceleration will stop or considerably diminish for an outlying cloud if it is occulted by

another closer to the centre. As these gas clouds are optically thin in the continuum this can only happen when the relative velocity of the two systems is such as to match some lines in the inner absorber with important transitions in the outer. This is absorption - absorption line locking and although other types can occur the principle is the same. When this process operates the lines become tied together in velocity space with a specific ratio of redshifts, R, dependent upon the wavelengths of the lines concerned.

Burbidge and Burbidge (loc cit.) laid great stress upon the number of systems found with R = 1.11, possibly caused by the Lyα /HI edge or HeII Lyα /HeII edge, but they made no attempt to estimate the statistical significance of the feature. Sargent and Boroson (1977) reanalysed the data, statistically, and came to the conclusion that there was only marginal evidence to support the existence of the peak. To complicate matters further Drew (1978) has also used a statistical method to gauge the significance of this feature and came to the conclusion that it was very likely to be real.

The second supposed evidence for the importance of radiation pressure in determining the line distributions was discovered by Perry and O'Dell (1978). They purportedly found a correlation significant at the 4σ level between the intrinsic luminosity of the source and ejection velocity of the absorbing matter. Unfortunately, the data used were inhomogeneous and the statistical technique, that of fitting a least squares line, left something to be desired. The advent of higher and more uniform quality data due to Weymann et al. (1979), Weymann et al. (1981) and Young et al. (1982a) made a more valid assessment of the true significance of the correlation possible (cf. Chapter II). In fact none was found in that work.

1.2.1.2 The Hydrogen only Systems

The possibility that the hydrogen only systems could be considerably different from those showing metals was discovered by Sargent et al. (loc cit.). They found that these hydrogen only lines were uniformly distributed in redshift and were not clustered as one might have expected had they arisen in galactic haloes. The thesis that they were primordial gas clouds was then proposed to account for this peculiar distribution. A separate investigation by Peterson (1978), who neglected to apply the Equivalent Width limit for the lines in the rest frame of the absorber, found that there was a steep dependence of the number density upon redshift. The result using the same data, apparently, still holds when an approximate correction is applied to allow for the variation of the observed Equivalent Width with redshift (cf. Weymann et al. 1981). This is in direct opposition to the results of Sargent et al. (loc cit.).

It should be borne in mind that in both studies the number of objects used was very small, on the order of a half dozen. In fact in a more recent paper Young et al. (1982b) have observed and analysed the spectra of three new high redshift quasars. On the basis of this sample they derive a steep dependence of the number density of hydrogen only systems upon redshift. The reason for this reversal is not clear but in such studies there is always the problem of higher order Lyman lines, eg. Lyβ, affecting the number density at short wavelengths. A significant number of higher order Lyman lines misidentified as Lyα will tend to flatten the derived redshift distribution of the supposed Lyα lines as it produces a spurious contribution at apparently lower redshifts.

Leaving aside the considerable unknowns associated with the large scale distribution of the hydrogen only systems there are still problems on the smaller scale. Specifically the existence, or otherwise of a peak at zero expulsion velocity similar to that for the CIV lines (cf. Section 1.2.1.1). Sargent et al. (loc cit.) noted that no such excess existed within the Lyα sample. A possible explanation is that if the multi - component model of Weymann et al. (1979) is correct then the increased density of background systems means that an excess comparable to that observed for the CIV peak would be lost in the noise (Weymann et al. 1981).

This difference may be accentuated by having Lyα weakened with respect to CIV in the clustered systems. Weymann et al. (1981) have counted the number of unidentified lines, and hence presumably Lyα, lying in the wings of Lyα emission in ten high redshift quasars. They found that the number of CIV lines with ejection velocities in the range $-3{,}000 < V < 0$ km/s was greater than the number of Lyα ones but that the situation was reversed for $0 > V > 3{,}000$ km/s.

In any case it is possible that the majority of the hydrogen only systems are produced in gas clouds containing metals as the general weakness of any corresponding metal lines would render these undetectable.

The only other information relating to these lines are that firstly, the clouds are apparently small (< 1 Mpc) as in observations of a another close pair of quasars no correlation was found between the distribution of hydrogen only systems in the two objects (Sargent et al. 1982). Secondly, that the clouds are not unusually hot, $T < 400{,}000$K, since high resolution studies of the line profiles show them to be generally unresolved, FWHM < 60 km/s

(Sargent et al. 1980).

1.2.2 Non - Cosmological Redshifts

For many years the only evidence in favour of a non - cosmological redshift component, not only in quasars but in galaxies as well, was produced by Arp (cf. Field 1973 and references therein) with minor contributions from other sources. These observations were based upon systems of peculiar appearance with discrepant redshifts. Typical of the quasar - galaxy and galaxy - galaxy associations was the famous NGC 4319/ Mkn 205 pair (cf. Figure 1.2) which it was claimed were connected by a luminous bridge (Arp 1971). If correct, then the substantially larger refshift of Mkn 205 (21,000 km/s compared with 1,800 km/s for NGC 4319) would be mainly due to some intrinsic mechanism within this object. The argument raged for a considerable number of years because of doubts about the the existence of the connection (cf. Arp et al. 1975), though it has now largely subsided without a definite conclusion.

The picture put forward by the non - cosmological camp (cf. Arp 1977) was that this system was the result of an explosive event in the nucleus of NGC 4319 which somehow produced young matter. Any newly formed object is then proposed to emit radiation, by an unspecified physical process, at longer wavelengths than older material (Arp 1977; cf. Chapter V). Thus, upon expulsion from the nucleus the new object (Mkn 205) would then be seen to have a redshift larger than that of the parent body, the luminous bridge being a relic of the ejection.

However, because of the subjective nature of such work, which precluded a priori statistical testing, it was only taken

seriously by the converted or by the credulous. Since then two improvements have taken place. Firstly, in an analysis of quasar - galaxy associations the regions around a homogeneous set of companion galaxies were searched for quasars (Arp 1981). The quasar candidates, having been selected by a UV excess criterion, were later verified by slit spectra taken on large telescopes. The study, in summary, concluded that 13 quasar - galaxy associations were found each with an a priori probability of occurence by chance of < 0.01, assuming a density of ten quasars per square degree. With a total sample of 34 companion galaxies the probability of this happening from a random distribution of quasars is 10^{-17}.

Moreover, Arp (loc cit.) has argued that this probability is an underestimate because of the lack of good plate material in 9 of the 34 fields which has not permitted reliable searches in those areas. Also, 5 of the UV excess candidates have not been observed spectroscopically because of insufficient telescope time. In all these cases the results were taken to be failures when calculating the statistics. Should any have been successes the probability would, of course, have been reduced further.

It is not possible to discount this result on the grounds that the objects are predominantly not quasars but are, for example HII regions belonging to the galaxy, because of the redshift discrepancies (these are of course, well known from slit spectra). Furthermore, although doubts have also been raised about the assumed background density of quasars, an increase by a factor of two in this would, it was argued, only raise the probability by 2^{13} to 10^{-13}. The same selection technique has been used in a control field in which the density is 6.7 (Arp and Surdej 1982) thus showing that the assumed number density is not grossly in error.

While this approach clearly represents a considerable improvement over the previous treatment by Arp of the statistics of non - cosmological redshifts it is still open to considerable criticism. Browne (1982) has noted that a fallacy exists within the statistical argument. A success is counted if a faint quasar falls within a small distance from the companion galaxy, or if a brighter quasar (due to its comparative rarity) is found within an increased radius. The radii are set in such a way as to give, on the hypothesis of a random quasar distribution, a probability of association < 0.01. However, the combined probabilities of these alternatives is obviously greater than the success rate for any one of them. Browne and Cohen (1978) have investigated the statistics of such searches and using that work Browne (loc cit.) concludes that 0.07 rather than 0.01 is a realistic estimate of the individual probability of association. Making this change and calculating the new binomial probability of thirteen successes from 34 trials reduces this to 10^{-7}.

This drop of ten orders of magnitude is impressive but has been compounded by Webster (1982a). It has been shown that the simple Poisson probability of association in each case differs from that as calculated by Arp (1981). The effect of this is to lower the number of successes from 13 to 6. The reason for the difference is not clear. It is possible that Arp has reduced the effective search area by allowing for that portion covered by objects, though this is entirely unproven. After these corrections the new binomial probability is now only 0.03, a change from Arp's original figure by some 15 orders of magnitude! Nevertheless, the statistics have still not been correctly treated because no weight is given to those associations with a probability > 0.01. This probability limit is purely arbitrary and a proper study would not separate the data into successes and failures but use all the information. Furthermore, the probability of association is a lower estimate for as previously discussed there were a number of

quasar candidates which did not have redshifts, and as such were regarded as failures. Also the individual probabilities were calculated on the basis of a quasar surface density somewhat in excess of that found by the same method in a control field.

An approach has been adopted by Zuiderwijk and de Ruiter (1982) who use a Kolmogorov - Smirnov test to compare the distribution of observed separations with that expected, which has the advantage of not binning the data. They find a probability of ~ 1% that the observed separation histogram is drawn from a random distribution of quasars and galaxies. Once again this is considerably less than the figure quoted by Arp (1981) but if correct then it implies a statistically significant excess of quasars close to companion galaxies. However, since the probability of association is a non - linear function of the surface density of quasars any non - Poissonian fluctuations, caused perhaps by clustering, will enhance the number of associations above that expected. If strong enough simple quasar - quasar clustering could then in principle reproduce the anomalous result and so whether this is due to a clustered distribution of quasars or some physical association of quasars and galaxies at very different redshifts it is not possible to say.

Barnothy (1974) has suggested that the number of quasar - galaxy associations could be enhanced by gravitational lensing and magnification of faint background quasars by the foreground galaxy or by its globular clusters. Because the surface density of faint objects is considerably greater than that of bright ones the probability of association is thereby increased. Canizaries (1982) has also considered this problem and has found that in the present context that sufficient magnifications cannot be produced over the required angular separation by particles of as low mass as galaxies.

The second major improvement in Arp's technique was the discovery and discussion by Arp and Hazard (1980) of aligned triplets of quasars. Although alignments of objects had been proposed before (eg. Arp 1970) these new examples were quite different for two reasons. Firstly, the deviations of the points from the line are two orders of magnitude less than in previous associations. Secondly, and more importantly from an observational viewpoint, all the objects involved here are quasars. Formerly unusual galaxies had also been included in the alignments. This means that a sample of objects in which to search objectively for aligned triplets may be defined a priori, thus removing the need to subjectively select galaxies with peculiar features.

In fact this is the first type of discrepant redshift grouping which is truly open to objective assessment. Unlike the former quasar - galaxy associations where the quasar searcher is aware of the relationship of the search area to the point of interest (the galaxy) and where it is possible, therefore, that a spurious effect may be produced because of increased diligence when near the galaxy. In the case of these aligned triplets their size is very much larger than the area visible at any one time to the quasar searcher. It is inconceivable that any mental correlation should carry over from one small area to the next in order that the observer should preferentially select quasars lying upon straight lines, especially as the field distortions induced by the objective prism will curve to varying degrees what would otherwise have been straight lines. Visually selected samples are, therefore, statistically unbiassed and suitable for objective searches for aligned triplets.

1.3 THESIS SUMMARY

Given the above summary of our present level of understanding and knowledge it is clear that a number of problems require resolution. The most fundamental of these, though usually considered to have been settled many years ago, is the question of the origin of the quasar redshift. Is it, as most astronomers believe, purely a doppler effect caused by the expansion of the universe, or alternatively is there a significant component peculiar to some objects?

It is proposed, in this thesis, to examine the evidence for non - cosmological redshifts and the constraints which may be placed upon any model purporting to explain them from observations of the absorption lines.

It has been recognised for some time that the quasar redshifts must be purely cosmological if the majority of the narrow absorption lines, especially those close to the emission lines, are produced extrinsically to the quasar. From Section 1.2 it may be seen that while most evidence appears to point vaguely in this direction, the report of a correlation between expulsion velocity and quasar luminosity (Perry and O'Dell loc cit.) strongly favours an intrinsic origin. The universality of narrow absorption lines in high redshift quasars means that the origin of these lines will have a powerful influence upon models for, and the size of, any non - cosmological component.

A prerequisite for any study to determine the size of the peculiar redshift component is to reassess with better and more homogeneous data and using more powerful statistical techniques the evidence for the proposed correlation between ejection velocity and quasar flux. If affirmed this would be very strong evidence against the extrinsic model. The existence of absorption lines could then not be used as immediate disproof of a

significant non - cosmological redshift component. This test has been carried out using the Weymann et al. (1979) and the Weymann et al. (1981) CIV data and a sample of Lyα lines taken from the literature. The selection criteria for these lines, together with the method of analysis employed and the results are described in Chapter II.

It is equally important to examine objectively the evidence which it is claimed indicates a non - cosmological redshift component. From consideration of Section 1.2.2 it appears that this may be most effectively obtained by an assessment of the significance of the numbers of aligned quasar triplets. A negative result in any such investigation (ie. one which would not require any physical associations) would not, however, of itself refute the non - cosmological redshift hypothesis. This is because the argument has been pressed upon a sufficiently wide observational front that a single battle is unlikely to conclusively decide the matter one way or the other. However, a null result would at least narrow the range of evidence put forward to support the model.

An investigation of the significance of alignments in a number of fields of quasar candidates, selected by visual inspection of Schmidt plates, has been carried out and is described in Chapter III. From the discussion of such samples in Section 1.2.2 it is clear that for this study the data are statistically unbiased.

If it is assumed that some of the Arp and Hazard (loc cit.) type alignments do imply significant non - doppler redshifts then it is only possible to apply any constraints to the size of this component derived from considerations of the absorption lines if it is known that those quasars have similar absorption properties to the norm. Such an investigation carried out in full would be most expensive in telescope time and as such not feasible. A partial study on one or two of the brighter quasars in alignments,

with the aim of determining their absorption line distributions, may be instructive if differences from normal were found.

It is thus fortunate that two of the bright quasars in the Arp and Hazard (loc cit.) 1146+111 grouping are close together on the sky. This gives the possibility of a simultaneous test for common absorptions, if the lines are extrinsic, between the pair of quasars and for any unusual line distributions. These two objects were observed on the Anglo - Australian Telescope with the RGO spectrograph and the Image Photon Counting System and are described in Chapter IV. They thus represent tests of both the extrinsic model for the production of the absorption lines and the normality, or otherwise, of the absorption line distributions in possible non - cosmological quasars.

Any investigation into peculiar redshifts would not be complete without some discussion of, and investigation into, the physical mechanisms proposed to explain this component. The most plausible method for the production of the peculiar redshift is gravitation, which has, after all, been observed in white dwarf stars (eg. Greenstein et al. 1977).

Material which is insufficiently supported will collapse into any gravitating body, thereby raising its gravitational redshift and giving it a positive doppler component if it is moving away from the observer. This rate of increase of redshift is calculable and may be expressed as a function of the particle radius and the central mass. The most accurate determinations of redshifts in quasars are for the narrow absorption lines as these are well defined features and are easily measured. For this reason the time variability of the absorption systems provide the most sensitive test of the model.

Arguments based upon the volume in a given redshift range at high gravitational redshift (Greenstein and Schmidt 1964) may be used to show that the central body must be at least as massive as normal galaxies. Clube (1977) has developed a theory by which masses may increase when they collapse and so can produce extremely massive bodies from initially moderate ones for a short period of time. If substantial peculiar, gravitational redshifts are required then this theory may be more suited to their production than General Relativity. Consequently, the calculations of the rate of infall are made within the context of this model. The theory is explored in Chapter V and the predictions confronted with observation.

The data produced by the COSMOS machine used in Chapter III to study the spatial distribution of quasar candidates also contains information on the object magnitudes . In two of the fields which were measured suitable photoelectric sequences exist which have not been previously used to calibrate the quasar samples. In Chapter VI, therefore, this task is undertaken for two reasons. Firstly, it is a test of the present performance of the COSMOS machine and secondly as a necessary precursor to any study of the number/ magnitude/ redshift relation for these quasar candidates. Unfortunately, sufficient redshift information does not currently exist to complete this latter task as those determined from objective prism spectra are highly dubious. Nevertheless, the advent of the UKST fibre optics system may repair the deficit and so this work is of considerable future value.

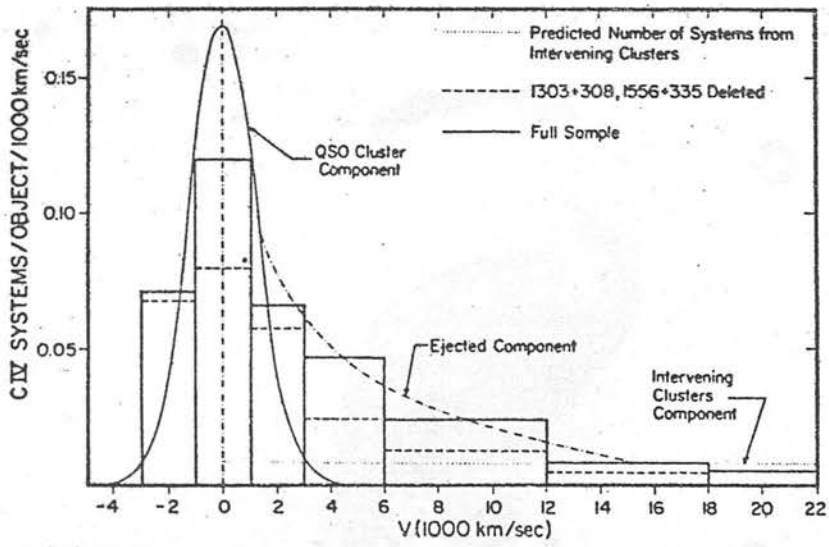

Figure 1.1 Histogram showing the distribution of CIV systems as a function of ejection velocity. The contributions from the three inferred components are also shown, schematically. (From Weymann et al. 1979).

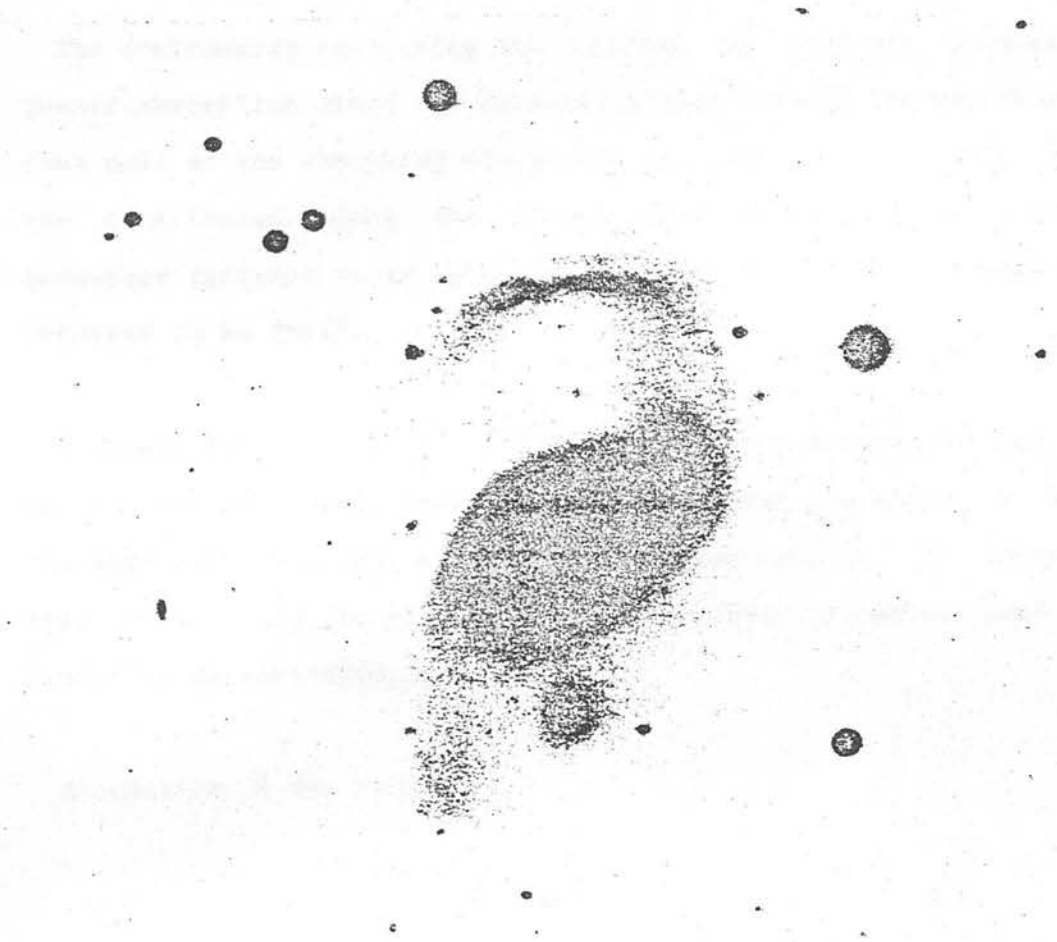

Figure 1.2 Photograph of the spiral galaxy NGC 4319 and the quasar Mkn 405. (From Field et al. 1973).

CHAPTER II

THE DISTRIBUTION OF QUASAR ABSORPTION LINES

2.1 INTRODUCTION

The controversy concerning the location of the gas producing quasar absorption lines has recently tended towards the hypothesis that most of the absorbing clouds are external to the quasar and are distributed along the line of sight (Weymann et al. 1979), hereafter referred to as WWPT); Sargent et al. (1980), hereafter referred to as SYBT).

However, Perry and O'Dell (1978) found a correlation, claimed to be at the 4σ level, between intrinsic quasar luminosity, F, and the expulsion velocity, B, of the absorption systems. If correct this could only be explained by an intrinsic mechanism, such as radiative acceleration.

A relation of the form -

$$B = KF^{1/2} \qquad 2.1$$

was proposed where K is a constant and -

$$B = \frac{(1 + Zem)^2 - (1 + Zabs)^2}{(1 + Zem)^2 + (1 + Zabs)^2} \qquad 2.2$$

and where Zem and Zabs are the emission and absorption redshifts respectively.

Unfortunately, the inclusion of absorption systems found in an inhomogeneous sample of objects extending from low redshift Seyfert galaxies to the most distant quasars could possibly produce strong redshift selection effects. In addition, the absorption line sample contained systems of a variety of different ionization states. Since Perry and O'Dell carried out their analysis other work has shown that not all types of absorption system necessarily have the same redshift distributions. SYBT (as discussed in Chapter I) noted that the hydrogen - only absorption lines are apparently distributed differently from the metal line systems.

The combination of these factors could have resulted in spurious correlations being found and it was obviously necessary to repeat the analysis using a more homogeneous data set and treating those absorption systems with different distributions separately.

Sufficient low ionization data (on MgII for example) does not exist to examine this sample in the desired manner. The analyses will thus be restricted to the hydrogen - only systems and to the medium and high ionization metal absorptions, represented by CIV. This will test whether either (or both) type of lines actually do exhibit the proposed correlation and hence will be important for deciding between models for the production of the absorption lines.

Although not yet completed, the sample of quasars observed by WWPT provided an initial set of CIV systems. This was extended using a sample taken from the literature by Weymann et al. (1981; hereafter referred to as WCS) giving a total of 41 quasars. The hydrogen absorption lines have also been selected in this work from published data. In all, 26 quasars satisfied the selection criteria.

This work has been published by Trew (1982).

2.2 THE STATISTICAL TESTS

For reasons of generality, and because there is no evidence that either the quasar fluxes or expulsion velocities are normally distributed a non - parametric correlation technique must be used - rather than a simple least squares regression. The great advantage of the former is that a correlation can be sought without foreknowledge of its exact functional form. This is provided that the two variables used in the analysis can be related to those which are physically important by monotonic functions, both of which vary in the same sense. A straight regression technique, as used by Perry and O'Dell (loc cit.), would not allow this. With such tests one would have to transform the variables into a plane in which the expected form of relation was known, for example linear.

The tests chosen are detailed below.

2.2.1 The Spearman Rank Correlation Coefficient

This test is the oldest and perhaps best known of all those statistics based upon ranks. It is the non - parametric equivalent of the most powerful of the parametric correlation coefficients, the Pearson r, but its efficiency is slightly reduced, being 91% (Siegel 1956). This means that 100 data pairs are required to give the same significance level from r (Equation 2.3) that can be achieved with 91 using the Pearson r. However, the considerable advantage of not having to make assumptions as to the underlying

distribution of the variables more than compensates for this loss.

The most convenient form for computing the Spearman Rank Correlation Coefficient is -

$$r = 1 - \frac{6 \sum_i (Xi - Yi)^2}{N^3 - N} \qquad 2.3$$

where there are N data pairs and each of the two variables is ordered independently, so that (Xi, Yi) represents the ranks of the variables for the "i"th datum. A correction to this formulation must be made if a large proportion of the data pairs have tied ranks, the appropriate relation, which is a generalization of Equation 2.3, may be found in Siegel (loc cit.). The range of the statistic is $0 < r < 1$, a high value indicating a stronger correlation. When computed, the significance of r can be estimated by calculating, for $N > 30$ -

$$T = r \sqrt{\frac{N - 2}{1 - r^2}} \qquad 2.4$$

where T is distributed according to the Student's T statistic with N - 2 degrees of freedom. For smaller samples probability tables exist to calibrate r (cf. Wall 1982).

2.2.2 The Mann - Whitney U Test

This is one of the most powerful non - parametric tests for the comparison of samples. When compared with the most efficient of the parametric tests, the Student's T statistic, its efficiency is 95% (Siegel loc cit.). Once again this is a minimal price to pay for the freedom from underlying assumptions.

Suppose that there are two samples with total numbers n(1) and n(2), where n(1) < n(2). To apply this test both samples are ranked independently and the number of values in n(1) which precede each of the n(2) are counted, summation of these gives U(1). If the n(2) set had been considered then U(2) would have been obtained but this is not necessary because -

$$U(2) + U(1) = n(2)n(1) \qquad 2.5$$

The smaller value of U(1) or U(2) is taken as the final U value, the sampling distribution of which under Ho is known (Ho is the null hypothesis which states that both samples are drawn from the same parent population). For larger samples, n(1) and n(2) > 8, it is easier to combine both data sets and rank the (n(1) + n(2)) observations. In this case -

$$U(1) = n(1)n(2) + \frac{n(1)(n(1) + 1)}{2} - R(1) \qquad 2.6$$

where R(1) is the sum of the ranks assigned to the n(1) sample. We also have -

$$\text{mean} = m = n(1)n(2)/2 \qquad 2.7$$

and the standard deviation, s, is given by -

$$s = \sqrt{\frac{n(1)n(2)(n(1) + n(2) + 1)}{12}} \qquad 2.8$$

Hence the significance, x, of a result U may be found by computing its difference from m in terms of the standard deviation, s.

2.3 DETERMINATION OF THE INTRINSIC FLUX

Of necessity, a luminosity based upon a broadband visual magnitude, mv, has been used in this work. At the mean redshift of the sample this corresponds to fluxes in the rest frame of the quasar at ~ 1800Å. To estimate the intrinsic luminosity per Å (F(1800)) at a constant wavelength in the quasar rest frame the following relations have been used, where Z is the emission line redshift.

$$F(1800) = 4\pi (rRo)^2 (1+Z)^3 lopt((1+\langle Z\rangle)/(1+Z))^{-K} \qquad 2.9$$

where -

$$\log(lopt) = \text{constant} - 0.4mv \qquad 2.10$$

The form of Equation 2.9 is such that K corrections are not necessary as, under the assumption of a power law of spectral index α, these have been included in the final term.

It has been shown (Mattig 1958) that -

$$rRo = \frac{c}{Hoqo^2(1+Z)}\{qoZ + (qo - 1)[(1 + 2qoZ)^{\frac{1}{2}} - 1]\} \quad qo > 0 \qquad \ldots 2.11$$

$$rRo = \frac{c}{Ho}\frac{\{Z(1 + Z/2)\}}{(1 + Z)} \quad qo = 0 \qquad \ldots 2.12$$

Substitution of these into Equation 2.9 gives that -

$$F(1800) = \frac{4\pi c^2}{Ho^2}\{Z^2(1+Z)((1+\langle Z\rangle)/(1+Z))^{-\alpha} lopt\}$$

for qo = 1

... 2.13

and

$$F(1800) = \frac{4\pi c^2}{Ho^2}\{Z^2(1+Z)(1+Z/2)^2((1+\langle Z\rangle)/(1+Z))^{-\alpha}\,Iopt\}$$

... 2.14

for qo = 0.

Tests upon the data have shown that the rankings of F(1800) are insensitive to the assumed cosmology for $0 < qo < 1$. Hence, qo = 0 has been arbitrarily adopted without fear of prejudicing the final result. Also, the values of F(1800) have been normalised to give a mean of unity. As most objects in the sample have not had their spectral indices measured, a mean value of 0.6 has been assumed for the entire sample (Richstone and Schmidt 1980).

The inclusion of emission lines in the visual passband will affect the estimation of the continuum flux. As the effects of such lines are redshift dependent, residual systematic errors correlated with Zem may still exist in F(1800). A simple calculation shows that the error introduced in this way is ~ 10 - 20% (cf. Section 6.4.2). From the discussion of these errors in Section 2.5 it will be seen that this is rather larger than the error associated with the adoption of a mean spectral index for the entire sample.

There is an apparent bias, a Malmquist type effect, in an analysis such as this which will tend to strengthen any correlation present, or produce a totally spurious one. It arises because both F(1800) and B are related to a third parameter - the object redshift. It is obvious that as the emission redshift increases any flux limited sample will progressively contain only intrinsically brighter and brighter sources. Furthermore, if these

objects are observed spectroscopically then the constant short wavelength cut off imposed, for example, by the atmosphere, produces, for a given line, a lowest possible observable absorption line redshift. This in consequence gives a maximum observable expulsion velocity, which will increase with Zem, cf. Equation 2.2.

To combat this, the samples have been analysed in two ways. Firstly, to search for a B/F(1800) relation and secondly, to look for a correlation between F(1800) and (B/Bmax), where Bmax is the maximum possible observable expulsion velocity. (Obtained by consideration of the wavelength range over which each object was observed.)

In summary, therefore, though the premise has been made that the form of the expected correlation is as given by Equation 2.1, it is possible simultaneously to test for any relationship in which B increases with rising F(1800).

2.4 THE SAMPLES

2.4.1 The CIV Lines.

The selection criteria for the CIV data from WWPT and WCS are summarized below. (They are described in more detail in those works.)

2.4.1.1 WWPT Data

Although this quasar sample is not complete to any flux limit the data are homogeneous, in that all the objects were observed with the same instrument and at the same resolution. It comprises 17 quasars, the spectra of which show a total of 34 CIV systems with B > 0. Acceptance of these absorption lines and quasars were subject to the following constraints -

i For the moderate redshift (CIV) sample 1.2 < Zem < 1.95.

ii Object visual magnitudes < 18.0.

iii Each object was observed at 2.5A resolution.

iv All identified lines had Equivalent Widths greater than a lower limit of 0.6 - 1.0A.

2.4.1.2 WCS Data

As this sample has been taken from the literature it may be less homogeneous and less complete than WWPT. Nevertheless, it is a complementary data set and after a few objects common to WCS and WWPT have been removed from it there were 24 quasars remaining, with a total of 50 CIV absorption systems.

The selection criteria were as follows -

i All objects had Zem > 1.9.

ii Observations must have been made with a resolution adequate to resolve the CIV doublet (~ 2.6A).

iii These observations also had to have wavelength coverage extending from B = 6,000 km/s to the red of CIV emission to B = 60,000 km/s to the blue.

In order to check, before combination, that the WWPT and WCS samples were statistically equivalent, the Mann - Whitney U Test (Section 2.2.2) was used to compare the distributions of F(1800) and (B/Bmax) in the two samples. It was found that the significance of any difference between the sets of (B/Bmax) was only 0.04σ. The difference between the sets of F(1800) values, however, was more significant, as might be expected on the grounds of decreasing completeness with increasing redshift. It was found that the WCS quasars ($\langle F(1800)\rangle = 0.79$) were brighter than the WWPT objects ($\langle F(1800)\rangle = 0.51$) at a confidence level of 1.5σ. Nevertheless, these differences are considerably less than the level of any believable correlation. The samples may thus be combined without fear of producing spurious, statistically significant results.

Table 2.1 lists those quasars contributing to the combined CIV sample, together with the intrinsic quasar luminosity and the number of CIV systems with B > 0.

2.4.2 The Hydrogen only Systems

The indentification of a hydrogen only system is more difficult than for a metal line, one as typified by CIV (which is perhaps the simplest of all absorptions to find) if a reasonable number of detections are desired. This is because as Lyα is the strongest transition many systems will not have corresponding higher order members of the Lyman series, if they arise in clouds of low column density. Furthermore, the choice of only those Lyα lines in which

identification is secured by definite metal counterparts would for this purpose be absurd, since both hydrogen and metal lines would then be forced to have the same redshift distributions. It was thus decided to identify, as Lyα, those otherwise unidentified lines shortward of Lyα emission with rest Equivalent Widths > 1A. This definition is very similar to that used by SYBT in their study of the distribution of Lyα lines.

The selection of the quasars and lines was as rigorous as possible -

i Only objects which have been observed at a resolution better than 7A were included. Subsequently, the resolution of each spectrum was degraded to 7A, to provide uniformity of data.

ii A further constraint was placed upon the amount of spectrum observed shortward of Lyα emission, in order to give reasonable data base in each object. This was set to 15,000 km/s.

The quasars in the sample are listed in Table 2.2, together with the quasar luminosity as calculated from Equation 2.14 and the number of Lyα lines in each, at the degraded resolution. In all, there are 462 acceptable Lyα lines in the 26 objects.

In order to determine whether quasars in the same luminosity range were being compared irrespective of the type of line system, the Mann - Whitney U Test was employed to compare those objects making up the CIV and Lyα samples. The result was that there was no difference between the two F(1800) distributions at a confidence level greater than 1.2σ.

2.5 RESULTS

The results of the Spearman Rank Correlation tests applied to the CIV and Lyα samples are displayed in Table 2.3.1 Here r and T are as described in Section 2.2.1. P is the resultant confidence level at which the null hypothesis of no correlation can be rejected. In the calculation of P the number of degrees of freedom has been taken to be the number of lines - 2. Implicit in this is the assumption that the individual absorption clouds are statistically independent.

Examination of the Table shows that a correlation between B or (B/Bmax) and F(1800) may be rejected at a confidence level of > 90%. On the basis of these results, it is clear that there is little evidence to support a correlation for either type of absorption system. However, this may not be a completely accurate reflection of the state of affairs because if all absorption lines are considered regardless of B, then it is inevitable that some intervening systems will occur, the distribution of which will, of course, be uncorrelated with the quasar luminosity.

Theoretical considerations suggest that it is very difficult to radiatively accelerate narrow absorption line clouds beyond 0.1 - 0.2 c (Beltrametti and Perry 1980). This result is corroborated by the B distribution of the so called "ejected" systems found by WWPT (cf. Section 1.2.1). Restriction of the range of B to a maximum of 15,000 - 30,000 km/s could thus provide the most favourable sample of lines in which to detect a radiatively accelerated component. In this case it is only necessary to repeat any analysis once because both B/F(1800) and (B/Bmax)/F(1800) are now equivalent.

The restricted Lyα sample comprises a total of 161 absorption systems in 26 quasars, with B < 15,000 km/s. The CIV data are composed of 52 lines distributed amongst 32 quasars, with B < 30,000 km/s. This upper limit to the ejection velocity has been increased over that for the Lyα in order to provide a reasonable number of systems. The results of these new analyses are shown in Table 2.3.2, the format being the same as for Table 2.3.1.

Again examination of Table 2.3.2 shows that at a confidence level of > 85% it may be asserted that no correlation exists between expulsion velocity and quasar flux. This must lead to the conclusion that at best only a very small proportion of absorption lines are expelled by radiation pressure or any other process the strength of which is correlated with the quasar flux. A similar study for a rather smaller sample of CIV lines appeared in press while this analysis was being undertaken (Peterson 1981). Although that work used a linear regression technique with all its inherent limitations (cf. Section 2.2), the result was in good agreement with that found here.

It must be remembered, however, that for observational reasons the luminosity used in this work has an effective rest wavelength ~ 1800A. But as the majority of the ejected matter is hydrogen (which has a steeply diminishing opacity shortward of the Lyman limit) and as the energy per octave is not observed to be increasing in this region most of the driving force will be produced by photons with wavelengths ~ 900A. Therefore, if the range of spectral indices is large enough, a correlation between F(900) and B need not imply the same between F(1800) and B. By propagation of errors (cf. Bevington 1969) estimates can be made of the necessary scatter in spectral indices to render a true correlation between F(900) and B unobservable.

In order to do this it is assumed that the correct relationship between F(900) and B is as given in Equation 2.1. This would be expected from an intrinsic production mechanism in which an excess of radiation pressure is responsible for the expulsion, provided that at the time of observation most of the absorbing clouds are experiencing no net force. Secondly, it is assumed that the continua in quasars may be represented by a power law with a single spectral index extending from the near UV to the soft X ray region. These assumptions then give that -

$$B = Kx^{-\alpha/2}F^{1/2}(1800) \qquad 2.15$$

where x is the ratio of the frequencies at which radiative acceleration is a maximum to that at which the quasar is observed (in the rest frame). By propagation of errors it is clear that -

$$s_B^2 = s_\alpha^2\left(\frac{\partial B}{\partial \alpha}\right)^2 + s_F^2\left(\frac{\partial B}{\partial F(1800)}\right)^2 \qquad 2.16$$

which becomes -

$$s_B^2 = 1/4\ s_\alpha^2\ B^2 \ln^2(x) + 1/4\ s_F^2\ B^2\ F^{-2}(1800) \qquad 2.17$$

A correlation will be undetectable for $s_B / B \sim 1$, giving -

$$4 \sim s_\alpha^2 \ln^2(x) + s_F^2\ F^{-2}(1800) \qquad 2.18$$

From Section 2.2 it is known that $s_F / F(1800) \sim 0.2$, substitution of which into Equation 2.18 gives $s_\alpha \sim 2.5$. This is an order of magnitude larger than that found by Richstone and Schmidt (loc cit.) although their spectral index distribution is somewhat skew. An alternative way of approaching this is to ask at what wavelength must the driving take place in order to have no observable correlation with an rms. scatter in the spectral index

of 0.5? A simple calculation from Equation 2.18 shows that this wavelength is ~ 30A, in the soft X ray region of the spectrum. This is somewhat embarrassing as many authors (eg. Kippenhahn 1978) have assumed a spectral break at wavelengths ~ 100A in order to freeze in the ionization state at a very high level and hence enhance the opacity of the lines which increases the accelerating force.

It would, thus, appear that no strong correlation exists between the UV flux and expulsion velocity and hence there is no radiative acceleration. While this conclusion is somewhat dependent upon the form of the relationship of B upon F it is rather difficult to understand, within the context of a radiative acceleration model, in what way one could contrive to have an index in Equation 2.1 of 2.5 rather than 0.5. Without such a change, unless the assumption of no net force is challenged, radiative acceleration simply does not appear to agree with the available data.

2.6 FURTHER TESTS

If there is no observational connection between the quasar and the absorption systems as discussed above then these may truly be external to the quasar and arise in galactic haloes. In that case it is possible to determine whether the current theory for the production of the peak absorptions is consistent with the observed clustering properties of low redshift Active Galactic Nuclei (eg. Longair and Seldner 1979). The results of these clustering studies show that powerful radio sources occur preferentially outside rich clusters. WWPT have suggested that the majority of the $|B| < 3{,}500$ km/s CIV systems were produced in the haloes of galaxies in the same cluster as the quasar. These would lead one to expect that radio loud quasars would have, on average, fewer absorption

systems with $|B| < 3{,}500$ km/s than the radio quiet ones.

For reasons of availability of data 5GHz fluxes were used in the search for a correlation between radio luminosity and the number of peak absorptions. For a number of objects 5GHz fluxes were not available and so, where possible, these were estimated from fluxes at longer wavelengths. Objects for which this was necessary are marked with an "e" in Table 2.4. Intrinsic fluxes, F, have been calculated from Equation 2.14, the spectral index being taken to be 0.5 (Bolton 1976) and $\langle Z \rangle = 1.89$.

It was fortunate that at the time of investigation a third homogeneous sample of CIV lines was released, due to Young at al. (1982; hereafter referred to as YSB). As has been discussed in Section 1.2.1 the distribution of the CIV lines in the YSB survey differs from those in the studies by WWPT and WCS. Whatever the reason for the difference neither sample is obviously superior and so both should be used for this work. In fact, analyses carried out on the WWPT and WCS samples alone produced similar results to those presented below, so the differences do not appear to be significant in the present context.

The YSB data consisted of 28 quasars showing 57 narrow absorption systems. However, a number of objects overlapped with the previous samples and on removal this reduced the sample to 17 objects and 23 lines, 7 of which had $|B| < 3{,}500$km/s.

It still remains to be shown that <u>rich</u> clusters are necessarily implied by the numbers of peak absorptions discovered. If, in a sample of N quasars, all of which have redshifts sufficient to show CIV, n absorption systems are found, then the implied mean number of cluster galaxies, is -

$$N(\mathrm{Gal}) = (n/N)(R/r)^2 \qquad 2.19$$

where R, r are the cluster and halo radii respectively, assuming the same density profiles for the cluster and haloes. It is unlikely that within the cluster enviroment, with the heightened possibility of gaseous stripping, the galactic halo radii will be larger than those inferred for field galaxies of ~ 100 kpc. These sizes have been calculated in order to explain the absolute numbers of metal absorption lines found in quasars (eg. Burbidge et al. 1977; cf. Section 1.2.1.1). Typical cluster dimensions on the order of one Mpc (Bahcall 1977) then give (R/r) ~ 10.

Examination of WWPT, WCS and YSB reveal that 60 quasars have redshifts > 1.2, making CIV observable. In these, 49 CIV peak absorptions are found. Those quasars showing CIV peak absorption lines are listed in Table 2.4, along with relevant data, N being the number of peak CIV absorption systems. The resultant estimated cluster richness is ~ 50 - 100 galaxies with M(B) < -19.5 (Ho = 100 km/s/Mpc). Given the uncertainties involved in the estimation of r (cf. WWPT) this richness is not expected to be accurate to better than a factor of several. As it is, this number is indicative of very rich systems, comparable to the Coma cluster (Godwin and Peach 1977).

Although the richness may be slightly reduced by multiple absorptions in haloes this is not likely to have an important effect because of the low velocity dispersion within them (Savage and Jeske 1981). Rather than produce separate absorption lines one would only expect this to give small scale splittings, which have not been included in the statistics.

For a number of objects 5GHz fluxes were not available and so, where possible, these were estimated from fluxes at longer wavelengths. Objects for which this was necessary are marked with an "e" in Table 2.4. Intrinsic fluxes, F, have been calculated

from Equation 2.14, the spectral index being taken to be 0.5 (Bolton 1976) and $\langle Z \rangle = 1.89$.

In order to test for any anticorrelation between quasar radio flux and the number of absorption lines in the peak, the velocity distributions in the radio loud and quiet objects have been compared, the dividing line having been set at a variety of intrinsic luminosities, Flim. The numbers above and below this dividing line, N(F<Flim) and N(F>Flim) respectively, are also listed. The Mann - Whitney U Test (Section 2.2.2) was used to search for any difference between the line distribution in the two samples.

The results of these tests are given in Table 2.5. The numbers in parentheses represent the situation when those objects for which radio fluxes are unknown are incorporated into the radio quiet bin. It should be noted that a value for F of 0.067 corresponds, roughly, to an observed flux of ~ 15mJy.

Examination of Table 2.5 shows that the majority of the peak absorptions occur in the radio loud objects. This result is somewhat surprising as it apparently contradicts what had been expected. Because of small number statistics the results are not highly significant, the Mann - Whitney test being most sensitive for samples of roughly equal size.

It is hoped that new data will soon become available which will permit further investigation of this matter. Professor R. J. Weymann, who has been informed of this result, is presently undertaking another survey of moderate redshift quasars for CIV absorption lines in order to increase the sample.

2.7 CONCLUSIONS

It has been shown that there is no detectable correlation between the quasar UV flux and the inferred ejection velocities of its absorption systems, in opposition to the earlier work of Perry and O'Dell (loc cit.). While this does not necessarily imply an extrinsic origin for these lines it does make it probable. Any alternative acceleration mechanism, for example shocks, would have to operate in such a way that their energy output was not correlated with the luminosity of the quasar and this is rather implausible.

It is, however, possible that at the time of observation a majority of the clouds are experiencing some net force. In this case there need be no relation between the ejection velocity and the continuum flux even if radiative acceleration is responsible for the expulsion.

An analysis of all available data suggests that there is a possible correlation between quasar radio flux and the number of absorption systems with absolute expulsion velocities $< 3{,}500$ km/s. This is a marginal result and at present it does not have immediate consequences as regards the probable formation site of the absorption lines because the physical significance of the observation is unclear. Hopefully, in the future this situation will change and the result, if confirmed, will be of some importance for theoretical models.

TABLE 2.1

Sample of Quasars for CIV analysis

Quasar	F(1800)	N	N(B < c/10)	Ref.
0002-422	0.827	2	1	2
0017+154	0.211	1	0	2
0024+224	0.286	1	1	1
0058+019	0.523	1	0	2
0100+130	1.691	1	1	2
0122-380	1.195	3	2	2
0151+048	0.321	3	0	1
0424-130	0.469	4	2	2
0453-423	0.848	2	1	2
0454+039	0.454	1	1	1
0528-250	0.636	2	1	2
0736-06	0.146	1	1	2
0802+103	0.166	1	1	2
0805+046	0.451	1	0	2
0848+164	0.649	1	1	1
0854+191	0.326	1	0	1
0856+170	0.230	1	1	1
0958+550	1.229	2	1	1
1011+250	1.840	2	2	1
1101-264	1.828	3	1	2
1126+101	0.145	1	1	1
1157+014	0.620	5	5	2
1223+228	0.667	2	2	2
1225+317	2.119	4	2	2
1226+105	0.210	1	1	2
1246-057	0.781	3	1	2

1256+357	0.232	3	2	1
1258+286	0.293	2	1	1
1303+308	1.770	7	7	1
1331+170	1.724	1	0	2
1416+067	0.276	1	1	1
1421+330	0.911	1	0	1
1448-232	0.310	2	0	2
1548+114b	0.573	3	2	2
1556+335	0.431	3	3	1
1756+237	0.187	3	2	1
2044-168	0.656	1	1	1
2126-150	1.293	3	0	2
2251+244	0.411	1	1	2
2351-154	1.126	1	1	2

References

1 Weymann et al. 1979 ApJ. 234, 33 (WWPT)

2 Weymann et al. 1981 Ann. Rev. Astr. & Astrophys. 19, 41 (WCS)

TABLE 2.2

Sample of Quasars for the Lyα analysis

Quasar	F(1800)	N	N(B < c/20)	Ref.
0000-398	0.241	10	7	1
0049-393	0.511	4	2	1
0100+130	1.704	35	5	1
0122-380	1.195	17	6	5
0130-403	0.097	15	10	1
0138-381	0.753	6	6	1
0207-398	0.787	4	4	1
0226-038	0.701	22	7	4
0237-233	1.101	4	4	1
0324-407	0.852	18	5	1
0424-131	0.469	8	7	8
0453-423	0.851	10	7	4
0457+024	0.359	12	6	8
0528-250	0.636	27	6	7
0642+449	0.465	22	4	2
0805+046	0.451	65	11	6
0820+296	0.223	24	9	4
0824+110	0.207	10	7	8
0830+115	0.352	41	10	8
1101-264	1.832	16	5	5
1225+31	2.232	17	4	1
1226+105	0.210	8	6	8
1331+170	1.724	7	1	3
2126-158	1.286	37	9	1
2251+244	0.411	14	6	4
2251-154	1.126	9	7	8

References

1 Boroson et al. 1978 ApJ. 220. 772

2 Carswell et al. 1975a ApJ. 195, 269

3 Carswell et al. 1975b ApJ. 196, 351

4 Carswell et al. 1976 A. & A. 53. 275

5 Carswell et al. 1981 MNRAS 198, 91

6 Jian - sheng et al. 1980 AAO Preprint

7 Morton et al. 1980 MNRAS 193, 399

8 Roberts et al. 1978 ApJ. 224, 344

9 Sargent et al. 1979 ApJ. 230, 49

10 Whelan et al. 1979 MNRAS 189, 363

11 Wilkerson et al. 1978 ApJ. 223,364

12 Wingert 1975 ApJ. 198, 267

13 Young et al. 1979 ApJ. 229, 891

TABLE 2.3.1

Corr.	r	T	P
CIV:			
(B/Bmax)/F(1800)	0.191	1.767	<9%
B/F(1800)	0.213	1.970	<6%
Lyα :			
(B/Bmax)/F(1800)	0.094	2.032	<4%
B/F(1800)	0.125	2.707	<1%

TABLE 2.3.2

Corr.	r	T	P
CIV:			
B/F(1800) (B < c/10)	0.197	1.421	<15%
Lyα :			
B/F(1800) (B < c/20)	0.120	1.529	<12%

TABLE 2.4

Sample of Quasars for analysis of the peak line distribution.

Quasar	F	N	Ref.
0024+224	0.433	1	4
0119-40	5.068	1	8
0151+048	0.017	1	12
0237-230	33.968	1	8
0424-13	2.906	3	8
0446-208	?	1	-
0528-250	19.643	1	8
0736-60	8.714	2	8
0802+103	3.577	1	8
0805+046	5.744	1	8
0835+580	2.616	2	1e
0848+164	<0.003	1	4
0856+170	0.500	1	6e
0957+561	0.181	1	7
0958+550	?	1	-
1101-264	<0.195	1	10
1115+080a	<0.003	1	9
1126+101	0.723	1	8e
1157+014	0.549	3	8e
1228+078	<0.012	1	12
1246-057	?	1	-
1246+377	<0.001	1	4
1256+357	0.038	2	12
1258+286	0.220	1	14e
1303+308	<0.012	3	12

1309-056	?	2	-
1416+067	5.728	2	8
1416+159	0.199	2	13e
1548+114b	<0.071	1	20
1556+335	0.929	2	5
1559+173	2.334	1	8
1756+237	3.637	1	8
2044-168	1.504	1	8
2251+244	9.086	1	8
2351-154	14.828	2	8

References

1 Brundage et al. 1971 AJ 76, 777

2 Colla et al. 1970 A. & A. Supp 11, 281

3 Condon et al. 1980a ApJ. 242, 486

4 Condon et al. 1980b Nature 283, 357

5 Davis 1971 AJ 76, 980

6 Ehman et al. 1974 AJ 79, 144

7 Noble and Walsh 1980 Nature 288, 69

8 Parkes Catalogue

9 Peacock 1982 Private Communication

10 Smith 1982 Private Communication

11 Smith and Wright 1980 Preprint

12 Sramek and Weedman 1980 ApJ 238, 435

13 Sutton et al. 1974 Aust J Phys Supp 33, 1

14 Willson 1971 MNRAS 151, 1

TABLE 2.5

Results of Mann - Whitney Analyses on peak absorptions

F(lim)	N(F<F(lim))	N(F>F(lim))	m	s	X
0.067	10(16)	33(33)	165(264)	34.8(46.9)	0.21(1.61)
0.133	11(17)	32(33)	176(272)	35.9(47.6)	0.46(1.75)
0.267	15(21)	28(28)	216(294)	39.2(49.5)	0.99(2.07)
0.667	20(26)	23(23)	230(299)	41.1(49.9)	1.49(2.28)
1.333	23(29)	20(20)	230(290)	41.1(49.1)	1.48(2.21)

CHAPTER III

AN ASSESSMENT OF THE SIGNIFICANCE OF QUASAR ALIGNMENTS

3.1 INTRODUCTION

Four sets of apparently perfectly aligned quasar triplets exhibiting curious redshift patterns have been identified by Arp and Hazard (1980). The physical significance of these associations is, however, not clear since alignments amongst random sets of data points can occur by chance. Indeed, the number of chance alignments increases strongly with the surface density of objects and the maximum length of association considered. It is necessary therefore, to apply objective criteria defining an alignment in order to assess the significance of the linearity of these quasar triplets.

To this end it has been possible to analyse five fields of quasar candidates, one of which includes the above triplets. Lack of complete redshift data, however, does not permit a similar treatment of the equally remarkable redshift patterns. Nevertheless, indications are made as to how this may be accomplished (cf. Section 3.6).

These quasar candidates were discovered in separate investigations by a number of investigators (cf. Section 3.3) by visual inspection of Schmidt plates each covering 20 - 25 square degrees of sky. Individually the samples contain 150 - 200 members, the majority showing strong line or UV excess spectra and

have magnitudes m < 19.8.

This work has been carried out in close collaboration with Dr. S. V. M. Clube of the Royal Observatory, Edinburgh and forms the basis of a paper by Trew et al. (1982).

3.2 THE ALIGNMENT DETECTION TECHNIQUES

Two procedures have been employed to define an alignment, each of which imposes a maximum scale size for the triplets of R degrees.

3.2.1 An Angular Approach

The first method constructs a straight line between all pairs of quasar candidates with separations < R. The resultant set of lines is searched for pairs of similar slopes and with a common (central) member. The maximum allowable difference between the slopes, e, is a free parameter and dictates the quality of the alignment (cf. Figure 3.1). If the triplet has a total length greater than R it is neglected.

It should, however, be noted that for pairs of quasars which are close together positional errors can produce an unacceptably large range of slopes. The propagation of such errors could produce spurious alignments by this procedure.

This technique is very similar to that developed by Broadbent (1980) and Kendall and Kendall (1980) for use in studies of ley lines between megalithic monoliths and which has subsequently been

employed in similar studies of quasar alignments (Zuiderwijk 1982; Webster 1982b). It is also akin to the use of a three point correlation function to search for triplets which have the shape parameter V on the order of unity (Groth and Peebles 1977; Section 4). However, unlike the three point correlation any effects due to clustering must now be taken into account separately.

This analysis can be applied in either (X, Y) space, as on the plate or in (RA, Dec) space, as on the sky, the latter being of potentially greater physical significance.

3.2.2 A Displacement Approach

The second procedure uses a linear acceptance window as opposed to an angular one. Each quasar is taken in turn to lie at the middle of the straight side of a semi - circle, the radius of which is R, cf. Figure 3.2. The use of a semi - circle eliminates any duplicity in the detection of alignments.

This "central" quasar defines one end of any possible alignment with other quasars falling inside the semi - circle. The procedure is to calculate the line joining this quasar to each other object within the area in turn and to determine the minimum distance, s, from this line of all quasars which lie at smaller radii. Any triplets in which s lies in the acceptance window are deemed to be alignments.

This method in which the line is defined by its end points avoids positional errors being magnified by extrapolation along the alignment. Notice, however, that no attempt has been made to calculate the best fitting line to the triplet, the alignment being completely determined by the positions of the flanking

objects. The deviation of the central point, s, is thus an underestimate of the goodness of fit of the line to the triplet.

As in Section 3.2.1 this test can be applied in both (X, Y) and (RA, Dec) space. However, because the arc of a great circle does not differ greatly from a straight line, over scales of a degree, estimates of the expected number of alignments produced by a random distribution of points are the same for both coordinate systems for R < 1 degree.

A comparison of the two above techniques applied to the fields of quasar candidates as well as a number of control samples (cf. Section 3.4), showed little difference in the numbers of detected alignments at comparable sizes of the acceptance window for R < 1 degree and x < 2 arc - minutes. However, the first method is less convenient in practice and is significantly more susceptible to propagating positional errors. Because of these practicalities it was decided to concentrate on the latter technique in this work.

The displacement method has also been used by Edmunds and George (1981) in their study of the numbers of alignments expected from computer generated fields of random points.

3.3 THE SAMPLES

The method for determining the positions of the objects was the same for all fields. The unvignetted portion of corresponding direct plates were scanned by the COSMOS measuring machine at the Royal Observatory, Edinburgh in Image Analysis Mode (IAM) with an 8 micron increment and a 32 micron spot size. A fuller description of the COSMOS machine and its measuring modes may be found in Chapter VI. With the exception of the $15^h\ 52^m\ +48^\circ$ field

each of the direct plates was an UKST J plate (IIIaJ emulsion and Schott GG395 filter) of ~ 70 minutes exposure. For this northern field a Palomar Schmidt IIaE plate of 50 minutes duration was used to determine the object positions.

All plates were measured with a 7% threshold cut above the local sky intensity. For objects in the magnitude range 18 - 20 the rms. error of the position of the intensity weighted image centroids has been estimated by having plates J6124 (cf. section 3.3.4) and J3593 (cf. Section 3.3.5) remeasured after a rotation of the plate within the machine by a right angle. The data have then been compared, the positions in one being transformed into the coordinate frame of the other by use of a second order polynomial. The rms. difference between the observed and expected positions was 3.5 microns for J6124 and 4.0 microns for J3593. This compares well with previous estimates (Stobie et al. 1979).

The transformation from (X, Y) to (RA, Dec) was performed using a number of astrometric standard stars distributed across the plate. Unfortunately, the COSMOS intensity weighted centroids of these images can be severely affected by off - centre haloes which surround them (caused by internal reflections within the glass of the plate). To combat this the IAM data were reanalysed with a threshold cut of 125% above the local sky intensity. This value is not critical, provided that it is sufficiently large to remove the haloes. The best method for determining the correct value is to have a small area measured in Mapping Mode. These data may then be converted using the Starlink programme E2D into IAM format at a given threshold. It is thus possible to obtain an empirical estimate for the threshold sufficient to remove the haloes. The positions of the objects so determined compared well with those found from profile fitting COSMOS Mapping Mode (MM) data. The astrometric transformation was carried out using a standard Gauss

- Jordan Polynomial fitting routine. In practice a third order polynomial was employed. Theoretically this should remove most of the Schmidt induced distortions (cf. Anderson 1971).

It will be noticed in the subsequent sections that in each of the fields the rms. error in the mean fit is substantially greater than the positional errors (the UKST plate scale is 1 arc - second = 14.89 microns). This discrepency is presumably due to magnitude effects on the plate, or induced by the COSMOS measuring process. However, uncertainties in the catalogue positions of the standard stars may also be present due to accumulated errors in their proper motions. This latter explanation is corroborated by the low rms. error in the field centred on $15^h\ 52^m +48^o$ (Section 3.3.3) with respect to the others as the AGK3 catalogue used is more up to date than the SAO which predominates in all the other fields.

Details of the fields searched are given below.

3.3.1 South Galactic Pole (SGP)

UKST prism plate UJ3682P was searched by Clowes and Savage (cf. Clowes 1981) for emission line and Ultra Violet excess (UVX) objects. This plate was an unfiltered IIIaJ emulsion of 70 minutes exposure. The detected number of probable quasar candidates, ie. those which have an 80 - 90% chance of being true quasars, was 146 within the central 4.5 x 4.5 degree area. This gives a mean surface density of 7.2 per square degree.

The reliability of the quasar candidates found in this field has been assessed by higher dispersion observations of a subset by Clowes and Savage using the Anglo - Australian Telescope and the IPCS. Thence, the probability estimates given above.

A number of Parkes radio sources lying inside the field did not correspond to images visible on the direct plate and as such could not be used to extend the quasar sample. This was probably due to inaccuracies in the quoted positions in the Parkes catalogue as one of these sources was later identified as an already optically discovered quasar candidate, but only after revision of the radio position by 30 arc - seconds (Savage and Wright 1981). This experience was such as to discourage any further attempts in the following fields.

The conversion from (X, Y) positions measured on the direct plate J3721 to (RA, Dec) was accomplished using a grid of 60 SAO and PERTH70 stars distributed evenly across the area. The rms. error in the fit was 1.2 arc - seconds.

3.3.2 $11^h\ 40^m +10^\circ$

Hazard (1981) has carried out a search for emission line and UVX quasar candidates on UKST prism plate UJ4054P. This plate is an unfiltered IIIaJ emulsion of 60 minutes exposure.

The number of probable quasar candidates found within the central 5.2 x 5 degree area was 189. This gives a surface density of 7.2 per square degree. The optically selected sample was supplemented by a small number of radio quasars found in a survey at Molongo (cf. Arp and Hazard loc cit.). The reliablility of the detections, again 80 - 90%, was determined by obtaining slit spectra for approximately two dozen candidates using the Palomar 200" telescope (Hazard loc cit.)

Positions on the Celestial sphere were produced from the (X, Y) coordinate system, the direct plate measured was J4288, using a map of 65 SAO, PERTH70 and AGK3 stars. The rms. error in the transformation was 1.0 arc - seconds.

3.3.3 $15^h\ 52^m\ +48^o$

Unlike the other fields this sample of 123 objects within 4.5 x 4.5 degrees, resulting in a surface density of 6.1 per square degree, was selected by Arp and Surdej (1982) solely on the basis of UV excess. These were found from the appearance of the objects on a plate taken in two colour passbands. Only sources estimated to have $U - V < -0.4$ were chosen.

It is more difficult to assess, without much large telescope time, the efficiency and reliability of this technique. Arp and Surdej claim on the basis of a small subset for which slit spectra were obtained, that the overall contamination is < 10%.

Not having access to the original plate material used in the search the POSS plate E1404 was used to provide positions. Unfortunately, the field centres were slightly different (Δ RA, Dec ~ 1 degree) placing the quasar candidates into the NW corner of the plate. Nevertheless, the positional accuracy does not appear to have suffered as with 109 SAO and AGK3 standards the rms. scatter about the mean fit was only 0.7 arc - seconds, the best of any of the fields studied.

It may seem somewhat anomalous when studing blue objects to use a IIaE emulsion, the reason was simply that this plate was of considerably better quality than its short exposure IIaO counterpart.

3.3.4 $01^h\ 12^m\ -35^\circ$

UKST prism plate UJ4532P (60 minutes exposure) was searched visually for emission line and UVX objects by Savage and Chen (Savage et al. 1982). It has a high quasar surface density of such objects - 11.2 per square degree. There are a total of 283 probable quasar candidates within the central 5 x 5.1 degree area measured by COSMOS.

Unlike the previous fields this quasar candidate sample has not yet been studied on large telescopes. Nevertheless, it is believed that the experience of Savage in such studies means that it is unlikely that the high surface density is due to misclassification of "normal" stars as quasar candidates and that the contamination is similar to the SGP, ~ 10%.

Positions for the quasar candidates were taken from a COSMOS measure of a glass copy of J6124, the original being a Survey quality plate. The astrometric reductions were performed using 102 SAO and PERTH70 standards, the final rms. error being 1.0 arc - seconds.

3.3.5 $01^h\ 44^m\ -40^\circ$

He and Smith (He et al. 1982) have performed a search for emission line and UVX quasar candidates on prism plate UJ3690P (75 minutes exposure). A total of 293 emission line candidates were found within 4.7 x 5.2 degrees.

As with the $01^h\ 12^m - 35^\circ$ field this sample has a high surface density of 12.0 quasars per square degree. Also in common with the above field the sample has not been studied on large telescopes, though there is an overlap between this field and a portion of the CTIO and Curtis Schmidt surveys (Hoag and Smith 1977; Smith 1975). Six of the eight CTIO and Curtis Schmidt quasars which lie within the measured area were found in this search. Observations have also been made of a number of emission line and UVX quasar candidates selected by the same searchers in another field on the Palomar 200" telescope (He 1982). From this it was discovered that 80 - 90% of the emission line candidates were confirmed as quasars, but only ~ 30% of the UVX objects were verified. Hence the restriction of the sample to the emission line candidates.

All quasar candidate (X, Y) positions were obtained from plate J3593 and converted into (RA, Dec) by 79 SAO and PERTH70 standards. The rms. error about the mean transformation was 1.2 arc - seconds.

3.4 THE CONTROL SAMPLES

A simple calculation suffices to give a first approximation for the expected number of alignments arising by chance from a total sample of N objects, uniform surface density p, maximum alignment length R and window half - width x, where $x \ll R$.

Consider Figure 3.2: the number of other quasars falling inside a rectangular box of width 2x and length R is -

$$N(\text{box}) = 2pxr \qquad 3.1$$

and within the annulus of radius r and width dr, will be -

$$N(ann) = \pi p r\, dr \qquad 3.2$$

Hence, the number of possible alignments with r < length < (r + dr) occurring in this semi - circle is -

$$dE = 2\pi p^2 x r^2\, dr \qquad 3.3$$

and so the total number from the sample -

$$E = N\int dE = N\int_0^R 2\pi p^2 r^2 x\, dr \qquad 3.4$$

$$= 2\pi p^2 x N \int_0^R r^2\, dr \qquad 3.5$$

$$E = 2/3\,\pi p^2 x N R^3 \qquad 3.6$$

This, however, is an overestimate because of edge effects, ie. the loss of possible alignments which cross the sample boundaries, cf. Section 3.5. Furthermore, the non - linear dependence of E upon p means that for a non - uniform surface density the fluctuations about the mean result in an increased number of alignments. A further deviation from the expected numbers can occur if two quasars are sufficiently close together that their separation is < x. In this case all objects within the semi - circle will form alignments. This proximity correction is expected to be considerably less severe than the edge and clustering effects while x << R. Moreover, it would be expected to show up in an examination of the relative separations of the points.

Many of the difficulties in determining the expected number of alignments may be avoided if a differential technique is employed, comparing the numbers of detected alignments in observed fields with those obtained using identical criteria in test fields having the same number of randomly distributed points. In practice, of course, the observed fields of quasars may exhibit clustering

(real or artificial) which does not occur in the random simulation fields, thereby producing deviations between observed and expected numbers of alignments. One way to allow for this is to represent any differences among exact and loose alignments alike by an appropriate slowly varying correlation function and to attribute any remaining residuals that are significant to an unspecified physical cause. Another is to use a "lateral perturbation" technique, altering the coordinates of each observed quasar in a random fashion by an amount that is just large enough to destroy any alignments of interest, but yet small enough to preserve any larger scale clustering. We can then compare observed and expected alignments differentially without reference to the absolute clustering. Though there are comparatively minor elements of subjectivity in both procedures, one in the choice of correlation function, the other in the choice of perturbing function, these are sufficiently unrelated that any residual excess or deficit of alignments in the observed fields which is common to both procedures can be seen as evidence for an objectively real effect.

The first method employed was to produce the expected number of alignments by constructing control fields using Monte - Carlo techniques each containing the same number of sources as the data to be reproduced. A number of control fields were constructed with the points distributed across the same area as their real counterparts. In practice, available computer time and the difficulty of applying the two point correlation functions (cf. Section 3.7) limited the number of such fields. Ten was initially regarded as providing a satisfactory balance between these constraints and the reliability of the statistics produced. Comparisons between the means and standard deviations derived from analyses on 10 and 100 fields agreed to within 10%.

3.5 EDGE EFFECTS

The finite size of the samples will result in the loss of a number of alignments which cross the boundaries. The magnitude of such an effect will, naturally, depend upon the shape of the area and the ratio of the maximum alignment length to the sample dimensions.

All the sample areas considered are approximately square. So, consider Figure 3.3, where S is the sample dimension and R is the maximum alignment length. Let E(A) be the number of alignments expected, without edge effects, from area A. In this case the expected number of alignments with regard to edge effects will be -

$$E = E(A) + E(B)(1 - F) \qquad 3.7$$

where F is the proportion lost in the strip around the edge of the sample, area B. From Equation 3.6 we have that -

$$L = \frac{E}{E(A) + E(B)} = \frac{(S - 2R)^2 + 4R(S - R)(1 - F)}{S^2} \qquad 3.8$$

let $X = R/S$

$$\Rightarrow \qquad L = 1 - 4X(1 - X)F \qquad 3.9$$

F may be estimated as follows. Within each semi - circle the number of alignments lost will be reduced roughly in proportion to the area falling outside the sample boundary (as represented by the shaded area in Figure 3.4). Hence, the fraction lost is -

$$F = \frac{1/4R^2(a - \sin(a))}{1/2\,\pi R^2} = \frac{(a - \sin(a))}{2\pi} \qquad 3.10$$

The mean separation of the objects lying within area B from the sample boundary gives a mean value for a of <a> -

$$\langle a \rangle = 2\cos^{-1}\left(\int_0^R \frac{dN(1)}{dl} l \, dl \Big/ R \int_0^R \frac{N(1)}{dl} \, dl \right) \qquad 3.11$$

$$= 2\cos^{-1}\left(\int_0^R (S-2l) l \, dl \Big/ R \int_0^R (S-2l) \, dl \right) \qquad 3.12$$

$$= 2\cos^{-1}([R/2 - 2/3RX]/2(1 - X)) \qquad 3.13$$

$$\langle a \rangle = 2\cos^{-1}\left\{ \frac{1 - 4/3X}{2(1 - X)} \right\} \qquad 3.14$$

Equations 3.9, 3.10 and 3.14 may now be combined and the expected losses due to edge effects determined. In practice this will be an underestimate because for alignments with lengths < R the fractional area loss per semicircle is greater. The proportion of missed alignments thus increases.

Figure 3.5 is a graph of L plotted as a function of the maximum alignment length together with experimental values determined by comparing the mean of 100 fields of constant density with the number of alignments expected from Equation 3.9. Examination of this Figure shows that firstly, in order to keep edge effects to a minimum, R < S/4. For the sample dimensions in this study this requires R ~ 1 degree. Secondly, it may be seen that while L is slightly underestimated at large X this difference is small and may be explained as above.

3.6 THE REDSHIFT PATTERNS

If it is assumed that an ejection process is responsible for the production of triplets it is possible, in a simplified model, to relate the redshifts of the outlying members of the quasar triplet to their relative separations. Unfortunately, in a completely general ejection model there are too many free parameters for a unique solution. Consider Figure 3.6, a central object, at a cosmological redshift Zo, ejects two secondary "quasars" colinearly with velocities in the rest frame of the central source of B(1) and B(2). Let the observed redshifts of these ejected particles be Z(1) and Z(2) as seen by a distant Earth observer. Because of the Doppler effect Z(1) and Z(2) will both be larger than Zo if the transverse velocity dominates. If, alternatively, the first order Doppler effect is dominant then the approaching particle will have a redshift less than Zo.

It is obvious that the observed redshifts of the flanking particles will, if ejected, be the combination of the cosmological redshift of the parent with a Doppler component. These must be decomposed in order to give a complete solution.

The convention used hereafter is that the observer is at rest in the primed reference frame and the central particle is stationary in the unprimed. The x direction has been chosen to be parallel to the line of sight and so to the direction of expansion of the Universe.

Now, from Special Relativity, length contraction shows that the general form for the Doppler shift is -

$$(1 + Z) = \gamma (1 + V'(x')/c) \qquad 3.15$$

where -

$$\gamma = \frac{1}{(1 - V'^2/c^2)} \; ; \qquad V'^2 = V'^2(x') + V'^2(y') \qquad 3.16$$

If a line of rest wavelength lo is observed at l and the total redshift, Z, is made up of two components Z(a) and Z(b) then -

$$l = (1 + Z(b))(1 + Z(a))lo \qquad 3.17$$

hence -

$$(1 + Z(a)) = \frac{(1 + Z)}{(1 + Z(b))} \qquad 3.18$$

thus in this application where the total redshifts Z(1) and Z(2) are a combination of the systemic redshift Zo and the individual doppler shifts, Equation 3.18 becomes -

$$\frac{(1 + Z(1))}{(1 + Zo)} = \frac{1 + B(1)\cos(a)}{\sqrt{(1 - B^2(1))}} \qquad 3.19$$

and -

$$\frac{(1 + Z(2))}{(1 + Zo)} = \frac{1 - B(2)\cos(a)}{\sqrt{(1 - B^2(2))}} \qquad 3.20$$

for the daughter particles. This gives relations between the absolute redshift values and the ejection velocities of the ejecta.

Also from Special Relativity we have from the Lorentz transformations that -

$$V'(y') = \frac{V(y)}{\gamma(1 + UV(x)/c^2)} \qquad 3.21$$

and -

$$V'(x') = \frac{U + V(x)}{(1 + UV(x)/c^2)} \qquad 3.22$$

Where γ is the Lorentz factor corresponding to the systemic velocity, that of the central object. So, consider Figure 3.6. The transformed velocities of the two particles in the primed

reference frame are -

$$V'(y':1) = \frac{cB(1)\sin(a)}{\gamma(1 + UB(1)\cos(a)/c)} \qquad 3.23$$

and -

$$V'(y':2) = \frac{cB(2)\sin(a)}{\gamma(1 - UB(2)\cos(a)/c)} \qquad 3.24$$

However, because particle 1 is moving away more quickly than 2 it exhibits an increased time dilation. This serves to reduce the apparent rate of separation of the particle from the centre. The corrected apparent transverse velocity is -

$$V'(app) = \frac{V'(y')}{1 + V'(x')/c} \qquad 3.25$$

and hence the observed ratio of separations will be -

$$\frac{q(2)}{q(1)} = \frac{\left\{\frac{cB(2)\sin(a)}{(1 - UB(2)\cos(a)/c)}\right\}\left\{1 + \frac{U/c + B(1)\cos(a)}{1 + UB(1)\cos(a)/c}\right\}}{\left\{1 + \frac{U/c - B(2)\cos(a)}{1 - UB(2)\cos(a)/c}\right\}\left\{\frac{cB(1)\sin(a)}{(1 + UB(1)\cos(a)/c)}\right\}} \qquad \ldots \quad 3.26$$

which after simplifying gives -

$$\frac{q(2)}{q(1)} = \frac{B(2)(1 + B(1)\cos(a))}{B(1)(1 - B(2)\cos(a))} \qquad 3.27$$

Let us return to the consider the redshifts imparted to the ejected particles as a result of their velocities. Using Equation 3.16 it can be shown that -

$$\frac{\gamma(V')}{\gamma(V)} = (U)(1 + V(x)U/c^2) \qquad 3.28$$

substitution of which into Equation 3.15 gives -

$$1 + Z = \gamma(U)\gamma(V)(1 + V'(x')/c)(1 + V(x)U/c^2) \qquad 3.29$$

and substituting for $V'(x')$ from Equation 3.22 -

$$1 + Z = \gamma(U)\gamma(V)(1 + V(x)U/c^2 + U/c + V(x)/c) \qquad 3.30$$

letting $\gamma(V(i)) = \gamma(i)$ -

$$\Rightarrow \frac{1 + Z(1)}{1 + Z(2)} = \frac{\gamma(1)(1 + B(1)U\cos(a)/c + U/c + B(1)\cos(a))}{\gamma(2)(1 - B(2)U\cos(a)/c + U/c - B(2)\cos(a))} \qquad \ldots 3.31$$

which simplifies to -

$$\frac{(1 + Z(1))}{(1 + Z(2))} = \frac{\gamma(1)}{\gamma(2)} \frac{(1 + B(1)\cos(a))}{(1 - B(2)\cos(a))} \qquad 3.32$$

but substituting from Equation 3.27 -

$$\frac{(1 + Z(1))}{(1 + Z(2))} = \frac{\gamma(1)}{\gamma(2)} \frac{B(1)}{B(2)} \frac{q(2)}{q(1)} \qquad 3.33$$

hence -

$$\frac{(1 + Z(1))}{(1 + Z(2))} = \frac{B(1)}{B(2)} \sqrt{\frac{1 - B^2(2)}{1 - B^2(1)} \frac{q(2)}{q(1)}} \qquad 3.34$$

With the assumption of colinear ejection from a central source Equation 3.34 gives a unique relationship between the redshifts and the relative separations. Combination of this with Equations 3.19 and 3.20 then define the physical parameters of the model. Inversion of these is rather complicated but possible. A solution is only required for one of the physical parameters, the others may be evaluated by substitution. After some rearrangement the three Equations may be combined to give that -

$$X^2\{(D - E)^2 - 4D\} + 2X\{E(D - E) + 4D\} + E = 0 \qquad 3.35$$

where -

$$D = \frac{1 + Z(1)}{1 + Zo}\left\{1 + \frac{q(1)}{q(2)}\right\} \qquad 3.36$$

and -

$$E = \frac{1 + Z(1)}{1 + Z(2)}\left\{\frac{q(1)}{q(2)} - 1\right\} \qquad 3.37$$

and where $X = 1/B^2(1)$. It is therefore possible, on the assumption of ejection, to precisely define the physical characteristics of the system.

It is possible also from Equation 3.27 to calculate the expected relative length distributions of the triplets, if assumptions are made concerning the ejection velocities. It may safely be taken that the distribution of a, the angle between the line of ejection and that to the observer, is random. So letting $B(1) = bB(2)$ we have that the ratio, U, of the shorter separation to the total length is either -

$$U = \frac{q(1)}{q(1) + q(2)} = \frac{1 + bB(2)\cos(a)}{(1 + b)} \qquad 3.38$$

or -

$$U = \frac{b(1 - B(2)\cos(a))}{(b + 1)} \qquad 3.39$$

depending upon the nomenclature adopted for the objects

Figures 3.7, 3.8 then show the distribution of relative lengths for $0 < B(2) < 1$ and $0 < B(2) < 0.5$ respectively, where the B(2) values are drawn randomly from within the ranges specified. Each

of these Figures contains two plots,

a/ b = 1, corresponding to symmetrical ejection of two equal masses.

b/ $0.1 < b < 10$, a random distribution of relative ejection velocities constrained such that $B(1) < 1$.

The vertical scales on these diagrams are in arbitrary units. Comparison of Figures 3.7b and 3.8b shows that the form of the expected distribution is in this case reasonably independent of the maximum expulsion velocity. The general shape of the other plots is also similar. However, very a symmetric alignments are not possible in the second because of the low value of the maximum expulsion velocity. This means that the effect of the light travel time is kept to a minimum and thus enhances the contrast between the numbers of symmetric and assymmetric triplets.

3.7 THE RESULTS

Analyses were first applied to the SGP and $11^h\ 40^m + 10^\circ$ fields with, as previously noted (cf. Section 3.5), a maximum search radius of 1 degree and for $0 < x < 1$ arc - minutes.

Tables 3.1a and b show the numbers of alignments with $R < 1$ degree found and expected as a function of the half - width of the acceptance window, x. In this application the numbers are cumulative with x. N is the number of alignments detected in the real quasar samples, M is the mean number produced by the control fields, s being the standard deviation and E is the number expected on the basis of Equation 3.6, corrected for edge effects. Examination of the Tables shows that E agrees closely with the

mean number found by experiment in the control fields. It should also be noted that, as expected, the numbers of alignments detected in (X, Y) and (RA, Dec) space are very similar. The comparison between the real and expected detection rates is, however, not as good. This is especially apparent in the $11^h\ 40^m$ $+10^o$ field where the numbers diverge significantly at large window half - widths. A similar effect in the SGP field is rather weaker, although there is evidence for a marginally significant excess at small window sizes, $x \sim 4$ arc - seconds.

At first sight, the discrepancy might be taken as evidence of real alignments in excess of those attributable to chance. There are two possible reasons for a divergence. Firstly, it is possible that if the alignments are real structures there is a degree of variability in the production mechanism which gives two trajectories differing by several degrees; although simple conservation of momentum considerations might lead one to expect perfectly aligned triplets. Secondly, any clustering present in the data will increase the number of detected alignments. This is apparent from Equation 3.6, where we see that $E(x) \propto p^2$ and thus those areas with an excess of objects are not completely compensated by those which are deficient. A comparison of clustered real data with unclustered control fields thus gives an apparent excess. Without a precise theory it is not possible to quantify the first effect, but the second, a priori, is likely to occur.

In an attempt to allow for clustering the two point correlation function for each field has been determined, the curves can be seen in Figures 3.9, 3.10. The error bars are given by -

$$\Delta w(i) = \sqrt{\frac{1 + w(i)}{N(i)}} \qquad 3.40$$

where w(i) is the value of the two point correlation function at

that separation and N(i) is the number of pairs contributing to w(i) (Peebles 1973). Sharp (1979) has investigated the accuracy of this expression and found that generally it is an overestimate by about a factor of two.

It is not suggested that the observed two point correlation functions necessarily imply real spatial clustering of the quasars. It is equally probable, if not more so, that the observed clustering is caused, for whatever reason, by an uneven detection rate.

So, using an approximation in which the distribution of points was biassed by the distance from their nearest neighbours, the observed two point correlation functions were imposed on the sets of otherwise random control fields. The comparison of the real two point correlation functions with the mean of that for the clustered control fields can also be seen in Figures 3.9, 3.10. Agreement in both cases is within the statistical errors. The determinations of M etc. were then repeated and the results are displayed in Tables 3.2a, b. The format is the same as Table 3.1 except that in this case no attempt has been made to estimate E. Exact agreement between real and control data is not to be expected because of statistical fluctuations in the correlation functions. Even so, a comparison of Tables 3.1 and 3.2 shows that, as expected, the effect of clustering is to lower the significance of the alignments in the real data.

Because the number of "real" alignments at large acceptance windows continued to exceed that produced by the clustered control fields a further series of simulations were run in an attempt to reproduce, by trial and error, the observed number of alignments at large acceptance windows ($x > 10$ arc - seconds) and to test whether the resultant mean two point correlation function differed significantly from that observed. Tables 3.3a and b illustrate the

"best fit" to the observed numbers of alignments as a function of window size. The mean correlation functions for the sets of control field are again shown in Figures 3.9 and 3.10. These agree with the observed curves to within the statistical errors. However, it must be stressed that the correlation functions producing the best fit are not unique.

Thus, with the general aim of forcing agreement between the observed and simulated data at large window sizes where any observed "alignments" are not expected to be of physical significance, it has been shown that there is no pronounced excess of alignments in the real fields at small window sizes $x < 10$ arc - seconds when $R < 1$ degree. Nevertheless, there are persistent signs of a slight overabundance of alignments in both fields at $x \sim 4$ arc - seconds. There are ~ 60 alignments with acceptence windows in the range $2 < x < 6$ arc - seconds and with $R < 1$ degree, when ~ 40 are expected. The effect, though marginal, is significant at the 2σ level.

It has been checked independently that the $x \sim 4$ arc - second peaks are not special artefacts of the method used here for detecting alignments by submitting these fields to testing by the other procedure based upon the distribution of triangles described by the quasar triplets (cf. Section 3.2.1). The feature was reproduced by this method and also by Webster (1982c) using the same data and similar techniques.

The subsequent availability of three new fields, $15^h\ 52^m\ +48^\circ$, $01^h\ 12^m\ -35^\circ$ and $01^h\ 44^m\ -40^\circ$ have opened the possibility of testing further the significance of the $x \sim 4$ arc - second peak. The two point correlation functions for these new fields are shown in Figures 3.11, 3.12 and 3.13. The experience gained in the previous analyses suggests slight changes in any further work. Having shown that there is no significance in the numbers of loose alignments

(ie. large x) it is fully justified to use these to determine directly the effects of clustering. This considerably simplifies the task and permits the use of a larger number of control fields because it is now not necessary to generate clustered control samples. This in turn allows an increased confidence in any features detected. The distribution of the numbers of detected alignments in these control fields were consistent with a Poisson distribution about the mean.

The revised method involves the calculation of a statistic T(x) (cf. Equation 3.35), which is a measure of any difference between the observed and the average expected numbers of alignments in the range x to x + dx (dx = 2 arc - seconds) so that the numbers are now calculated differentially with respect to x rather than cumulatively as before.

$$T(x) = \frac{\{O(x) - ax^{-b} E(x)\}}{\{ax^{-b} E(x)\}^{1/2}} \qquad 3.41$$

Here O(x) is the observed number of alignments in the real samples with half - widths in the range x to x + dx, while E(x) is the corresponding number for the mean of the unclustered control fields. In all five fields combined these numbers are, typically, 137 and 100 $\pm$ 10 respectively, while a and b are parameters which allow for the effects of two point clustering in the real data by increasing E(x) to the mean level of O(x).

It is implicit in this method that only deviations from the mean level are of significance, the difference between the means of O(x) and E(x) being consistent with clustering in the real data (cf. above). The functional form of the correction is the same as that found by Peebles (loc cit.) for the two point galaxy correlation function, and as such is a reasonable a priori representation of the effects of clustering. The range of x has

also been increased to 2 arc - minutes to give a better defined zero point. Given that the distribution of E (at each value of x) is Poissonian implies that $\Sigma T^2(x)$ is identical to χ^2, thus permitting a simple probablistic interpretation of the results. Best fitting values for the free parameters a and b and the corresponding ΣT^2 (or χ^2) probability of the observed distribution T(x) have been sought for each field by minimizing $D^2 = \Sigma T^2(x)$ over the full range of x. The results are given in Table 3.4. Contour plots of the D^2 surfaces used in the minimization are shown in Figures 3.14 - 3.19, from which it is clear that the minima are well defined.

The assumed form of the clustering function, though plausible, is somewhat arbitrary. It may be equally defensible to assume that the loose alignments are of no physical significance, and thus to minimize any differences between the observed and model clustered distributions in the arbitrary range $x > 30$ arc - seconds with $b = 0$, analagous to the first method of analysis used. The probabilities from the D^2 test of the observed distributions in the range $x < 25$ arc - seconds that then emerge are also given in Table 3.4. It turns out that departures of the observed numbers of alignments from those expected are fairly insensitive to any plausible adjustments of a and b.

Differential large scale clustering effects between the real and simulated fields could in principle influence the statistics. However, any such effect is small as the observed two point correlation functions show no anticlustering on scales of about a degree which otherwise would have been expected. In Figures 3.20 - 3.24, T(x) values are plotted for each field, assuming $b = 0$ and in Figures 3.26 - 3.30 similar plots are shown for the best fitting a and b values, limiting the range in both cases to $x < 30$ arc - seconds for clarity of presentation. Inspection of these Figures reveals marginally significant excesses in three fields

for x ~ 4 arc - seconds. In order to test further the significance of these peaks, the separate fields have been combined to produce a total distribution of T(x), shown in Figures 3.25, 3.31. It is clear from these Figures that these peaks, though individually barely significant, together represent a quite distinct feature. Calculation of the D^2 statistic gives that the probability of the observed T(x) distribution occurring by chance is in the range 10^{-3} - 10^{-4}.

Closer examination of Figures 3.25, 3.31 shows that two other peaks are perhaps of greater significance than might be expected. Either these are evidence for other prefferred shapes or alternatively suggest that the assumed distribution is not a good one. Differentiation between these is possible by setting the significance of the 4 arc - second peak to zero and then repeating the χ^2 test upon the remaining histogram. This will determine whether the underlying T(x) distribution is adequately described by poisson fluctuations about the mean. For the total of the five fields considered, the removal of the peak resulted in a probability of 30% that the observed and expected distributions were drawn from the same parent population. It is thus probable that the assumption that D^2 is identical to the χ^2 distribution is a good one and that the other peaks are not of significance.

One possibility is that despite all efforts to remove its effects the clustering in the real data is in some way responsible for this peak. As an independent test of this peak we have used the "lateral perturbation" technique to generate 100 randomly perturbed fields per real data set, the standard deviation of the displacements in quasar position being 1 arc-minute. These fields were analysed and the results after averaging were compared with the real data as before (assuming a = 1, b = 0). This produced a total distribution plot T(x) which was identical to Figures 3.25 and 3.31 in all essential respects. Not only is the excess of

alignments at x ~ 4 arc-seconds still present to the same degree but the mean level is approximately zero, indicating that the real data had not been so greatly perturbed as to transform it into a random distribution. It is clear, therefore, that the expected numbers are not grossly in error and that simple clustering of the data is not responsible for the 4 arc - second feature.

It is worth restating that not only is the effect not produced by the coordinate transformations employed, as it is present in analyses carried out on both (RA, Dec) and (X, Y) surfaces but it is detection technique independent. Indeed it is not obvious that any process in the plate measurement and reduction would produce an artificial feature of this kind (cf. Section 3.8), so either it is a somewhat improbable chance deviation from truly random fields or it is representative of a real property of the quasar distribution on the sky.

It is possible, therefore, that the five fields of quasar candidates have an excess of 41 tight alignments over the 137 expected after allowance for clustering (or 86 over 92 expected if no such correction is applied). It is not altogether obvious how this excess relates to any possible number of true physical alignments in space because if physical alignments exist then the number of such systems will increase linearly with the number of quasars considered. On the other hand the number of chance alignments will increase more strongly than this, cf. Equation 3.6, and so a real effect may be lost in the noise. The large sample sizes and high surface densities of the $01^h\ 12^m\ -35^\circ$ and $01^h\ 44^m\ -40^\circ$ fields are, therefore, not as may have been expected necessarily conducive to the detection of a physical excess.

As an additional test of the significance of this peak the relative quasar separations V=q(1)/q(2) and U=q(i)/(q(1) + q(2)) have been measured for each peak alignment choosing q(i) such that

$U < 0.5$ (as with Equations 3.38 and 3.39). This gave distribution functions F11(U) and F12(V) for all alignments with half - widths between 2 and 4 arc - seconds. Similar control samples using non - peak alignments gave functions F21(U) and F22(V). Distribution functions F01(U) and F02(V) associated with the excess peak alignments can thus be derived -

$$F0i(q) = F1i(q) - (137/179)R\ F2i(q) \qquad 3.42$$

where R is the ratio of the numbers of alignments in the peak and control bins. The distributions are illustrated in Figures 3.32a - d, together with those of the control samples, suitably normalised. Comparisons of this kind, if significant, can in principle be expected to reveal differences if a physical mechanism giving rise to the excess produces U values correlated with the line - of - sight orientation as well as characteristic dimensions (V values). Firstly it should be noted that the lack of a peak in F01(U) and F21(U) at $U \sim 0$ shows conclusively that proximity effects (cf. Section 3.4) are not important in the analyses.

All that can be said at present, considering the range of theoretical U distribution illustrated in Figures 3.7 and 3.8, is that the data are consistent with a random ejection model.

3.8 CONCLUSIONS

Before coming to any final statements it must be recognised that these are crucially dependent upon the availability of complete samples. In particular, if the redshift patterns are of importance and there is any bias in the detection technique, which for example excludes low redshift quasars, could cause underestimation

of the number of alignments, as the central objects in each of the Arp and Hazard alignments have low redshifts. Similarily, the inclusion of any non - quasars, for which physical alignments are inconceivable, will lead to an underestimation of the significance of any result. Such imponderables are outside the scope of this investigation.

The only positive result which has emerged is the marginal (3 - 4σ) excess for structures of dimensions R < 1 degree, x ~ 4 arc - seconds. Confirmation of the reality of this will require similar studies in additional fields of quasar candidates. However, if, for the moment, the reality of the 4 arc - second peak is assumed, then some explanation must be sought and some idea given of the intrinsic sizes implied for the associations.

A simple ejection model in which all three particles (the parent and the daughters) take up some momentum from the explosion will, in general, produce a non - linear association. If the intrinsic shape of all alignments is the same, then the probability density of x varies as sin(x).

Projection effects may, therefore, produce a peaked distribution with a non - zero mean. One might expect that on the basis of this model the flanking bins should also show numbers in excess of those expected. The fact that such wings are not observed may be explained in two ways: firstly, as a problem with the signal/ noise in the data. Secondly, larger scale variations will tend to be removed by the clustering correction technique.

Comparisons of the length of the alignment with its width show that the velocity given to the parent is a small fraction (~ 0.1% - 1%) of that imparted to the flanking objects. The determination of the relative masses is dependent upon the energy distribution in the ejection process but if there is equipartion of energy then

the daughter particles have only a few percent of the mass of the parent.

A second possibility is that the preferred, non - zero, value of x is produced by observational effects rather than by some intrinsic production mechanism, remembering that the line is not the best fitting one to the triplet but is determined solely by the flanking objects. The most obvious method for accomplishing this is to deform perfect, x = 0, alignments by differential refraction. In an ideal world such distortions would be removed in the (X, Y) to (RA, Dec) conversion, However, errors in the positions of the standard stars and uncertainties in the plate constants may mean that this is not achieved in practice. It is of importance, therefore, to calculate the size of this effect.

A good estimate may be made by assuming a plane parallel, homogeneous atmosphere of refractive index (1 + k). For an object at a zenith distance z, measured at the top of the atmosphere, the deviation A caused by refraction will be -

$$A = k \tan(z) \quad \text{radians} \qquad 3.43$$

thus converting k into arc - seconds the differential refraction becomes -

$$dA = 58\{\tan(z(1)) - \tan(z(2))\} \qquad 3.44$$

As all alignments have lengths less than one degree then z(1) - z(2) must also be less than one degree. The telescope records show that each plate was taken at transit and that the values of the zenith distances are small. Substitution into Equation 3.44 give typical deviations of only ~ 3/4 arc - second and so this mechanism is inadequate for the production of the observed 4 arc - second peak from perfect alignments.

Relativistic aberration has also been proposed as a mechanism for producing misalignments by Hoyle and Narlikar (Hoyle 1981). In order for this process to operate however there must be a significant motion of the triplet in the plane of the sky as seen by an observer on earth. The magnitude of this velocity, V, may be calculated for small misalignments from -

$$X = \frac{1}{8} \frac{V/c}{\sqrt{1 - V^2/c^2}} \sin(A) \sin(K) R^2 \qquad 3.45$$

(a derivation of this is given in the above reference), where X and R are the alignment half - width and length respectively and A and K are the colatitude and Position Angle of the triplet as seen from the earth. Substitution of X = 4 arc - seconds and R = 1 degree into Equation 3.45 shows that V = 10,000 km/s. This is considerably greater than the usual random velocities of galaxies and as such is not consistent with the identification of the central body with a previously normal object. While this problem may be circumvented by the assumption of repeated ejections the model then becomes somewhat over - elaborate.

Returning to the physical characteristics implied, if the excess alignments are produced by an ejection, the mean triplet half length is ~ 0.35 degrees. This corresponds to physical dimensions of ~ 5 Mpc ($z \sim 0.5$, Ho = 100 km/s/Mpc, qo = 0), typical of rich clusters. Assuming that the central redshifts of the alignments are generally similar to those discovered by Arp and Hazard (loc cit.) (ie. $0.5 < z < 1$). The density on the sky of rich clusters is (Abell 1958) 1 - 2 per square degree compared with a surface density of excess alignments ~ 0.4 per square degree (mpg < 20). If the central quasars are associated with rich clusters then a maximum production rate per cluster of one every ~ 100 Myr appears to be implied.

Whatever its origin, it should be noted that, if real, there is a ~ 20 - 25% probability that any single alignment of the kind selected by Arp and Hazard is physically significant. These probabilities of course increase if the actual redshift values are of importance. This, however, is the only strong evidence for a statistically significant excess of aligned triplets and the significance is dependent upon the correctness of the identification of D^2 as χ^2.

Final resolution of the nature of the peak probably requires a change of emphasis or similar analyses on a large number of presently unavailable new fields. The most promising new direction is an assessment of the significance of the quasar redshift patterns, which has been shown to be related to the relative separations of the particles, at least in restricted models. Unfortunately, it has not been possible to establish whether any such patterns, similar to those reported by Arp and Hazard (loc cit.) exist along a significant proportion of the alignments discovered here as most of the quasar candidates do not have reliable redshifts. In any case it is difficult to quantify the significance of such trends as the redshift selection effects differ from one detection technique to another and are difficult to quantify (cf. Hewitt and Burbidge 1980). In a sample which has been produced by a variety of techniques, therefore, assumption of a single underlying redshift distribution may hide real, or produce spurious, results.

Further progress will only be possible when more high quality data sets become available. To improve the statistics these should cover at least comparable areas to those considered here and should use a more objective method for finding the quasar candidates to improve the uniformity of detection and reduce, or at least enable quantification of, the redshift selection effects.

Finally, it may be of interest to examine one of those Arp and Hazard (loc cit.) associations which instigated the project, although now the alignments have been selected in a totally objective manner, unlike in the Arp and Hazard (loc cit.) work. Their $11^h\ 30^m + 106^\circ$ grouping is shown in Figure 3.33, except that here all those triplets aligned to better than 4 arc - seconds in (RA, Dec) space have been included. It may be chance but the overall structure now appears to take on a fan like appearance with one of the original triplets changing into a quadruplet. The original triplets are quasrs A, D, E and F, H, I. Quasar E actually contributes to two other triplets in addition to the quadruplet. Redshifts, where these have been determined from spectroscopic observations on a large telescope or can be uniquely found from the prism spectra, are shown alongside the objects.

TABLE 3.1

Number of Alignments found in (RA, Dec) space; random data Figures for (X, Y) space are given in parentheses.

a Field; SGP

x"	N	M	s	(N - M)/s	E
1.	4 (4)	3.2 (3.0)	2.04 (2.05)	0.39 (0.49)	3.5
2.	12 (12)	5.6 (7.0)	2.42 (2.58)	2.64 (1.94)	7.0
4.	23 (23)	11.5 (13.4)	3.81 (4.43)	3.02 (2.17)	14.1
6.7	29 (30)	21.2 (21.2)	6.43 (5.71)	1.21 (1.69)	23.6
10.	39 (40)	31.0 (31.0)	9.23 (9.32)	0.87 (0.97)	35.2
20.	91 (91)	64.5 (65.7)	17.63 (17.85)	1.50 (1.42)	70.5
34.	154 (154)	106.8 (107.9)	19.82 (19.70)	2.38 (2.34)	119.8
67.	277 (274)	213.1 (214.9)	28.84 (28.43)	2.22 (2.32)	236.0

b Field; $11^{h}\ 40^{m}\ +10^{\circ}$

x"	N	M	s	(N - M)/s	E
1.	5 (4)	3.9 (4.2)	1.20 (1.14)	0.92 (-0.18)	4.6
2.	10 (10)	8.9 (9.2)	1.97 (1.87)	0.56 (0.43)	9.1
4.	35 (35)	17.5 (17.7)	4.93 (5.21)	3.55 (3.32)	18.2
6.7	46 (47)	28.8 (29.0)	7.13 (6.99)	2.41 (2.58)	30.6
10.	77 (77)	44.6 (45.2)	9.51 (9.73)	3.41 (3.27)	45.6
20.	139 (139)	88.4 (89.8)	13.09 (13.63)	3.87 (3.61)	91.2
34.	226 (226)	147.3 (149.3)	23.19 (24.38)	3.39 (3.12)	155.1
67.	423 (423)	299.9 (305.2)	43.79 (46.94)	2.81 (2.51)	305.5

A correction has been applied to E to allow for the loss of alignments at the edge of the field.

TABLE 3.2

Number of Alignments found in (RA, Dec) space; clustered data Figures for (X, Y) space are given in parentheses.

a Field; SGP

x"	N	M	s	(N - M)/s
1.	4 (4)	4.1 (4.3)	1.73 (1.14)	-0.06 (-0.26)
2.	12 (12)	7.9 (8.3)	3.75 (3.50)	1.09 (1.06)
4.	23 (23)	14.6 (14.5)	5.87 (6.06)	1.43 (6.70)
6.7	29 (30)	24.1 (24.7)	7.40 (7.45)	0.66 (0.71)
10.	39 (40)	37.2 (36.8)	9.75 (10.24)	0.18 (0.31)
20.	91 (91)	73.5 (69.5)	12.95 (14.06)	1.35 (1.53)
34.	154 (154)	126.1 (121.2)	21.58 (22.83)	1.29 (1.43)
67.	277 (274)	247.6 (245.6)	32.26 (28.87)	0.91 (0.98)

b Field; $11^h\ 40^m +10^\circ$

x"	N	M	s	(N - M)/s
1.	5 (4)	7.3 (5.2)	3.83 (3.39)	-1.53 (-0.35)
2.	10 (10)	13.3 (10.8)	4.88 (5.31)	-0.68 (-0.15)
4.	35 (35)	25.5 (22.8)	7.01 (7.24)	1.36 (1.69)
6.7	46 (47)	36.7 (35.6)	7.44 (12.24)	1.25 (0.93)
10.	77 (77)	53.9 (53.9)	10.47 (14.39)	2.21 (1.60)
20.	139 (139)	113.1 (103.7)	20.73 (24.39)	1.50 (1.45)
34.	226 (226)	183.1 (176.6)	35.11 (35.28)	1.24 (1.40)
67.	423 (423)	355.0 (357.6)	57.39 (60.71)	1.18 (1.18)

TABLE 3.3

Number of Alignments found in (RA, Dec) space; "best fit" clustering.

Figures for (X, Y) space are given in parentheses.

a Field; SGP

x"	N	M	s	(N - M)/s
1.	4 (4)	4.5 (4.4)	2.13 (2.17)	-0.23 (-0.18)
2.	12 (12)	8.7 (8.7)	3.25 (3.16)	1.02 (1.03)
4.	23 (23)	16.7 (16.8)	4.96 (4.97)	1.27 (1.25)
6.7	29 (30)	27.0 (27.0)	5.32 (5.27)	0.38 (0.57)
10.	39 (40)	40.9 (40.7)	8.40 (8.40)	-0.23 (-0.17)
20.	91 (91)	83.9 (83.4)	9.54 (9.54)	0.74 (0.80)
34.	154 (154)	144.5 (144.0)	16.12 (16.12)	0.59 (0.62)
67.	277 (274)	293.2 (293.7)	36.83 (36.82)	-0.45 (-0.45)

b Field; $11^{h}\ 40^{m}\ +10^{o}$

x"	N	M	s	(N - M)/s
1.	5 (4)	7.0 (7.0)	2.98 (2.71)	-0.67 (-1.11)
2.	10 (10)	14.1 (14.6)	4.72 (4.53)	-0.87 (1.02)
4.	35 (35)	28.1 (29.2)	7.02 (6.68)	0.98 (0.87)
6.7	46 (47)	42.4 (44.1)	9.49 (8.46)	0.38 (0.34)
10.	77 (77)	66.1 (68.3)	11.43 (10.08)	0.95 (0.86)
20.	139 (139)	129.4 (139.3)	18.00 (17.76)	0.53 (-0.02)
34.	226 (226)	218.6 (225.7)	28.86 (26.44)	0.26 (0.01)
67.	423 (423)	432.4 (442.7)	48.08 (45.07)	-0.20 (-0.44)

TABLE 3.4

Field	Nqso	p $\square^{\alpha-1}$	a	b	P	a	b	P	Ref
SGP	146	7.2	1.382	-0.021	0.03	1.319	0	.30	2
$11^h\,40^m+10^\circ$	189	7.2	1.178	0.096	0.25	1.276	0	.07	3
$15^h\,48^m+48^\circ$	123	7.1	0.866	0.233	0.01	0.951	0	.002	1
$01^h\,12^m-35^\circ$	283	11.2	1.527	-0.022	0.08	1.500	0	.02	5
$01^h\,44^m-40^\circ$	293	12.0	1.350	0.028	0.08	1.392	0	.05	4
Total	1034	-	1.364	0.026	3×10^{-4}	1.384	0	10^{-4}	-

References

1 Arp H. C. & Surdej J. 1982 A & A 109, 101

2 Clowes R. G. 1980 PhD Thesis, University of Edinburgh

3 Hazard C. 1982 Private Communication

4 He X. T., Smith M. G. & Trew A. S. 1982 In preparation

5 Savage A., Trew A. S., Chen J. & Weston T. 1982 Preprint

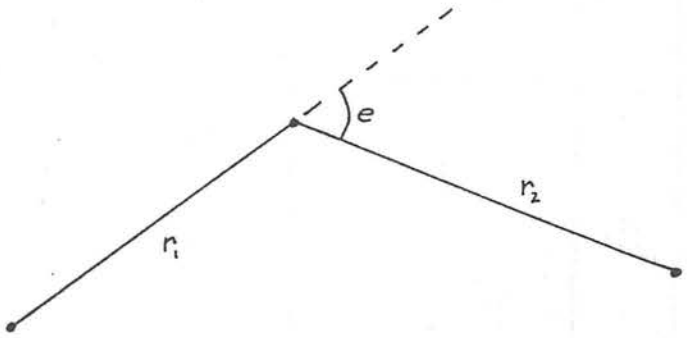

Figure 3.1 Definition of the angle of deviation, e, used to detect alignments by the Angular method (cf. Section 3.2.1).

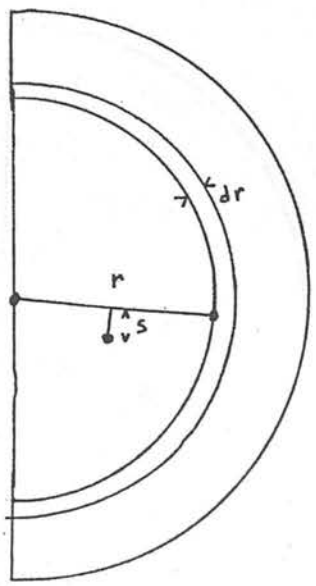

Figure 3.2 Description of the method used to detect alignments by the linear deviation of the central point from the mean line (cf. Section 3.2.2).

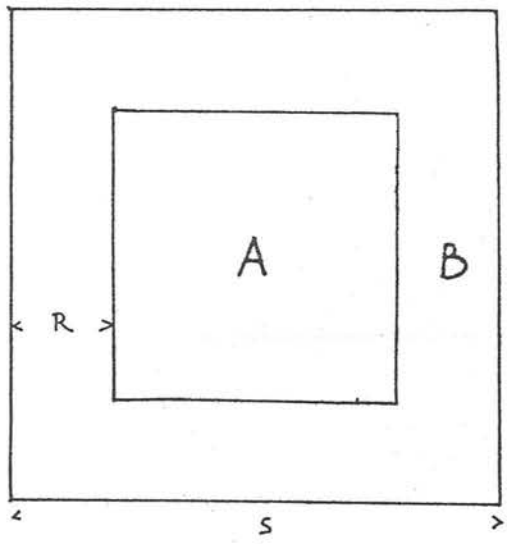

Figure 3.3 The division of the total area used to calculate the fraction of alignments lost due to edge effects. Only those quasars lying in area B will be affected by this problem.

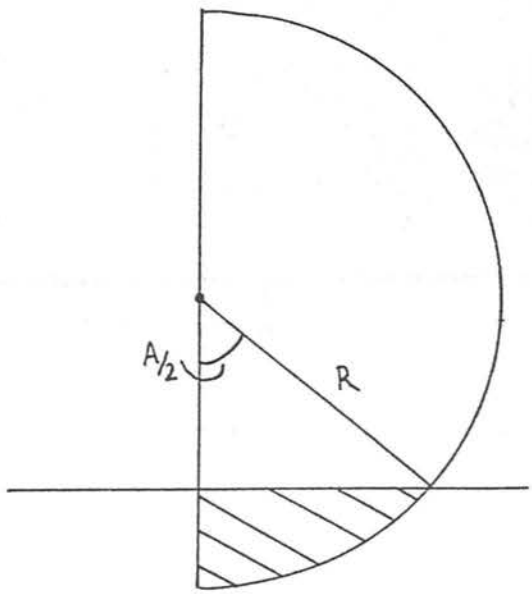

Figure 3.4 Estimation of the fractional area lost per semi - circle due to the finite size of the sample.

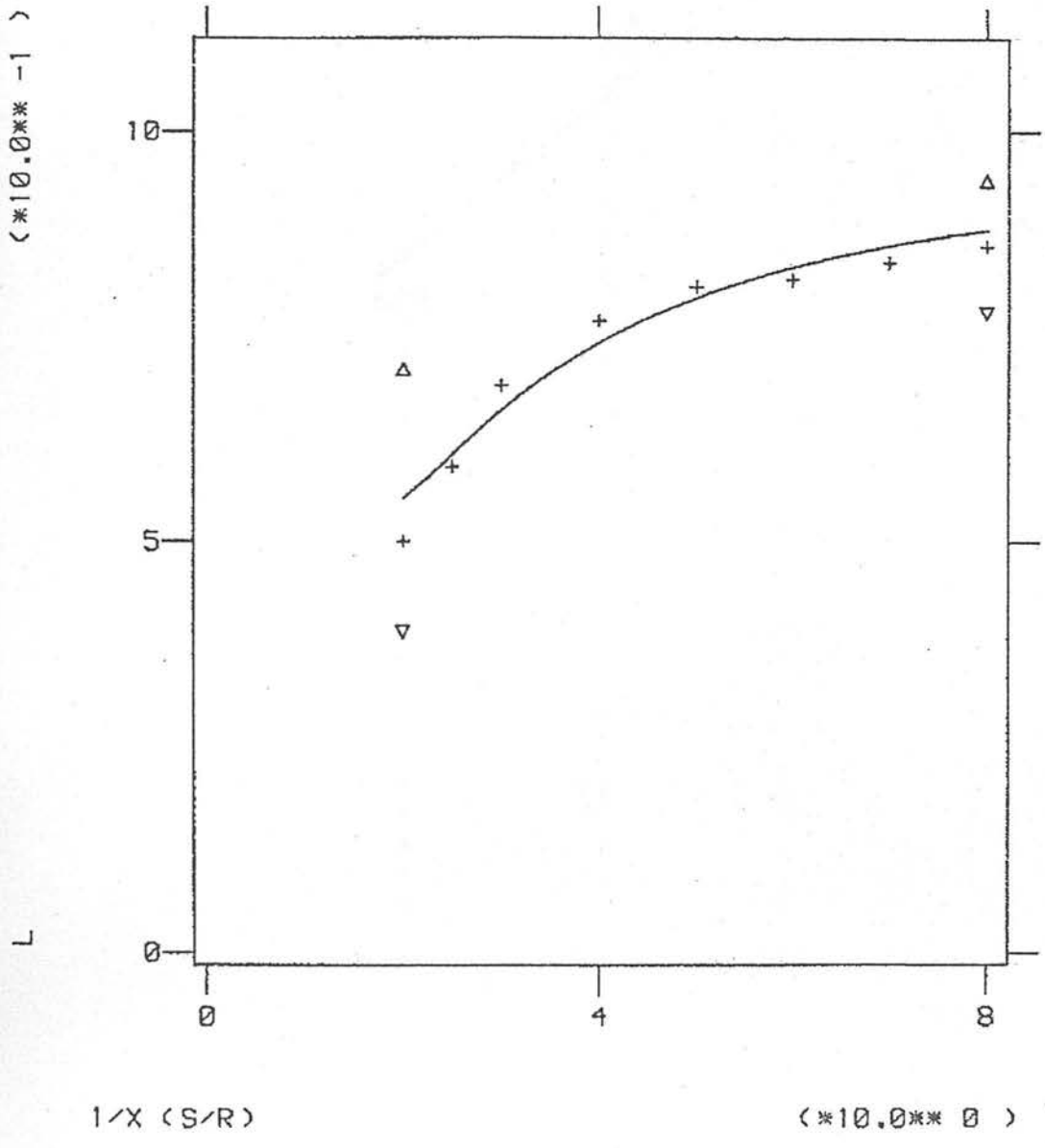

Figure 3.5 Comparison of the number of alignments compared to that expected without regard to edge effects, L, plotted as a function of the maximum alignment length. The theoretical curve is compared with empirically derived points.

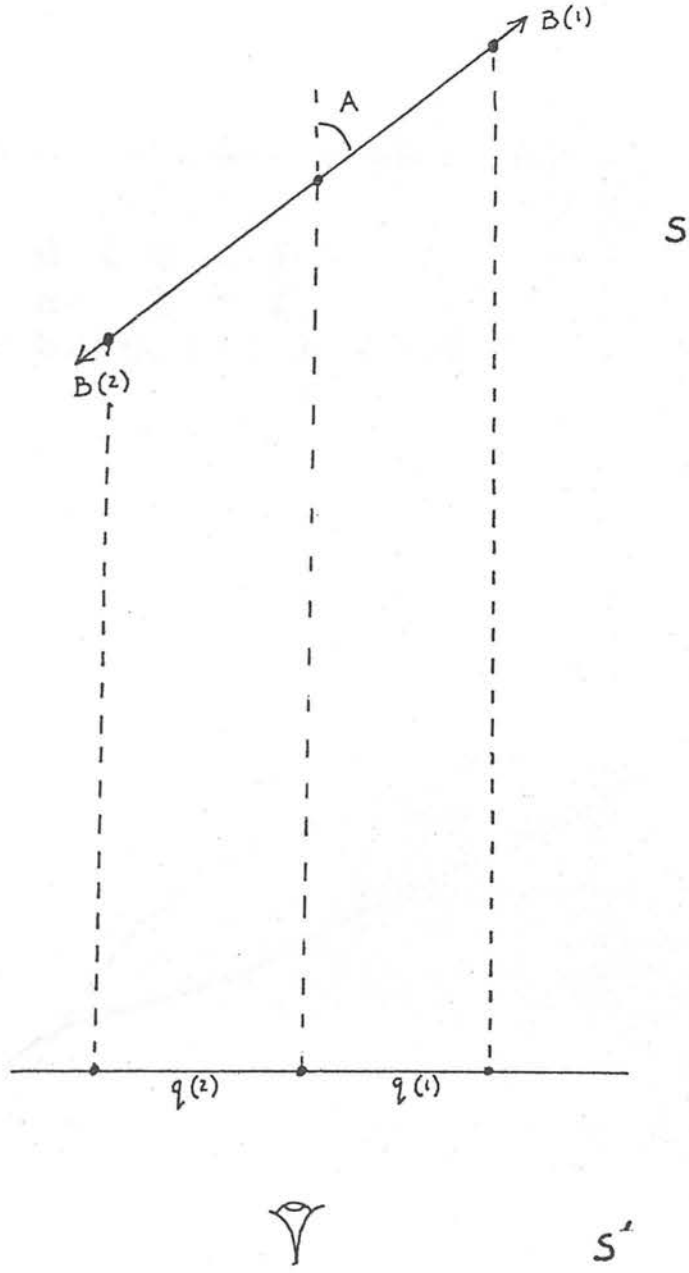

Figure 3.6 The geometry of the ejection model, B(1) and B(2) are as measured in the rest frame of the parent body, as is the ejection angle to the line of sight, A. The redshifts and separations are as determined by the Earth observer.

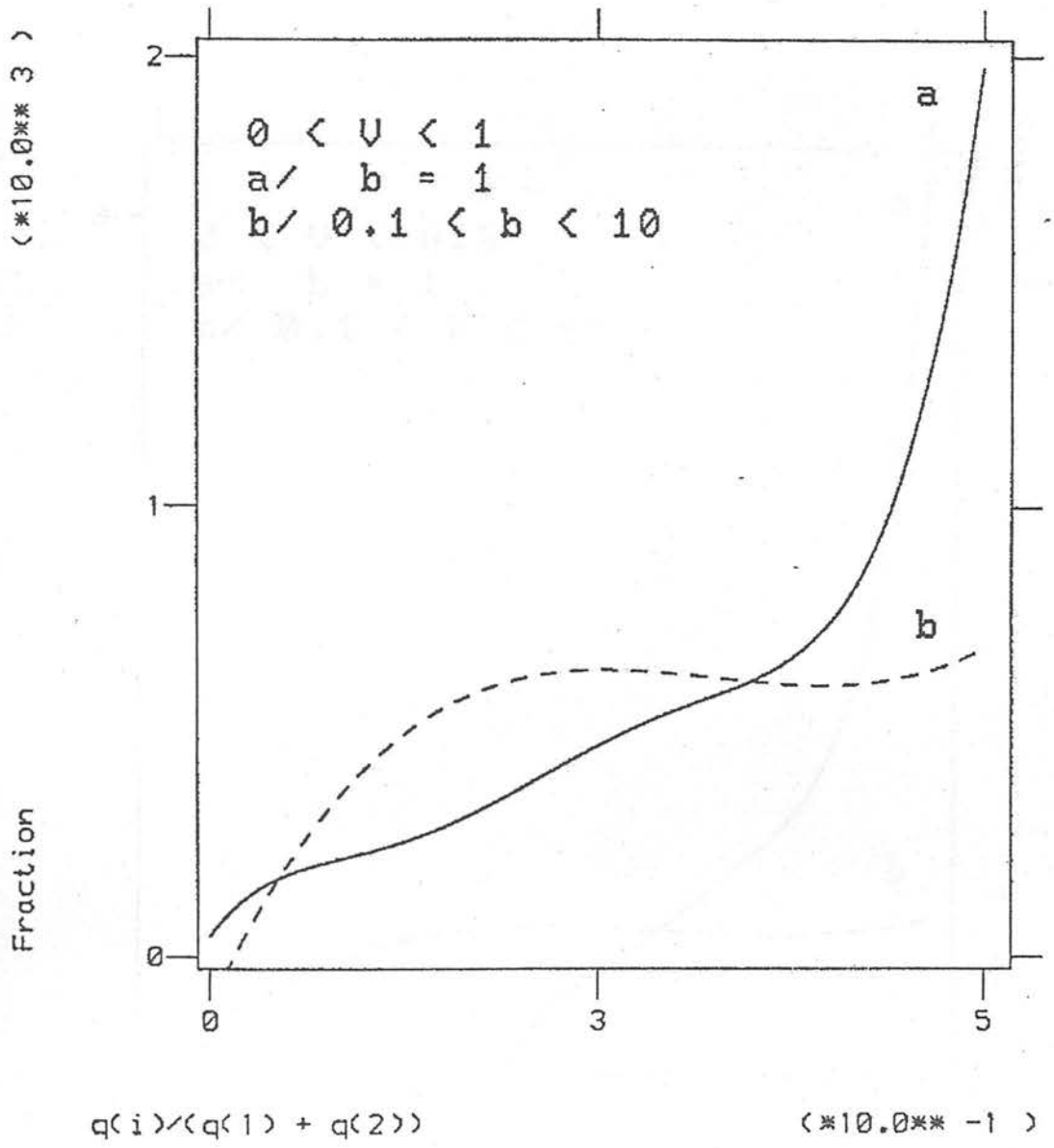

Figure 3.7 The distribution of relative separations, shorter side to total length, expected from colinear ejection with B(2) < 1.

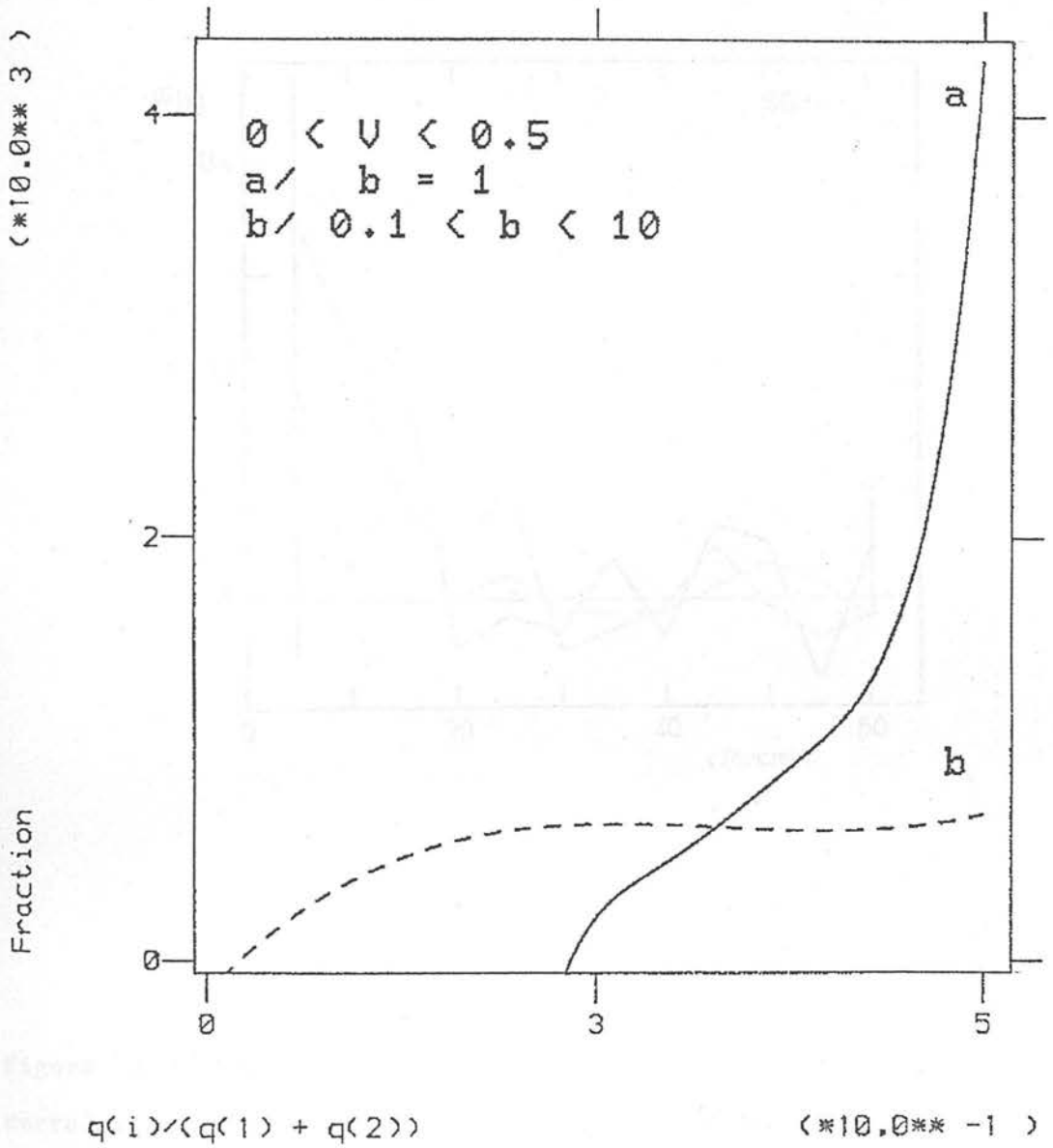

Figure 3.8 The distribution of relative lengths, as in Figure 3.7, except now B(2) < 0.5.

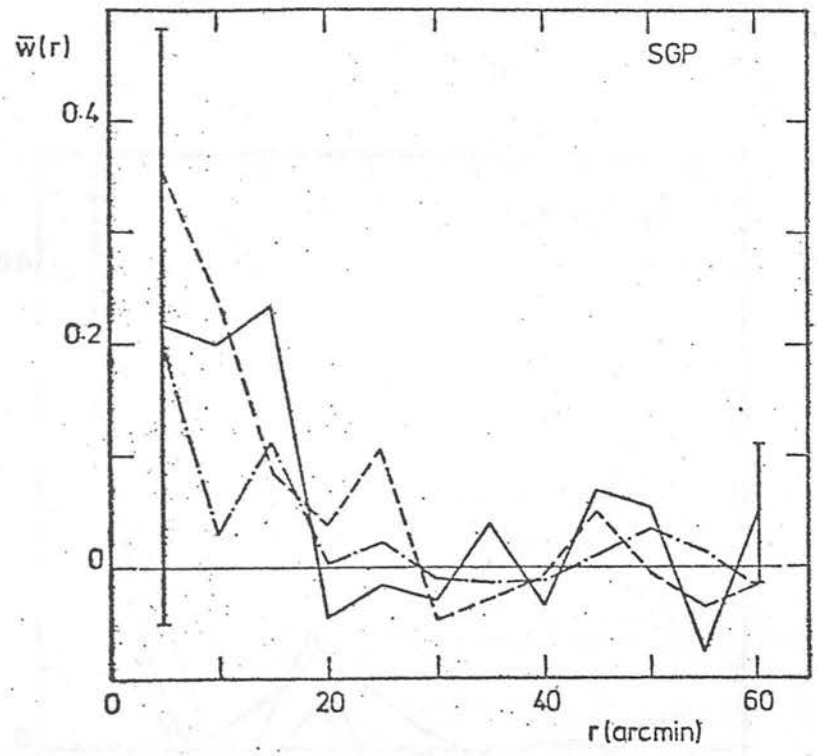

Figure 3.9 Comparison of the real and imposed two point correlation functions for the SGP. The solid line is the observed correlation function, the dotted line is the mean correlation function of the control fields approximating that of the real data. The dashed line is the mean correlation function which gives the best fit to the observed number of alignments.

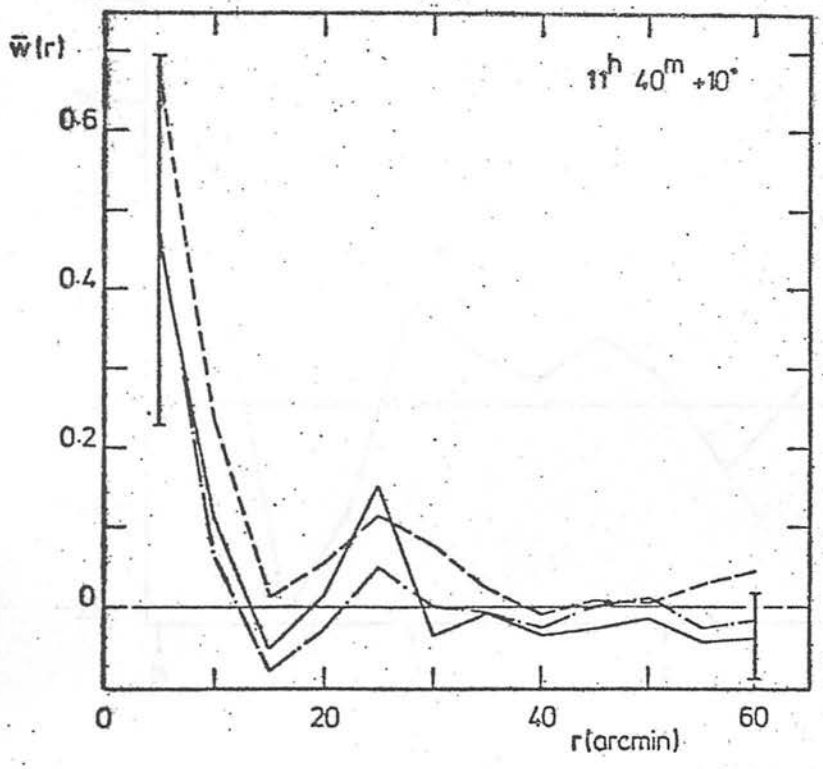

Figure 3.10 Comparison of the real and imposed two point correlation functions for the $11^h\ 40^m+10^\circ$ field. The line symbols are the same as for Figure 3.9.

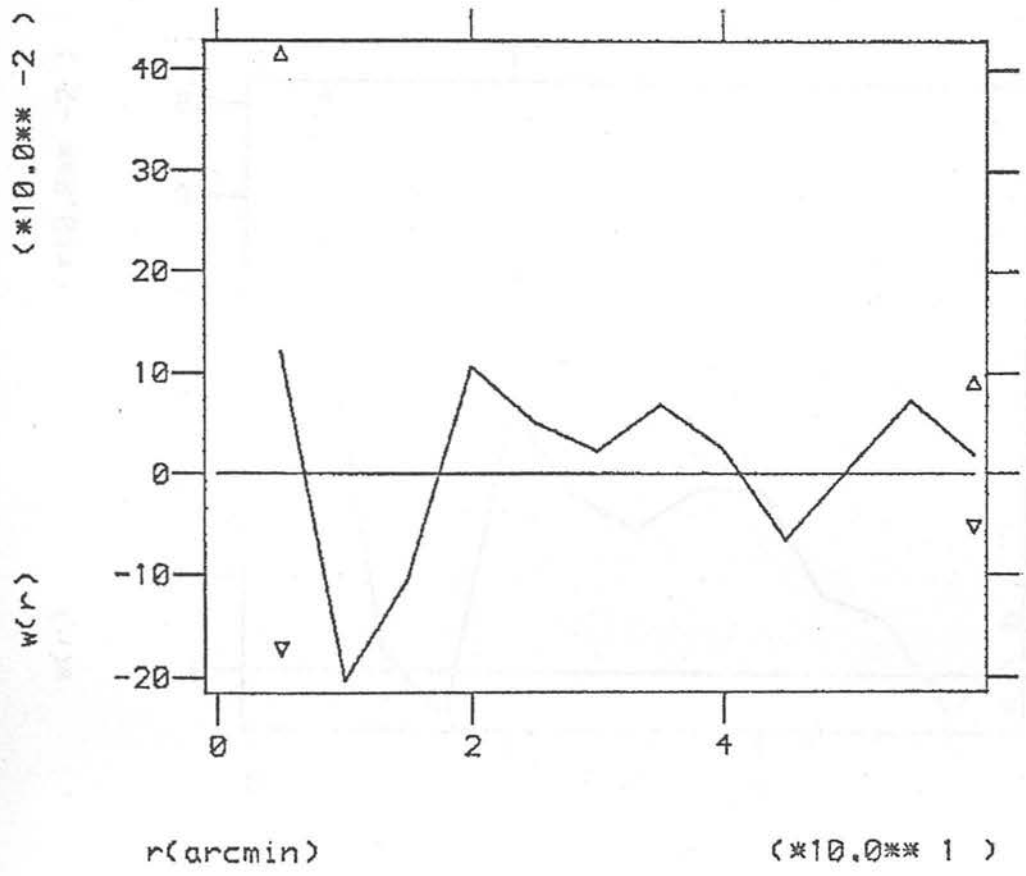

Figure 3.11 Observed two point correlation function for the quasar candidates in the $15^h\ 52^m$ $+48^\circ$ field. The error bars are as given by Equation 3.36.

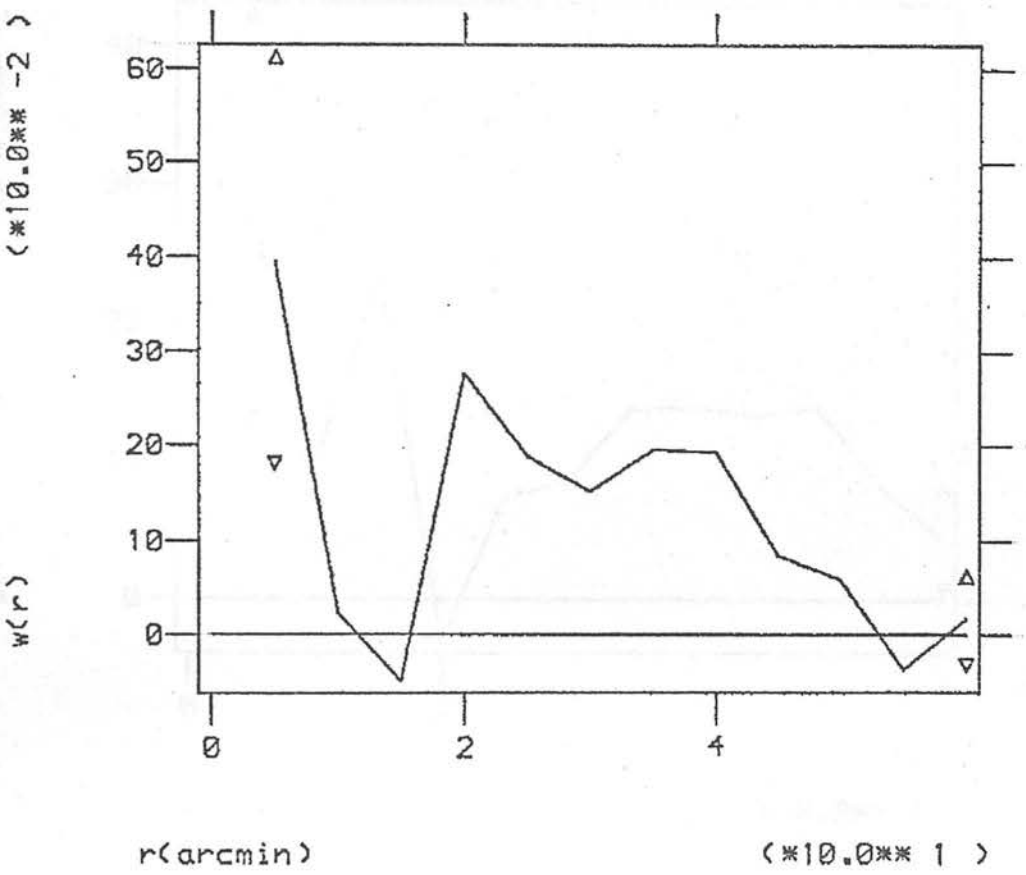

Figure 3.12 Observed two point correlation function for the quasar candidates in the 01^h 12^m -35° field, error bars as in Figure 3.11.

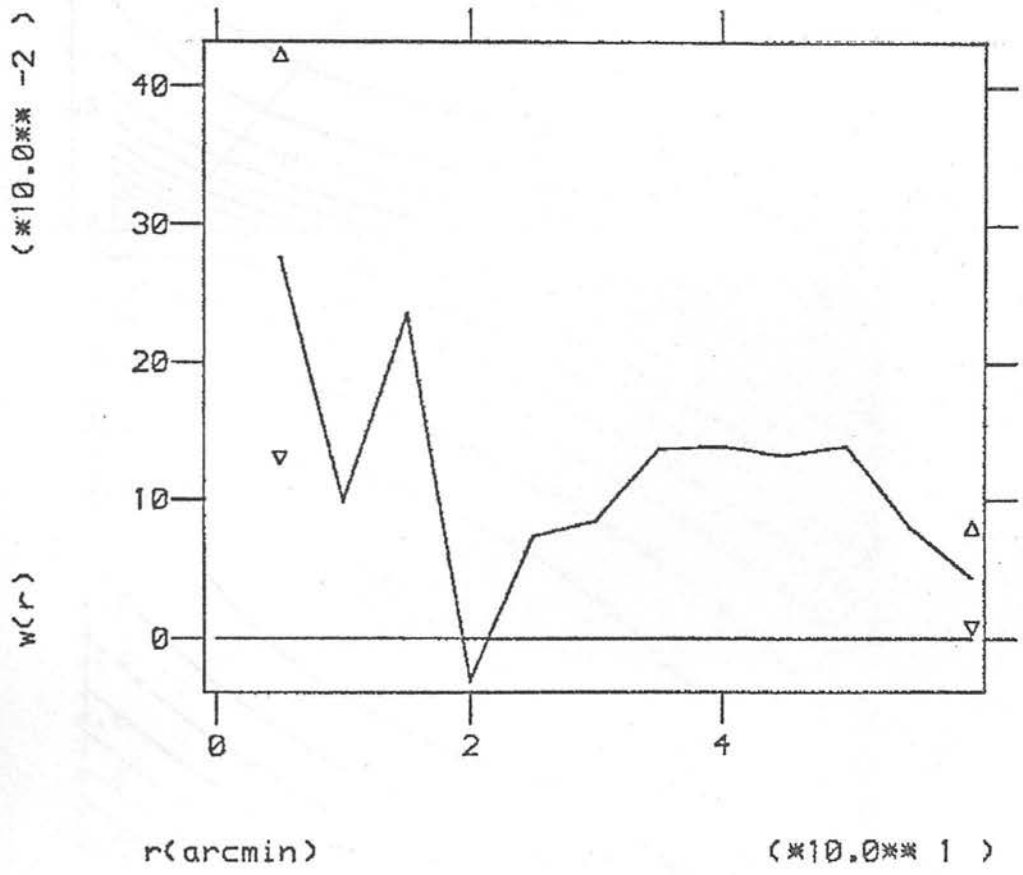

Figure 3.13 Observed two point correlation function for the emission line quasar candidates in the $01^h\ 44^m\ -40^\circ$ field. Error bars as in Figure 3.11.

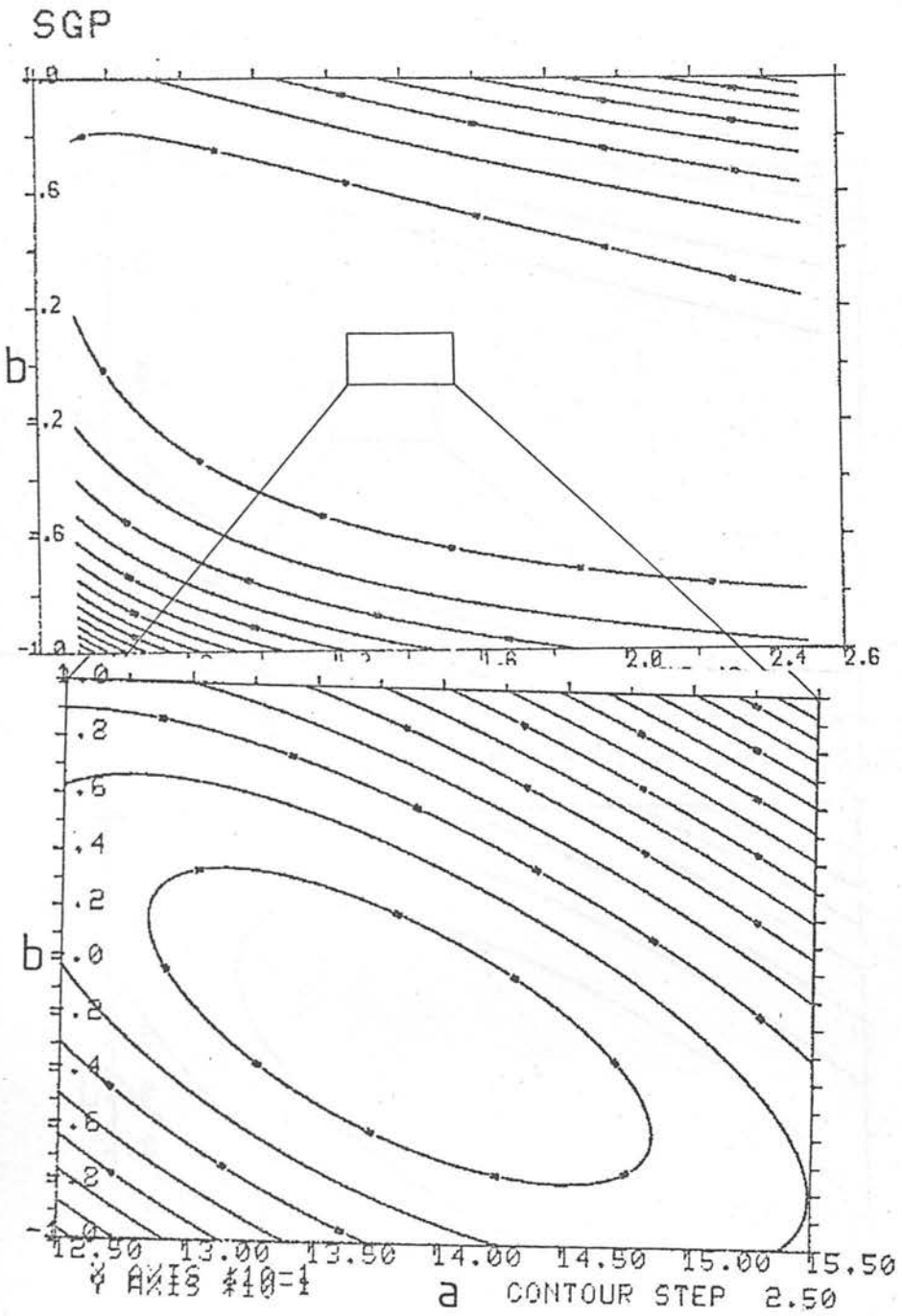

Figure 3.14 Contour plots of the D^{λ} surfaces used to detect the best fitting values of a and b (the parameters defining the form of the clustering correction) for the quasar distribution in the SGP. The lower plot is an expansion of the marked region in the upper.

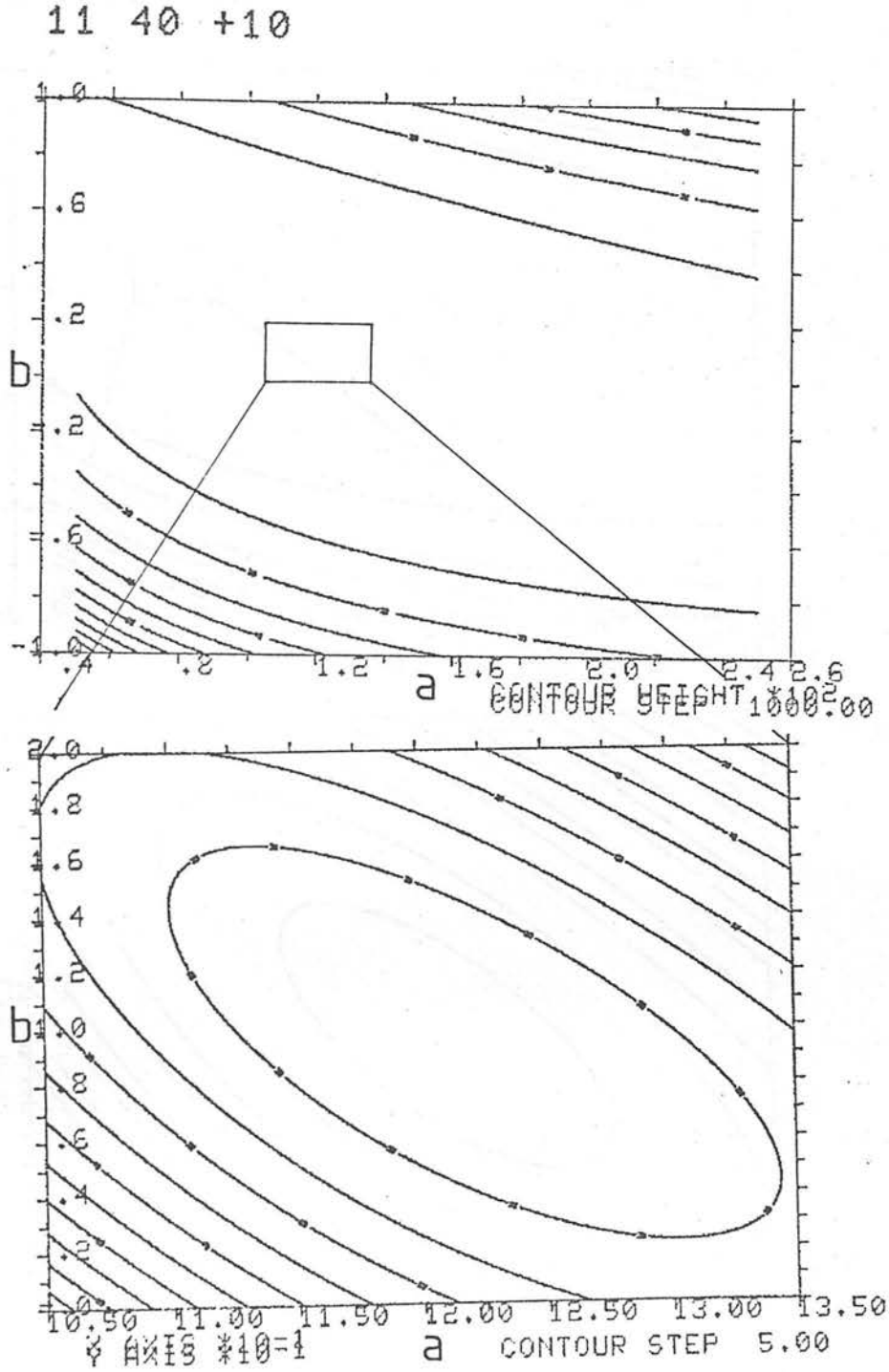

Figure 3.15 Contour plots of the D^2 surface for the $11^h\ 40^m\ +10^\circ$ quasar distribution. Axes as in Figure 3.14.

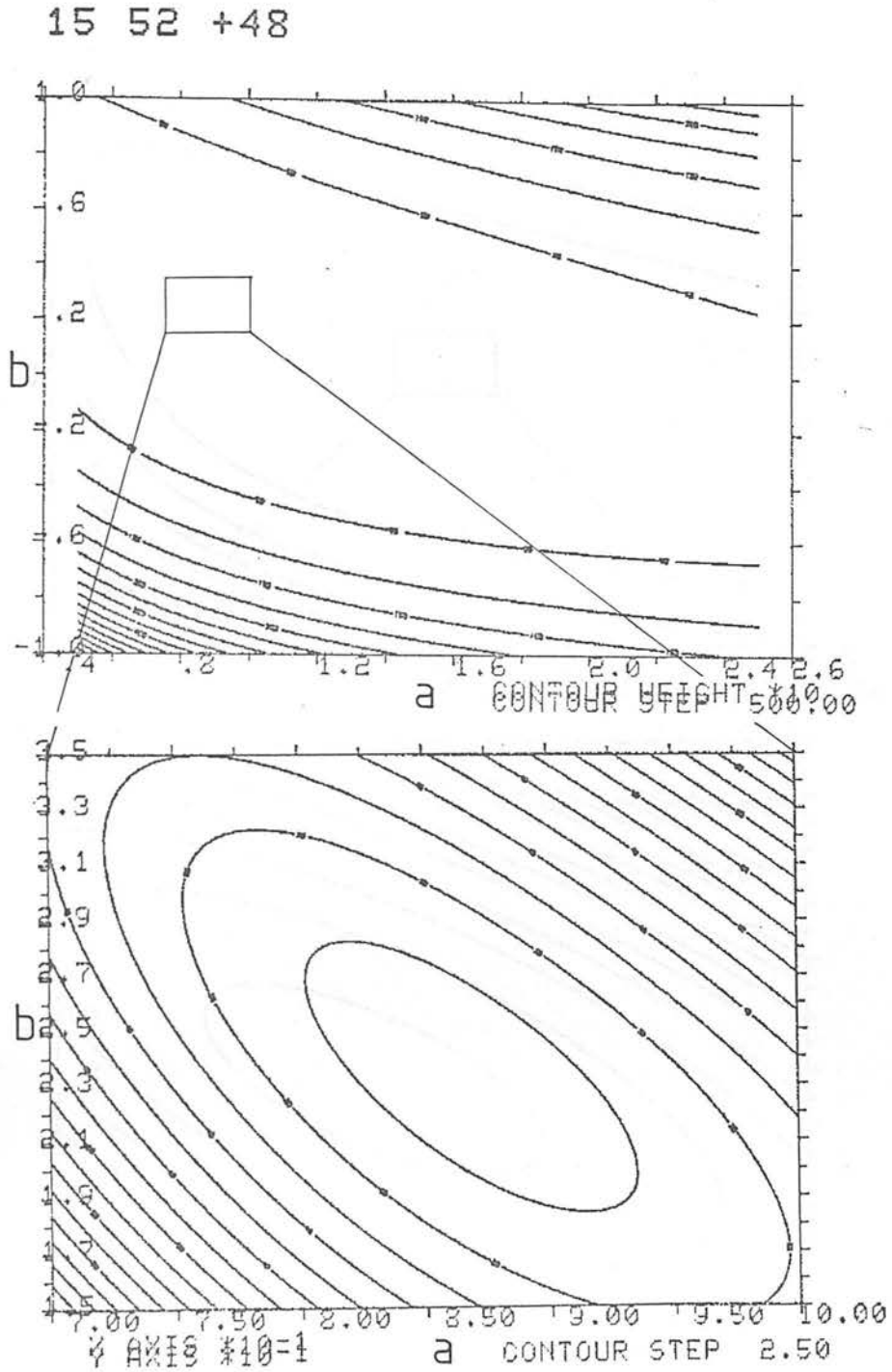

Figure 3.16 Contour plots of the D^2 surface for the quasar distribution in the 15^h 52^m $+48^\circ$ field. Definitions as in Figure 3.14

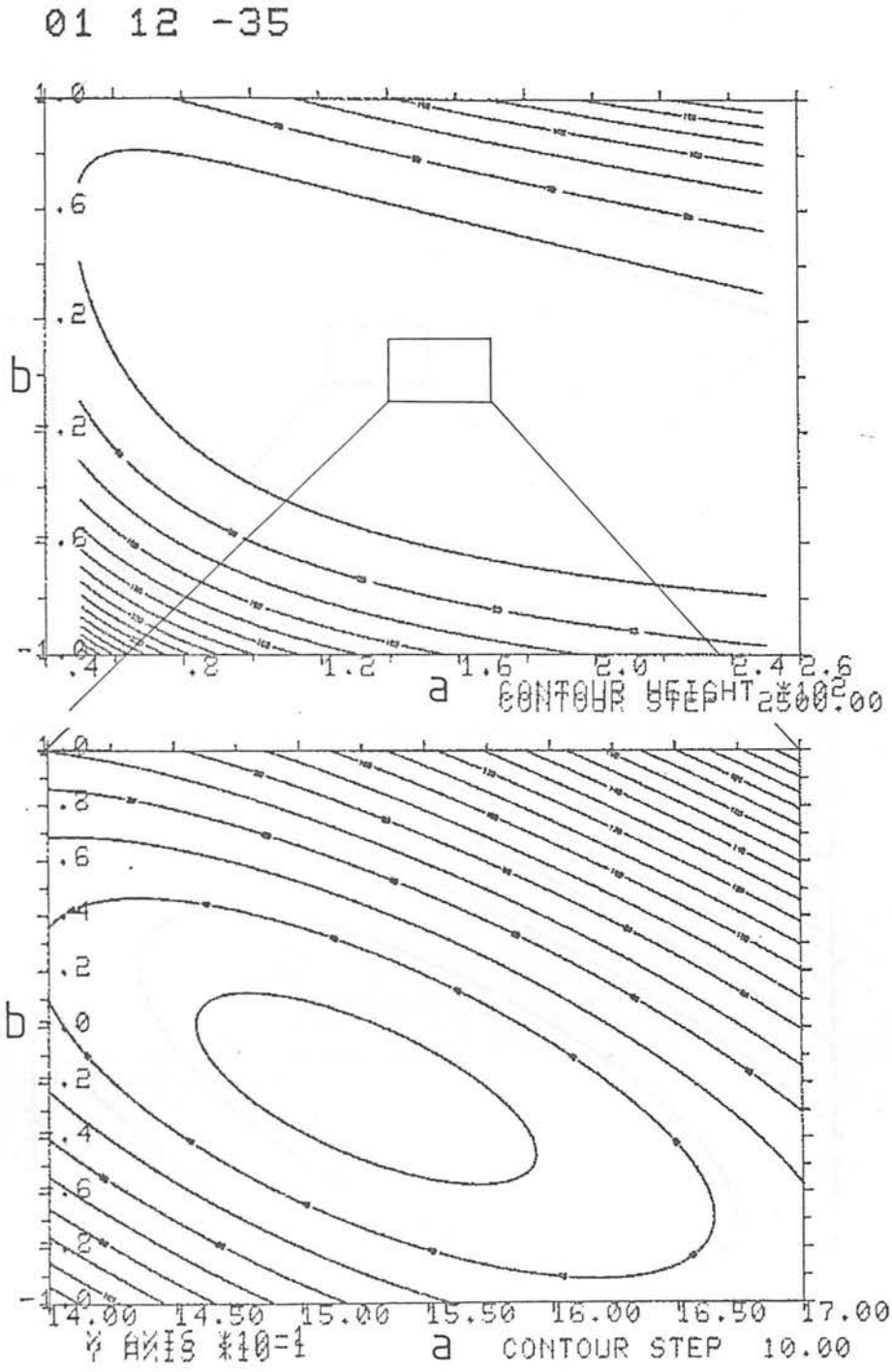

Figure 3.17 Contour plots of the D^2 surface for the quasar distribution in the $01^h\ 12^m\ -35^\circ$ field. Definitions as in Figure 3.14

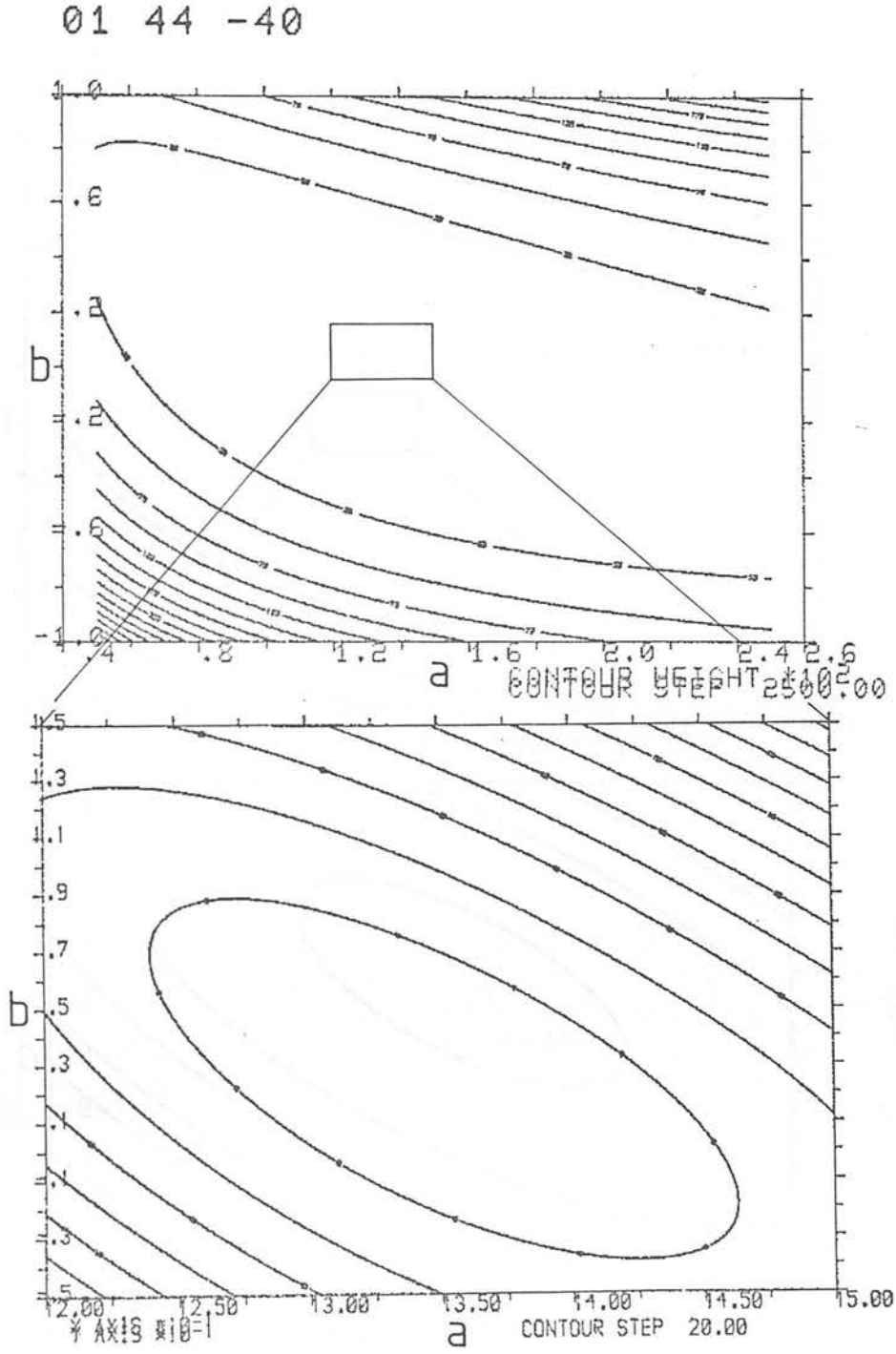

Figure 3.18 Contour plots of the D^2 surface for the quasar distribution in the $01^h\ 44^m\ -40^\circ$ field. Definitions as in Figure 3.14

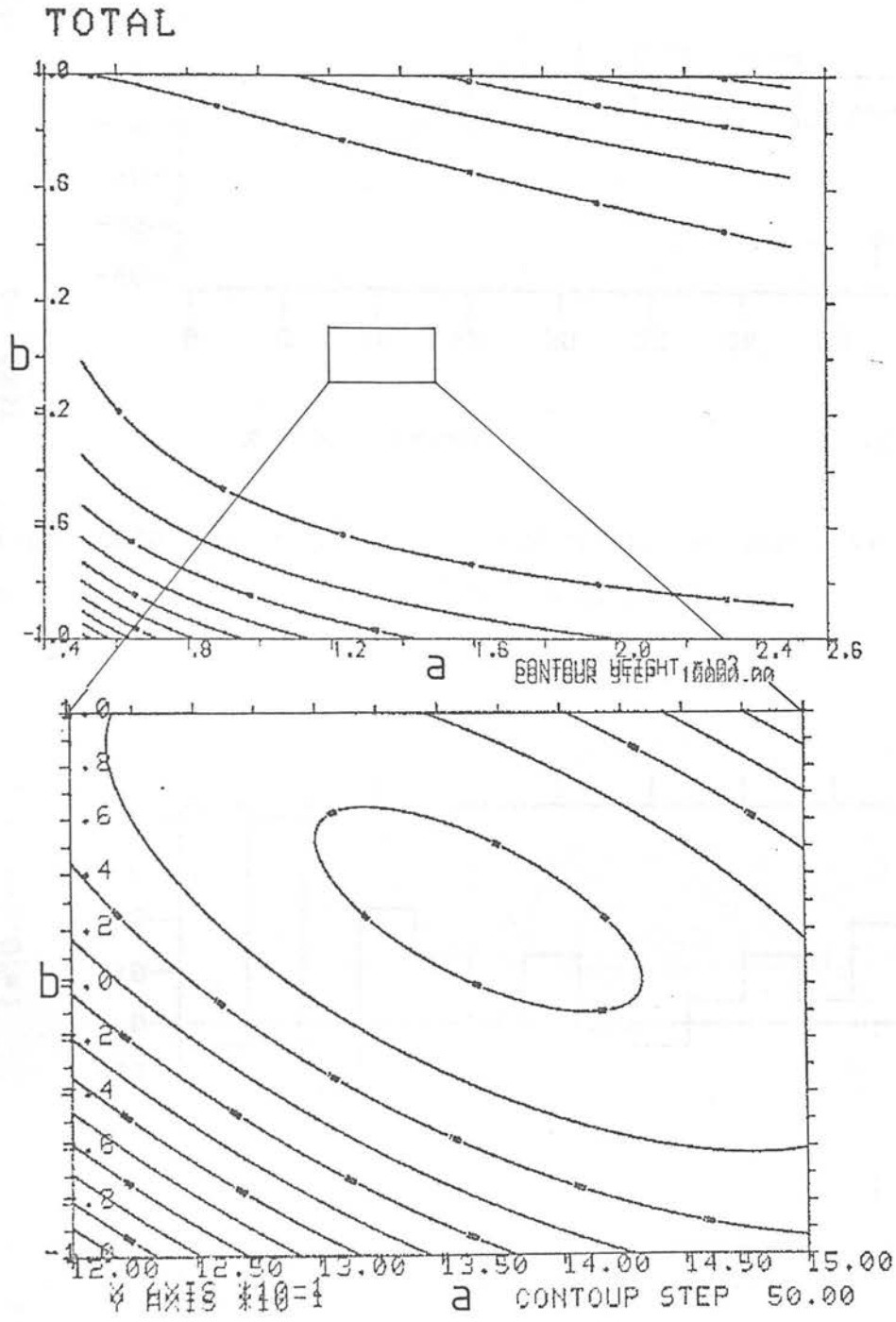

Figure 3.19 Contour plots of the D^2 surface for the total quasar distribution in the five fields. Definitions as in Figure 3.14.

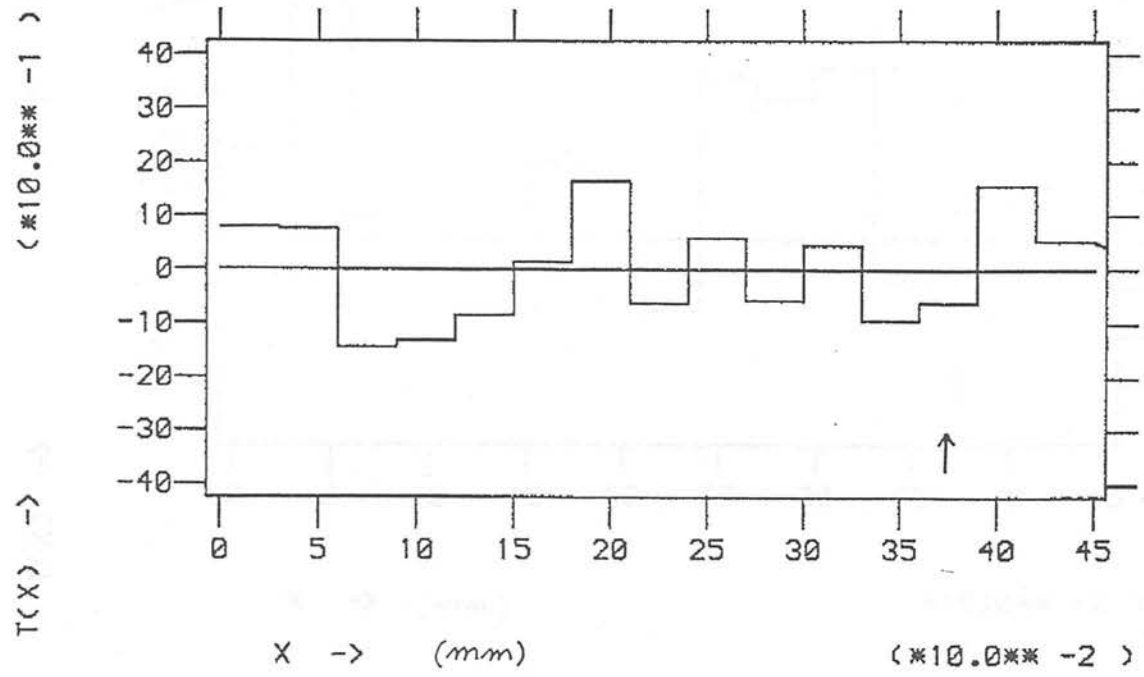

Figure 3.20 Plot of T(x) for the SGP field. The arrow marks the maximum value of x to which D^2 (b = 0) is evaluated.

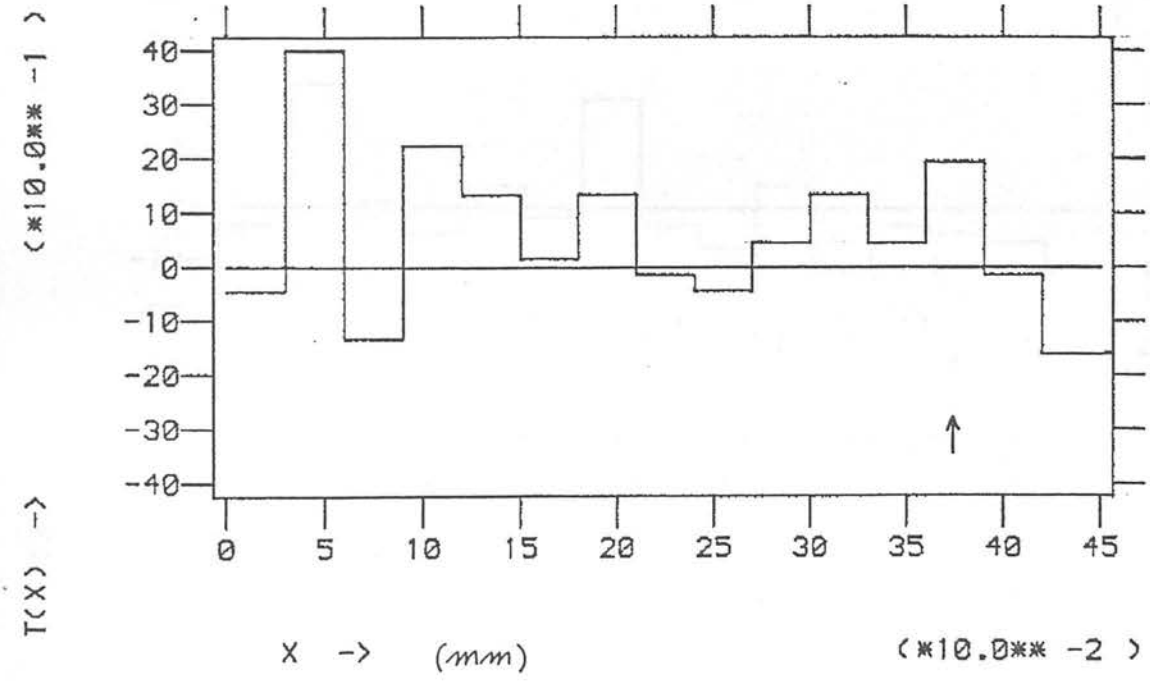

Figure 3.21 Plot of T(x) for the $11^h\ 40^m$ $+10^o$ field. The arrow marks the maximum value of x to which D^2 (b = 0) is evaluated.

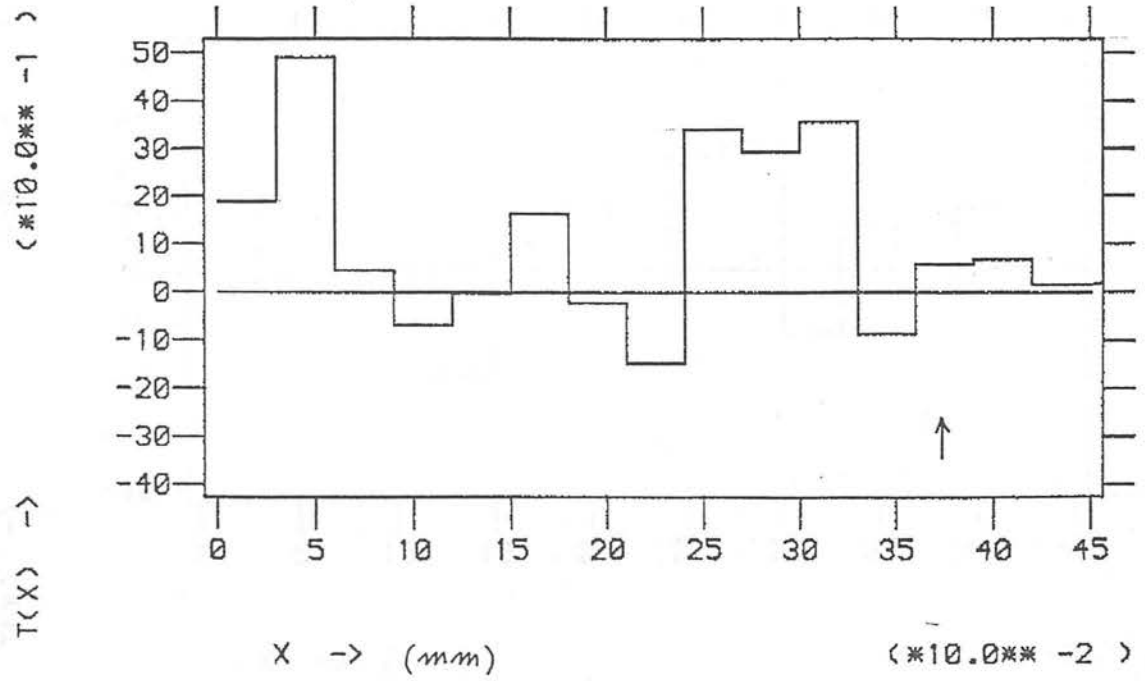

Figure 3.22 Plot of T(x) for the $15^h\ 52^m$ $+48^\circ$ field. The arrow marks the maximum value of x to which $D^2(b = 0)$ is evaluated.

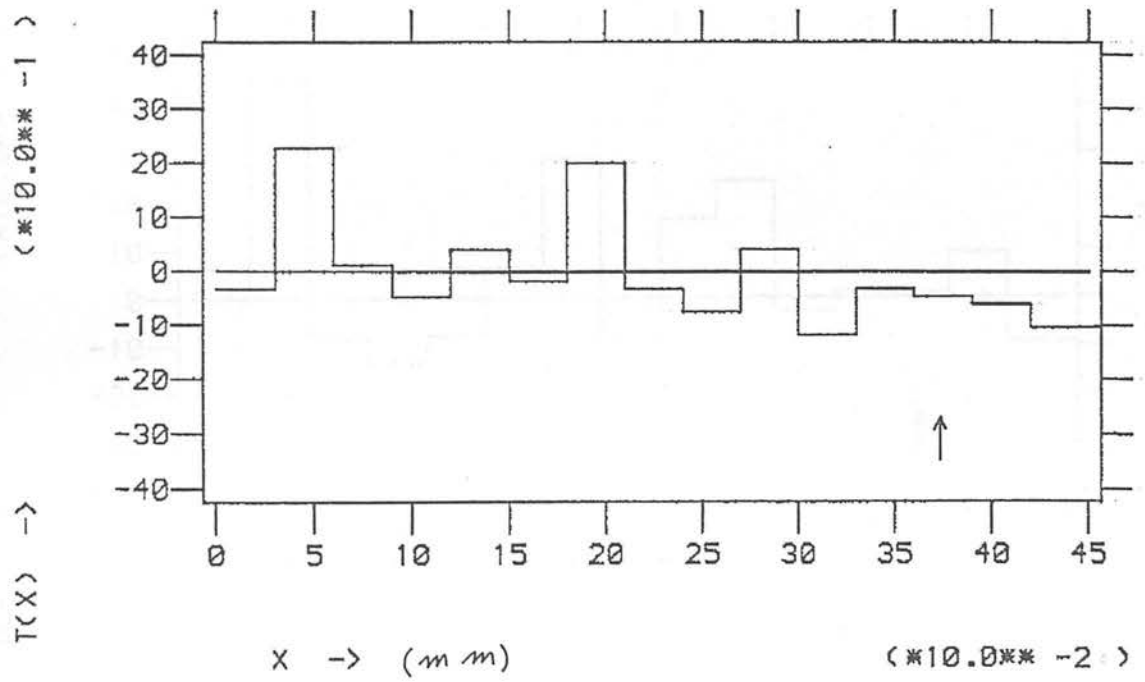

Figure 3.23 Plot of T(x) for the $01^h\ 12^m$ -35° field. The arrow marks the maximum value of x to which $D^2(b = 0)$ is evaluated.

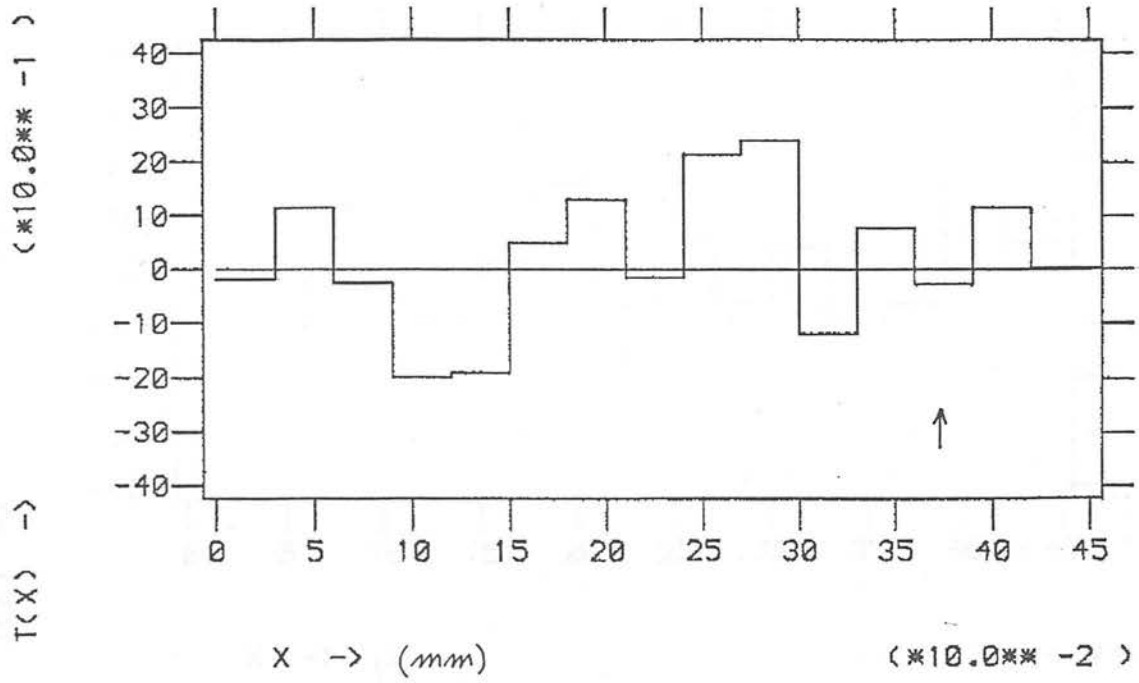

Figure 3.24 Plot of T(x) for the 01^{h} 44^{m} -40° field. The arrow marks the maximum value of x to which $D^{2}(b = 0)$ is evaluated.

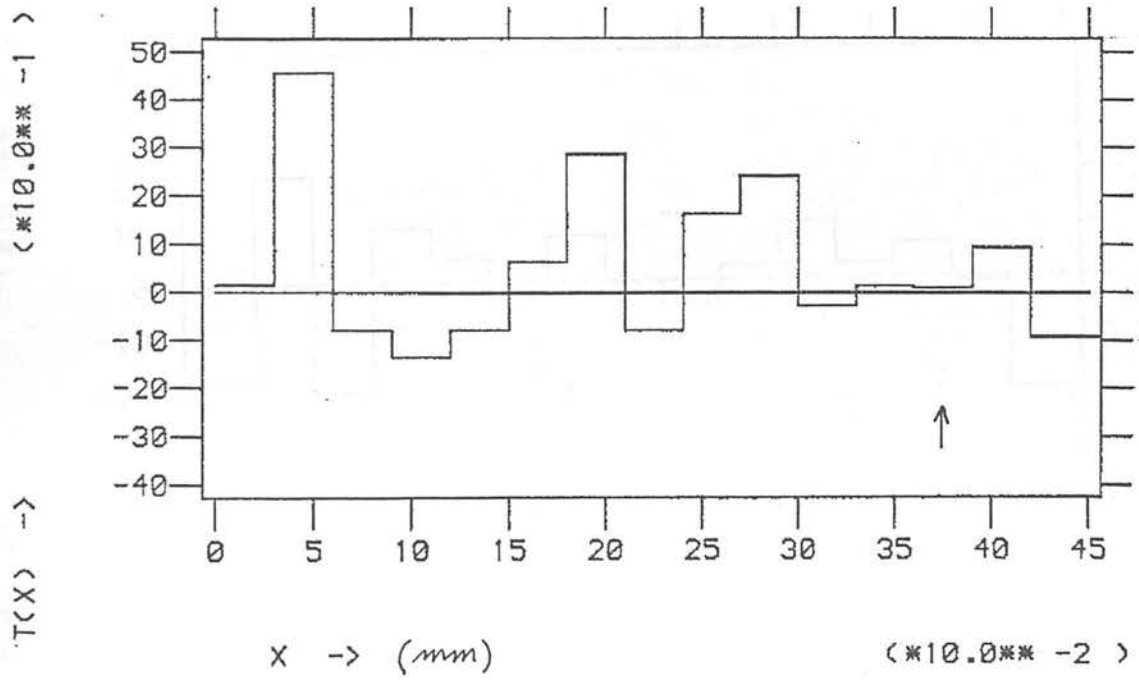

Figure 3.25 Plot of T(x) for the total of the five fields considered above. The arrow marks the maximum value of x to which $D^{2}(b = 0)$ is evaluated.

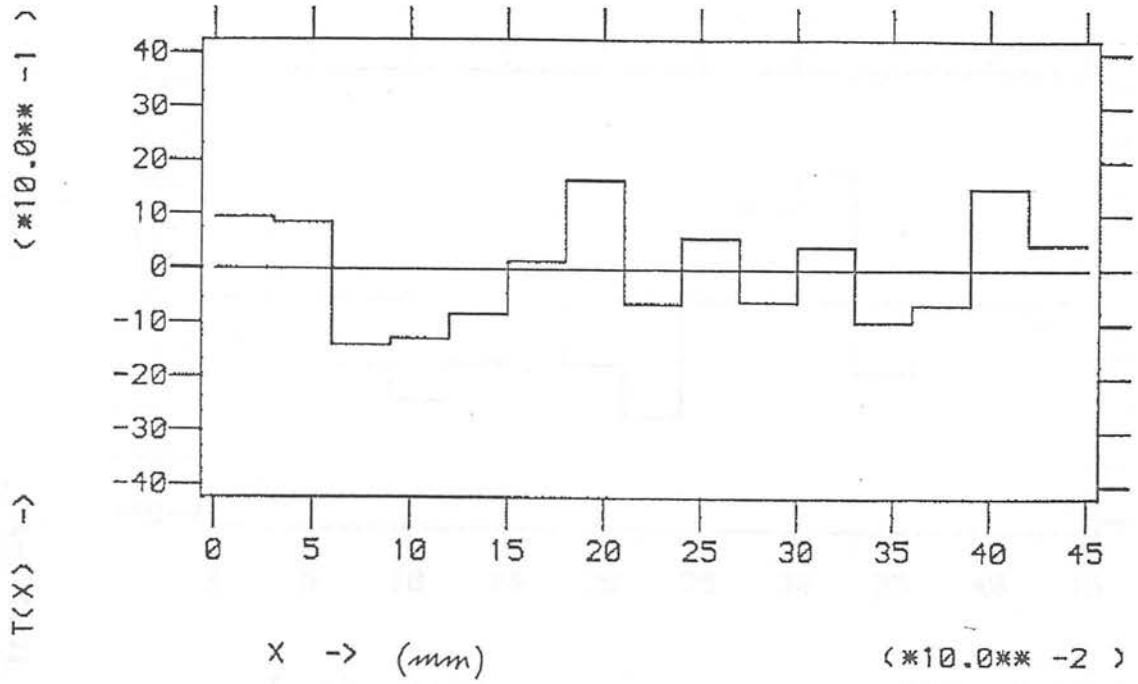

Figure 3.26 Plot of T(x) as in Figure 3.20 for the SGP field, except that now best fitting a and b values have been used to correct for clustering.

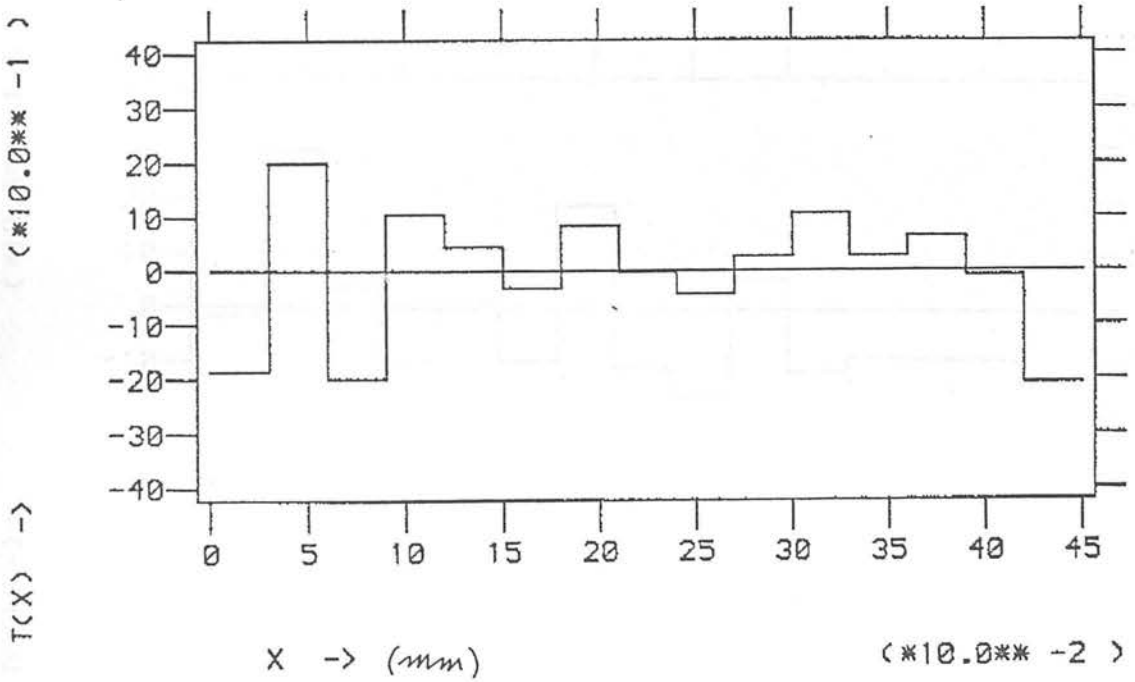

Figure 3.27 Plot of T(x) as in Figure 3.20 for the $11^h\ 40^m\ +10^\circ$ field, except that now best fitting a and b values have been used to correct for clustering.

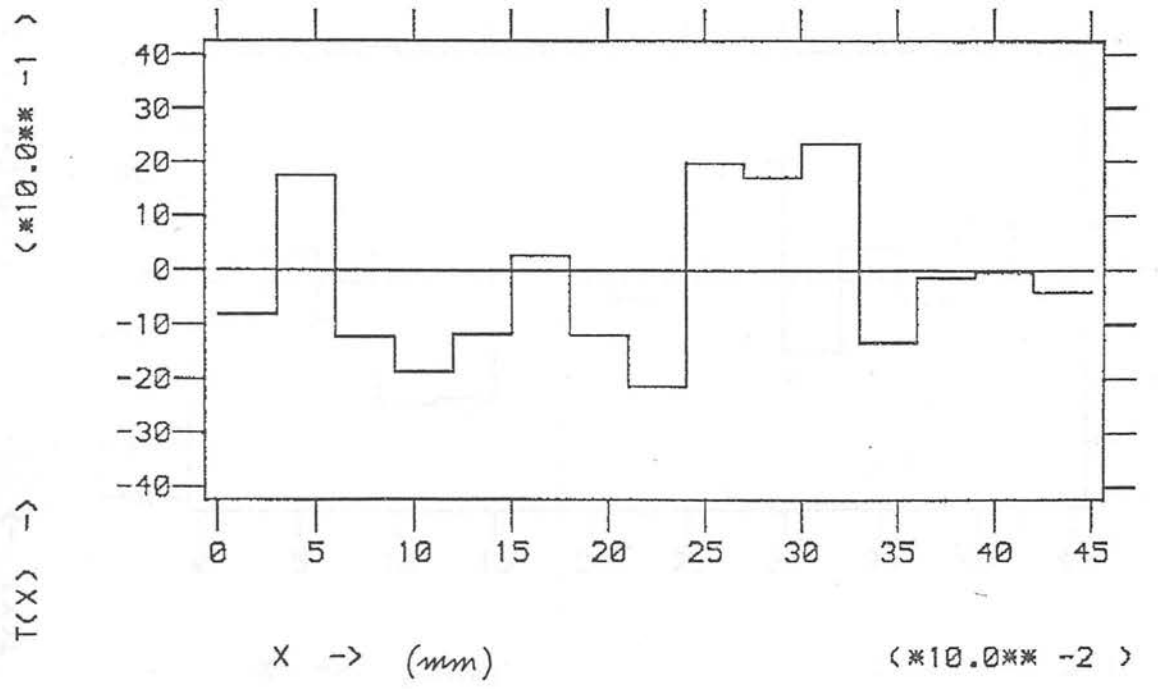

Figure 3.28 Plot of T(x) as in Figure 3.20 for the $15^h\ 52^m\ +48^\circ$ field, except that now best fitting a and b values have been used to correct for clustering.

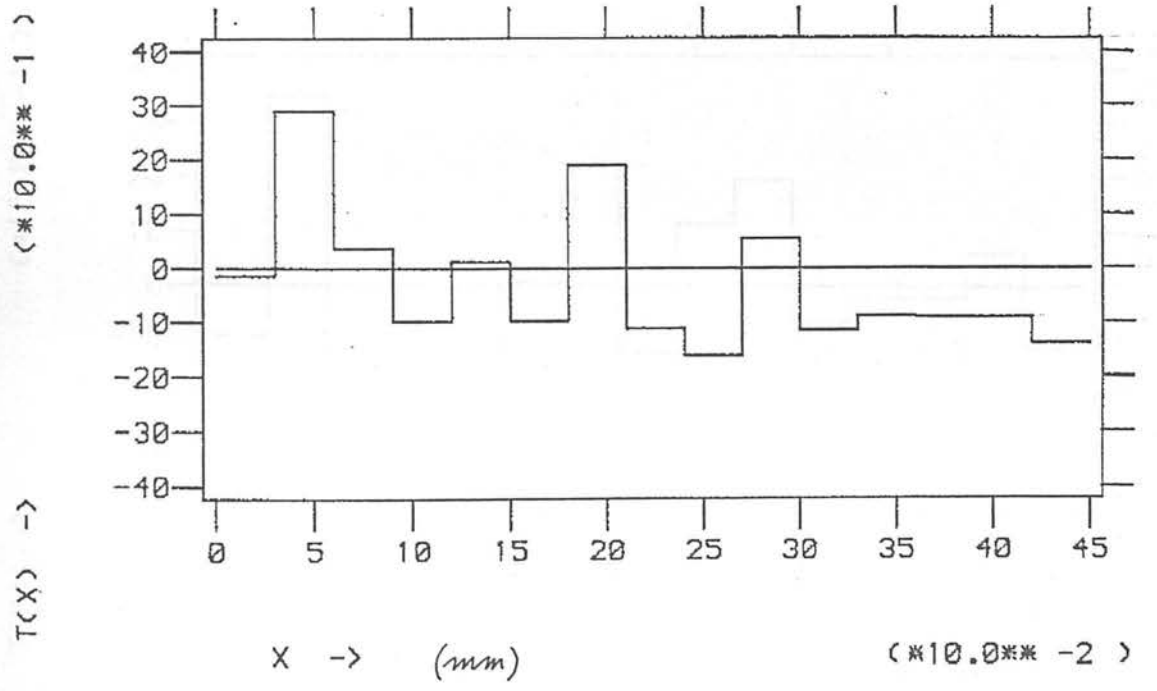

Figure 3.29 Plot of T(x) as in Figure 3.20 for the $01^h\ 12^m\ -35^\circ$ field, except that now best fitting a and b values have been used to correct for clustering.

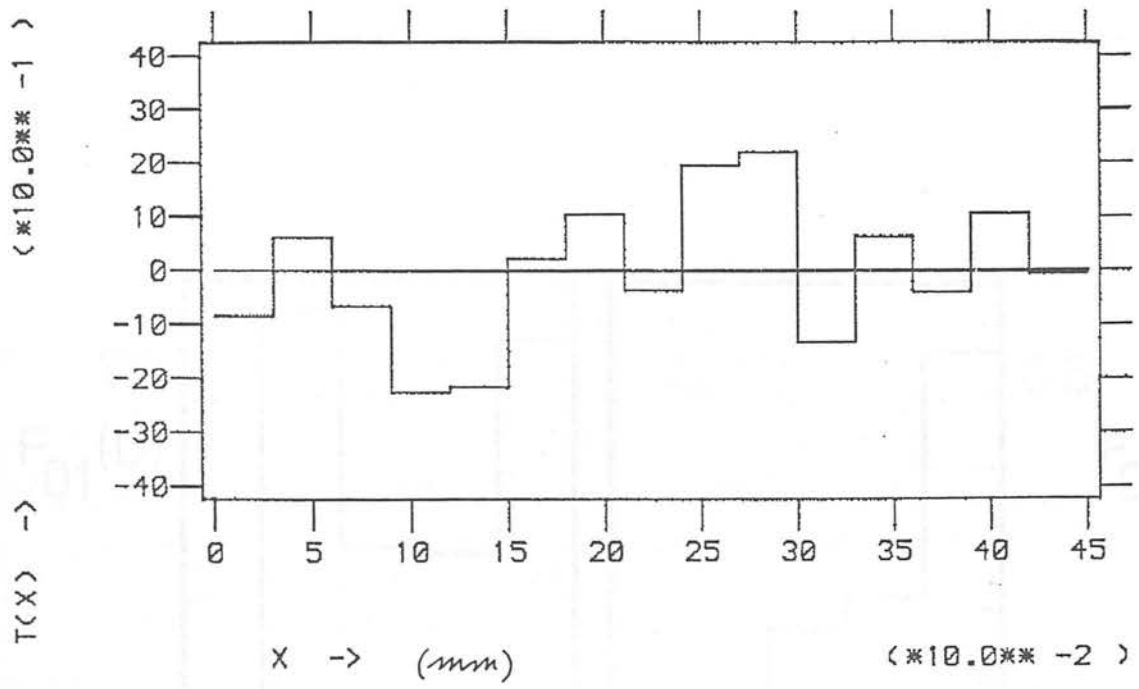

Figure 3.30 Plot of T(x) as in Figure 3.20 for the $01^{h}\ 44^{m}\ -40^{\circ}$ field, except that now best fitting a and b values have been used to correct for clustering.

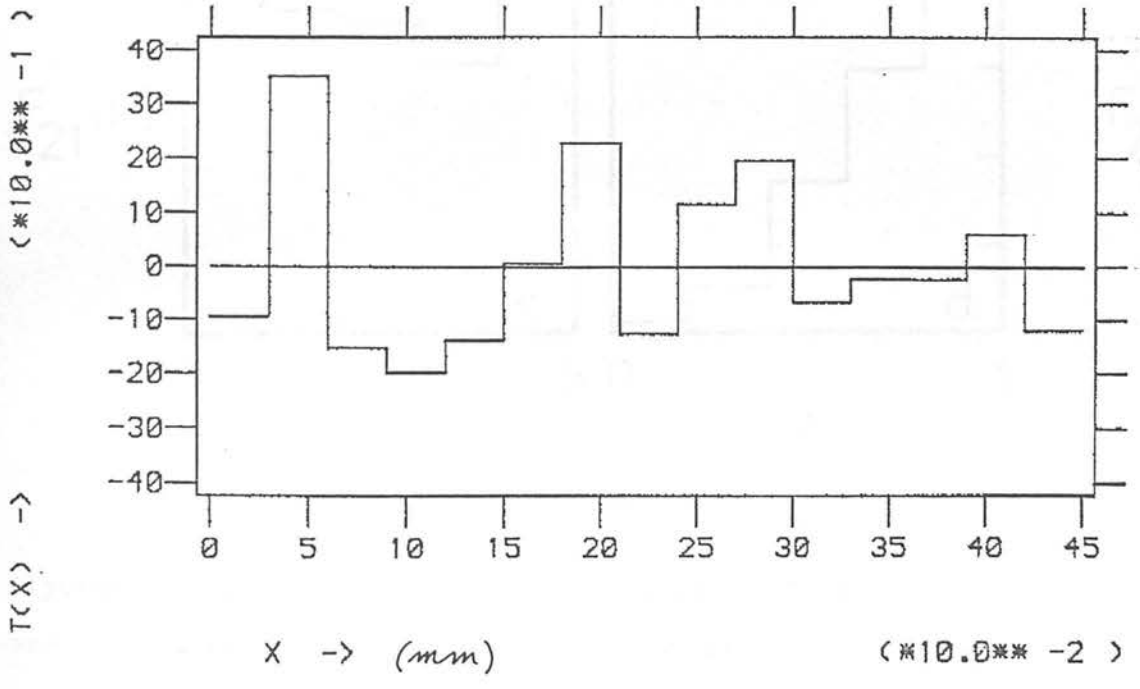

Figure 3.31 Plot of T(x) as in Figure 3.20 for the total of the five fields, except that now best fitting a and b values have been used to correct for clustering.

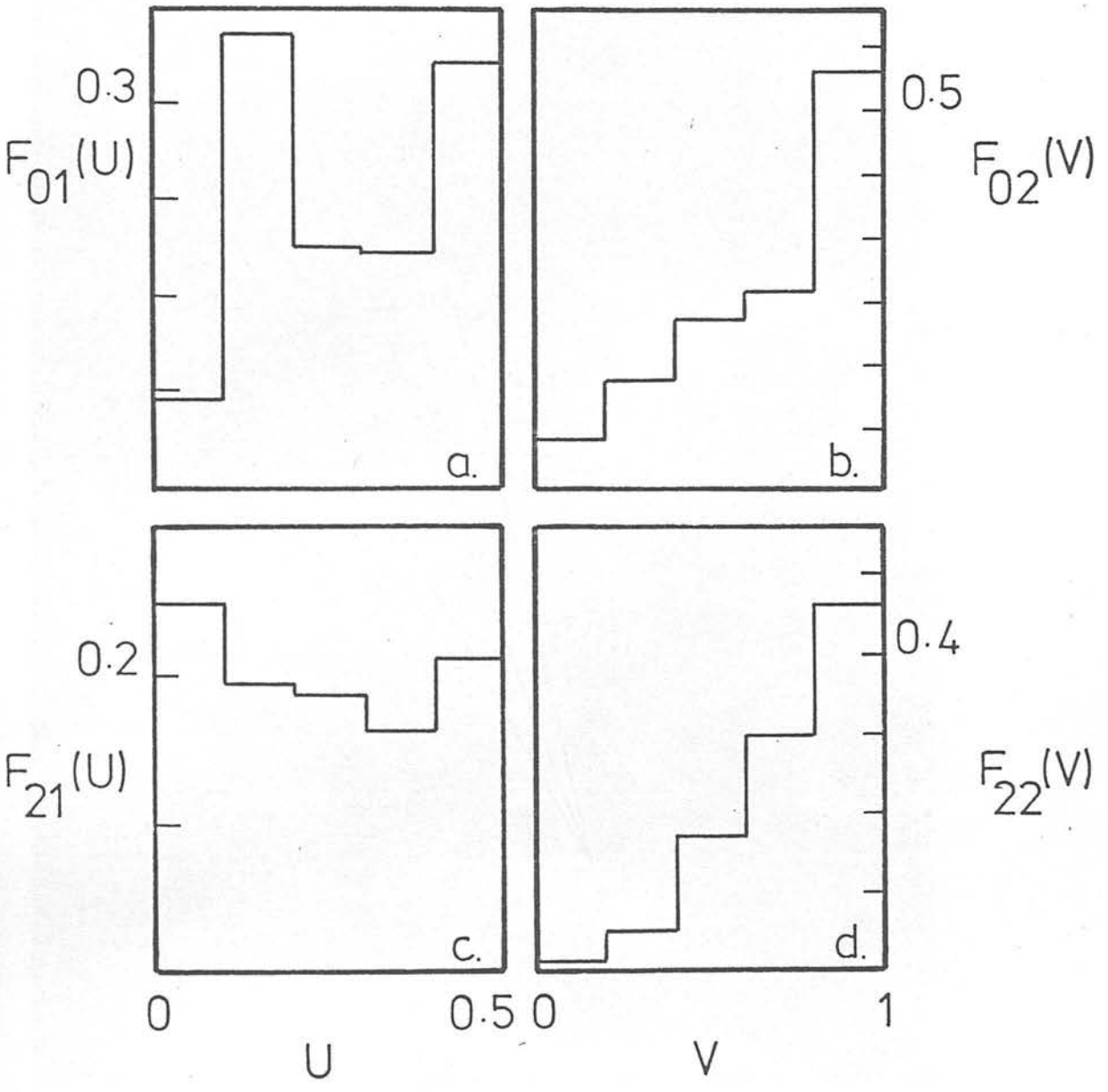

Figures 3.32a, c The frequency distributions of U for the excess and control alignments are shown (F01 and F21 respectively).

Figures 3.32b, d The frequency distributions of V for the excess and peak alignments.

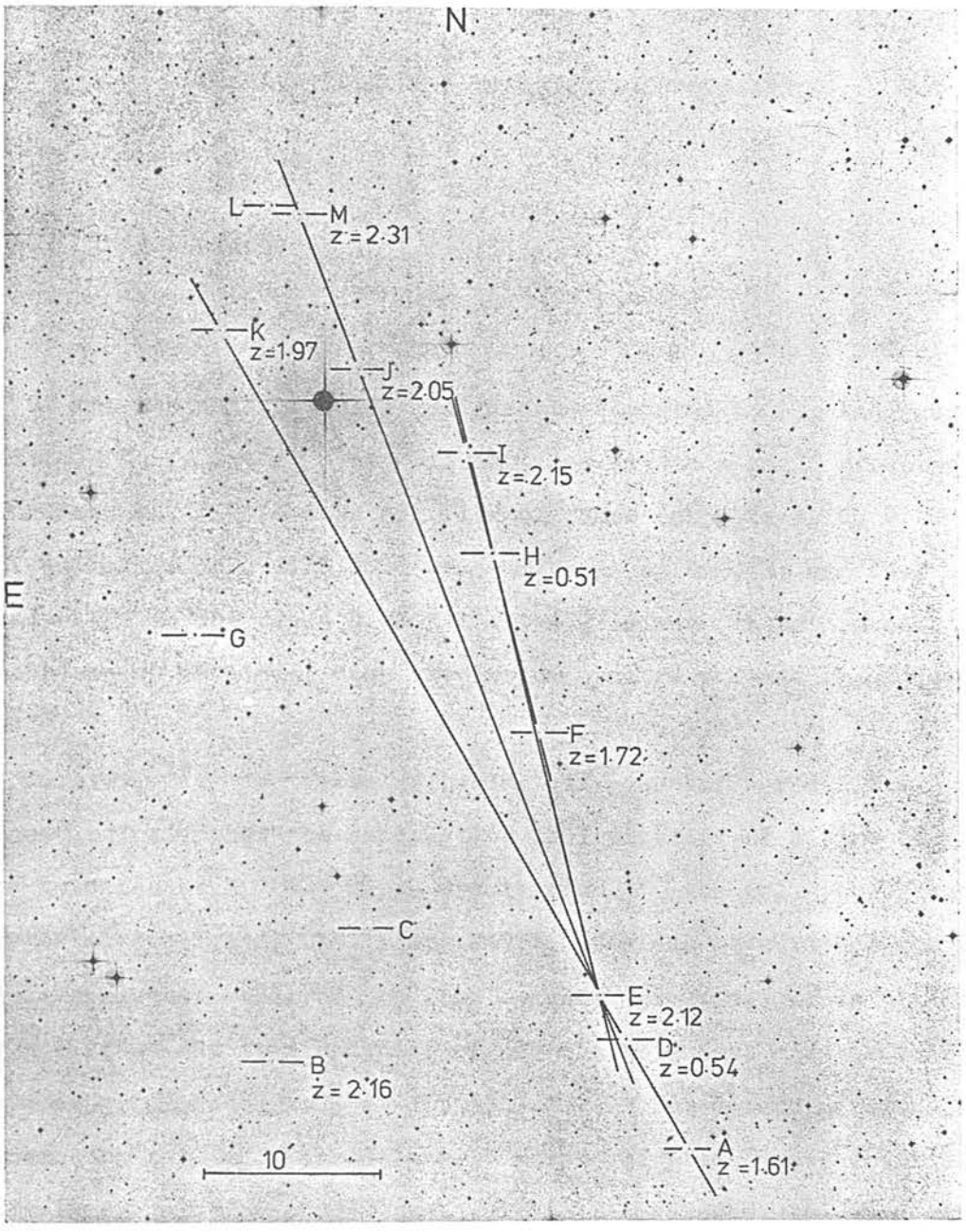

Figure 3.33 Photograph of a region of the $11^h\ 40^m +10^\circ$ field from plate J4288 surrounding the Arp and Hazard $11^h\ 30^m +106^\circ$ group. All probable quasar candidates are marked with redshifts when these are known. (Photograph courtesy of Photolabs, Royal Observatory Edinburgh)

CHAPTER IV

OBSERVATIONS OF A CLOSE PAIR OF QUASARS

4.1 INTRODUCTION

Of the two sets of quasar alignments reported by Arp and Hazard (1980) one, at $11^h\ 46^m +11^\circ\ 30'$ lies across a small grouping of quasars, cf. Figure 4.1. All five of these (objects B, C, D, E and G as marked) are within 10 arc - minutes on the sky and four have redshifts in the range $0.86 < Z < 1.10$. Given these facts, two reasons for obtaining high resolution spectra present themselves.

Firstly, it is very probable, if quasar redshifts are cosmological, that the association is indicative of a rich cluster of galaxies at $Z \sim 1$. Close examination of the only photographic material available, UKST plate J4288, provides no evidence for any galaxy cluster centred on the quasar grouping. This is not surprising, as at a redshift of one the brightest cluster members are expected to be at B (~ J(UKST)) ~ 24 - 26, depending upon the cosmoslogical and evolutionary models adopted (Bruzual 1981). A simple calculation shows that without reference to the close redshift agreement between four of the quasars (which is difficult to quantify) the probability that this association should arise by chance is ~ 0.05% (assuming a density of ten quasars per square degree). Even allowing for the total area of sky surveyed for quasars, optimistically estimated to be 500 square degrees, this still makes the grouping unlikely as the result of a random quasar

distribution in space.

If true, then observations of these objects might be expected to show correlations in their absorption line spectra indicative of common gas clouds along the line of sight, perhaps located within the cluster itself. This would then provide the first direct evidence that high redshift absorption lines arise in regions physically distinct from the quasar.

The second reason for observing these objects is that the quasar grouping contains three objects which belong to two of the peak alignments found in Chapter III, and are thus prime candidates for having significant non - cosmological redshifts. If the majority of absorption lines are produced in intervening galactic haloes then such objects would have very different absorption line distributions from the norm. Because of the small number of objects observed a null result, in which the distribution of expulsion velocities was normal, would not necessarily have a significant effect upon theories of non - cosmological redshifts. However, one might plausibly argue for a constancy in quasar absorption line properties (cf. Chapter V) and thus extend any conclusions to the quasar population as a whole. On the other hand, the discovery of an abnormal line distribution would be most embarassing for the conventional model.

Three of the five quasars are rather faint for high resolution spectroscopy, the remaining two, however, are of suitable brightness, mv ~ 18.0 and are separated by only 160 arc - seconds, corresponding to ~ 1 Mpc at a redshift of one (Ho = 100 km/s/Mpc, qo = 0). These two objects are B and G in Figure 4.1

The observations were made on the Anglo - Australian Telescope as the result of an award of three half nights of dark time by the Panel for the Allocation of Telescope Time (PATT) and were made

with the guidance of Dr. R. F. Carswell.

4.2 THE INTEGRATION TIME

A necessary preliminary to making observations is to estimate the required integration time. In the case of the detection, at a predetermined significance level, of narrow, deep absorption lines this is relatively easy. The narrowness of the lines means that the object continuum, sky and detector backgrounds remain constant across the line, so simplifying the calculation. Define the following parameters -

A = the projected pixel area on the sky (sq. arc - seconds).
l = number of line increments under image.
d = the line width or resolution element, whichever is larger (channels).
C = observed rate of object photons in the continuum (per A per s).
e(i) = observed rate of object photons in the "i"th channel in the line (per channel per s).
s = sky background rate (per sq. arc - second per A per s).
B = detector background (per channel per s).
W = Equivalent Width to be detected (A).
r = desired number of Standard Deviations of detection.
n = Number of A/channel.
T = necessary integration time (s).

by the definition of Equivalent Width -

$$W = n \sum_i \frac{(CT - Te(i)/n)}{CT} \qquad 4.1$$

where the summation is applied across the line. In which case -

$$\sum_i e(i) = Cn(d - W/n) \qquad 4.2$$

So, if it is required to detect the line at a level of r standard deviations and it is assumed that the counting statistics are Poissonian then -

$$nT\sum_i (C - e(i)/n) > r\sigma \qquad 4.3$$

where -

$$\sigma^2 = T\{\sum_i e(i) + 21d(snA + B)\} \qquad 4.4$$

thus substituting from Equations 4.2 and 4.4 into Equation 4.3 we get -

$$T > \frac{r^2}{C^2W^2}(C(nd - W) + 2d(Asn + B)) \qquad 4.5$$

from Equation 4.5 it is clear that the optimum conditions for detection are when the instrumental resolution matches the line width. Once the line becomes resolved then the integration time increases linearly with the dispersion.

In the above discussion the emphasis has been upon the fluxes which reach the detector, because it is these which determine the signal/ noise ratio. Unfortunately, in general the detected fluxes will not be simply related to the object magnitude but will depend upon seeing and light loss within the instrument. In the most straightforward case of a cylindrical profile, diameter D, for the stellar energy distribution within the seeing disc, the detected object photon rate C is related to the magnitude, m, by -

$$C = \{1 - (A - \sin(A))/\pi\}10^{\frac{m_e - m}{2.5}} \qquad 4.6$$

where -

$$\cos(A/2) = S/D \qquad 4.7$$

and where S is the slit width in arc - seconds and me the magnitude at which the detector registers 1 count per s per A.

Calculation may now be made of the required integration time for given observing conditions. It is recommended that this time be calculated for at least the 5σ detection of the lines in order to allow for uncertainties in determining the continuum level.

The above analysis has been independently derived and checked observationally by Dr. R. F. Carswell (1982).

4.3 THE OBSERVATIONS AND PRELIMINARY REDUCTIONS

The Anglo - Australian Telescope (AAT) is situated on Mount Woorut, near Coonabarabran in New South Wales, Australia at a height of 3819 feet above mean sea level. This site is shared by a number of smaller instruments, including the UK Schmidt Telescope.

The main mirror of the AAT is hyperboloidal in shape and 154" (~ 3.9m) in diameter and has a focal length of 41.5 feet (12.7m) giving an f ratio at the prime focus of ~ 3.3. Several secondary mirrors are available, the largest of which gives a Cassegrain focal ratio of f/8, the others provide f/15 Cassegrain and f/36

Coude foci.

The RGO spectrograph, for which two cameras are available, one an 25cm focal length Cassegrain - Maksutov system, the other a 82cm focal length f/5.5 spherical mirror. This is mounted at the f/8 focus (plate - scale = 6.7 arc - seconds/ mm) and is normally used with the Image Photon Counting System (IPCS) (Boksenberg 1972; Boksenberg and Burgess 1973). Only the former camera was used for these observations. The spectrograph slit has a maximum length of ~ 250 arc - seconds, though portions may be isolated by the use of Dekker apertures. Its width is continually variable from 0.07 to 16.75 arc - seconds and the entire slit assembly may be rotated in position angle.

Data to enable subsequent wavelength calibration ("scrunching") of the spectra may be obtained from observations of a Copper - Argon arc lamp, the light from which can be deflected into the optical path. Neutral density and colour filters, which may also be inserted, are sometimes necessary to limit the intensity of this beam. It is also possible to remove point to point spatial variations in the detector sensitivity by observation of a tungsten lamp located on the same turret as the comparison arc. However, as the lamp is observed through the RGO spectrograph any large scale variations will not be correctly removed because of the different colour temperatures of the tungsten filament and night sky which produce different intensity distributions in the Y (dispersion) direction. In order to correct for any such sensitivity changes white dwarf stars, for which the absolute spectral fluxes are known, must be observed. These may then be used to calibrate the wavelength response of the detector.

The IPCS can detect, locate and count individual photons up to a maximum rate of ~ 1 event per pixel per second. The system in its newer, two dimensional mode provides an array of 2048 x 250

pixels, though not all of these need be used. Indeed, edge effects limit the usable size to ~ 2044 x 235 for celestial objects and (because of vignetting in the internal mirror used to deflect the light of the reference beam into the optical path) to ~ 2044 x 220 for calibration arcs etc.

The spectral response of the S20 cathode used in the IPCS detector peaks at ~ 4100A. The overall sensitivity quoted in the IPCS manual of 1 count per second per A near 5500A for a star with V = 15 implies an overall quantum efficiency of the telescope and spectrograph system of ~ 1%. However, general experience with the data discussed later and also from other observers (eg. Carswell 1982) indicates that this number is probably an overestimate by about a factor of two.

A certain amount of simple reduction, such as sky subtraction, may be carried out as the data are acquired. The result can be displayed giving the observer a real time picture of the progress of the observations. The raw data are written to tape at the end of each integration ready for proper analysis later.

Further details of the AAT and instruments may be found in a variety of AAO reference manuals.

The observations were made on the nights of 28 - 29 and 29 - 30 January, 1982 with Dr. P. W. J. L. Brand using the 25 cm camera and grating 1200V in first order. This gives a nominal reciprocal linear dispersion of 33A/mm. The grating was used blaze to collimator as in this configuration a considerably better ratio of actual to projected slit width is obtained. This means an increased observable object flux as the slit can be opened more widely while still matching the instrumental resolution.

Each channel was 15 microns wide, which corresponded to 0.5A and with a projected slit width of approximately three channels gave a resultant spectral resolution of 1.5A. The IPCS was used in the two dimensional mode, each line increment was 2.25 arc - seconds across (X gain low). The camera format used was 2044 x 130 pixels, giving an extent of 300 arc - seconds along the slit.

The journal of observations is shown in Table 4.1. The proximity of the two objects enabled both to be observed simultaneously through Dekker 50 (clear aperture), for which the necessary slit Position Angle was 241 degrees.

Exposures, typically of 100s duration, were made of the Cu - Ar arc every 25 minutes during the night through neutral density filters (with ND = 1.3) so that any pixel shifts (cf. AAO Newsletter No. 13) may be subsequently allowed for. Because of instrumental problems with the IPCS control computers it was not possible to bracket the observations with flat field exposures and only one was taken at the end of each night, these were of 10,000s exposure.

Each spectral frame was reduced separately using the Edinburgh Spectral Reduction package (ESP) on the Royal Observatory, Edinburgh node of the Starlink network of Vax 11/780 computers. The first step in the reduction is to remove the small scale sensitivity variations in the detector. This was done by finding such fluctuations in the flat field and correcting for these in the data.

Because of S distortion in the IPCS, the amount of which is dependent upon position on the camera cathode, it is not possible using the long slit mode to straighten all the spectra at the time of observation. Consequently, a routine was written and incorporated within the ESP programme to correct for these

distortions. For each object an area around the spectrum was extracted from the data, this was typically 10 to 15 increments wide and 2040 channels long. The data were compressed in the dispersion direction into 20 segments of length 102 channels. For each of these segments the mean and standard deviation of the counts in the line increments were determined and that increment containing the maximum flux located. If this peak contained sufficient counts that it exceeded the mean by three standard deviations then this was taken to be the centre of the spectrum in that segment.

A series of points defining the overall shape of the spectrum were thus determined and fitted with a third order polynomial. Interpolation using this function enabled calculation of the necessary shift at the position of each channel in order to straighten the spectrum. In practice, it is not possible to reduce the number of line increments containing object flux beyond three, as the size of the seeing disc distributes the light over at least two increments.

Removal of the sky background was achieved by subtracting the same number of line increments of sky from those deemed to contain the object (plus sky). The sky data were chosen from close to the quasar spectra in order that problems with residual S distortion should be kept to a minimum.

The wavelength scale was determined by a mean of arcs taken before and after each exposure. Because the above method for removing S distortion relies upon having a spectrum which covers only a small number of line increments it is not suitable for correcting the arc spectra. Consequently, in order to prevent the introduction of wavelength shifts the calibration arcs were taken from the same line increments which contained the object. Any S distortion should, therefore, only broaden the lines rather than

shift them systematically with respect to the object.

The mean rms. error in calibrating the wavelength scale was only 0.2 of a bin or about 0.1A. This was accomplished by fitting, using a least squares method, a fifth order polynomial. All measured wavelengths are as in vacuo and have been corrected to heliocentric values.

Finally, the wavelength response of the detector was removed by the empirical determination of this function from observations of the white dwarf star L970-30 and then applying the appropriate correction. The reduced data from the individual frames were then added together, the resulting totals are shown in Figures 4.2a - d.

4.4 THE EMISSION LINES

Examination of Figures 4.2a - d shows that in 1146+11B there is only one emission line visible. In the other, 1146+11G, there are two obvious emissions. Before the Equivalent Width and wavelength of these can be found it is necessary to estimate the level of the underlying continuum. In quasars the wide extent of the lines means that small errors in this can have relatively large effects upon the determined line position and strength. Some idea of the size of this problem may be gained by repeated attempts to set the continuum level and to observe the effect upon the derived parameters.

The procedure used to determine the continuum level was to select regions on either side of the line which were believed, from visual inspection, to be free from strong features. The average flux and central wavelength in these regions were

calculated and a straight line interpolated between these points. This fitted line was taken to be the true continuum level allowing estimation of both the Equivalent Width and centroid of the emission feature.

The emission line Equivalent Widths were simply determined by integrating the number of counts above and below the continuum. The ratio of these gives the Equivalent Width. As noted above, uncertainties in setting the continuum level will affect the determination of the Equivalent Width. Repeated attempts at continuum estimation showed that the rms. error in the observed Equivalent Width was $\pm$ 5A.

The centroid of the emission line was determined in two ways. Firstly, by finding the centre of gravity of the line (cf. Equation 4.12). Clearly, this method gives more weight to the central portions of the line, which contain more flux, and relatively little to any wings. The second approach does the opposite, in that it is those portions far from the peak which are given most weight. It was initially developed by Schneider and Young (1980) and it involves the convolution of the line profile with a gaussian of width similar to that of the line. This gaussian has been split in the centre and one half has been reflected about zero giving no weight to the line peak and most to the edges. The central wavelengths determined in this way are given in Table 4.2, though these agree to within the formal errors to those found by the former method. This obviously indicates that all the emission lines in the two quasars have symmetric profiles.

In 1146+11G the identification of the emission lines is clear, the ratio of wavelengths being indicative of SiIV + OVI and CIV. The redshifts of the individual lines (2.121 and 2.118 respectively) differ by only 300 km/s, or 5A at the position of the CIV emission. This is only about 20% of the line width, and

while it is slightly outside the formal error for the position of the line centroid such differences are common in quasars and are perhaps caused by differences in line profiles or variations in the central wavelength due to different contributions of blended lines.

If this redshift is correct then the CIII] line should be at a wavelenght of 5960A. Examination of Figure 4.2c shows that no strong feature is visible at this wavelength. This line is common in high redshift quasars and a low resolution spectrum by Arp and Hazard (1980) is claimed by the authors to have a weak feature at the correct wavelngth. While there are small undulations in the continuum in this region, none are convincing emission lines. It should be remembered that S distortion is severe in this region and small errors may exist in the continuum level.

For the other object, 1146+11B, the situation is not quite so clear if one must rely upon these data alone. The single emission line could be either MgII (in which case CIII] would be just off the end of the spectrum) or it could be Lyα. The absence of an obvious Lyα forest, seen in virtually all high redshift quasars, argues for the former identification. This is borne out by the lower resolution observations of Arp and Hazard (loc cit.) in which the redshift is secured by a number of lines. The redshift has thus been taken to be 1.107.

4.5 THE ABSORPTION LINES

Upon completion of the data reduction the observer is left with a wavelength calibrated, sky subtracted and flat fielded spectrum. If there are no features in these data then they should have a poisson distribution about the mean, though because of the sky and

detector backgrounds the noise is higher than that expected simply on the basis of the observed counts. In the presence of spectral lines the fluctuations about the continuum are also raised above that expected from the statistics. It is these features which, as absorption lines, it is hoped to detect.

The method described hereafter is similar to that used by Young et al. (1979).

4.5.1 Continuum Fitting

The continuum has been determined by the following procedure. Suppose that the final object spectrum consists of a series of counts, where N(i) is the number in the "i"th channel. These data have been divided into 51 segments of 40 channels width and within each the mean level has been determined by calculating -

$$U = \frac{\sum_{i}^{N_b} N(i)}{Nb} \qquad 4.8$$

and the actual variance by -

$$S = \frac{\sum_{i}^{N_b-1} (N(i) - U)^2}{Nb - 1} \qquad 4.9$$

where Nb is the number of channels contributing to the segment. If the data did not contain any features then the fluctuations about the mean should have a poisson distribution, with variance, S(t) -

$$S(t) = \frac{\sum_{i}^{N_b} S(N(i))}{Nb} \qquad 4.10$$

where -

$$S(N(i)) = \left\{\frac{1 + f(i)}{1 - f(i)}\right\} N(i) \qquad 4.11$$

and where f(i) is the ratio of the sky and detector backgrounds to the object counts in the "i"th channel. Deep absorption lines or noise spikes, however, will increase the fluctuations about the mean and raise S above S(t). In that event the channels within the segment were searched for the one which deviated most from the mean. This point was rejected and U, S and S(t) were redetermined with Nb reduced by one.

If the observed variance still exceeded that expected, then the next most deviant point was rejected and the process repeated, stopping when $S < S(t)$. If the number of points removed exceeded twenty then that segment was ignored. The continuum level at the average wavelength of the channels was deemed to be the mean count level (U) of the remaining channels.

The set of wavelength/ continuum level points from all the acceptable segments were interpolated using cubic splines to give the continuum level, C(i), at each channel. Interior knots were placed at each point, except for the second from either end. This is necessary in order to obtain a unique fit (eg. Schoenberg and Whitney 1953). As extrapolation with spline functions is not possible the first and last twenty channels have not had the continuum level determined. Consequently, no search for lines has been made in these regions.

Experiments with artificial spectra showed that this technique fitted the continuum to within 5%, even in the presence of many strong and narrow lines. In the real data, however, it is possible that the continuum may be depressed by many weak absorption lines or be perturbed by non - statistical fluctuations. It is unlikely in the observations described here that the former of these

problems is severe as the line densities longward of Lyα emission observed in most quasars are low.

4.5.2 Detection of Absorption Lines

Any objective technique for the detection of absorption lines must be constructed in such a way so as to select all those lines with strengths greater than some lower limit and with minimal contamination from noise. The following procedure has been adopted which applies a lower limit to the Equivalent Width, though in the case of variations in the signal/ noise across the spectrum this minimum will not be constant, but rise as the data become more noisy.

By definition, the centroid of the line is given by -

$$L = \frac{\sum_i 1(i)\ (C(i) - N(i))}{\sum_i (C(i) - N(i))} \qquad 4.12$$

where the summations are made across the M channels which form the line and 1(i) are the wavelengths of each channel. Also by definition the Equivalent Width of an absorption line is -

$$W = A \sum_i (1 - N(i)/C(i)) \qquad 4.13$$

where A is the number of Angstroms per channel. The summation is again performed across the line width. By similar considerations to those used to obtain Equation 4.4 the variance of the Equivalent Width may be shown to be -

$$S(W) = \frac{M(1 + 2f) - W}{C} \qquad 4.14$$

if the counting statistics are Poissonian. Here f and C are the mean fractional sky contribution and mean continuum flux at the line respectively. Clearly, to minimize S(W) the value of M should be kept as small as possible, ie. to the full width of the line at zero intensity.

The variance in wavelength of any detected lines may be determined by partially differentiating Equation 4.14 with respect to N(i). This gives -

$$Nc\ W\ S(L) = (1(i) - \langle 1 \rangle)\ S(N(i)) \qquad 4.15$$

After rearrangement and substitution from Equation 4.13 we have for lines with a gaussian profile -

$$S(L) \sim \frac{S(W)}{W^2} \frac{M^2}{12} \qquad 4.16$$

Once the continuum level has been found, as above, the detection of lines was accomplished by the following technique. A box with a width of M channels was stepped along the data by increments of one channel at a time. At each position of this box the central wavelength, Equivalent Width and respective variances were calculated in those channels. If the Equivalent Width of the possible line was greater than four standard deviations of W then it was accepted as a true feature.

Such a method may detect strong features more than once at different relative positions of the selection window and line. In these cases the multiplicity was removed by determining the mean wavelength of all those lines separated by less than M channels, the contribution of each being weighted by its Equivalent Width. This mean wavelength was then adopted as the true wavelength of the line, the Equivalent Width of which was taken to be the maximum Equivalent Width of any component.

For the RGO spectrograph and IPCS combination the maximum resolution is 2.6 - 2.8 channels (IPCS Manual). This is approximately the full width at half intensity of any unresolved features and so for a gaussian resolution profile the full width when the intensity has dropped to 1% of the peak value is about 2.5 times this number, or 7 channels. Consequently, M was somewhat arbitrarily set to seven, a choice which was confirmed by close examination of the line profiles.

The lines detected by the above method are listed in Table 4.3 and are marked on the spectra in Figures 4.2a - d. This Table is laid out as follows: the observed (in vacuo) wavelengths and Equivalent Widths of the lines are listed in columns 1 and 2 respectively, while 3 and 4 contain their standard deviations. The remaining coulumns are defined in Section 4.5.3.

4.5.3 Indentification of the Absorption Lines

The method used to identify the absorption lines is essentially that of Bahcall (1968). A set of standard lines commonly observed in quasar absorption systems were compared with the observed lines. Using these it was possible to form a matrix of redshifts in which each observed line is compared with every one in the standard package. Any absorption systems will then be seen as a peak in the redshift distribution. This histogram, therefore, may be expected to show the redshifts of the systems.

The standard line set was taken from the list of Aaronson et al. (1975), though only the stronger transitions with wavelengths > 1000A were included. While some selection techniques (eg. Aaronson et al. loc cit.) impose extra conditions based upon the relative strengths of the lines and ionizational considerations these have

not been applied here because of the relatively low signal/ noise and paucity of the data. The wavelengths of the standard lines give a range of redshifts from 0.4 to 4.9, though in practice the upper redshift limit was set to be only somewhat greater than the emission redshift. The lines are listed in Table 4.4 and the resultant redshift histogram for 1146+11G is shown in Figure 4.3. The corresponding distribution for 1146+11B is similar to Figure 4.3, though features are less obvious because of the smaller number of lines and the resultant rise in the signal/ noise.

Not all peaks in such diagrams need represent true absorption systems, especially when the number of lines is small. Spurious features may be produced by the repeated identification of a single line with both members of a close doublet, eg. CIV. In order to determine which peaks are real the proposed identifications within each were checked. Any spurious systems can thus be removed, the remaining true ones have been used to identify the lines listed in Table 4.3 and are marked on the redshift histogram in Figure 4.3. In this Table columns 5 and 6 give the name and rest wavelength of ion identified with the absorption, while in 7 the resultant redshift is tabulated.

As may be seen from Table 4.3 only 50% of the absorption lines have been identified in the two objects. This is a common occurence in quasar spectra, the remaining lines being postulated to be the strongest members in otherwise weak systems.

In 1148+11G there are two identified redshift systems -

Zabs = 2.1201. This system contains only two lines, a CIV doublet, and is located close to the emission line peak. The implied expulsion velocity is only ~ 100 km/s and as such is a member of the peak in the CIV redshift distribution discussed

by Weymann et al. (1979).

Zabs = 1.9556. This system contains three lines, a CIV doublet and the SiIV 1402A line. The ejection velocity for this system is 16,200 km/s.

In 1146+11B there is only one identified redshift system, this low number of absorption lines is common amongst low redshift quasars -

Zabs = 0.6868 This system contains only two lines and while they are clearly a MgII doublet the implied ejection velocity, 66,000 km/s, is high but not unknown in other quasars.

4.6 CONCLUSIONS

In order to make a believable indentification of any absorption systems with a common source the redshift would have to be closer together than ~ 500 km/s, if the absorber is proposed to be a single galactic halo or group of galaxies. Unfortunately, no systems were found in both objects which satisfied this condition. However, half of the lines remain unidentified in each object and it is just as likely that these would appear as common to both. In this case the acceptance criterion has been altered such that any two lines should be closer together than 8A, which corresponds to a difference in wavelength/ wavelength of ~ 500 km/s.

Searching the spectra of the two objects for any such features shows that a line in 1146+11B at 4669.48A is matched by one in 1146+11G at 4676.33A. This wavelength shift is only 450 km/s, within the dispersion velocity of a small group of galaxies. The probability of this occuring by chance may be calculated by noting

that in the low redshift object there are two unidentified lines in 2,000A of spectrum, while in 1146+11G there are five. The probability of two lines being separated by $\pm$ 8A is thus 8%. This is, therefore, suggestive of an association but is, unfortunately, not conclusive.

Although the number of detected absorption systems is small, the distribution of redshifts is completely consistent with that found in studies of other objects (eg. Weymann et al. 1979). Therefore, in those objects in which there is the greatest probability of there being a significant non - cosmological redshift component, there is no evidence for an abnormal expulsion velocity distribution. This would have been expected if the absorptions had been produced outside the quasar and the magnitude of any peculiar redshift component been large.

TABLE 4.1

Journal of Observations

Object: 1146+11B

RA	Dec	Date	Wavelength Region	Time (s)
11 46 07.83	11 03 50.6	28-29 Jan 1982	5010-6120	6000
		29-30 Jan 1982	4020-5050	7000

Object: 1146+11G

RA	Dec	Date	Wavelength Region	Time (s)
11 46 17.12	11 05 06.9	28-29 Jan 1982	5010-6120	6000
		29-30 Jan 1982	4020-5050	7000

TABLE 4.2

Emission Lines

Object: 1146+11B

λ(vac)	ID		Z	EW (Observed)
5895	MgII	2798	1.107	33

Object: 1146+11G

λ(vac)	ID		Z	EW (Observed)
4376	SiIV	1397	2.121	45
	+ OVI	1402		
4829	CIV	1549	2.118	51

TABLE 4.3

Absorption Lines

Object: 1146+11B

Wavelength	W(A)	s(L)	s(W)	ID	λ(ID)	z(ID)
4669.484	0.62	0.19	0.14			
4716.803	0.56	0.19	0.13	MgII	2796.35	0.6868
4730.438	0.58	0.21	0.14	MgII	2803.53	0.6873
4758.608	0.56	0.21	0.14			

Object: 1146+11G

4146.764	0.51	0.21	0.11	SiIV	1402.77	1.9561
4231.633	1.12	0.18	0.11			
4553.867	0.39	0.17	0.11			
4575.810	0.44	0.10	0.10	CIV	1548.20	1.9556
4581.509	0.42	0.08	0.10	CIV	1550.77	1.9543
4676.326	0.51	0.07	0.10			
4830.512	0.72	0.09	0.10	CIV	1548.20	2.1202
4838.483	0.39	0.21	0.09	CIV	1550.77	2.1201
5245.548	0.89	0.21	0.18			
5864.956	0.89	0.17	0.17			

TABLE 4.4

Standard Ion Wavelengths

Ion	Wavelength	Ion	Wavelength
HI	1215.67	MgII	2803.53
	1025.72		2796.35
CI	1656.92	SiII	1260.42
CII	1334.53		1193.28
CIV	1550.77		1190.42
	1548.20	SiIII	1206.51
NV	1242.80	SiIV	1402.77
	1238.81		1393.76
OVI	1037.63	FeI	2523.61
	1031.95		2484.02
MgI	2852.97	FeII	2600.18
			2382.76
			2382.76

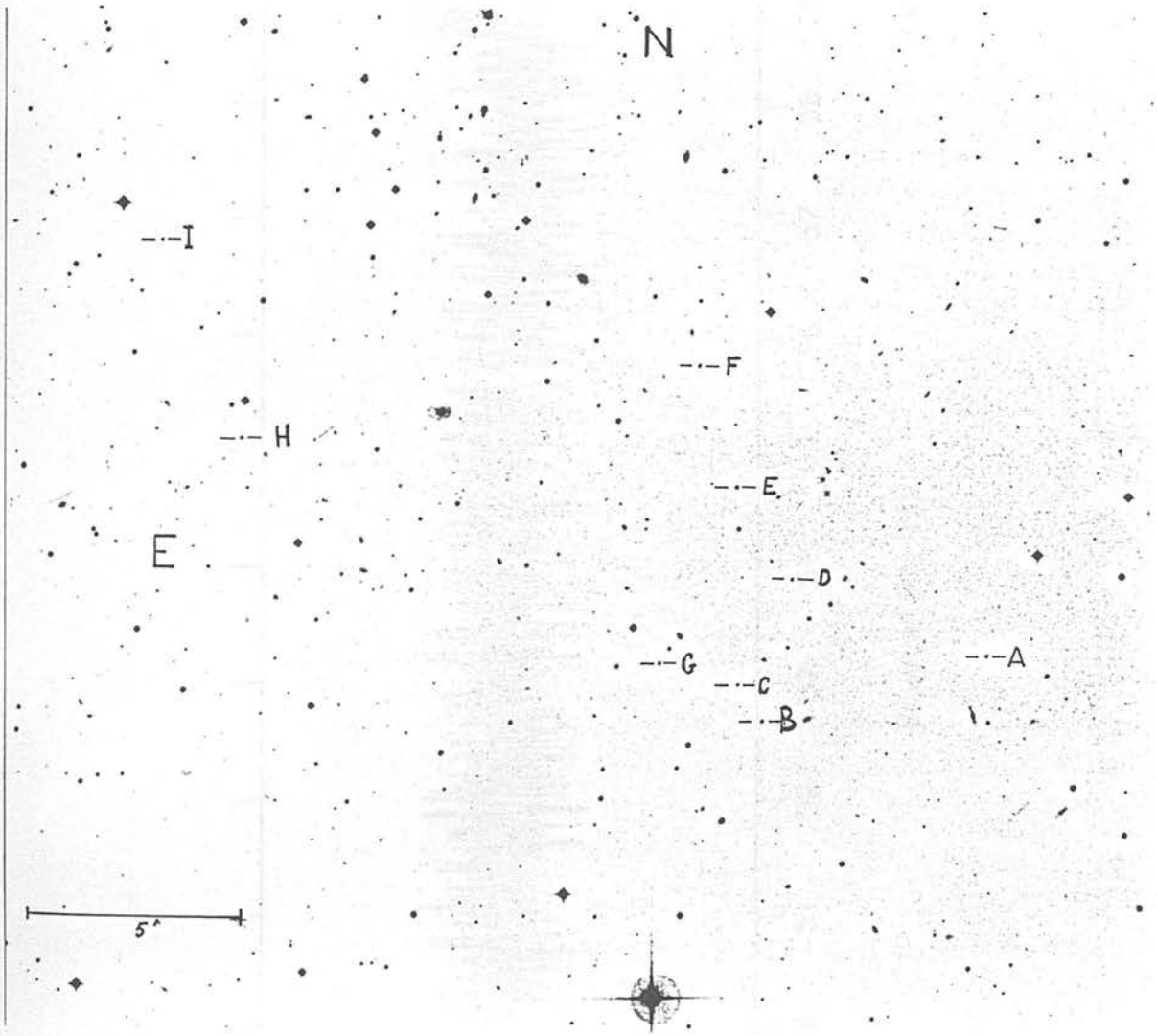

Figure 4.1 Photograph of the region of the $11^h\ 46^m +11^\circ\ 30'$ field from plate J4288. All probable quasar candidates are marked. (Photograph courtesy of Photolabs, Royal Observatory, Edinburgh.)

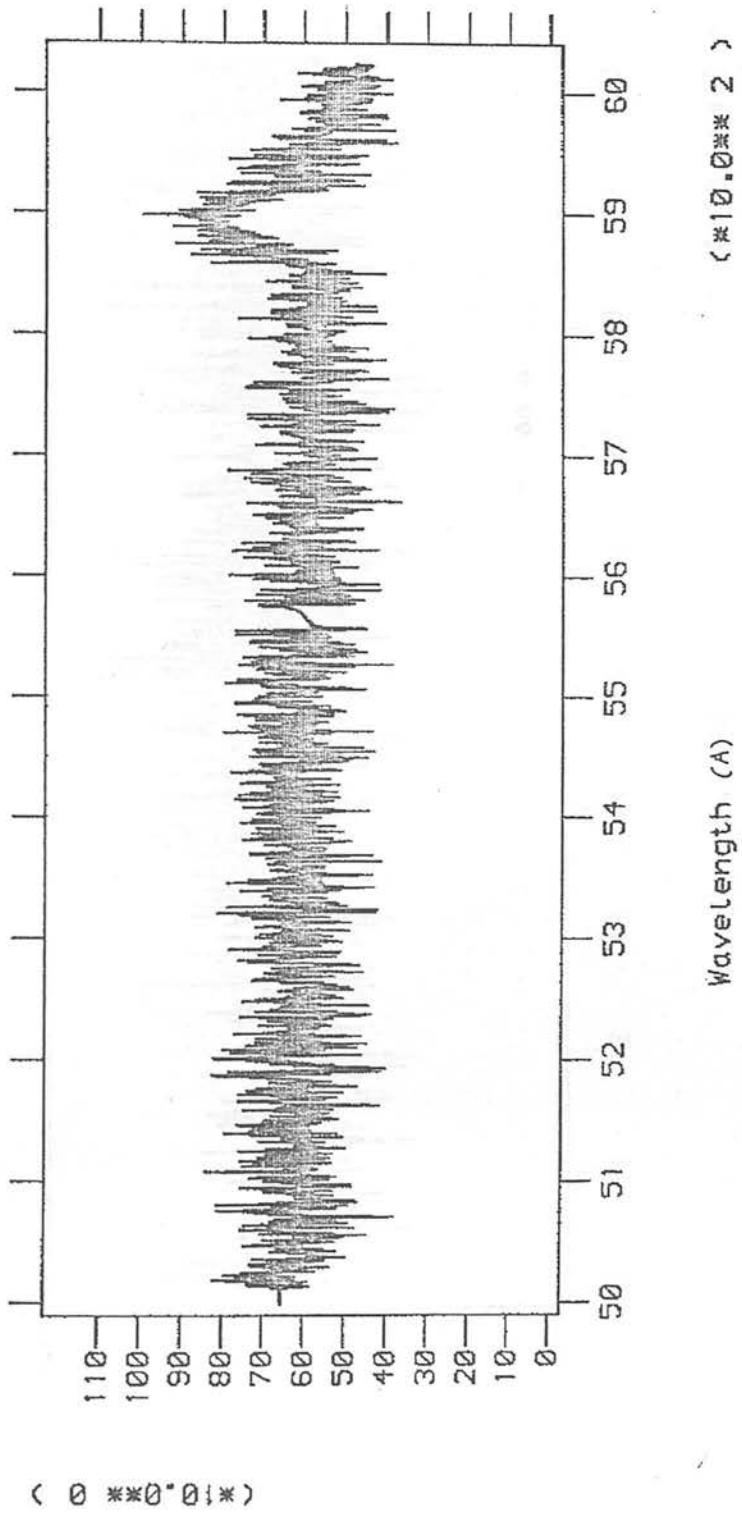

Figure 4.2a Spectrum of 1146+11B produced from the addition of five integrations covering the range from 6,000 - 5,000A. The absorption lines found are marked.

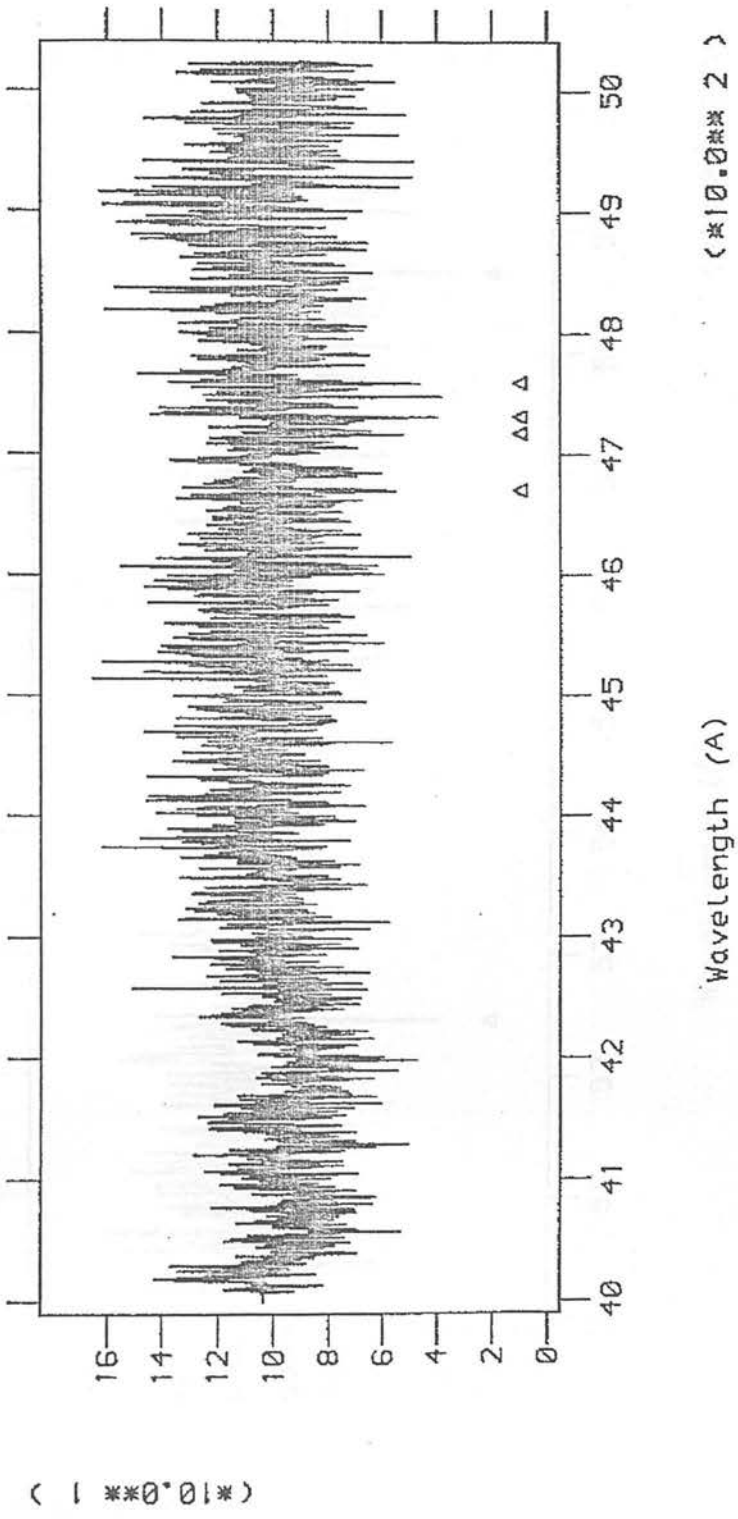

Figure 4.2b Spectrum of 1146+11B produced from the addition of five integrations covering the range from 5,000 - 4,000A. The absorption lines found are marked.

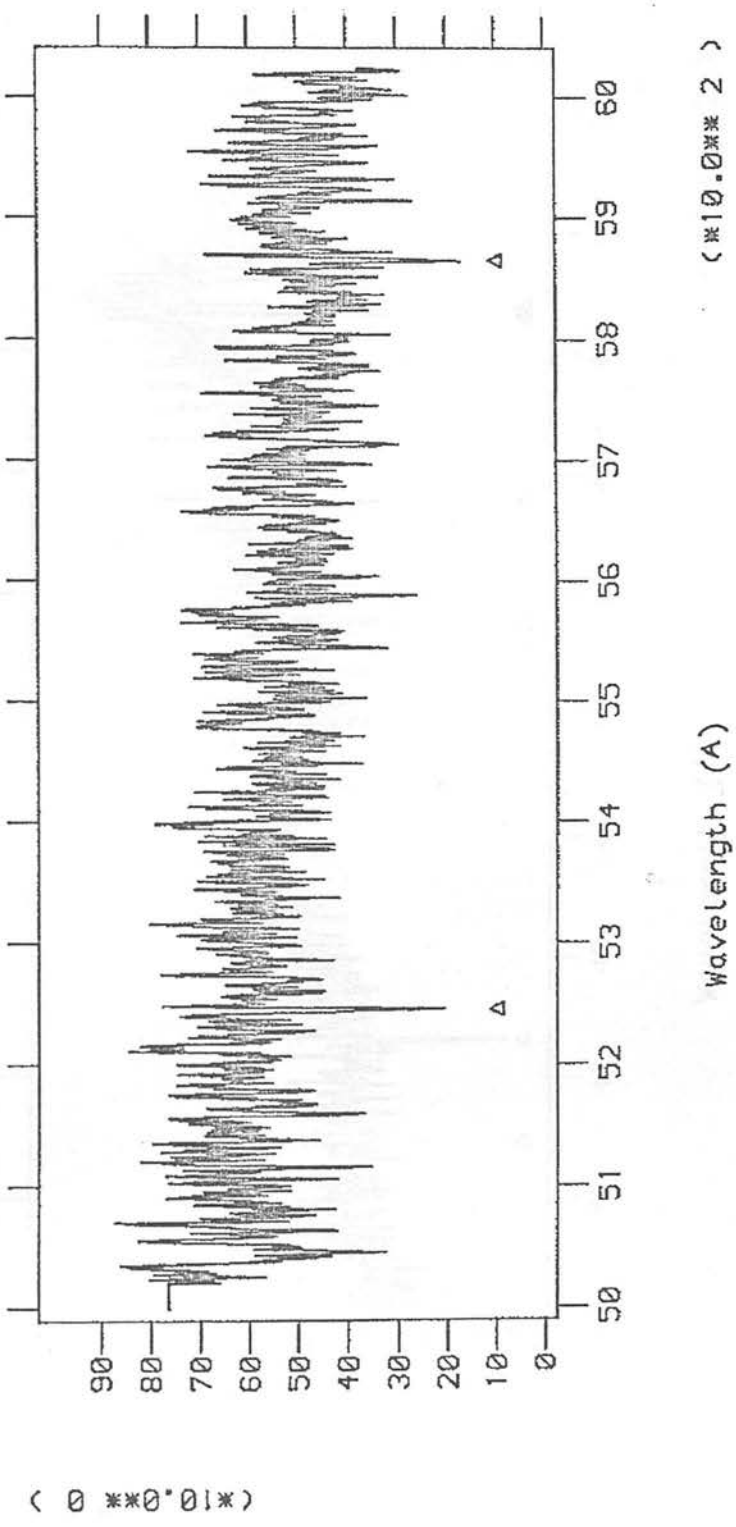

Figure 4.2c Spectrum of 1146+11G produced from the addition of five integrations covering the range from 6,000 - 5,000A. The absorption lines found are marked.

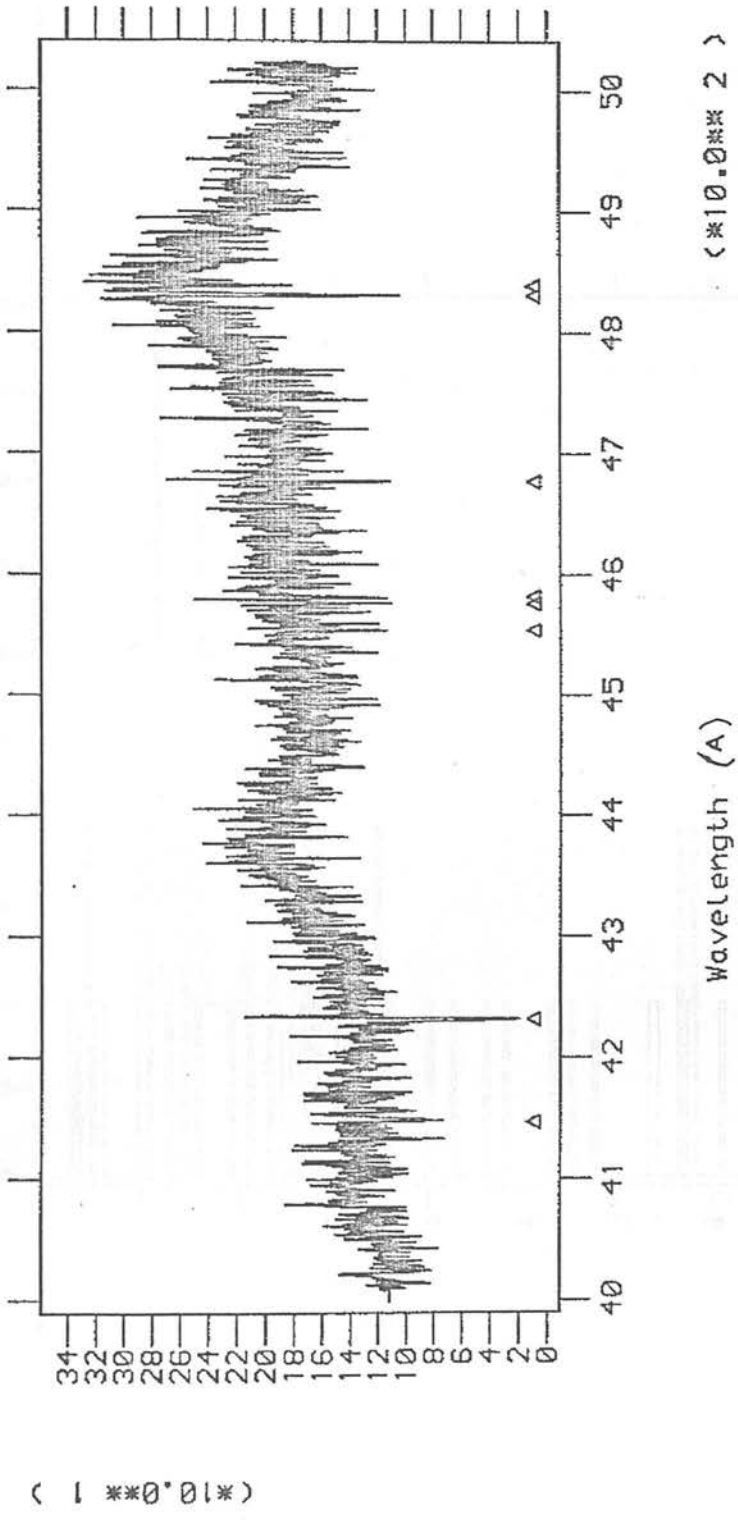

Figure 4.2d Spectrum of 1146+11G produced from the addition of five integrations covering the range from 5,000 - 4,000A. The absorption lines found are marked.

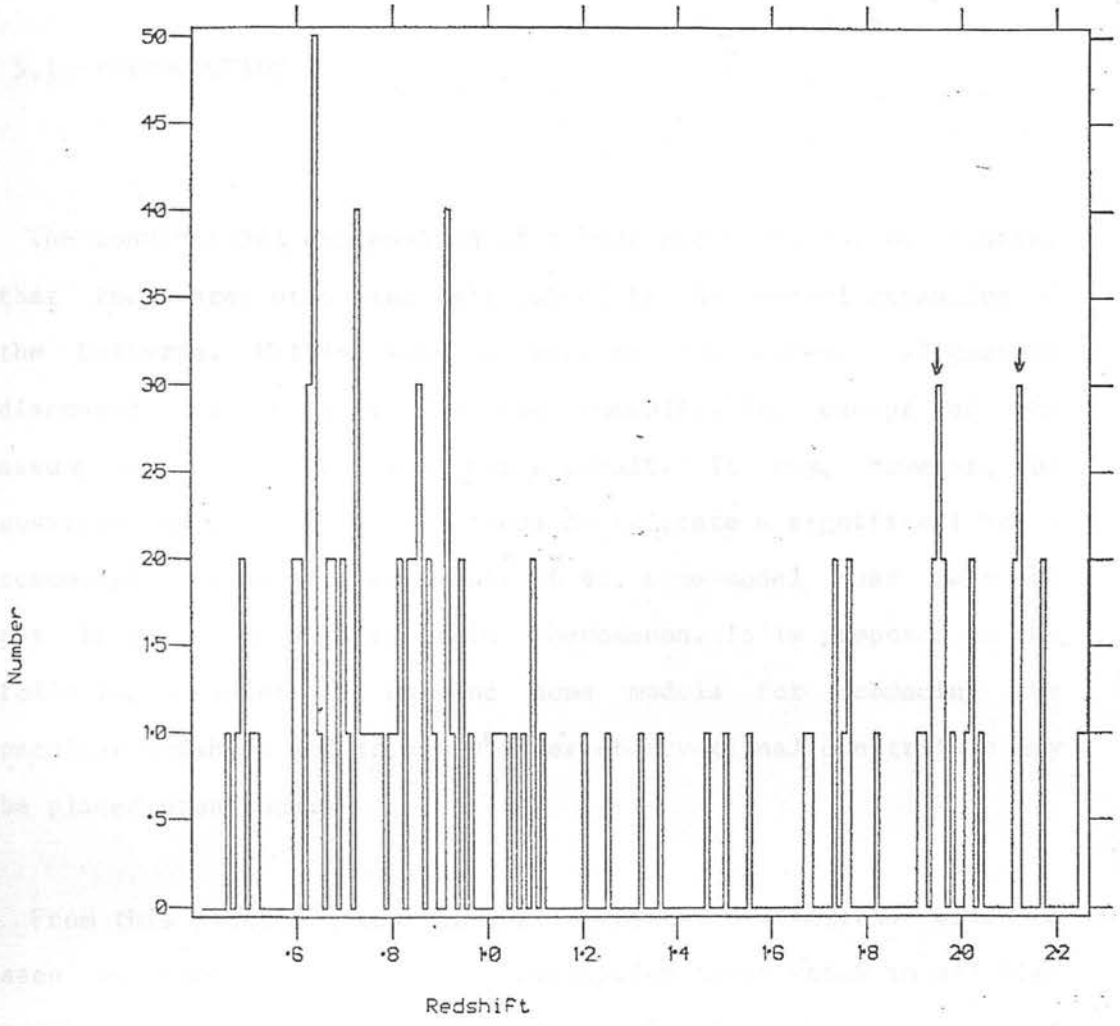

Figure 4.3 Plot of the matrix of redshifts formed by the comparison of standard wavelengths with the absorption lines observed in 1146+11G. Those peaks representing the absorption systems are marked.

CHAPTER V

NON - COSMOLOGICAL REDSHIFT MODELS

5.1 INTRODUCTION

The conventional explanation of quasar redshifts is, of course, that they are predomina tely caused by the general expansion of the Universe. Within such a picture the excess alignments discussed in Chapter III are inexplicable, except on the assumption that these are a chance result. It may, however, be possible that such observations do indicate a significant non - cosmological redshift component. If so, some model must then be put forward to explain this phenomenon. It is proposed in the following chapter to examine some models for producing the peculiar redshift and to see whether observational constraints may be placed upon them.

From this point of view the most important limitations will be seen to come from the narrow absorption lines which in all high redshift quasars cover a large range of redshifts up to (and slightly beyond) that for the emission lines. This includes the only such quasar examined which lies in a peak alignment (cf. Chapter IV). In order for any non - cosmological redshift model to be tenable it must, therefore, produce these lines internally since only if the quasars have purely cosmological redshifts can extrinsic absorption take place with normal matter.

The leading proponent of non - cosmological redshifts, Arp, has advocated a theory in which "youth" is reponsible for the peculiar redshifts. The precept is that certain atomic constants evolve with time in such a way that young objects emit radiation at intrinsically longer wavelengths than older material and therefore give the impression of being at higher redshifts. Thus, when explosive events in galactic nuclei produce, in some unspecified manner, objects composed of new matter, these are observed, after expulsion, to have higher redshifts than the parent and are recognised as quasars or compact companion galaxies (eg. Field et al. 1973).

This picture has been extended and placed upon a more physical framework by Hoyle and Narlikar (1974). The theory attempts to explain redshifts not solely by the doppler effect but by appealing to an extra mechanism in which the mass of atomic particles varies with time. It is postulated that new matter may be created spontaneously (Narlikar 1977a) but at initially infinitesimal mass. As time progresses the mass increases, the functional form of m(t) depends upon the space - time metric chosen for matter generally, where t is now not the Cosmic epoch but the time since the creation of the matter. For the Einstein - de Sitter metric (ie. one incidentally in which the Universe expands to infinity but only reaches it at zero velocity) the masses are quadratically dependent upon time. Consider the effect of this upon the wavelength of emitted radiation; for example the simple Bohr model of the one electron atom predicts the frequency, f, of radiation emitted in the transition from states of orbital quantum number l to n to be -

$$f = mK\left\{\frac{1}{n^2} - \frac{1}{l^2}\right\} \qquad 5.1$$

where K is a term involving only atomic constants not expected to be time dependent, e and h. From this it is clear that as the

system evolves the frequency of radiation increases and hence the apparent redshift diminishes.

Within this model the production of quasar absorption lines implies that one is observing an object composed of a series of shells of matter of varying ages, the smaller the shell radius the younger it is (Narlikar 1980). Unfortunately, the detailed physics of this have not been worked out yet, and as such is not directly amenable to observational testing. However, in common with other theories in which a significant non - cosmological redshift component is invoked this model predicts no correlation between the emission line Equivalent Width and redshift. This might be expected from conventional theories because of stretching of the spectrum. As reported by Narlikar (1977b) no correlation was found in a small sample of objects examined. However, this is not surprising considering the large range in other observed quasar properties. This lack of a complete physical picture and the large quantity of new physics contained makes it preferable to first try more conventional theories for the peculiar component.

This is by no means the only theory which tries to explain redshifts by means other than the doppler effect. Other models abound, such as tired light mechanisms, temporal variation of physical constants. As these are comprehensively reviewed by Pecker (1977) they need not be described in more detail here. None have received much attention with the exception of gravitation. The existence of gravitational redshifts have been known theoretically for many years and have been observed in compact objects, such as white dwarfs (eg. Greenstein et al. 1977). Obviously, the problem of the non - cosmological redshift in quasars is many orders of magnitude larger than the component observed in white dwarfs, nevertheless the mechanism has the merit of having been observationally verified, at least in the weak field regime.

the available volume in which to place any emitting or absorbing matter at high redshift is very small. This constraint was used by Greenstein and Schmidt (1964) to discount significant gravitational redshifts in quasars. It was argued that in a gravitational well the magnitude of, and the spread in, redshift across the region (given by the line shift and width respectively) characterised the volume in which the matter must be contained. Combination of the size of this volume with other details known about the line region, such as the matter density, showed that for reasonable central masses there was insufficient space in which to hold enough matter to produce the quasar emission lines.

This objection can be circumvented if the central mass is made large because then the volume between redshift Z and Z + dZ is increased and it becomes possible to contain the required amount of gas. Unfortunately, in most cases the implied central masses are very large, being comparable to or greater than that of typical galaxies. Within conventional models it is thus extremely difficult to overcome this constraint.

The difficulty posed by the argument of Greenstein and Schmidt (loc cit.) has partially been responsible for the development by Clube (1977) of an alternative theory of gravity. This model, based upon Lorentz's euclidean space/ absolute time theory rather than Einstein's theory of Relativity, is characterised by the retention of a material aether, ie. one possessing a non - zero rest mass and energy. Two fundamental differences produced by this

are that the local speed of light and rest mass change according to the level of the gravitational potential. It is possible to show that in order for the theory to be consistent with -

i The observed rate of advance of the perihelion.

ii The dependence of the natural frequency of an atomic oscillator on the gravitational potential.

iii The light delay times for propagation through a spatially varying gravitational field.

iv The observed amount of gravitational deflection of light.

then the relations between the rest mass and local velocity of light upon the gravitational potential are well determined (Dicke 1961; Atkinson 1962). Slight differences do exist between the forms of m and c obtained in these two studies because of an extra constraint imposed by Atkinson (loc cit.), but both forms agree in the limit of small potentials. As this is the only regime in which tests have been made both are equally viable. Clube (1977) has adopted the formulation of Dicke (loc cit.), namely that within the potential well of a point like source -

$$m = mo \exp(3GM/r) \qquad 5.2$$

$$c = co \exp(-2GM/r) \qquad 5.3$$

where mo and co are the values of the particle rest mass and speed of light in a region of zero gravitational potential. Thus while the theory is highly unconventional within the framework of modern physics, it does appear to be observationally valid, and it does have other predic tions which are as yet untested (Clube 1982).

It is clear from Equations 5.2 and 5.3 that in a strong field considerable differences between the aether theory and General Relativity occur. In the former the non - conservation of rest mass produces an effect known as "supermass" - the apparent increase to an external test particle of the gravitational attraction of a body which lies in a deep potential well. Thus, an initially small mass will act like a larger one for the length of time for which the supermass effect persists. It must be stressed that, as will be shown later, this does not challenge conservation of energy.

A new quasar model has been built upon the basis of this theory and is one in which a large disc (100 pc) of matter periodically accumulates in the plane of the galaxy by the accretion of gas expelled from stars by the stellar wind (Bailey and Clube 1978). The problem of the stability of such a system against dissipation by supernovae has been investigated by Bailey (1978) who concluded that given a small, 10^4 Mo, central heat sink the disc was stable. Different models of the ISM, without this heat sink, have come to the opposite conclusion (eg. Bregman 1978). Such studies, however, have sufficient uncertainties that the problem is by no means resolved.

If it assumed that the scheme is as derived by Bailey (loc cit.) and Bailey and Clube (loc cit.) then the gaseous disc grows until the onset of gravitational instability. At this point a proportion of the matter goes to form stars. Strong turbulence driven by massive OB stars leads to a rapid inward (viscous) transport of matter into the galactic nucleus. Thus the core grows and forms a low mass ($\sim 10^6$ Mo), relatively low entropy spinar (eg. Ginzburg and Ozernoy 1977). The late evolution of such objects is unknown but it is probable that they become unstable and collapse. The effect of this is to increase the self gravity of the body and by

the supermass effect to raise its mass. Depending upon the exact details of the final state, ie. the forces responsible for supporting the body etc., the mass is increased by some factor. Because little is known about the physics of the collapsed state it is not possible at present to predict the size of this enhancement but it may be as large as a factor of a thousand million.

For a period of time, therefore, a galactic nucleus develops a very deep potential well and may have a mass considerably larger than normally associated with galaxies. This enhanced mass, hence, avoids the problem raised by Greenstein and Schmidt (loc. cit.). A more detailed review of the model and its observational consequences may be found in the literature (eg. Clube 1977, Clube 1980).

Unlike a Black Hole (the predicted endpoint of the collapse of a massive body within General Relativity) the final state in the aether theory is only semi - stable. This may be seen by differentiating Equation 5.2 applied to an isolated self gravitating body which shows that the collapsing supermass will, when the potential becomes large, begin to expand again. Furthermore, it is an observational requirement since there is no evidence for the existence of hypermassive galactic cores on the order of 10^9 - 10^{11} Mo in our or other (stable) galaxies. It is further probable (Clube 1978) that the accreted matter surrounding the supermass may become rotationally unstable. This leads to the ejection of smaller, though still supermassive, objects by centripetal force. If these ejecta move with relativistic velocities and hence escape from the parent body they then may appear as aligned quasar triplets. Alternatively, if the speed of expulsion is below the escape velocity for the galaxy then the expelled masses become the progenitors of spiral arms (Clube 1978).

Certain features of this aether theory make it more suitable, perhaps, as a source of the excess redshifts, if these are large, than more conventional gravity theories. The radial variation in the gravitational potential produces a distribution of peculiar redshifts within a single body. Thus it is feasible to reproduce naturally the redshift distribution of the absorption systems if these are clouds at varying distances from the central mass.

As in General Relativity, however, it is obvious that a mass placed in this gravitional field will respond, unless supported, to the attraction by falling in towards the centre. This is especially true in this alternative theory because it is presumed that the system was stable before the advent of the supermass and hence completely unprepared for the excess forces. As absorption lines are not observed to vanish sponanteously it may be supposed that rapid collapse does not happen very often. The absence of obvious radial motions may therefore be used to place constraints upon any model in which gravity produces the excess redshift. It is proposed to use the predicted rate of fall of particles as an observational test of the allowed parameters of this model.

While most attention has been placed upon the absorption systems the same arguments may, of course, be applied to the emission line regions. These have not been, and will not be, discussed explicitly for the practical reason that it is more difficult to accurately determine the line centroid for a broad emission line than for a narrow absorption line. Moreover, the range of experimental definitions of the centre of an assymmetric line creates the possibitity of spurious effects when comparing the analyses of different workers. Since there is no obvious advantage in using the emission lines (they have redshifts which are not significantly in excess of that for the absorption systems and presumably are, therefore, no deeper in the potential well) they

will be neglected in the following analysis.

5.2 THEORY

5.2.1 The Model

Consider a system in which an observer is sitting at rest with respect to a collapsed supermass which was created at time t = 0. Initially, a test particle was located at some distance from the central body and was at rest. When the particle is released it will, under the gravitational attraction of the central mass, fall towards the centre. This motion brings the particle into regions of progressively higher gravitational potential and hence redshift. Any light emitted by the falling particle, therefore, will exhibit an increasing redshift due to the sampling of deeper portions of the potential during the collapse and also due to the doppler effect. If the test particle is identified as a cloud of absorbing gas then this inward passage will show itself as a variation in the redshift of the absorption line system. It is, therefore, of considerable interest to determine the rate of change of redshift as a function of redshift and of the central mass.

This picture is a good approximation to the situation in which a supermass becomes active in the core of a rotationally supported body such as a galaxy. Though there are two practical points which should be borne in mind -

i Strictly, the mass used in the computation should not be that of the supermass but only the increase in mass. This is because the initial rotation of the system supports it against

the pull of the original nucleus, thus counteracting that fraction of the new core mass. If the enhancement factor is large, however, this correction is small.

ii The rotation of the body will also affect the size of the doppler redshift by temporally changing the proportion of transverse to linear velocities. It is, however, a good approximation to assume that this ratio is constant during the time taken for the test particle to fall into the core. Even if the rotational velocity of a particle at a radius of 10 pc were 100 km/s (sufficient to support it against a 10^8 M⊙ core, typical of the Galaxy (eg. Oort 1977)) then the orbital time is 700,000 yr, whereas the collapse phase, for a 10^{11} M⊙ supermass, will be seen later to last on the order of one to ten years, dependent upon the initial conditions.

Of course, under the assumption of purely circular galactic orbits the initial radial velocity of the test particle will indeed be zero.

5.2.2 Lagrangian Mechanics

The identificaton of a Lagrangian within Lorentzian mechanics or Relativity is more difficult than in classical mechanics (Goldstein 1974). This is because it is now not simply the difference between kinetic and potential energies, although the partial derivative with velocity of the Lagrangian is still the momentum. The choice of the Lorentzian Lagrangian, for example, can only be made by making an initial guess and checking that it satisfies Lagrange's Equation and for consistency with conservation of energy. Nevertheless, there are problems which, like this one, are best tackled by the use of Lagrangian

mechanics. In this vein Clube (1977) has adopted a Lorentzian Lagrangian of the form -

$$L = mc^2 \gamma^{-1} \qquad 5.4$$

where -

$$\gamma = (1 - V^2/c^2)^{-1/2} \qquad 5.5$$

So, it is required to determine dZ/dt. Within the context of the model in which the absorbing matter is located within gas clouds outside the central mass, the problem is particularly simple as the mass may be treated as a point source. Then we have for the gravitational redshift -

$$Z = \frac{GM}{co^2 r} \qquad 5.6$$

M being the mass of the central body and r the distance of the test particle from it. Given the above information it is possible to evaluate Lagrange's Equation -

$$\frac{d}{dt}\left(\frac{\partial L}{\partial \dot{r}}\right) = \frac{\partial L}{\partial r} \qquad 5.7$$

While it is possible to use this Lagrangian directly to determine the particle's orbit it is simpler to first show that the form of Equation 5.4 satisfies conservation of energy and then to use this conservation law to calculate the orbit.

Consider a conservative system in which the force, F, equals -del(V), where V is the potential. Also, let this potential be velocity independent, and then if the Lagrangian is not an explicit function of time the total time derivative of the Lagrangian is -

$$\frac{dL}{dt} = \sum_j \frac{\partial L}{\partial x(j)} \frac{dx(j)}{dL} + \sum_j \frac{\partial L}{\partial \dot{x}(j)} \frac{d\dot{x}(j)}{dL} \qquad 5.8$$

where the x(j) are the orthogonal coordinates of the system. Now by substitution of Lagrange's Equation we have that Equation 5.8 may be rewritten as -

$$\frac{dL}{dt} = \sum_j \frac{d}{dt}\left(\frac{dx(j)}{dt} \frac{\partial L}{\partial \dot{x}(j)}\right) \qquad 5.9$$

from which it follows that -

$$\frac{d}{dt} \{L - \sum \dot{x}(j)(\partial L/\partial \dot{x}(j))\} = 0 \qquad 5.10$$

and hence -

$$L - \sum_j \dot{x}(j)(\partial L/\partial \dot{x}(j)) = \text{constant} \qquad 5.11$$

in this particular example substitution for the Lagrangian from Equation 5.4 gives -

$$mc^2\gamma^{-1} - mc^2\left\{\dot{r} \frac{\partial}{\partial \dot{r}}\left(1 - \frac{\dot{r}^2 + r^2\dot{\theta}^2}{c^2}\right)^{1/2} + \dot{\theta} \frac{\partial}{\partial \dot{\theta}}\left(1 - \frac{\dot{r}^2 + r^2\dot{\theta}^2}{c^2}\right)^{1/2}\right\}$$

$$= \text{constant} \qquad 5.12$$

which simplifies to -

$$mc^2\gamma^{-1} + mc^2\gamma(\dot{r}^2 + r^2\dot{\theta}^2)/c^2 = \text{constant} \qquad 5.13$$

and thence -

$$\gamma mc^2 = \text{constant} \qquad 5.14$$

Energy conservation is thus implicit in the form of Equation 5.4. It is now possible to begin the calculation of the rate of change of redshift.

The simplest approach is to split the total change in redshift into its two components, gravitational and doppler, called Z and z respectively. These may be recombined later. A proper treatment in which the motion is not assumed to be purely radial is very complicated. The particle orbit and the redshift time dependence must then be computed numerically.

5.2.3 The Gravitational Redshift

Starting with the calculation of the rate of change of gravitational redshift we have from Equation 5.14 that -

$$e = mc^2\gamma \qquad 5.15$$

where e is the total energy of the particle. The effect of the variation in the potential is to change the state of the test body as typified by its rest mass, velocity etc.. The new velocity taken up by the particle produces an initial Lorentz factor γ_o. Hence, substituting for m and c from Equations 5.2 and 5.3 implies that -

$$\gamma = \gamma_o \exp(Z) \qquad 5.16$$

It is clear from the foregoing discussion that the functional dependence of γ_o upon Z is simply exp(Zi), where Zi is the value of the gravitational redshift at t = 0. So, by the definition of the Lorentz factor this becomes for purely radial motion -

$$1 - \frac{1}{c^2}\left(\frac{dr}{dt}\right)^2 = \exp\{-2(Z-Zi)\} \qquad 5.17$$

$$\left(\frac{dr}{dt}\right)^2 = c^2(1 - \exp\{-2(Z-Zi)\}) \qquad 5.18$$

That this equation of motion reduces to the Newtonian one in the weak field, low velocity regime it is simple to show that this approximates to -

$$\frac{1}{2}\left(\frac{dr}{dt}\right) = co^2\left\{\frac{1}{r} - \frac{1}{ri}\right\}\frac{GM}{co^2} \qquad 5.19$$

which is clearly the usual conservation of energy equation for a freely falling system moving from a radial separation ri to one of r.

Using Equation 5.6 Equation 5.18 gives -

$$\left(\frac{dZ}{dt}\right)^2 = \frac{Z^2 co^4}{G^2 M^2} \exp(-4Z)(1 - \exp\{-2(Z-Zi)\}) \qquad 5.20$$

There is an ambiguity, as always, when taking a square root about the sign of the expression. In this case it is known that in the low redshift regime the falling particle will show an increasing and hence positive rate of change of redshift. Therefore letting $K = co^3/G$ -

$$\frac{dZ}{dt} = \frac{KZ^2}{M}\exp(-2Z)\ (1 - \exp\{-2(Z-Zi)\})^{\frac{1}{2}} \qquad 5.21$$

In the limit of a particle starting from infinity, Equation 5.21 takes on a particularly simple form because then Zi = 0. In this case the rate of change of Z with time is a maximum for a given value of Z, since the body has had the maximum time for the acceleration to act before reaching this radius.

A graphical representation of this function is shown in Figure 5.1. The three functions shown are for Zi = 0, 0.5 and 1.0 respectively. The abscissa is the gravitational redshift (not to be confused with that actually observed) and the ordinate is the rate of change of redshift per second. The calculations have been made for a central mass of $10^{11} M_{\odot}$.

The form of the curve is somewhat unexpected in that it contains a stationary point. This means that below some radius the rate of infall begins to decrease rather than having a continued acceleration. The reason for this is rather difficult to visualise as it is direct conflict with everyday experience. However, it is caused by the variation in the local speed of light (cf. Equation 5.3). As the particle drops into the potential well it is initially moving non - relativistically and is accelerating. When its motion brings it into regions in which the speed of light is significantly lower than the value in free space then the particle will find itself prematurely relativistic. It is well known that it becomes progressively more difficult to accelerate a relativistic body and so the rate of acceleration slows. A point will come, since the local speed of light is dropping exponentially, when, in order to remain below the local light speed, the infalling material must actually decelerate, hence the turning point in Figure 5.1.

5.2.4 The Doppler Redshift

Calculation may now be made of the magnitude of the second component in the observed redshift, namely the doppler effect. As in Special Relativity the form for the doppler redshift within the aether theory is -

$$1 + z = (1 - V^2/c^2)^{1/2}(1 + Vr/c) \qquad 5.22$$

where Vr is the component of velocity parallel to the line of sight and V is the total velocity, though this must now be interpreted as an absolute motion with respect to the aether reference frame. An angle term, A, may be introduced to allow for the projection factor between the particle's motion and the line of sight, which as shown in Section 5.2.1 is not likely to be strongly time dependent and is taken as a constant. The major uncertainty in A comes not from its possible time variability but from the unknown orientation of the system to the line of sight.

Noting the Z dependence of the Lorentz factor given in Equation 5.16, differentiating Equation 5.22 then gives -

$$\frac{dz}{dt} = \exp\{Z-Zi\}\{(1 + AV/c)\frac{dZ}{dt} + A\frac{d}{dt}(V/c)\} \qquad 5.23$$

Since the motion is purely radial we have that -

$$V = -\frac{dr}{dt} \qquad 5.24$$

The negative sign arises because of the sign convention. So, from Equation 5.21, after a little rearrangement it is clear that -

$$\frac{dr}{dt} = -co\ \exp(-2Z)(1 - \exp\{-2(Z-Zi)\})^{1/2} \qquad 5.25$$

hence -

$$\frac{d}{dt}(V/c) = \frac{d}{dt}(1 - \exp\{-2(Z-Zi)\})^{1/2} \qquad 5.26$$

$$= \exp\{-2(Z-Zi)\}(1 - \exp\{-2(Z-Zi)\})^{-1/2}\frac{dZ}{dt} \qquad 5.27$$

Substitution into Equation 5.22 then gives -

$$\frac{dz}{dt} = \frac{KZ^2 \exp\{-Z-Zi\}\{(1 - \exp\{-2(Z-Zi)\})^{\frac{1}{2}} + A\}}{M} \qquad 5.28$$

A plot of (dz/dt) against gravitational redshift; as representative of the radial separation of the particle from the central body, is shown in Figure 5.2, again illustrated for three values of the initial redshift, 0, 0.5 and 1.0. As before, the supermass is assumed to be 10^{11} M⊙ and A has been taken as 0.5. Not unexpectedly, considering the form of Equation 5.28 and the dependence of dz/dt upon dZ/dt, the curve also contains a stationary point. This is again due to the lowering of the local speed of light in regions of high potential as discussed above. It is obvious that as the particle slows to remain below the speed limit the magnitude of the doppler effect will diminish.

5.2.5 The Total Peculiar Redshift

The two components of redshift must now be combined to give the total rate of change of redshift. Using the "Addition Law" (cf. Section 3.6) we have that -

$$(1 + Zt) = (1 + Z)(1 + z) \qquad 5.29$$

From Equation 5.25 it is possible to substitute in for the particle velocity as a function of the gravitational redshift to give -

$$(1 + Zt) = (1+Z)\exp\{Z-Zi\}(1 + A(1 - \exp\{-2(Z-Zi)\}^{\frac{1}{2}}) \qquad 5.30$$

This is a monotonically increasing function with Z and is

illustrated in Figure 5.3. It covers a smaller range in gravitational redshift than Figures 5.1 and 5.2 in order to expand the interesting region close to the origin. While for the present purpose the rate of change of total redshift is more interesting than its absolute value, the latter this provides constraints upon viable model parameters. Differentiating Equation 5.29 we get -

$$\frac{dZt}{dt} = (1 + Z)\frac{dz}{dt} + (1 + z)\frac{dZ}{dt} \qquad 5.31$$

From the above work analytic forms have been derived for dz/dt, dZ/dt and (1 + z) in Equations 5.21, 5.28 and 5.22 respectively, the (1 + Z) factor merely being an extra term in the dependent variable. These terms may be substituted into Equation 5.31 and dZt/dt determined -

$$\frac{dZt}{dt} = \frac{KZ^2}{M}\exp\{-(Z-Zi)\}\{(1 + Z)(A + (1 - \exp\{-2(Z-Zi)\})^{1/2}) + (1 + A(1 - \exp\{-2(Z-Zi)\})^{1/2})(1 - \exp\{-2(Z-Zi)\})^{1/2}\} \qquad \ldots 5.32$$

The graph of this function is illustrated in Figure 5.4 for Zi = 0, 0.5 and 1.0. The abscissa being, as in the previous Figures, the gravitational redshift component. Considering the aforementioned turning points in the gravitational and doppler components the shape of this function is as expected.

The functional forms of Equations 5.21, 5.28 and 5.32 are very interesting because of the inverse dependence of the rate of change of redshift upon M. While this may be opposite to what might have been expected the explanation is rather simple. What is of interest is the rate of change of the gravitational potential at a given value of that potential (determined by dZ/dt and Z respectively). In a 1/r potential the ratio of these is inversely proportional to M, ie. for a larger central mass a given depth in

the well occurs at a larger radius and thus has a lower gradient than for a small mass. Hence, particles at a given gravitational redshift will be seen to evolve more rapidly the smaller the central mass. This is of the utmost importance because upper limits on the time variation of the redshift give lower limits upon the central mass.

The question about the timescale on which this collapse phase operates is still unresolved as the preceding discussion has been in terms of the radial separation of the test particle from the central core. To answer this it is required to determine r(t), or equivalently Z(t). With a little manipulation the integral of Equation 5.21 will give this relationship. Unfortunately the form of the integrand is sufficiently complex that an analytic solution does not exist. Progress can only be made, therefore, by numerical integration. This technique has been applied to Equation 5.21, giving a form for Z(t) which is illustrated in Figure 5.5, and to Equation 5.32 giving Zt(t), which is shown in Figure 5.6. The abscissae are the time in years since the particle was released, the ordinates being the gravitational and total redshifts respectively. The calculations have been made, as before, for Zi = 0, 0.5 and 1.0 and for a central body of 10^{11} Mo, conversion for other masses being trivial.

Examination of these graphs show that the particle spends most time during the collapse phase at small gravitational redshifts. This is not surprising since it is initially moving relatively slowly and the linear extent of regions of high redshift becomes progressively smaller. For the model parameters as given the time taken for a particle to collapse from a region of low potential (Z = 0.001)into the core is about 10 yr, although this depends upon the initial redshift. This time increases linearly with the mass of the central body.

Within a dynamical theory such as this it is possible to have blueshifted lines produced by the material of the far side of the collapsing system if the doppler effect is the main contributor to the peculiar redshift. In practice, however, these lines will not be observed as those normally seen in quasar spectra have rest wavelengths in the blue or UV. Thus blueshifted absorption lines would be moved away from the visible spectral window and be unobservable. Although there exist lines in the far red which would theoretically be visible these would not be selected because identification of the absorptions is so biassed towards those lines with rest wavelengths in the blue. Hence, the only clouds which are seen spectroscopically are those for which the gravitational component is dominant or those which are moving away from the observer. The lack of negative redshifts is thus not a constraint upon the model.

5.3 THE OBSERVATIONS

In order to determine the rate of change of redshift indicated by the observations those quasars which have been observed for absorption lines over a timescale of about or greater than ten years have been selected from the catalogue of Ellis and Phillips (1979) and by a search of more recent literature. Only those absorption systems which contained at least 5 lines were used in order to increase the accuracy of the absorption redshift and also the certainty of identification.

There were a total of six quasars which had been observed at high resolution over the requisite period and for which reliable analyses of the absorption data existed. These objects, together with the absorption line redshifts are listed in Table 5.1. The six quasars exhibited twelve acceptable absorption systems, No

being the number of lines in each. In this Table the year given is the nearest date to the epoch of observation, though in a number of instances the analyses were not carried out until some time later. Some of the redshifts quoted as being at the same epoch are not separate observational estimates but have been produced by independent analyses of the same data. These have been included in order to give an estimation of the typical measurement error in the centroid of the absorption lines. Some idea of this may also be obtained by determining the standard deviation of the absorption line redshifts about the mean for the system. This number, s, has been found for each absorption system and is also given in Table 5.1.

A straight line was then fitted by a least squares method to the data for each system. With the exception of the Zabs = 1.965 system in 0119-046 for which only two observations exist, the redshifts were weighted by the inverse of the variance, $1/s^2$, in order to discriminate against the less well determined absorption line redshifts. In cases where the evaluation of s has not been possible a value of 10 has been assumed, though for the present purpose this is not critical. The slope of the line, which is the best fitting rate of change of redshift, is listed in Table 5.2 along with the redshift of the absorption system. The goodness of fit of the least squares line to the points may be estimated by examination of Figures 5.7a - 1. These plots show the data, with the standard deviation on the points when known, and the best fitting line for each of the absorption systems.

It is possible to estimate the standard deviation, s(m), of the best fitting slope by calculating -

$$s^2(m) = \frac{\sum_i w(i)}{\sum_i w(i) \sum_i w(i)x^2(i) - \left(\sum_i w(i)x(i)\right)^2} \qquad 5.33$$

where x(i) are the values of the abscissa at each of the data

points and w(i) are the corresponding weights. A derivation of this is by Bevington (1969). The value of s(m) has been determined for each of the data sets and are listed in Table 5.2 beside the least squares slope.

The mean absolute rate of change of redshift is $1.5 \pm 1.3 \times 10^{-4}$ per year, though when the signs are taken into account this drops by an order of magnitude and in fact becomes negative. Comparison of the mean absolute rate of change of redshift with the measurement errors in redshift, s, and the standard deviation of that slope, s(m) show that the uncertainties are an order of magnitude larger than any variation. This implies that the data are consistent with no evolution outside the observational errors.

5.4 COMPARISON OF THEORY AND OBSERVATION

From Section 5.3 it is known that the maximum allowable value for dZ/dt is $\sim 1.5 \times 10^{-4}$ over a baseline of a year. This corresponds, roughly, to a rate of 5×10^{-12} per second. What has not been determined is the ratio of gravitational to doppler redshifts making up the total non - cosmological component. This fraction depends upon the value of the initial gravitational redshift, Zi. In order to assess the effect of this parameter upon the final implied mass the determination has been made for each value of Zi. Examination of Figure 5.3 gives the magnitude of the gravitational component, for a particular value of Zi and for a set total peculiar redshift. Substitution of this into Equation 5.32 will then give the rate of change of total redshift as function of the central mass. In fact for a total redshift of 2 and with A = 0.5 the results are identical to within a factor of two and give $M \sim 10^{16}$ Mo.

The reason for this close agreement in the implied central masses irrespective of Zi is because the interior particles are more strongly accelerated, though for a shorter time, than the exterior ones. These effects thus partially cancel giving an impulse which is constant to a first approximation.

Such exceptional central masses are also implied by plausibility arguments based upon the constraints first noted by Greenstein and Schmidt (loc cit.). Absorption lines are observed to be very narrow, the full width being on the order of 50 km/s. This implies that the ratio of the cloud radius to the distance from the central source is ~ 10^{-4}. Typical absorption systems have hydrogen column densities of ~ $10^{19} cm^{-2}$ (cf. Weymann et al. 1981). Assuming that the gravitational redshift is ~ 1 then in order to contain the required amount of matter within the radii secified by the line width and displacement the cloud density, p (in particles per cc), must be -

$$p \sim \frac{3 \times 10^{17}}{M} \qquad 5.34$$

where M is the central mass in units of solar masses. The general absence of excited fine structure lines in absorption systems may be used to place upper limits on the electron density within the cloud (Bahcall and Wolf 1968). Estimates of the implied densities have been made in a few cases (eg. Williams and Weymann 1976) and give $p < 10$. Evaluation of the central mass from Equation 3.32 then gives $M > 3 \times 10^{16}$ Mo.

With such large masses it is highly probable that any surrounding structure would be disrupted or at least highly disturbed by the gravitational forces if the supermass was to exist for too long. The necessary lifetime for disruption may be calculated for a body, such as the Galaxy, which is predominantly

supported by rotation. Let the model galaxy be one in which a central core of mass Mc is surrounded by a mass distribution and where M(r) is the mass of this extended component interior to r. If, because of some traumatic event, the core becomes supermassive with a new mass of Ms then the outlying matter will experience a net radial force of magnitude -

$$Fr(r) = \frac{G(Ms + M(r))}{r^2} - \frac{G(Mc + M(r))}{r^2} \qquad 5.35$$

$$= \frac{G(Ms - Mc)}{r^2} \qquad 5.36$$

The system will disrupt after a lifetime of Ms which is sufficient to have the impulse of Fr(r) equal to the original rotational momentum of the particles, ie. when -

$$\frac{G(Ms - Mc)}{r^2} t = V(r) \qquad 5.37$$

where V(r) is the rotational velocity at r. Given that initially the system was stable it is clear that -

$$V^2(r) = \frac{G(Mc + M(r))}{r} \qquad 5.38$$

hence, letting Ms = xMc -

$$t = \frac{1}{(x - 1)}\sqrt{\frac{(Mc + M(r))r^3}{GMc^2}} \qquad 5.39$$

in the case of Ms >> M(r) >> Mc then Equation 5.39 reduces to -

$$t = \sqrt{\frac{M(r)r^3}{GMs^2}} \qquad 5.40$$

It should be noted that $M(r)r^3$ will diminish with decreasing r

provided that the radial density profile decreases less rapidly than r^{-5}, if the material is in the form of a disc, or as r^{-6} if it is in a sphere. Within our Galaxy the density within the disc scales as an exponential and the halo as an inverse cubic (eg. Caldwell and Ostriker 1981). So, evaluation of Equation 5.39 for the edge of the halo will give an upper limit for the stability time for the body as a whole. Thus, taking r = 20kpc, M(r) = 10^{11} M⊙, Mc = 10^{6}M⊙ (cf. Oort 1977) and x = 10^{10} gives the permissable lifetime as ~ 1,000yr. In the case of a series of outbursts the possible lifetime is increased as the particle will perform a random walk, if the recurrence time is short with respect to the escape timescale. This will raise the stability lifetime by a factor of n, where n is the number of periods of activity.

The implied lifetime for the central mass is very short considering that some quasars must have been active for many millions of years in order to have produced the extensive double lobe radio sources. It is, of course, possible that these objects are atypical in some way, or that the underlying galaxy has been, or will be, destroyed by the activity. The numbers of such sources are sufficiently small that this does not pose much of a problem from the point of view of the numbers of disrupted galaxies expected. Destruction, however, cannot be used as an escape route if long lived massive quasars exist in many ordinary galaxies. It is possible to estimate the lifetime of the active period by a simple statistical argument. Suppose that all the quasars have cosmological redshifts which are less than one. If it is assumed that space is euclidean, which has the effect of giving the maximum volume contained within a given redshift limit, then the volume inside a cone of half opening angle, a, is -

$$V = \frac{1}{3}\pi \tan^2(a)\frac{c^3 z^3}{Ho^3} \qquad 5.41$$

which for a = 1/2 degree and z = 1 gives V = 2.2×10^{6} Mpc^3 (Ho

= 100 km/s/Mpc). Thus, if the space density of galaxies is constant and equal to the local value of 0.06 galaxies per Mpc with M(B) < -16 (Davis and Huchra 1982) then the total number enclosed is 130,000. The observed surface density of quasars of ~ 10 per square degree (eg. Veron and Veron 1982) implies that -

$$\frac{10}{1.3 \times 10^4} = \frac{\text{Quasar Lifetime}}{\text{Galaxy Age}} \qquad 5.42$$

on the assumption that every galaxy may produce a quasar. Setting the age of galaxies ~ 15 Gyr gives the length of the quasar period ~ 1Myr. This is two to three orders of magnitude larger than the permitted age derived from the stability arguments above and apparently is a direct rebuttal to the model. Although the lifetime of the active period may be reduced by increasing the volume available to produce the quasars, ie. by increasing the number of galaxies available, this is only possible in the radial direction and in order to reconcile the two ages the upper limit to z must be increased to ~ 5 - 10, larger than the observed maximum quasar redshifts.

This discrepancy will be exacerbated if a non - euclidean space is assumed and if the range of galaxies capable of producing quasars is reduced, though this may be partially offset by evolution of the galactic space density.

There are three possible ways in which the above timescales may be reconciled -

i To assume that the infalling material is supported, perhaps by a very hot, tenuous gas. This would permit lower central masses to have reduced rates of infall and so satisfy these observational constraints. Such a system is, of course, Rayleigh - Taylor unstable, though this will only be important if the timescale for the instability to develop is short

compared to the period between observations.

For a cloud which is ~ 1 pc across and at a temperature of 50,000K the sound crossing time is ~ 50,000 yr. Since the Rayleigh - Taylor instability will grow with a velocity only slightly less than the sound speed it is clear that the clouds will be dissipated sufficiently slowly that the sudden disappearance of absorption systems, due to cloud destruction, would be very unlikely.

ii The foregoing analysis assumes that the gravitational field in the neighbourhood of the test particle is equivalent to that generated by a point source. If this is not the case then the estimates for the central mass would not be valid. In order to reduce the gradient of the field without increasing the mass of the core a model would have to be invoked in which the supermass was composed of a number of smaller bodies distributed cospatially with the absorbing material. This "plum pudding" model would then have a potential well which had a relatively flat bottom and so the absorbing clouds would not experience the strong accelerating force.

The geometry of this new central region is not obvious since some of the absorbing clouds must cover the continuum source and line emitting regions completely because the stronger absorptions are observed to have black cores. This requires that the heat source be centrally concentrated and thus uncorrelated with the mass distribution. It is further probable that if there are more than two supermassive bodies then the gravitational slingshot mechanism (Saslaw et al. 1974) will eject masses into the galaxy, thereby altering the form of the potential well.

iii In a real galaxy the particles have a transverse velocity due to the initial rotation. Because the total velocity of the test body must not exceed the local speed of light the existence of a second velocity component will reduce the maximum radial velocity and hence the rate of increase of redshift. This does not require that the rotational velocity of the particle be relativistic before the onset of the supermass as its velocity is boosted by the drop in the potential. It is unlikely, however, given the magnitude of the transverse velocity observed in the Galaxy, that this will reduce the rate of redshift increase by the required factor of 100 - 1,000.

Although such models may prove to be correct in the end they are becoming somewhat over - elaborate. The use of Occam's Razor to remove them from consideration may, therefore, be justified.

5.5 CONCLUSIONS

Arguments suggest that the most plausible and least revolutionary means for the production of peculiar redshifts within quasars is gravitation. It is further argued that conventional gravity theories do not lend themselves to the manufacture of the large non - cosmological components desired. Attention is thus focussed upon an alternative theory due to Clube (1977).

It has been shown that on the assumption of a point - like gravitational source the constancy of the absorption line redshifts in quasars places a lower limit on the mass of the central object if it is to explain peculiar redshifts by gravitational means. This mass is, in the mean, $\sim 10^{16}$ $M_\odot$ and as such is considerably in excess of the normal mass of galaxies.

It has also been possible to show that within a rotationally supported body, similar to the host Galaxy, the lifetime of such an object, integrated over the age of the Universe, must be less than ~ 1,000 - 10,000 yrs or else the gravitational perturbation would be sufficient to destroy the galaxy. However, from statistical arguments based upon the observed numbers of quasars and galaxies it is possible to show that the quasar phenomenon must last for at least ~ 7×10^{-5} times the age of the Universe, or ~ 1 Myr. As this is two to three orders of magnitude greater than the stability time this provides a strong discrepancy between the present state of the theory and observation.

The observational limits upon the rate of change of absorption line redshifts, therefore, place strong constraints upon those quasar models employing gravity as a source of peculiar redshift.

TABLE 5.1

Data for the comparison of absorption line redshifts as a function of time.

Year	Zabs	s ($\times 10^{-4}$)	No.	Ref.
Object: 0058+019				
1967	0.6128	3.6	9	10
1967	0.6128	3.4	9	2
1967	0.6129	?	6	1
1969	0.6127	4.0	10	11
1975	0.6118	3.3	6	15
Object: 0119-046				
1967	1.9659	9.7	7	13
1977	1.9633	1.4	7	17
Object: 0237-233				
1967	1.9484	45.0	8	7
1968	1.9555	8.2	15	10
1975	1.9551	5.9	10	5
Object: 0237-233				
1967	2.2017	8.0	9	10
1968	2.2015	10.5	8	4

1975	2.2013	5.0	8	5

Object: 0237-233

1968	1.3648	4.7	10	10
1968	1.3642	3.4	6	4
1975	1.3644	3.7	8	5

Object: 0237-233

1968	1.6564	5.0	6	10
1968	1.6560	9.1	6	4
1975	1.6558	6.3	5	5
1978	1.6568	4.6	6	6

Object: 0237-233

1968	1.6715	5.0	6	10
1968	1.6706	8.2	8	4
1975	1.6714	2.3	8	5
1978	1.6714	8.1	6	6

Object: 0802+103

1966	1.9460	7.5	11	9
1966	1.9470	15.0	16	16
1967	1.9458	7.1	14	3
1968	1.9468	?	14	1
1975	1.9453	19.0	12	19

Object: 0805+046

1971	2.8754	10.0	11	14
1971	2.8758	?	16	1

1980	2.8772	10.0	8	12

Object: 0805+046

1971	2.4739	8.2	10	14
1971	2.4745	?	17	1
1980	2.4757	8.0	14	12

Object: 1256+357

1969	1.8366	2.4	5	8
1977	1.8328	5.0	5	17
1979	1.8320	?	6	18

Object: 1256+357

1969	1.8952	11.0	6	8
1977	1.8976	17.0	5	17
1979	1.8980	?	6	18

References

1 Aaronson et al. 1975 ApJ 198, 13

2 Bahcall & Feldman 1970 ApJ 161, 389

3 Bahcall et al. 1967 ApJ 149, L11

4 Bahcall et al. 1968 ApJ 153, 689

5 Boksenberg & Sargent 1975 ApJ 198, 31

6 Boronson et al. 1978 ApJ 220, 772

7 Burbidge 1967 ApJ 147, 845

8 Burbidge 1969 ApJ 155, L43

9 Burbidge et al. 1966 ApJ 144, 447

10 Burbidge et al. 1968 ApJ 152, 1077

11 Chan & Burbidge 1971 ApJ 167, 213

12 Chen et al. 1981 MNRAS 196, 715

13 Kinman & Burbidge 1967 ApJ 148, L59

14 Lynds 1971 ApJ 164, L73

15 Peterson et al. 1977 ApJ 218, 605

16 Stockton & Lynds 1966 ApJ 144, 451

17 Weymann et al. 1977 ApJ 213, 619

18 Weymann et al. 1979 ApJ 234, 33

19 Williams et al. 1975 ApJ 202, 296

TABLE 5.2

Rates of change of absorption line redshifts

QSO	Zabs	dZ/dt (per yr)
0058+019	0.613	-12.8 ± 5.1 $\times 10^{-5}$
0119-046	1.965	-26.0 ± 9.8
0237-233	1.955	-1.8 ± 14.2
0237-233	2.201	-4.4 ± 10.6
0237-233	1.364	-0.1 ± 6.6
0237-233	1.656	3.4 ± 6.2
0237-233	1.671	1.9 ± 6.5
0802+103	1.946	-1.1 ± 22.4
0805+046	2.875	16.4 ± 15.7
0805+046	2.474	15.1 ± 12.7
1256+357	1.837	-46.5 ± 6.9
1256+357	1.895	30.0 ± 25.3

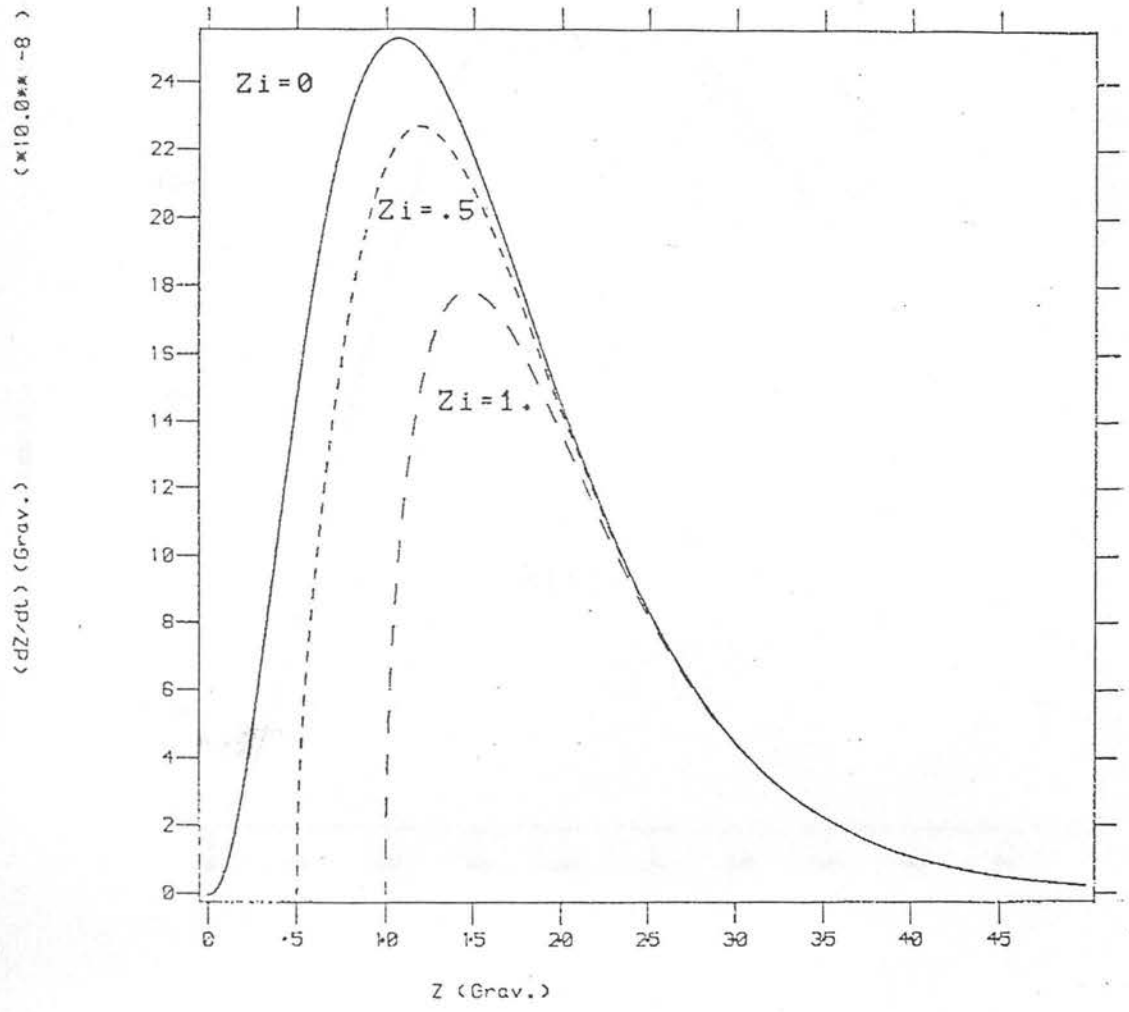

Figure 5.1 The dependence of the rate of change of gravitational redshift plotted against the gravitational redshift. The ordinate is in units of change of redshift per s., calculated for a central mass of 10^{11} Mo.

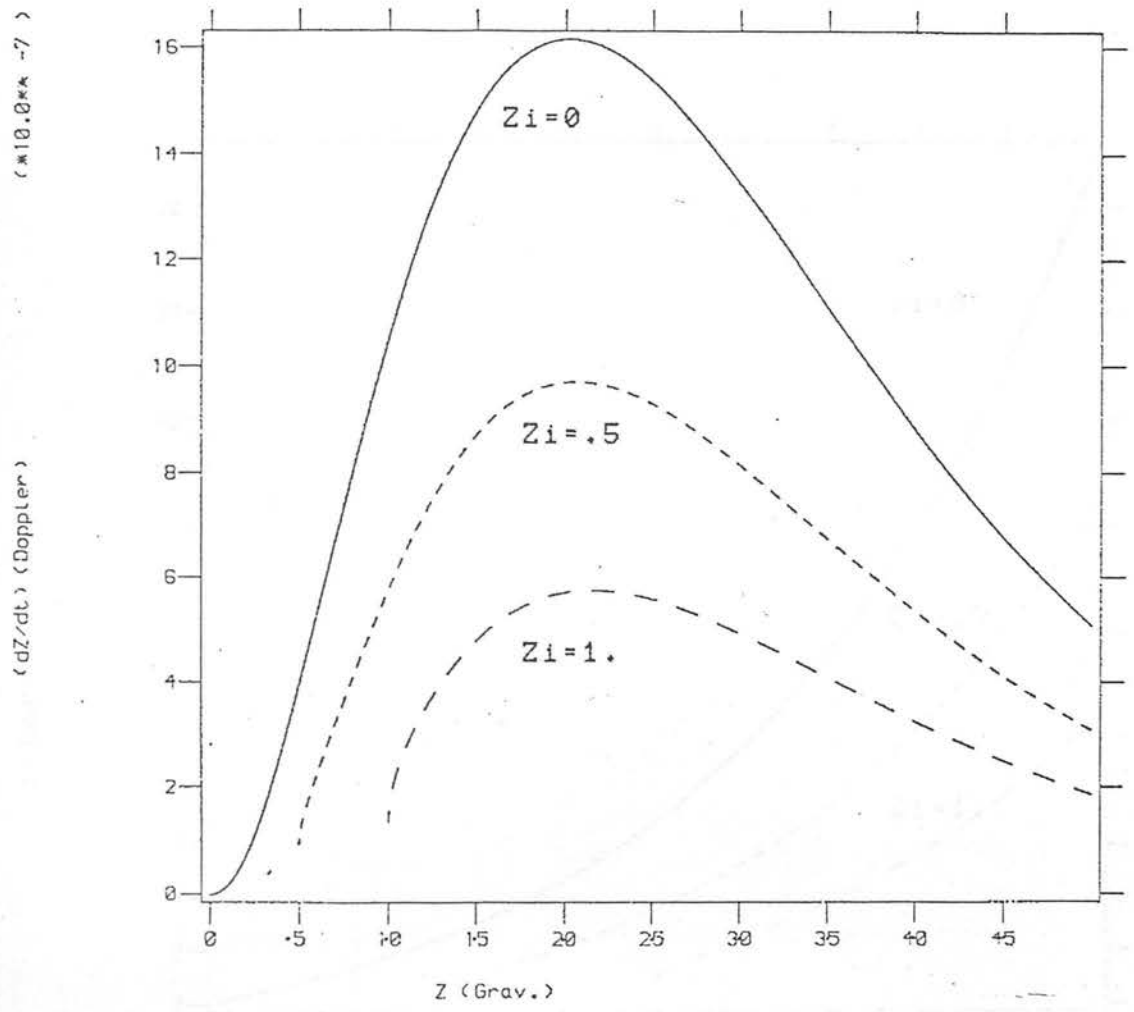

Figure 5.2 The dependence of the rate of change of doppler redshift plotted against the gravitational redshift. The ordinate is in units of change of redshift per s., calculated for a central mass of 10^{11} Mo.

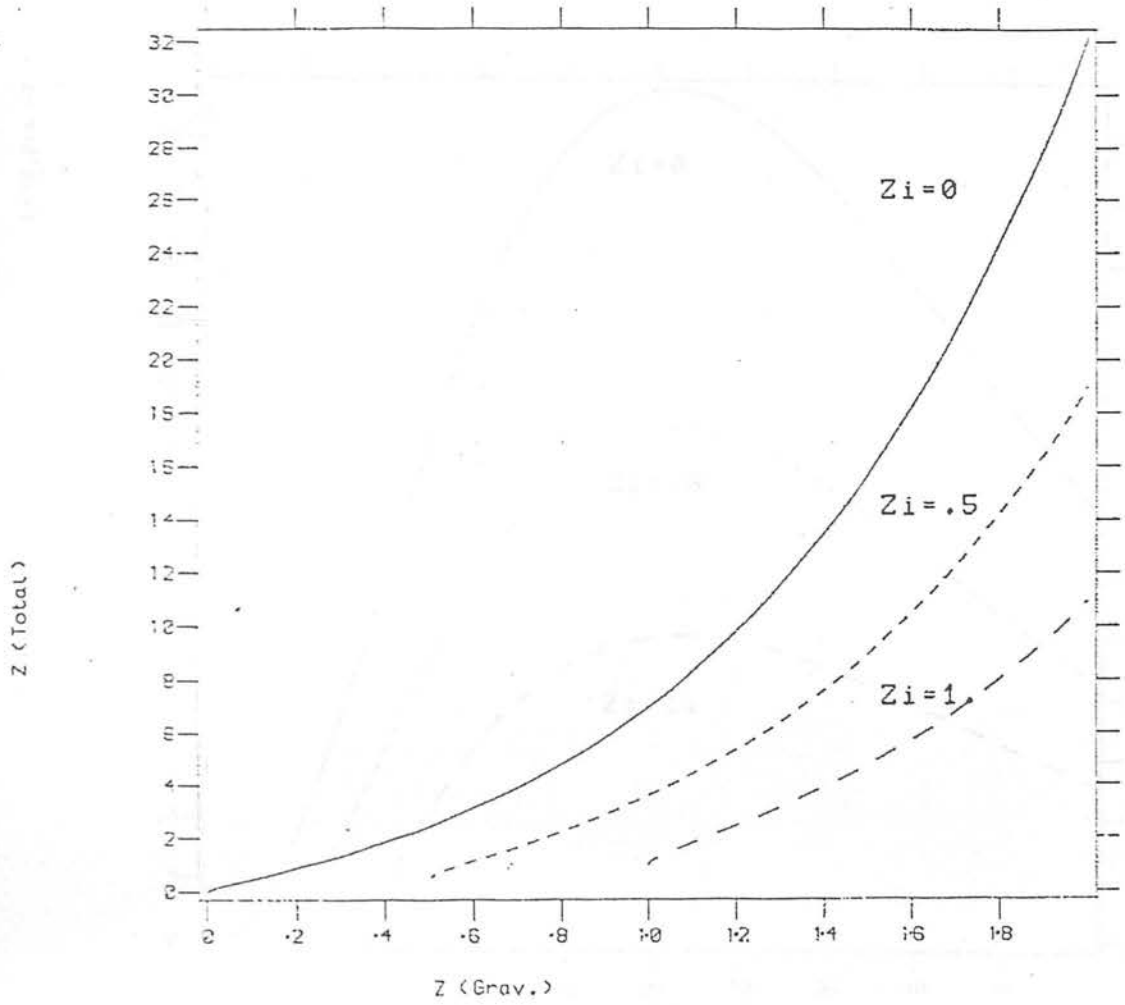

Figure 5.3 The total redshift, gravitational and doppler components combined, is shown as a function of the gravitational redshift.

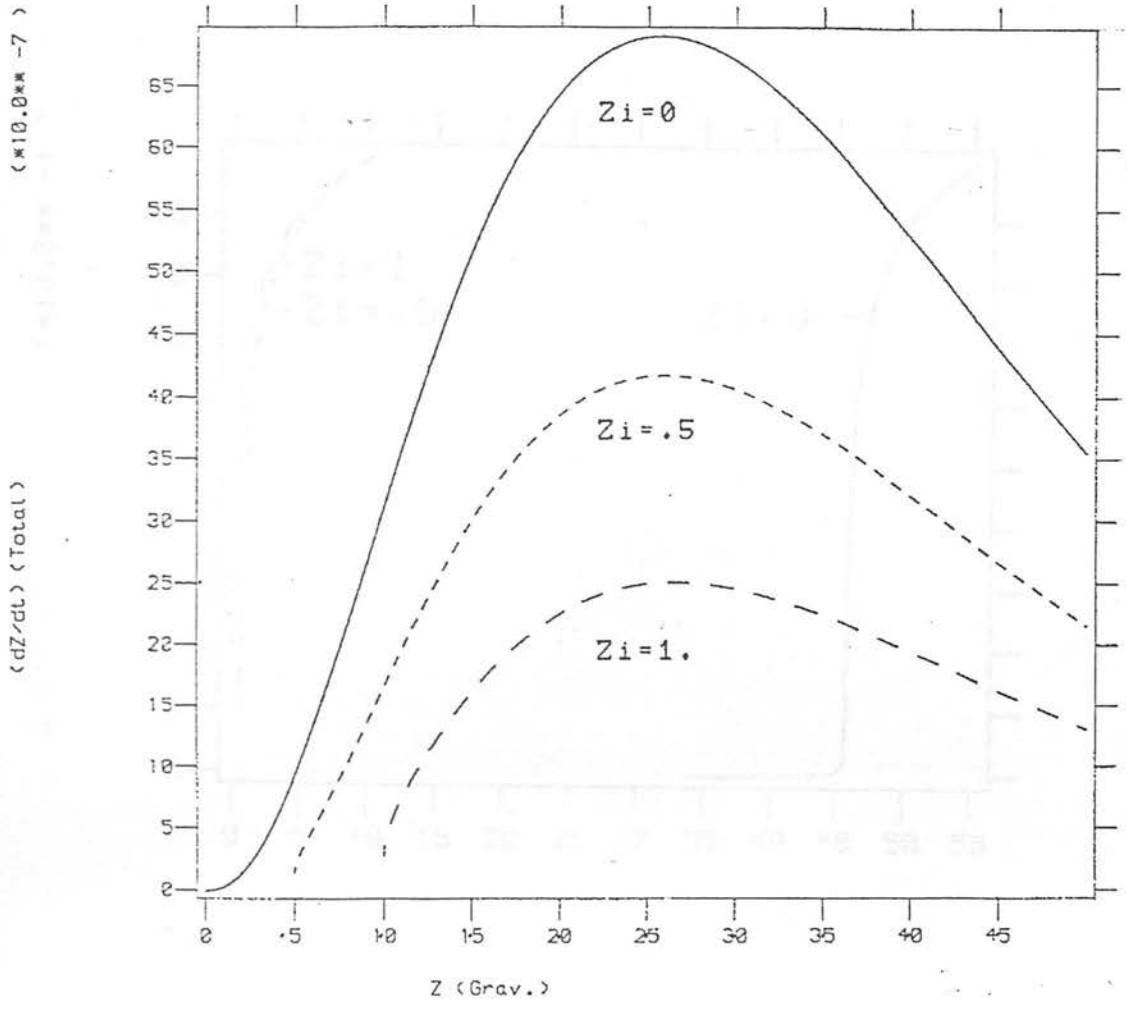

Figure 5.4 The dependence of the rate of change of total, gravitational plus doppler, redshift plotted against the gravitational redshift. The ordinate is in units of change of redshift per s., calculated for a central mass of 10^{11} Mo.

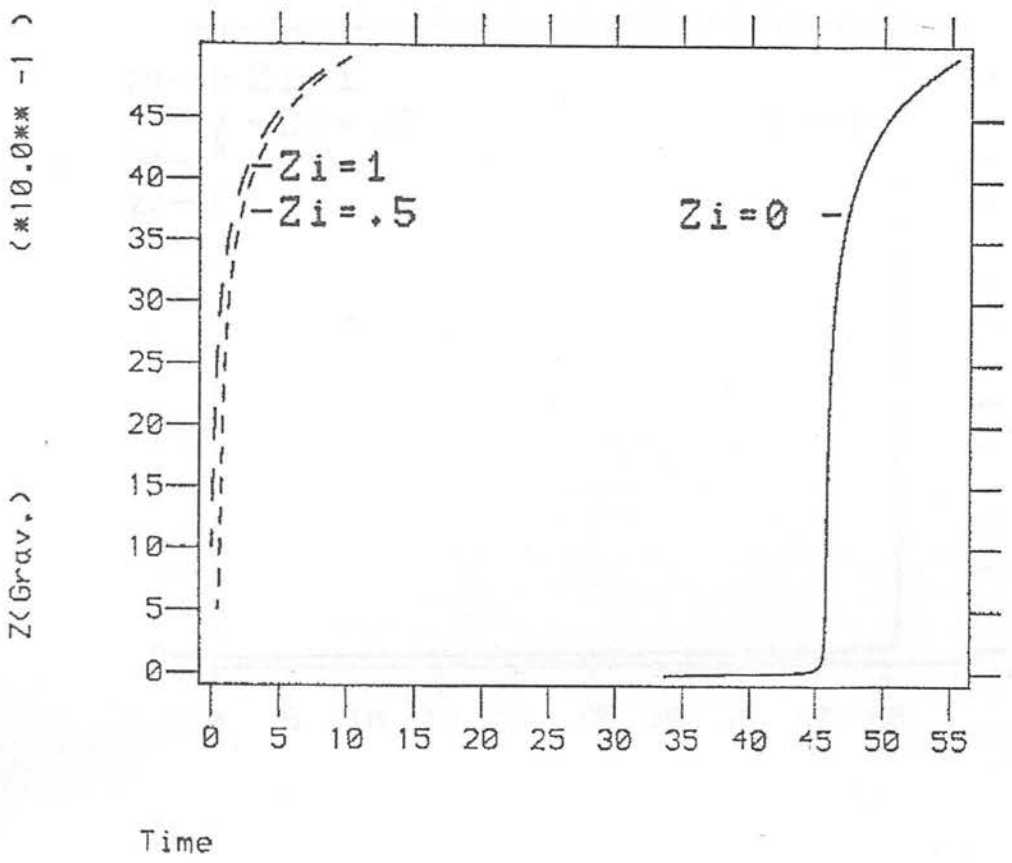

Figure 5.5 A graph of the gravitational redshift, equivalent to an inverse radial separation of the test particle and central body, plotted as a function of time. The zero point (t = 0) being taken from the point when the Z = 0.001. The abscissa is in years since release.

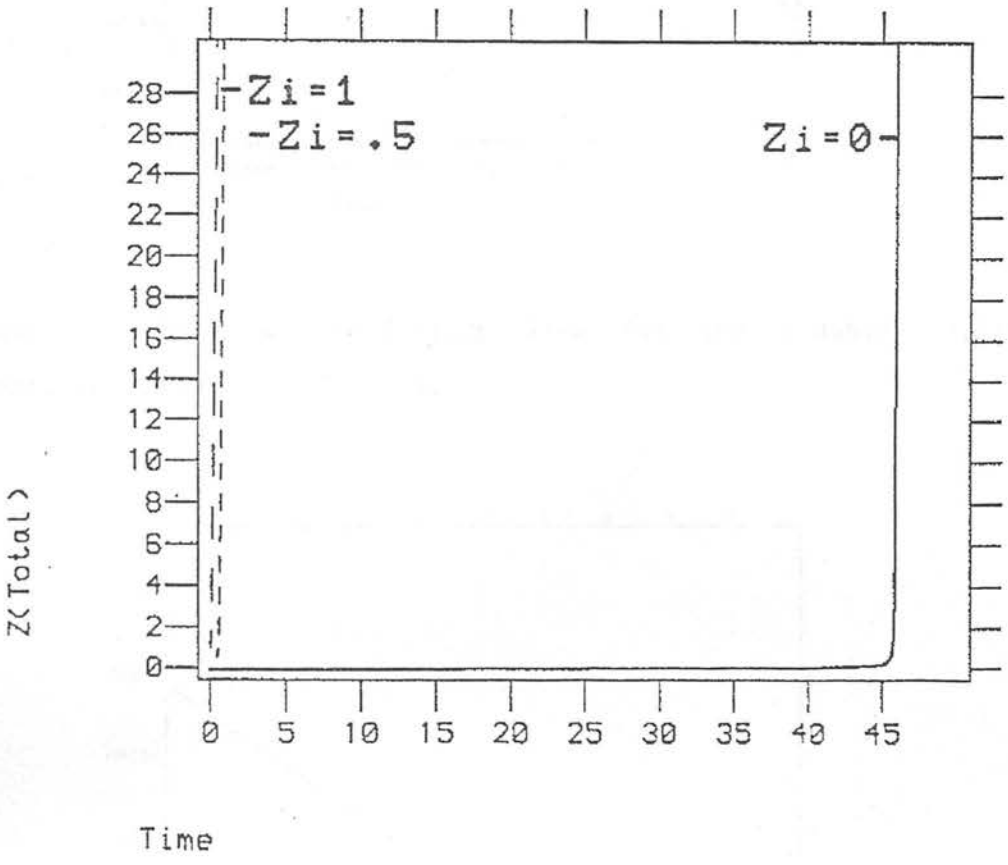

Figure 5.6 A graph of the total redshift as a function of time. The definitions are as for Figure 5.5.

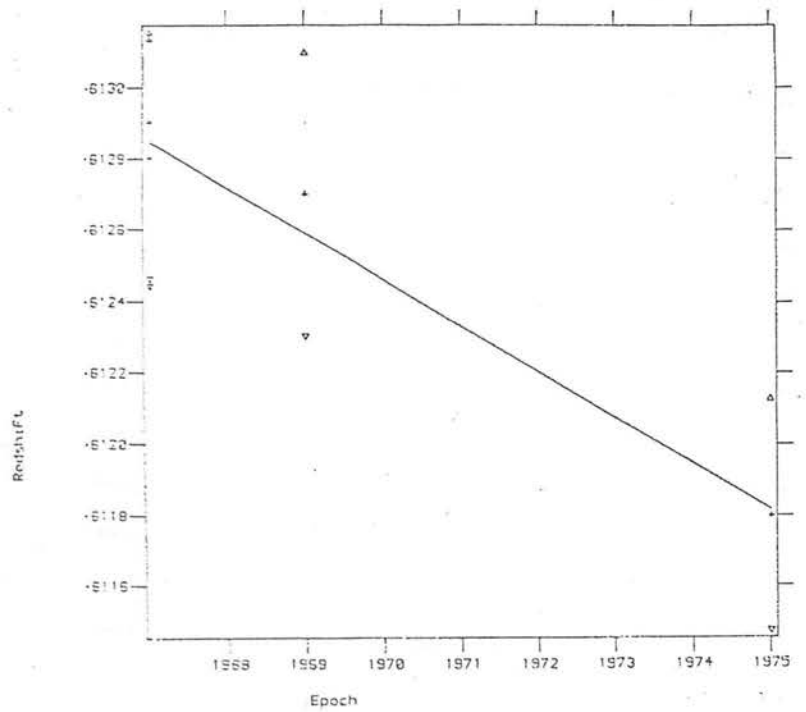

Figure 5.7a Data and best fitting line for the redshift 0.613 absorption system in 0058+019.

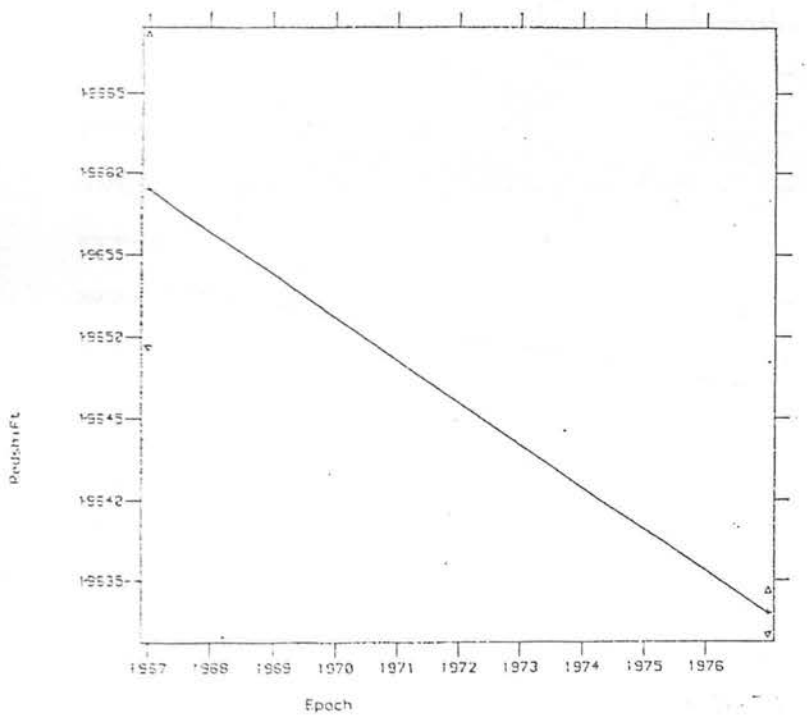

Figure 5.7b Data and best fitting line for the redshift 1.965 absorption system in 0119-046.

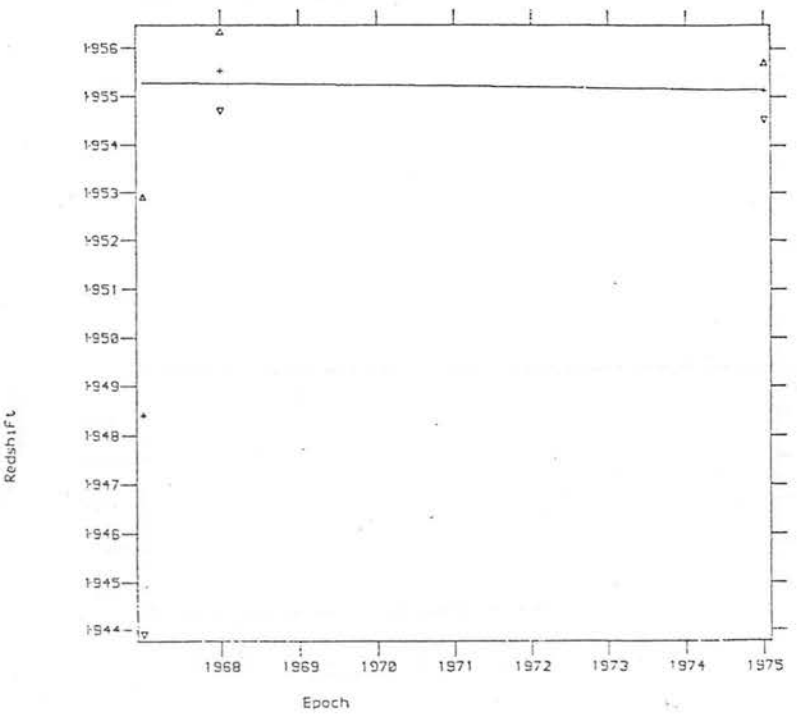

Figure 5.7c Data and best fitting line for the redshift 1.955 absorption system in 0237-233.

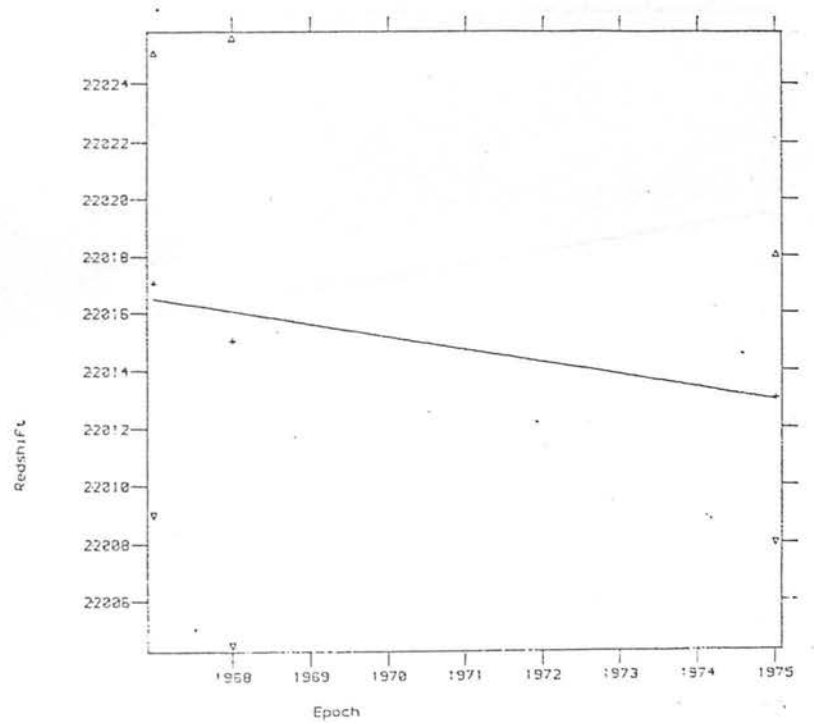

Figure 5.7d Data and best fitting line for the redshift 2.201 absorption system in 0237-233.

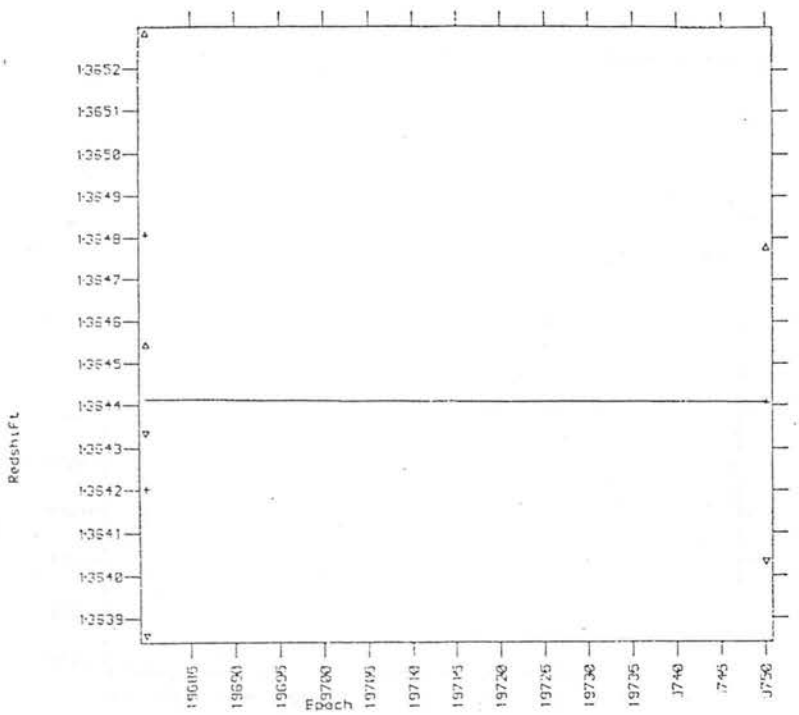

Figure 5.7e Data and best fitting line for the redshift 1.364 absorption system in 0237-233.

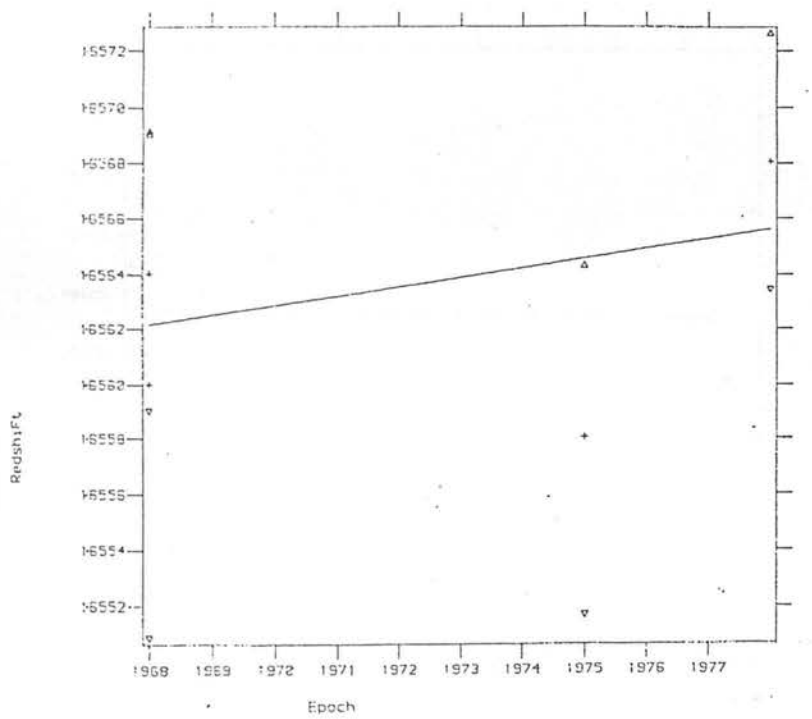

Figure 5.7f Data and best fitting line for the redshift 1.656 absorption system in 0237-233.

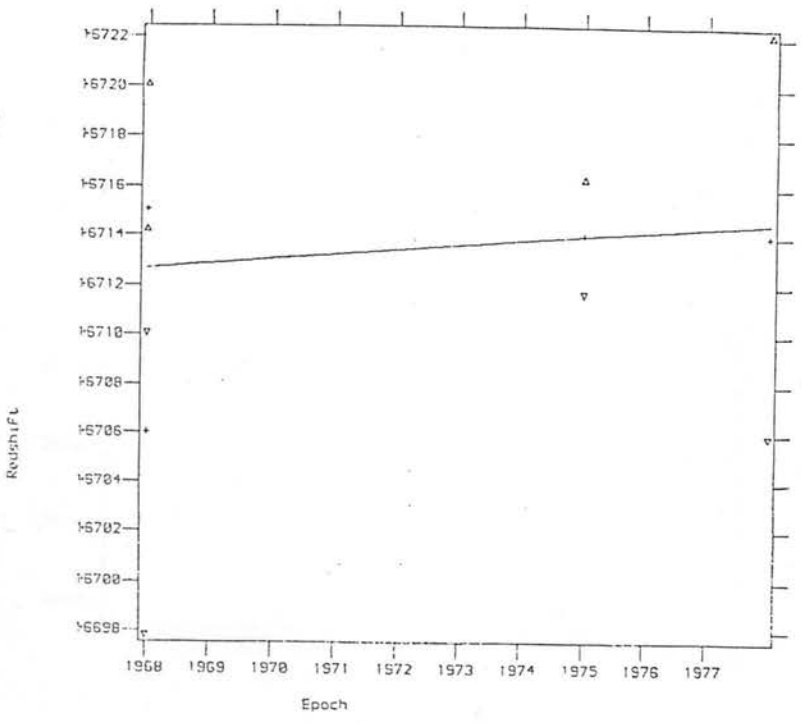

Figure 5.7g Data and best fitting line for the redshift 1.671 absorption system in 0237-233.

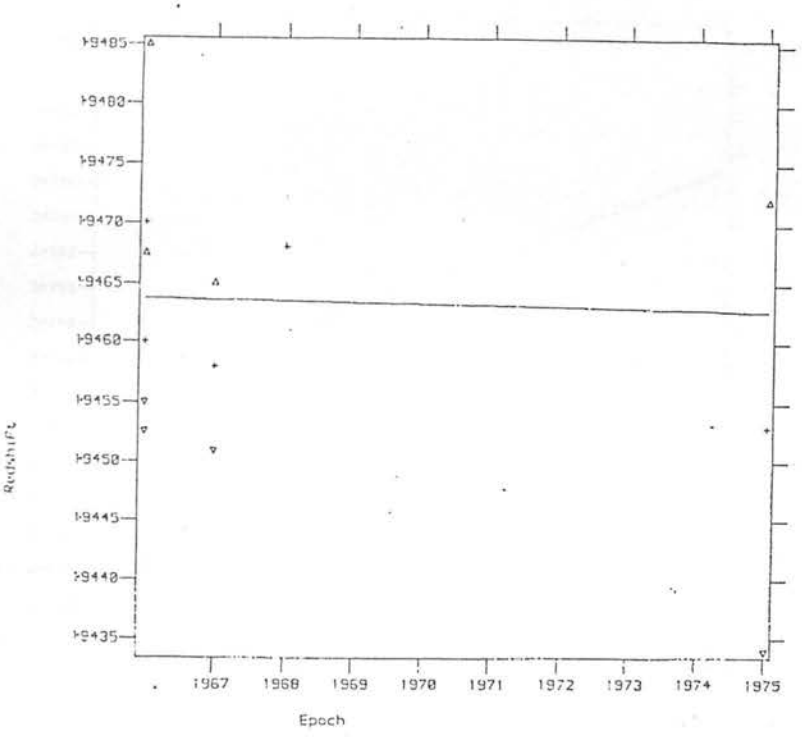

Figure 5.7h Data and best fitting line for the redshift 1.964 absorption system in 0802+103.

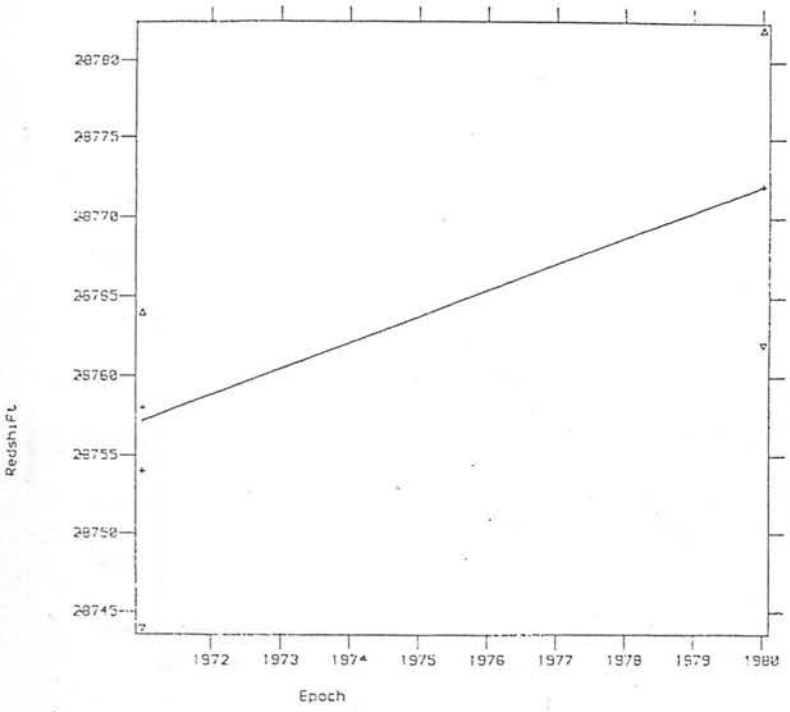

Figure 5.7i Data and best fitting line for the redshift 2.875 absorption system in 0805+046.

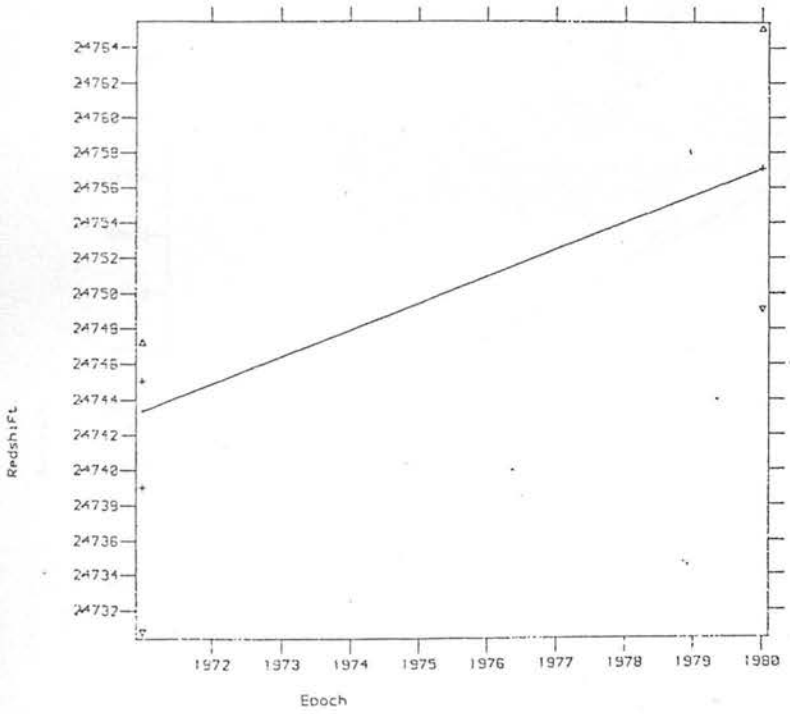

Figure 5.7j Data and best fitting line for the redshift 2.474 absorption system in 0805+046.

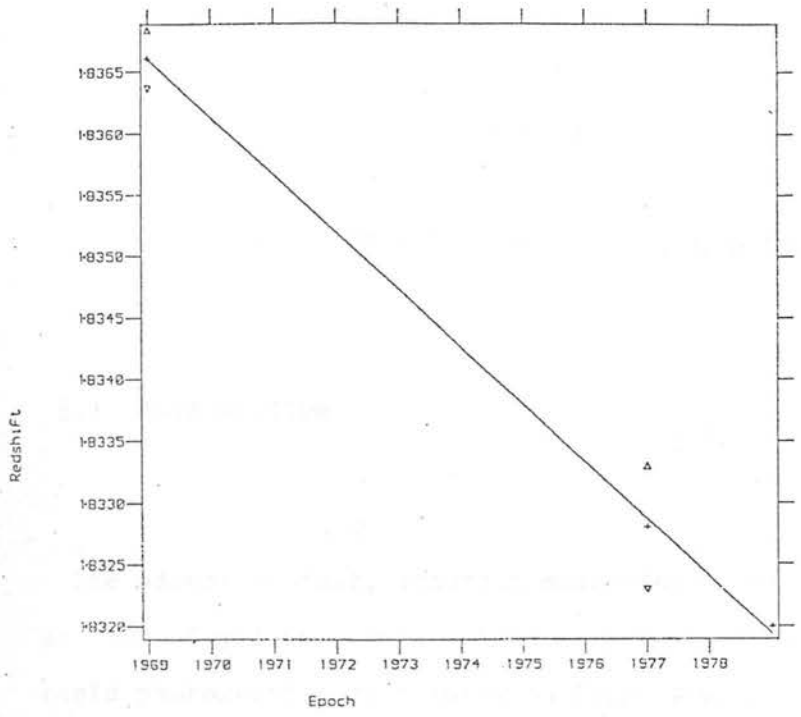

Figure 5.7k Data and best fitting line for the redshift 1.837 absorption system in 1256+357.

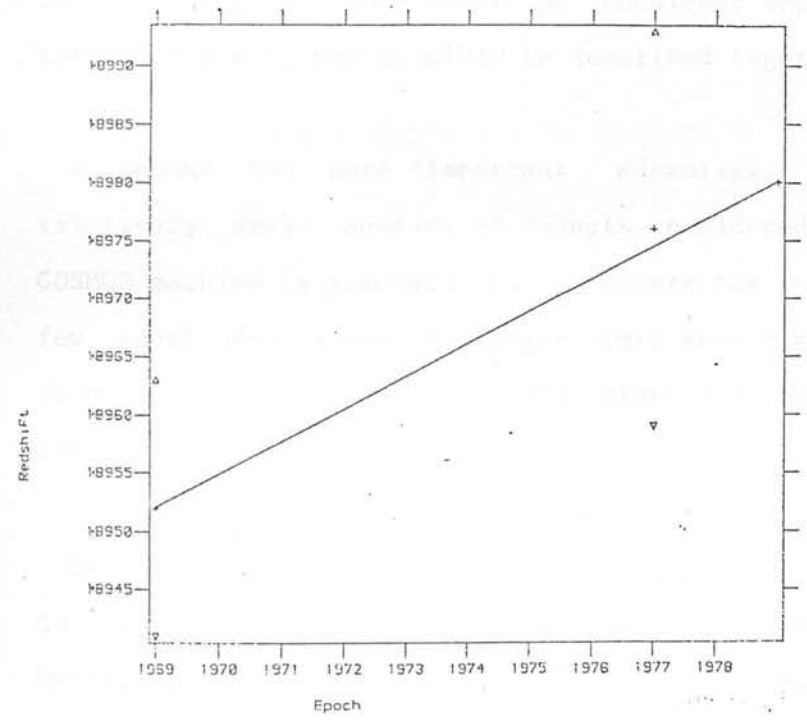

Figure 5.71 Data and best fitting line for the redshift 1.895 absorption system in 1256+357.

CHAPTER VI

PHOTOGRAPHIC PHOTOMETRY OF QUASAR CANDIDATES

6.1 INTRODUCTION

The advent of fast, accurate measuring machines such as COSMOS at the Royal Observatory Edinburgh has led to the possibility of rapid photographic photometry on large samples of objects. It was thus a natural extension of the positional work using COSMOS described in Chapter III to use the same data to obtain magnitudes for previously uncalibrated samples of quasar candidates. Only two out of the five fields ($01^h\ 12^m\ -35^\circ$ and $01^h\ 40^m\ -40^\circ$) previously studied required such work. The techniques employed in each were identical and so may sensibly be described together.

A second and more important advantage, considering the relatively small numbers of objects considered here, is that the COSMOS machine is generally more accurate for images which are a few magnitudes above the plate limit than the more conventional techniques, such as using an Iris Diaphragm Photometer (Gilmore 1982).

Such a study is, of course, a necessary precursor of any attempt to derive the quasar number/ magnitude/ redshift relation. Unfortunately, because of the lack of redshift information a complete study is not possible as yet, though it is hoped to extend the work when more spectra become available. The simpler

and less informative magnitude distribution is possible to derive and is discussed later.

6.2 THE COSMOS MACHINE

This machine developed at the Royal Observatory Edinburgh (Stobie et al. 1979) performs measurements in two ways - Mapping and Image Analysis Modes (MM and IAM respectively), though only the latter will be considered hereafter.

The plate is scanned, raster fashion, by a light beam from a Cathode Ray Tube. The fraction of the light which is transmitted through the plate is recorded by a photometer. In such a system measurements are most naturally made in transmission space, the number of discrete transmission values permissible being limited by digitisation to 128. These may be converted into intensities by means of a transformation calibrated by previous measurement of the plate stepwedges. In practice, the intensity is expressed in terms of the Baker Density in the form -

$$\log(I(i)) = \gamma * \log\left\{ \frac{Tc - Tb}{T(i) - Tb} - 1 \right\} + \text{constant} \qquad 6.1$$

where Tc is the transmission level of clear plate, Tb is a machine constant, T(i) is the measured transmission level in the "i"th pixel and γ is the slope, or contrast, of the characteristic curve.

In IAM only those pixels which are above a set threshold, expressed as a percentage above the local sky background intensity, are recorded. This pixel map is subsequently reduced by COSMOS Image and Data Processing software to produce a list of

images, together with defining parameters, for the user. In this reduction a lower area cut is applied so that only images consisting of more than a given number of pixels are output, thus removing most of the grain noise from the final data.

The parameters supplied for each image are postion, size, shape and orientation, which are given in both intensity weighted and unweighted forms. In addition and most importantly for this work are the magnitude parameter, M(I), and the local value of the background sky intensity, Isky, are listed. M(I) is defined as -

$$M(I) = -250*\log\{\sum_{i}(I(i)-Isky)\} \qquad 6.2$$

Here I(i) is the intensity in the "i"th pixel as given by Equation 6.1 and the summation is performed over the image. It is, unfortunately, not possible to simply convert M(I) into magnitude for two reasons. Firstly, because of image saturation at bright magnitudes, the slope of the M(I)/magnitude relation changes from the expected 100 to ~ 50 (Reid and Gilmore 1982). The magnitude at which this occurs differs from plate to plate depending upon the exposure, seeing conditions etc.. In addition, the use of a thresholded intensity, ie. the total intensity in the image above the threshold, has the effect that at faint magnitudes proportionally greater and greater fractions of the image flux are lost. This will also modify the slope of the M(I)/ magnitude curve. In order to derive reliable magnitudes from the COSMOS data, the form of this relation must be found empirically from a previously calibrated magnitude sequence within the measured area (cf. Section 6.3).

The second problem is that the M(I) parameter must be corrected for sensitivity variations across the measured area, which are common with J plates (cf. Campbell 1981). In principle this is a simple matter. It is assumed that the sky is uniform so that any

changes in the background across the plate are sensitivity variations. Dividing the pixel (sky subtracted) intensities by the local sky intensity will thus remove the point to point variations and "flat field" the data -

$$M'(I) = -250*\log\{\sum_{i}((I(i) - Isky)/Isky)\} \qquad 6.3$$

Examination of Figures 6.1 and 6.2 show that once flat fielded the M(I) parameter is then very stable across the plate and that any position dependent parameter shifts are only at the one standard deviation level. Hereafter, all references to the COSMOS magnitude parameter are to the flat fielded version.

6.3 CALIBRATION OF COSMOS DATA

Close to, but just outside, the edge of the COSMOS data in both fields are previously determined stellar magnitude sequences. Although both of these lie in the vignetted region of the plate the level of vignetting is small, ~ 5% (Dawe 1981) and so does not appreciably affect the results. Considerably more serious is the "Malin Effect", which is a sensitivity variation across the plate. This is probably caused by water vapour desensitizing the emulsion. As air currents circulate more freely and hence bring more water vapour into contact with the plate at the edges than at the centre the desensitizing is non - uniform (cf. Campbell loc cit.).

The most efficient and accurate way to calibrate the COSMOS data under these circumstances is to set up secondary photographic sequences within the measured area which are calibrated by the primary ones. This transfer was accomplished using the Iris Diaphragm Photometer at the Royal Observatory Edinburgh. The use

of such machines is described by Schaefer (1981).

The method employed was as follows, each of the primary standards was measured along with the Iris radius for a neighbouring area of sky. Point to point variations may be removed by dividing through by the local sky reading (Schaefer loc cit.). In practice, the noise in the measurement was as large as any true variations and so this is of limited importance. An identical process was then carried out on the stars in the photographic sequence and finally the primary sequence was remeasured, to check for systematic differences - none were ever found. Transformations can then be applied to calibrate the COSMOS M(I) parameter in terms of magnitude.

As in both fields the plates measured were UKST J plates (IIIaJ emulsion and Schott GG395 filter, a non - standard combination). Any magnitudes forthcoming will be in this passband. Because the primary sequences only have B and V magnitudes a transformation must be made from these into J(UKST). Colour equations recently derived from UKST plates have been used (Blair and Gilmore 1982) -

$$J(UKST) = V + 0.72(B - V) \qquad 6.4$$

6.4 RESULTS

6.4.1 $01^h\ 12^m - 35^\circ$

The sample consists of 283 probable emission line and UV excess quasar candidates within the central 5 x 5.1 degree area measured by COSMOS.

The plate measured by COSMOS was a glass copy of a high quality Survey original, J6124. Figure 6.1 is a plot of the polynomial fit to the stellar ridge line (the locus of stellar images in a given parameter/ parameter space) in the log(Area)/ COSMOS Magnitude plane. This shows that the measure of this field is also of very high quality and any position dependent parameter variations are probably small. As the intrinsic characteristics of stars are invariant with respect to position on the plate any observed differences must be caused by field effects. Such plots cannot detect correlated errors in log(Area) and M(I) which would produce motions parallel to the ridge line. However, such problems are not common (Hewett 1982) but could be caused by background fog on the plate.

There are two photoelectric sequences for V < 20.7 in the Sculptor Dwarf elliptical galaxy (Hodge 1965; Kunkel and Demers 1977) which lies on the edge of the plate. The former consists of 14 stars, the latter of 17, though not all of these were measured as a number were too bright. Initially, these sequences were used separately to calibrate the Iris readings but both curves agreed so closely that they were combined. There were 6 stars common to both sequences of which two showed large, 1 - 2 magnitude, discrepancies in the quoted magnitudes (cf. Kunkel and Demers loc cit.) In both cases the values given by Kunkel and Demers were considerably closer to the mean relation between Iris reading and magnitude, so that these were accepted in preference to those of Hodge.

The J magnitude/ Iris calibration curve is shown in Figure 6.3, the data of Hodge (loc cit.) being the closed circles, those of Kunkel and Demers (loc cit.) are the open ones. These data have been fitted by a least squares minimization procedure with a second order polynomial of the form -

$$J(UKST) = -1.59\times10^{-5}\,Iris^2 - 2.92\times10^{-2}\,Iris + 22.79 \quad 6.5$$

This curve was defined by 22 standards. The rms. scatter about the line projected in the J direction was 0.15J. Using this empirical relation, J magnitudes for the photographic sequence were estimated by interpolation.

It is now possible to create an M(I)/J magnitude calibration curve using a photographic sequence totalling 62 stars, which was set up 30 arc - minutes distant. A finding chart is shown in Figure 6.4, with magnitudes derived from Iris measurements in Table 6.1. The relationship is illustrated in Figure 6.5 and has been fitted with a cubic spline, with two interior knots at M(I) = -350 and -490, shown by the arrows. The rms. deviation about the mean M(I)/ J curve was ~ 0.15J. This gives an estimated total rms. deviation in the final magnitudes of ~ 0.2J. Transformations of the known quasar M(I) values to J magnitude can now be made by interpolation from this curve.

The lack of other magnitude standards in the COSMOS measured area leaves open the possibility of systematic errors in the quasar magnitudes correlated with position on the plate. However, the magnitude histogram, Figure 6.6, for the quasar candidates compares well with previous estimates in differing fields discovered by the same technique (cf. Savage and Bolton 1979; Section 6.4.2). Also, the magnitude distributions derived in each of the four quadrants of the COSMOS area agree closely. Consequently any spatial effects are probably not larger than the random measurement errors. The stability of the COSMOS parameters, coupled with the constancy of the sky Iris radii between the photoelectric and photographic sequences, tend to confirm this conclusion.

A number of quasar candidates, 7 in total, which were obviously merged in the COSMOS data, were then removed, the revised magnitude distribution being shown in Figure 6.7. Subsequent examination on the Schmidt plate of the objects in the bright tail remaining in this diagram has shown that the majority are also probably merged images. Detection of such bright quasars on a deep plate is unlikely because of saturation of the spectrum which renders the emission features invisible, though a strong UV excess may still be recognised.

Eight quasar candidates do not have calculated J magnitudes because they are below the faint end of the photoelectric sequence, ie. J(UKST) > 20.8. The low magnitudes are due to these objects being extended and so suffering more severely than stellar images from thresholding within COSMOS. It is highly unlikely that objects which were actually this faint could be seen on the prism plate.

6.4.2 $01^h\ 40^m - 40^\circ$

The 293 quasar candidates used in Chapter III were supplemented in this study by an extra subset of UV excess objects, though the probability of these being true quasars is relatively small, ~ 20 - 30%. The complete sample then consisted of 689 objects within the COSMOS measured area of 4.7 x 5.2 degrees.

In this field Hawkins (1982) has set up an electronographic sequence extending to V ~ 23. This is very much fainter than is required or is possible to measure on the Schmidt plate. A lower limit of V = 21.8 was placed upon the magnitudes of the stars measured. The plate material used was a glass copy of the Survey quality original J3593. In total 25 electronographic standards

were measured with the Iris Diaphragm Photometer, the resultant Iris Radius/ J magnitude diagram is shown in Figure 6.8. This relation was fitted with a quadratic function -

$$J = 4.54\times10^{-5}\,\mathrm{Iris}^2 - 4.19\times10^{-2}\,\mathrm{Iris} + 22.72 \qquad 6.6$$

the rms. scatter in J being ~ 0.2.

The photographic sequence was displaced by 30 arc - minutes from the electronographic one and contained 68 stars. A finding chart is given in Figure 6.9 with magnitudes determined from the Iris readings listed in Table 6.2. As in the previous field no significant variations were detected in the sky Iris reading from the primary to secondary sequences, the COSMOS data were also very stable, cf. Figure 6.2, the format being the same as for Figure 6.1. J magnitudes for the photographic standards were obtained by interpolation from Equation 6.6.

This enabled a M(I)/ J magnitude calibration to be calculated which is shown in Figure 6.10. These data have been fitted with a second order polynomial -

$$J = -4.76\times10^{-6}(M(I))^2 + 1.38\times10^{-2}M(I) + 22.40 \qquad 6.7$$

which gives rms. errors of ~ 0.15J. Thus, the combined estimated random error in the final magnitudes was ~ 0.25J. So, using Equation 6.7 it was possible to calculate the quasar J magnitudes given their M(I) values.

An examination of the quasar magnitude histogram, cf. Figure 6.11, shows that these objects have a very similar distribution to those in the previous field. Merged and extended images have been removed as before. In this case, however, it is fortunate that the COSMOS area contains 8 CTIO (Hoag and Smith 1977) and Curtis

Schmidt (Smith 1975) quasars. Six of these have independently been discovered here. Due to spectroscopic observations on large telescopes each have reliable continuum magnitudes (Osmer 1980; Osmer and Smith 1980). It is, thus, possible to compare the magnitudes derived here with photoelectric measures.

Before any such comparison of the broadband J magnitudes obtained in this study with the photoelectric ones corrections must be made for the inclusion of emission lines in the former. In order to estimate the effect of this it is noted that the spectral response of the IIIaJ emulsion and GG395 filter combination is well approximated by a rectangular profile (Gilmore 1982) of width L (~ 2400A). So, by the definition of Equivalent Width, we have that the effect of an emission line, Equivalent Width = W, on the broadband flux is -

$$I(B) = I(C)(1 + W/L) \qquad 6.8$$

where I(B) and I(C) are integrated total broadband and continuum fluxes respectively. For each of the quasars in the CTIO and Curtis Schmidt surveys Osmer (loc cit.) and Osmer and Smith (loc cit.) quote the redshift and emission line Equivalent Widths. These data enabled the calculation of the total contribution within the J(UKST) passband of the emission lines. Table 6.3 lists these quasars, here W is the total emission line Equivalent Width within the J passband and m(C) the original CTIO or Curtis Schmidt photoelectric magnitude.

Before applying such corrections the magnitude system must be converted into J(UKST). It has been shown (Oke 1974) that the CTIO magnitudes are very close to visual ones and hence given the quasar (B - V) colour J(UKST) may be calculated from Equation 6.4. A mean value for (B - V) of 0.1 (Cheney and Rowan - Robinson 1981) has been adopted which gives the revised J(UKST) magnitudes listed

in Table 6.3, as m(CL). It is now possible to compare the photoelectric magnitudes with those determined in this study. These are listed in Table 6.3 as m(J). The comparison is also shown in Figure 6.12. The best fitting line has been constrained to have an intercept of zero. The slope of the line is, as would be expected, unity and the rms. scatter is 0.25J. It is, therefore, very unlikely that the photographic quasar magnitudes are systematically in error.

In order to increase the available data on those objects outside the COSMOS area ~ 400 quasar candidates have been measured on the Iris Diaphragm Photometer by Mr. X. T. He. A calibration of these data has also been made, the Iris/ J magnitude relation being shown in Figure 6.13. The best fitting line was determined by a least squares technique and has the form -

$$J = 5.38*10^{-5}*Iris^2 - 4.34*10^{-2}*Iris + 23.44 \qquad 6.9$$

Comparison of Equations 6.6 and 6.9 show that the agreement is close considering possible variations between different sets of Iris measures. The resultant magnitude distribution is given in Figure 6.14, which closely resembles that for the COSMOS data. A further 11 CTIO and Curtis Schmidt quasars lie in this region, cf. Table 6.4. The format is the same as in Table 6.3, and a magnitude comparison identical to that above has been applied. The data and best fitting straight line, again constrained to have an intercept of zero, are shown in Figure 6.15. The slope of the line is again unity, although the rms. error has increased to 0.35J. This is 50% worse than the scatter about the mean COSMOS relation and is an example of the increased accuracy possible at faint magnitudes with the COSMOS machine.

Closer examination of Figures 6.12 and 6.15 shows that two points in particular (those marked by arrows) are significantly, >

2σ, removed from the mean line. These are Curtis Schmidt quasars 94 and 88 respectively. It is not obvious in either case why this difference is so large. Presumably it is either caused by intrinsic variations in the objects or is the product of random errors in the photometry.

6.5 CONCLUSIONS

It has been possible, using transferred sequences, to calibrate the COSMOS magnitude parameter in terms of UKST J magnitude. The rms. accuracy of this final magnitude is estimated to be 0.25 J. From considerations of the COSMOS parameter/ parameter plots and from comparisons of a number of photographic and photoelectric magnitudes it appears that these magnitudes are stable over the plate.

The derived magnitude histograms for the quasar candidates are similar to previous distributions in other fields searched by the same technique and the data are of great value for future studies of the quasar space distribution.

TABLE 6.1

Photographic Sequence for $01^h\ 12^m-35^\circ$

No.	J Mag.	No.	J Mag.
1	14.34	32	19.32
2	13.70	33	20.00
3	14.60	34	18.75
4	14.49	35	19.90
5	14.53	36	20.29
6	14.93	37	18.62
7	14.86	38	18.85
8	15.73	39	18.85
9	15.26	40	20.16
10	16.02	41	18.39
11	15.26	42	19.77
12	16.06	43	18.59
13	17.36	44	19.54
14	17.19	45	20.67
15	17.26	46	19.22
16	16.77	47	20.51
17	16.66	48	20.88
18	17.29	49	18.69
19	20.38	50	19.97
20	19.09	51	19.38
21	17.43	52	20.19
22	18.01	53	20.41
23	17.46	54	19.58
24	18.89	55	18.85
25	20.38	56	19.32
26	20.13	57	19.09

27	20.44	58	20.44
28	18.11	59	19.48
29	19.09	60	20.41
30	18.25	61	19.41
31	18.85	62	20.13

TABLE 6.2

Photographic Sequence in $01^h\ 40^m - 40^\circ$

No.	J Mag.	No.	J Mag.
1	15.47	35	19.63
2	15.49	36	18.38
3	16.70	37	18.60
4	15.70	38	18.19
5	15.77	39	18.89
6	15.73	40	18.63
7	16.07	41	18.57
8	16.07	42	18.89
9	15.68	43	19.42
10	15.75	44	18.69
11	15.90	45	19.18
12	17.69	46	18.95
13	16.63	47	19.94
14	18.04	48	19.45
15	17.66	49	18.92
16	16.83	50	18.85
17	16.81	51	18.82
18	16.86	52	18.79
19	17.26	53	19.52
20	17.92	54	18.89
21	17.37	55	19.45
22	17.49	56	19.59
23	17.52	57	19.59
24	17.83	58	19.35
25	17.72	59	19.69
26	17.72	60	20.78

27	18.07	61	19.80
28	19.45	62	20.01
29	19.05	63	20.93
30	18.07	64	19.66
31	18.22	65	20.37
32	17.86	66	20.52
33	18.60	67	21.35
34	18.16	68	21.04

TABLE 6.3

Comparison of COSMOS Photographic and Photoelectic Magnitudes

No.	RA.	Dec.	Z	W	m(C)	m(CL)	m(J)
91	1 32 5.5	-39 56 25	2.21	200	18.6	18.5	18.6
92	1 32 53.3	-40 55 41	2.41	900	19.4	18.9	19.0
93	1 38 13.7	-38 8 10	2.87	400	17.6	17.4	18.0
94	1 49 17.9	-39 42 39	2.06	100	17.9	17.9	18.4
-73	1 31 48.4	-40 54 49	1.34	100	19.9	19.9	19.6
-74	1 32 9.6	-40 18 8	2.18	100	19.5	19.5	19.4

Negative Numbers are Curtis Schmidt Quasars.

TABLE 6.4

Comparison of Iris Photographic and Photoelectric Magnitudes.

No.	RA.	Dec.	Z	W	m(C)	m(CL)	m(J)
88	1 28 6.5	-41 8 52	2.38	350	18.7	18.5	19.2
89	1 30 50.5	-40 21 54	3.02	250	17.4	17.3	17.6
90	1 31 3.1	-40 27 35	1.48	100	19.0	19.0	19.1
-59	1 30 38.2	-41 37 56	1.32	150	19.7	19.7	19.3
-60	1 30 45.9	-40 25 49	2.16	100	19.2	19.2	19.0
-62	1 30 50.7	-40 38 13	2.39	300	19.0	18.8	19.1
-64	1 31 3.5	-40 27 23	1.48	100	19.0	19.0	19.1
-66	1 31 12.2	-41 32 19	1.55	200	20.2	20.1	20.0
-67	1 31 17.7	-41 23 26	1.24	100	19.7	19.7	19.8
-68	1 31 22.1	-40 11 16	1.90	200	19.8	19.7	19.4
-70	1 31 29.7	-40 8 15	1.65	200	20.0	19.9	19.4

Negative Numbers are Curtis Schmidt Quasars.

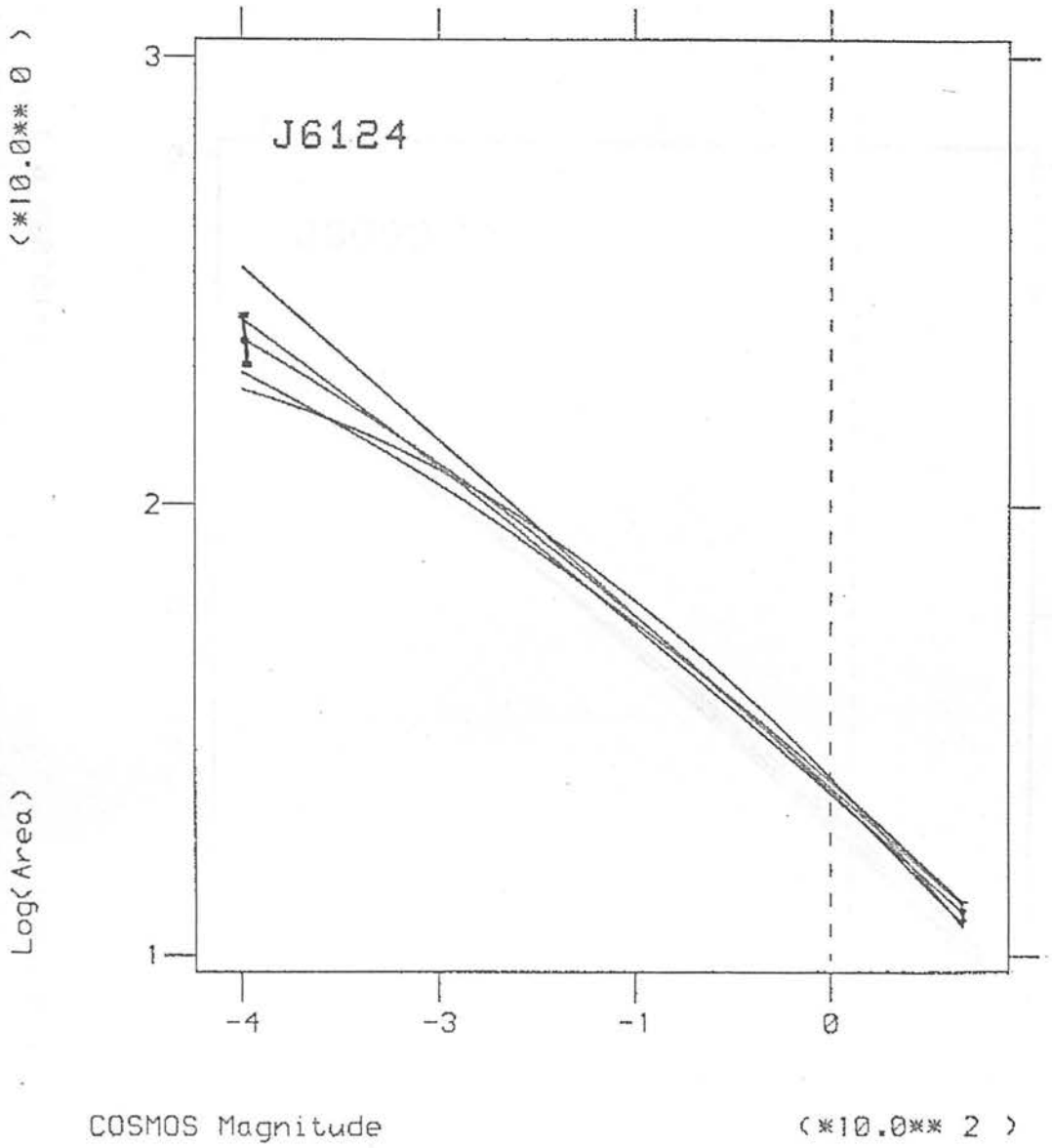

Figure 6.1 Polynomial fits to the stellar ridge lines in the M(I)/ log(Area) plane in five regions on the J6124 plate (the four corners and centre). The error bars are $\pm$ 1 sigma.

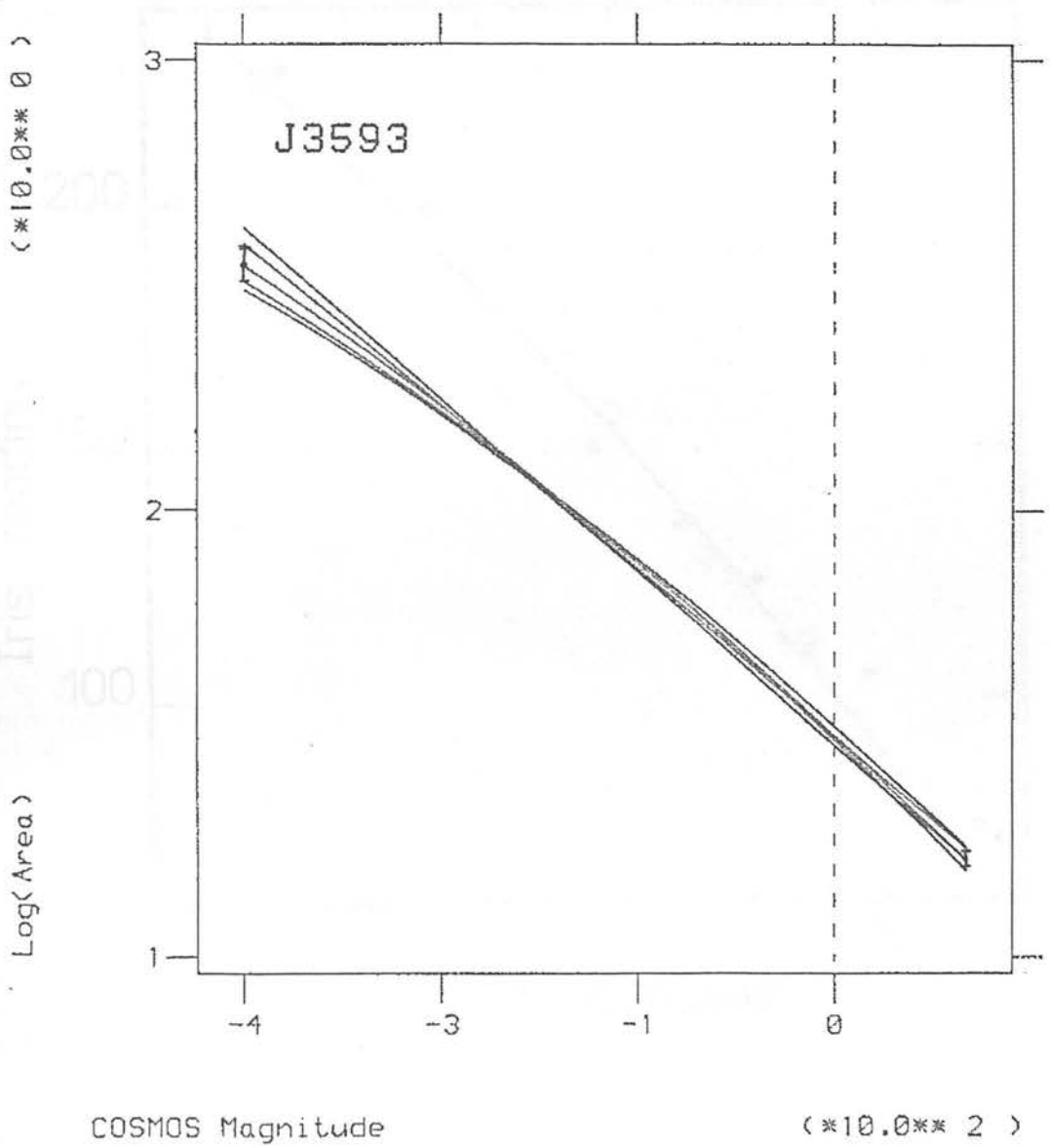

Figure 6.2 Polynomial fits to the stellar ridge lines in $01^h\ 44^m$ -40°. The definitions are as in Figure 6.1

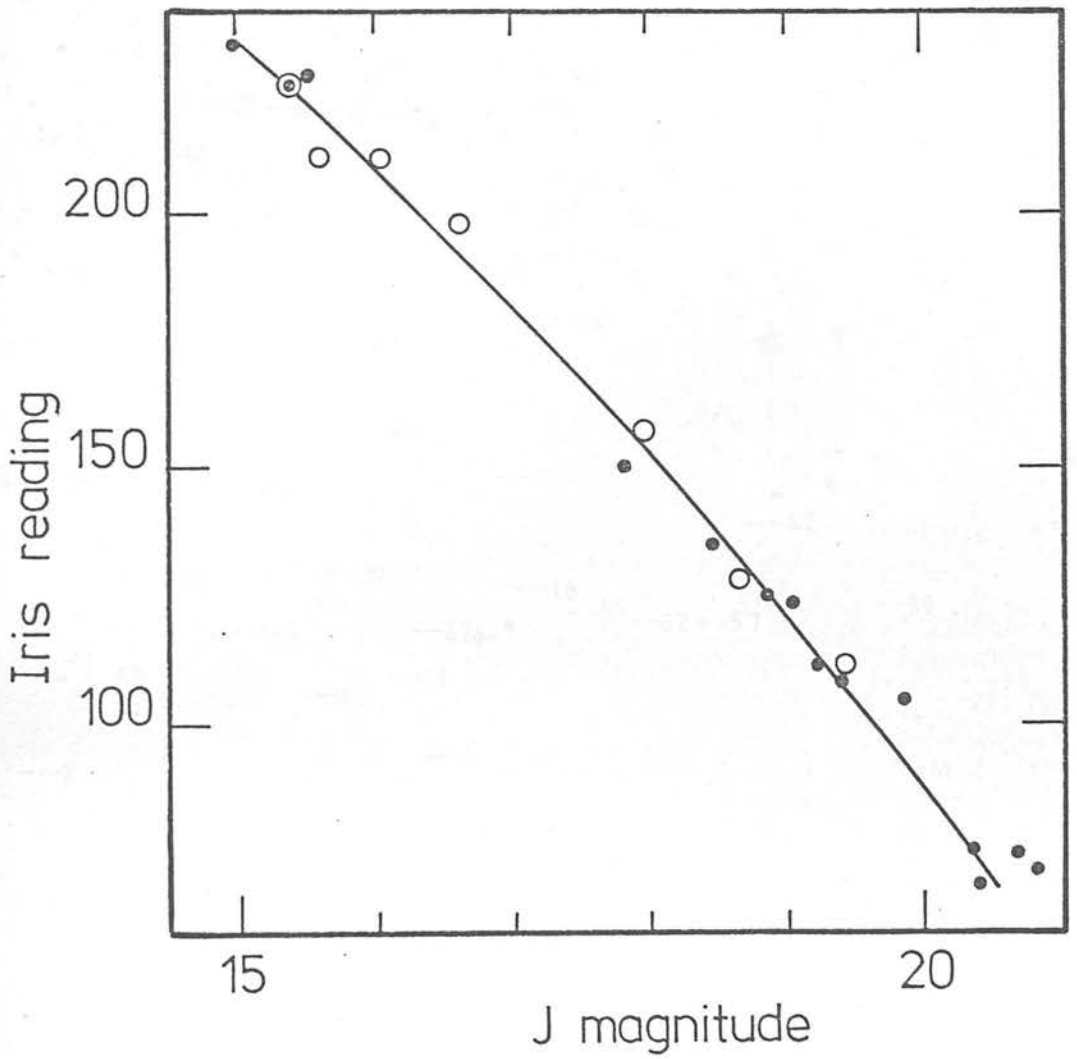

Figure 6.3 J magnitude/ Iris radius relation for the photoelectric sequences in the Sculptor Dwarf Elliptical. The data have been fitted with the quadratic function shown.

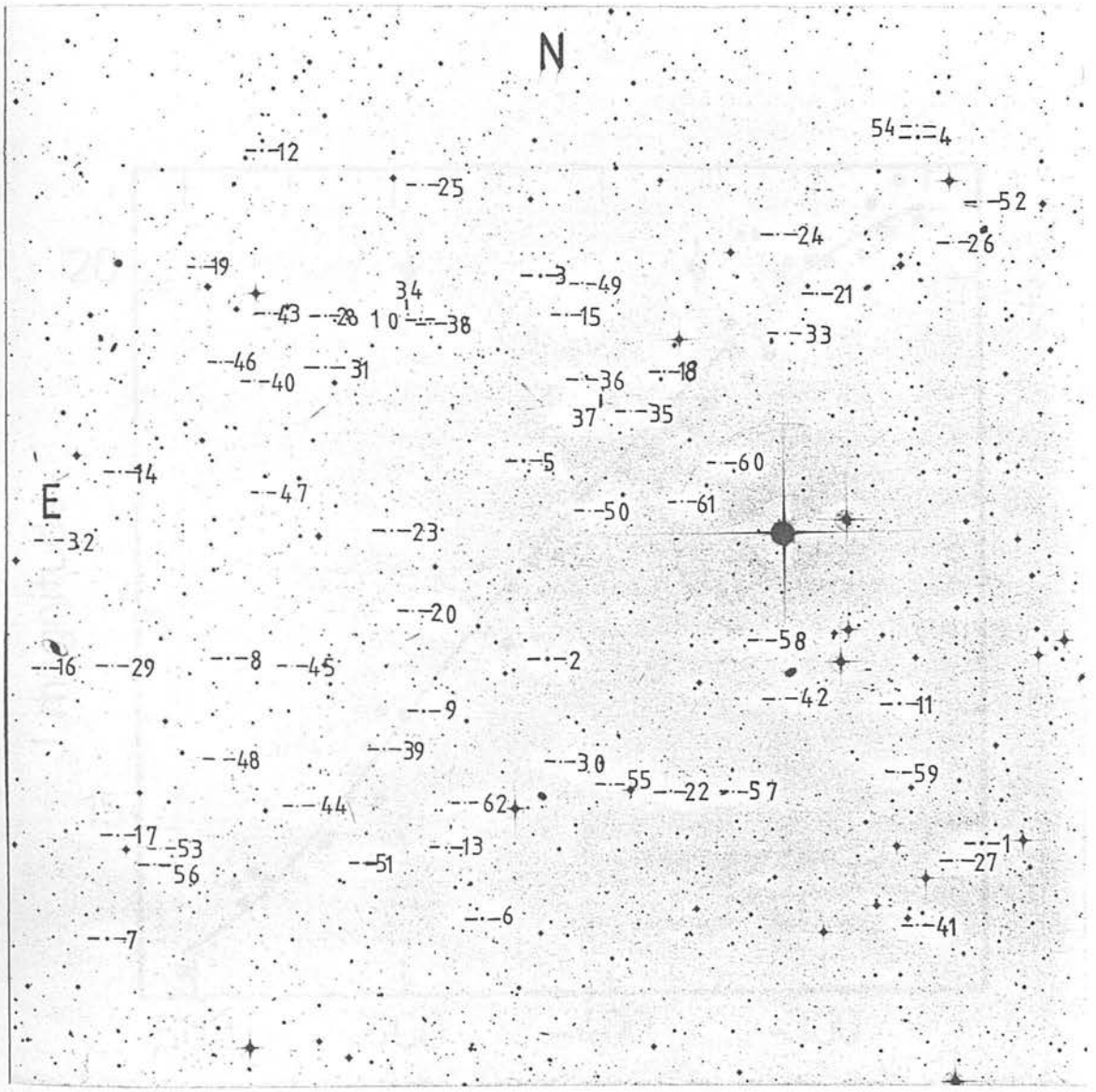

Figure 6.4 Finding chart for the photographic sequence set up in $01^h\ 12^m\ -35^\circ$ . . (Photograph courtesy of Photolabs, Royal Observatory, Edinburgh.)

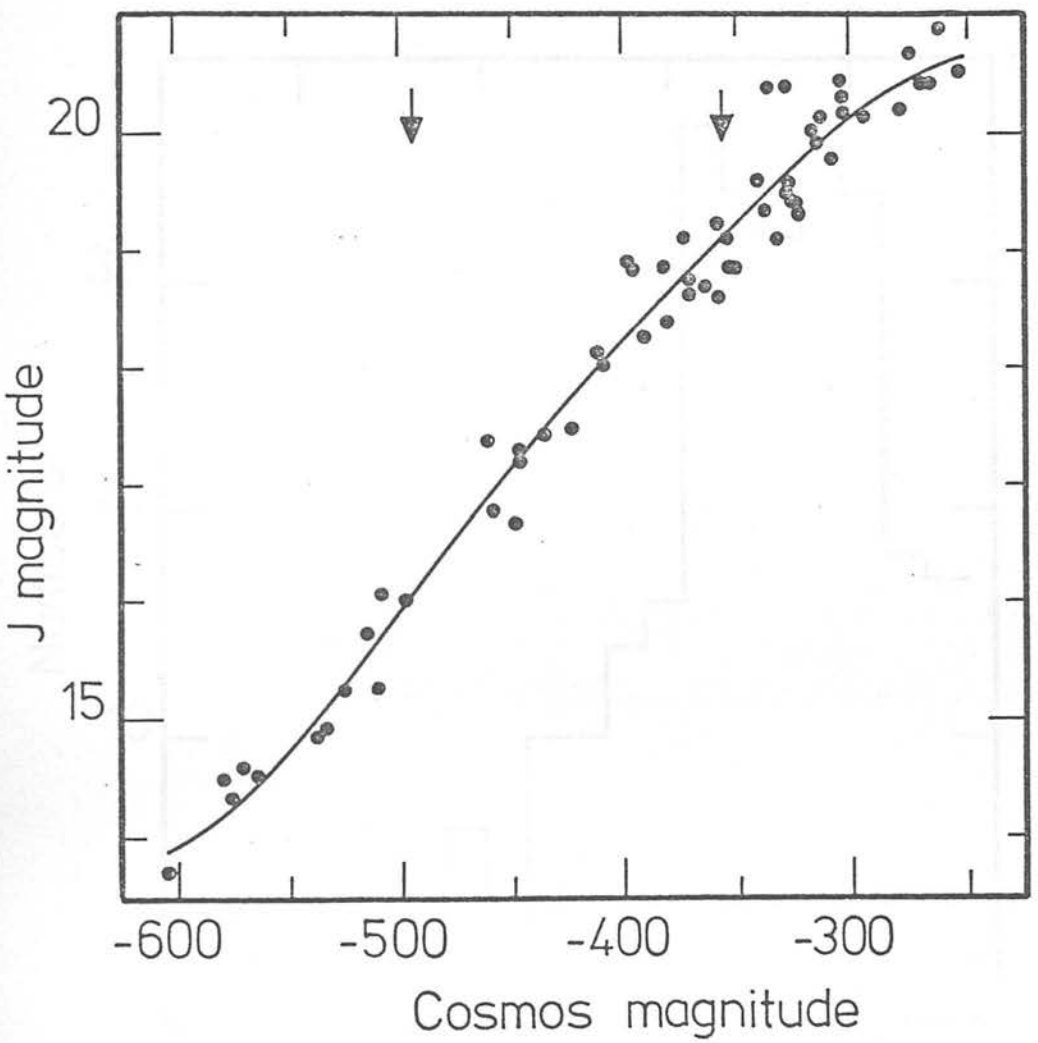

Figure 6.5 The relation between the sky corrected COSMOS magnitude and J magnitude for the photographic sequence in $01^h\ 12^m\ -35^\circ$. The data have been fitted with a cubic spline with two interior knots, marked by the arrows.

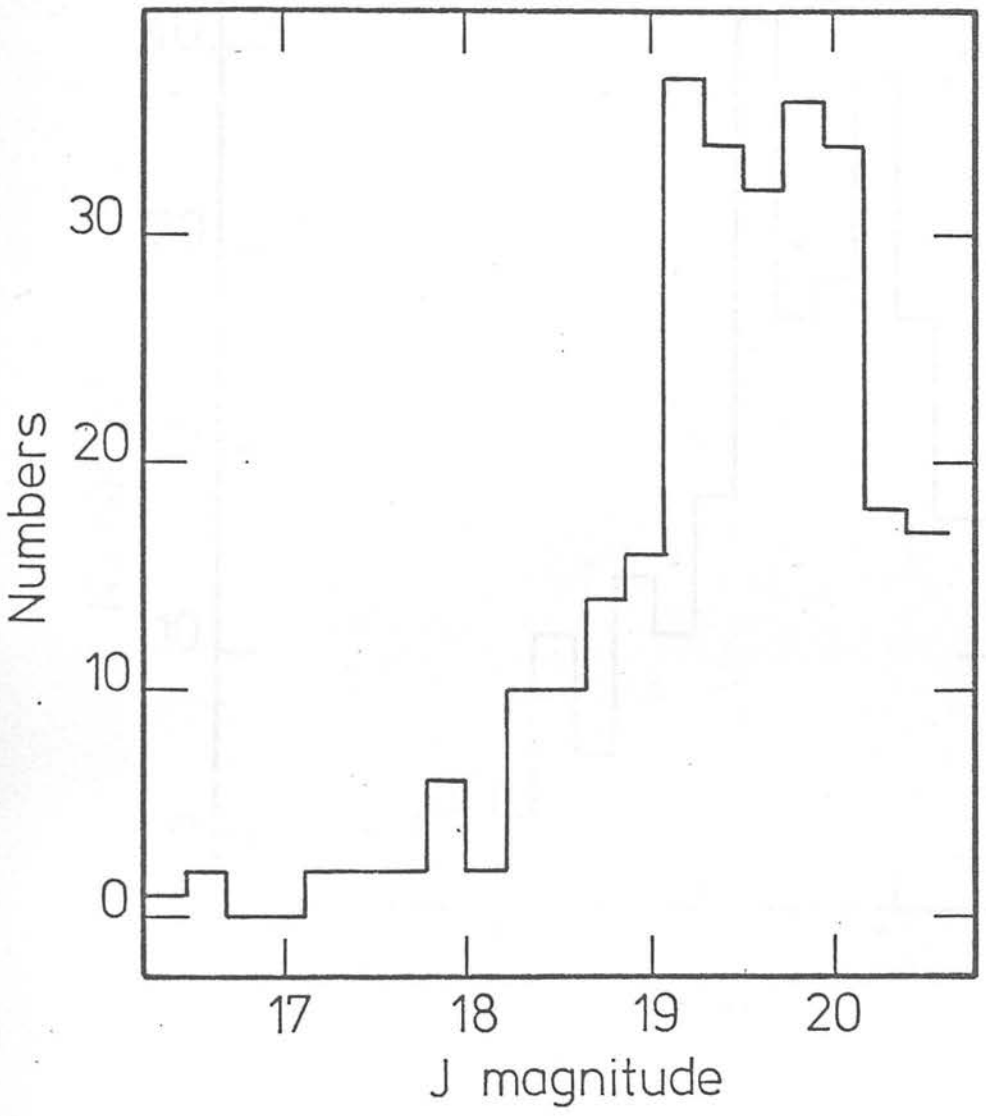

Figure 6.6 The distribution of quasar J magnitude in the $01^h\ 12^m$ -35° field.

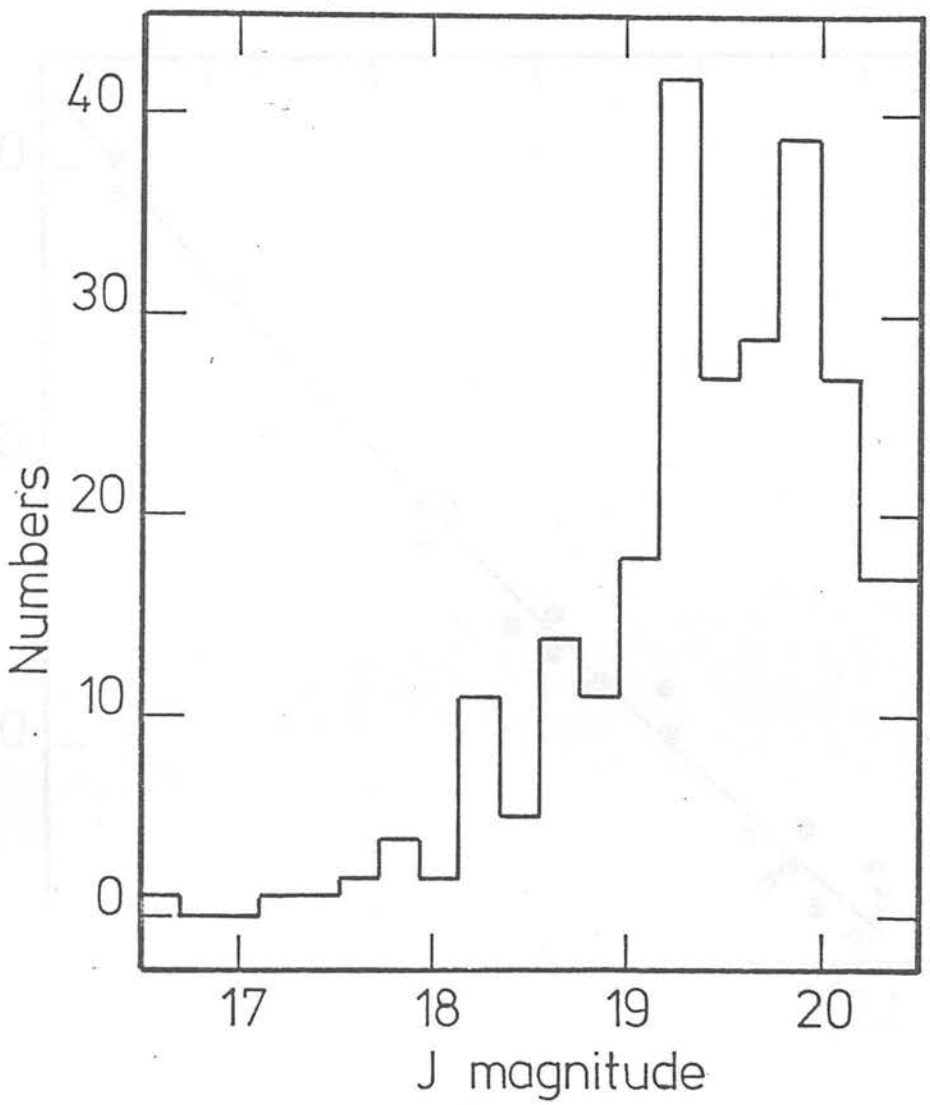

Figure 6.7 The J magnitude distribution for the quasars in the 01^h 12^m -35° field but with those known merged images removed.

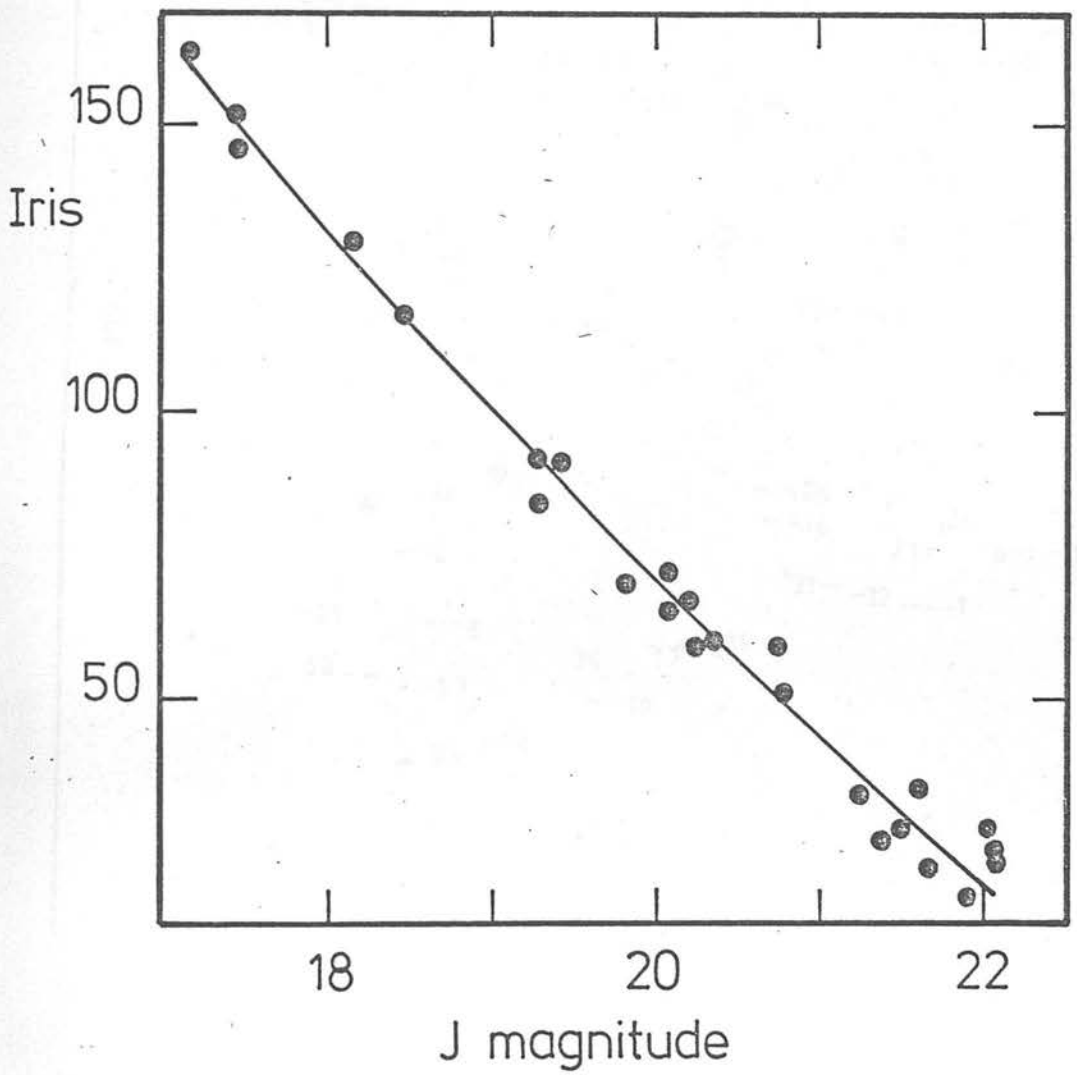

Figure 6.8 J magnitude/ Iris radius relation for the photoelectric sequences in the $01^{h}\ 44^{m}\ -40^{\circ}$ field. The data have been fitted with the quadratic function shown.

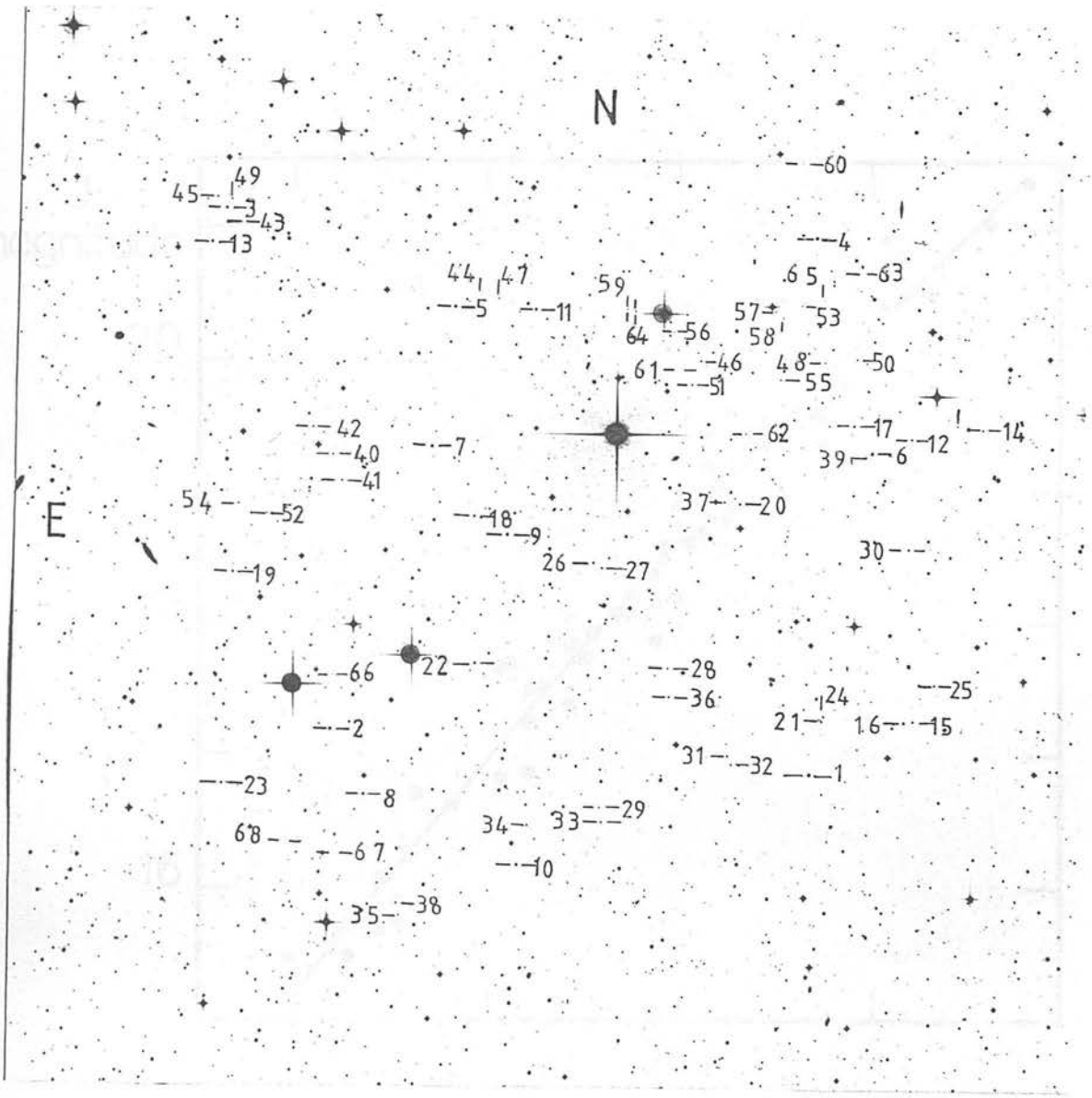

Figure 6.9 Finding chart for the photographic sequence set up in $01^h\ 44^m\ -40^\circ$. (Photograph courtesy of Photolabs, Royal Observatory, Edinburgh.)

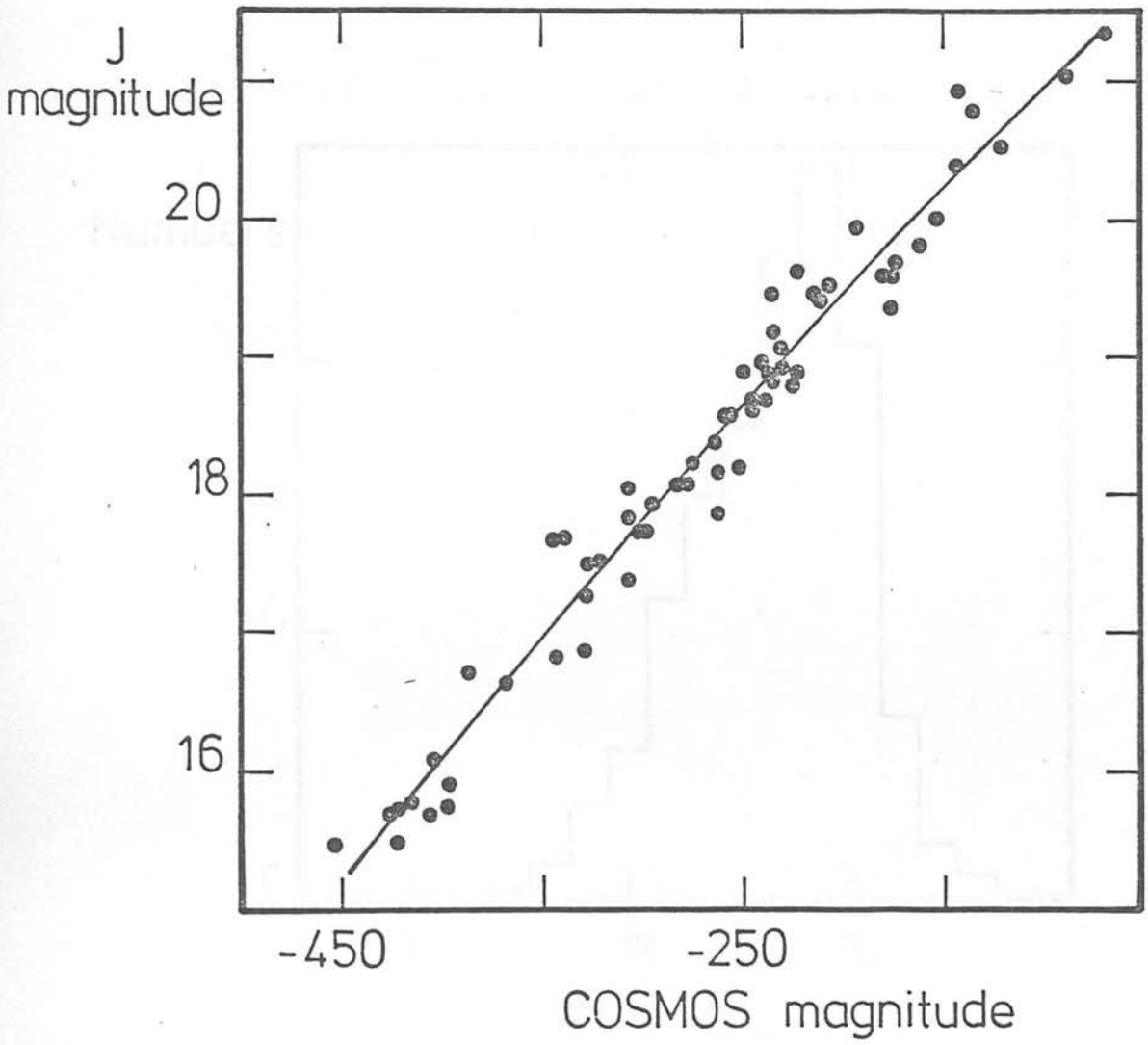

Figure 6.10 The relation between the sky corrected COSMOS magnitude and J magnitude for the photographic sequence in $01^h\ 44^m$ -40°. The data have been fitted with a quadratic function as shown.

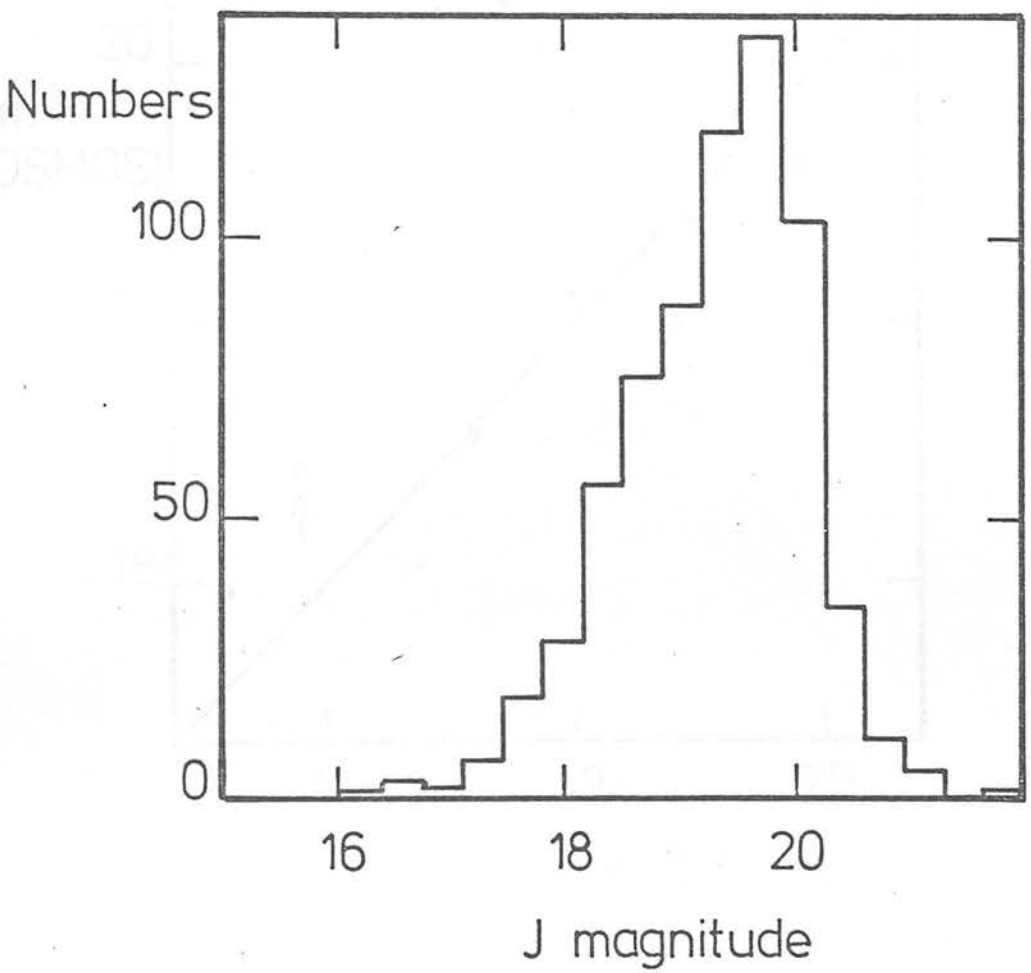

Figure 6.11 The J magnitude distribution for the quasars in the $01^{h}44^{m}$ -40° field but with those known merged images removed.

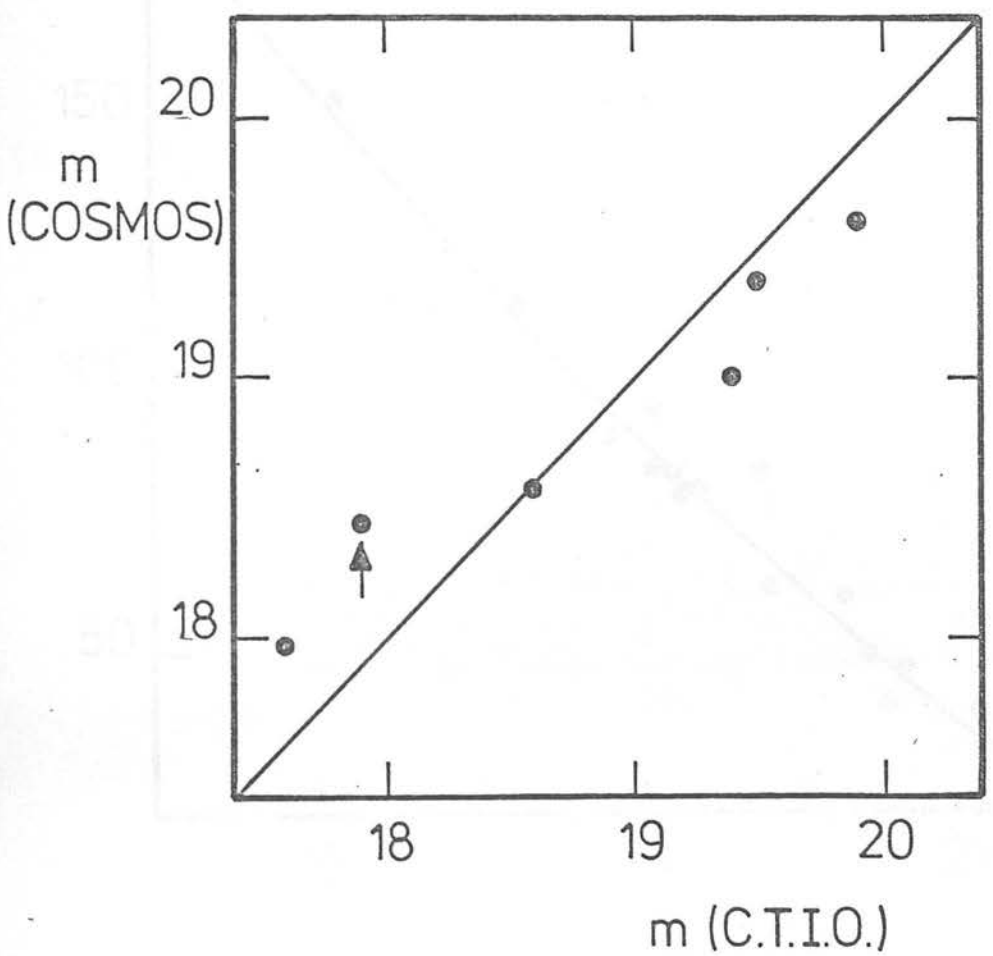

Figure 6.12 Comparison between the COSMOS photographic J magnitude and the corrected photoelectric magnitudes of the CTIO and Curtis Schmidt quasars. The line shown is the best fitting least squares line constrained to have an intercept of zero. For an explanation of the arrowed point see Section 6.4.2

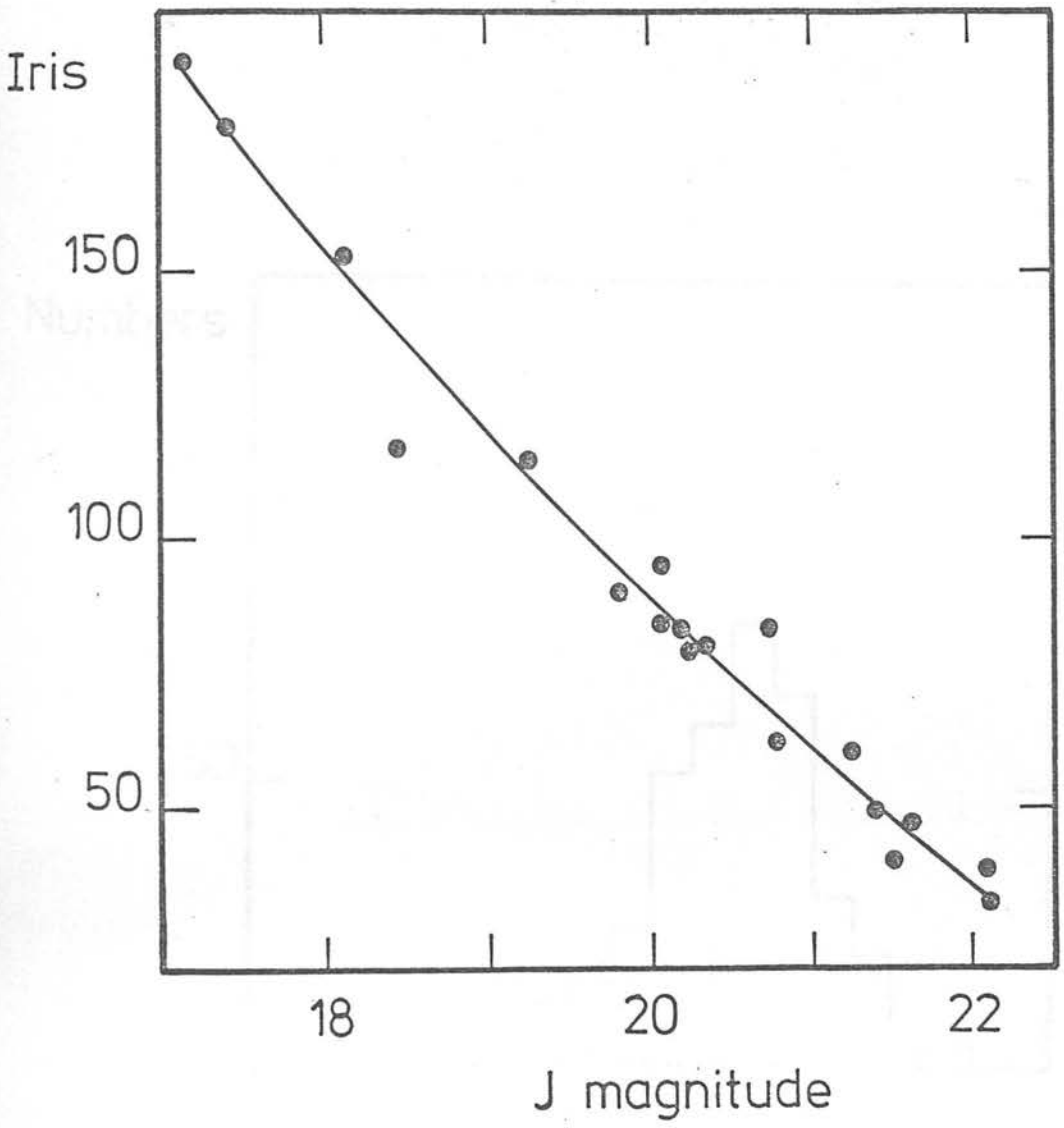

Figure 6.13 J magnitude/ Iris radius relation for the photoelectric sequence in $01^{h}\ 44^{m}\ -40^{o}$. These data have been fitted with the quadratic curve shown and used to calibrate the Iris readings of those quasars lying outside the COSMOS measured area.

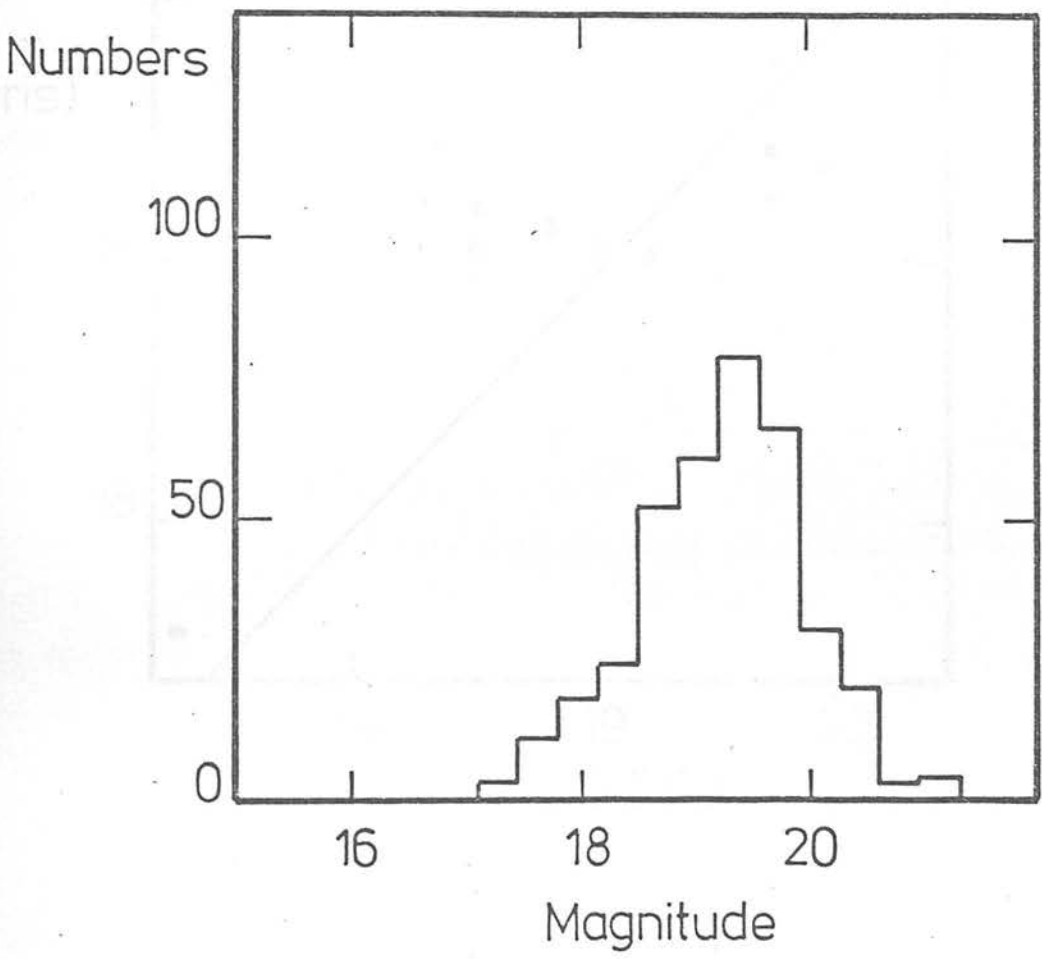

Figure 6.14 The J magnitude distribution for the quasars lying outside the COSMOS measured area with those merged objects removed.

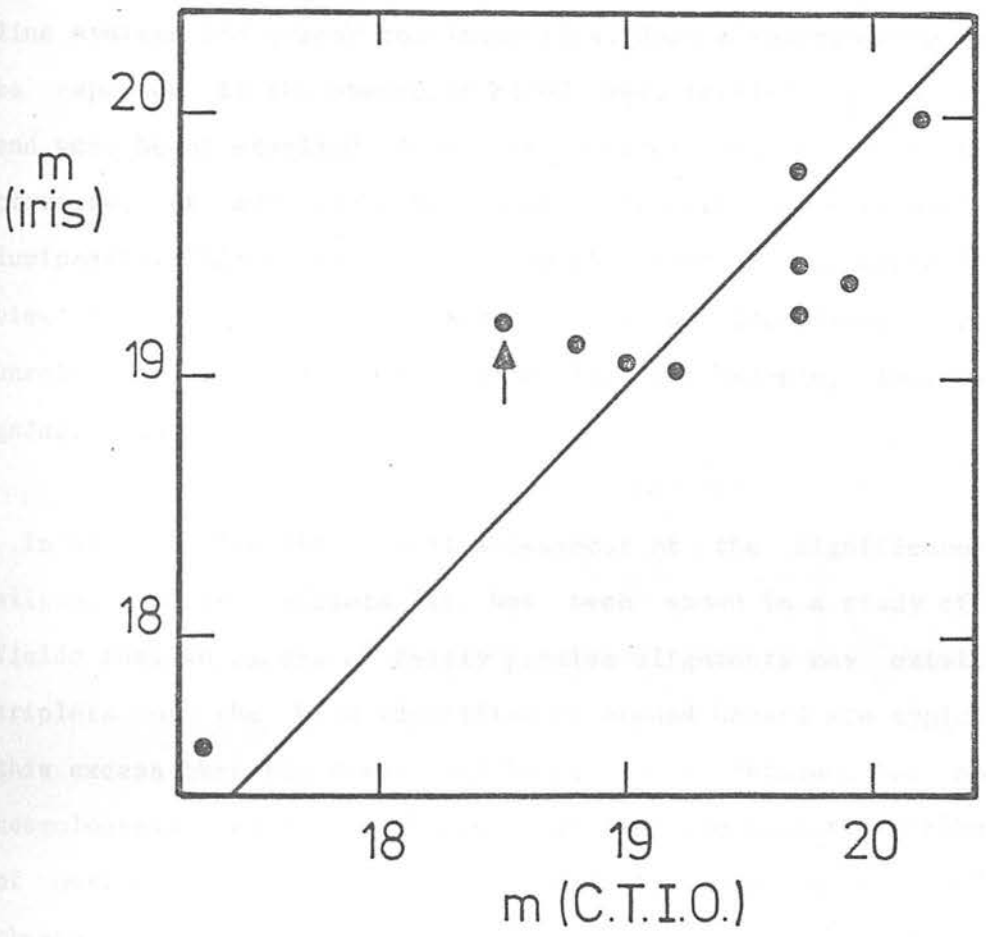

Figure 6.15 Comparison between the Iris photographic J magnitudes and the corrected CTIO and Curtis Schmidt photoelectric ones. The line drawn is the best fitting least squares line, constrained to have an intercept of zero. For an explanation of the arrowed point see Section 6.4.2.

CHAPTER VII

GENERAL CONCLUSIONS

An analysis of published data has shown that there is no correlation between inferred ejection velocities of absorption line systems and quasar contimuum flux. Such a relationship would be expected if the absorbing clouds were intrinsic to the quasar and were being expelled from the central source by radiation pressure, or any mechanism whose strength is correlated with luminosity. This removes one of the objections raised against the view that the gas producing the narrow absorption lines is unrelated to the quasar and resides in, for example, intervening galactic haloes.

In an objective statistical assessment of the significance of aligned quasar triplets it has been shown in a study of five fields that an excess of fairly precise alignments may exist. If triplets of the kind identified by Arp and Hazard are typical of this excess then the result may be considered evidence for non - cosmological redshifts. While studies of the quasar distribution of optically selected quasar candidates may be affected by observational selection effects, this appears not to be true in this case. Thus it is difficult to conceive of a bias in the search procedure which could account for an excess of alignments of a specific shape, especially as field distortions on prism plates would deviate alignments by an amount dependent upon the position of the triplet.

Further work is considered necessary to ascertain the significance of this result and it would be preferable to have future analyses carried out on data selected by some automatic and thus more objective technique.

It has also been shown that the properties of quasar absorption line systems may be effectively used to constrain non - cosmological redshift models in which any peculiar component is caused by gravitation. The implicit assumption that the redshift properties of absorption systems are reasonably similar for the quasar family as a whole has been borne out by AAT observations of two quasars lying in peak alignments. Thus if non - cosmological redshifts exist then these quasars have a large probability of having a significant peculiar redshift component.

COSMOS data have been used to detrmine the magnitudes of quasar candidates in two fields which were previously uncalibrated. This work is necessary before studies can be made of the number/ magnitude/ redshift relation for these samples. Unfortunately, sufficient redshift information does not exist, at present, to enable this to be determined. Nevertheless, such studies are of considerable importance for the understanding of quasar evolution and attention must be given to the problems of determining the redshifts of large numbers of faint quasar candidates. The fibre optic system planned for the UK Schmidt Telescope should provide an excellent means for enabling this work to be carried out.

APPENDIX I

IS THERE A β/L RELATION FOR ANY TYPE OF QSO ABSORPTION LINE SYSTEM?

A. S. TREW

University of Edinburgh and Royal Observatory, Edinburgh, Scotland

(Received 17 July, 1981)

Abstract. The possible correlation noted between the intrinsic quasar luminosity and the absorption line expulsion velocity is re-examined using homogeneous data sets for metal and Lα only line systems. The method of analysis is chosen to enable any reasonable form of correlation to be found. No correlation is detected at a confidence level >10%.

1. Introduction

The continuing controversy concerning the location of the gas-producing quasar absorption lines has recently tended towards the extrinsic hypothesis (Weymann *et al.* (1979), hereafter referred to as WWPT); Sargent *et al.* (1980), hereafter referred to as SYBT). One of the most suggestive pieces of evidence to the contrary was the possible correlation found by Perry and O'Dell (1978) between the intrinsic quasar luminosity and the expulsion velocity of the absorption system.

A relation of the form

$$\beta \propto L^{1/2} \tag{1}$$

was proposed at a significance level of 4 σ.

Unfortunately, the inclusion of a variety of types of absorption system in that work could have led to confusion as there is increasing evidence that different lines are not distributed in the same way (SYBT). It was therefore necessary to repeat the analysis using a more homogeneous data set and treating those with different distributions separately.

The metallic line systems are represented by C IV. Although it is not yet completed, the sample of quasars observed by WWPT provided an initial set of C IV systems. This was extended using another sample taken from the literature by Weymann, *et al.* (1981; hereafter referred to as WCS). The sample of hydrogen systems was also taken from published data. A total of 26 quasars satisfied the selection criteria.

2. The Samples and Statistical Tests

There is an apparent bias, the Malmquist effect, in analysis such as this which will tend to strengthen any correlation present. It arises because both F_{opt} and β are related to a third parameter – z_{em}. To combat this, the samples have been

Astrophysics and Space Science 82 (1982) 223–228. 0004–640X/82/0821–0223 $00.90.

analysed intwo ways, firstly for the β/F_{opt} relation and secondly by normalising the expulsion velocity with β_{max}, the maximum possible observable expulsion velocity, for each object individually.

The selection criteria for the C IV data are set out in WWPT and WCS and need not be repeated here. Although the quasar sample is not complete to any flux limit, the WWPT data is homogeneous in that all the objects were observed with the same instrument and at the same resolution. It comprised 17 quasars, the spectra of which showed a total of 34 C IV systems with $\beta > 0$. The WCS sample is somewhat less homogeneous and complete. It consisted of quasars with $z_{em} > 1.9$ and after a few objects common to both sets were removed there were 24 quasars remaining with a total of 50 C IV absorption systems.

In order to check that the WWPT and WCS samples were equivalent, the Mann–Whitney U Test (Siegel, 1956) was used to compare the distributions of F_{opt} and (β/β_{max}) in the two samples. It was found that the significance of any difference between the sets of (β/β_{max}) was only 0.04 σ.

The difference between the sets of F_{opt} values, however, was more significant as would be expected on grounds of decreasing completeness with rising z_{em}. It was found that the WCS quasars, $\langle F_{opt} \rangle = 0.79$, were brighter than the WWPT objects, $\langle F_{opt} \rangle = 0.51$, at a confidence level of 1.5 σ. As this was not a highly significant result, the two samples were combined.

The identification of a Lα system is more difficult than for C IV if a reasonable number of detections is desired. It was decided to use those lines, identified as belonging to known redshift systems, and to include any unidentified lines shortward of Lα emission which have $EW > 1$ A. This definition is very similar to that used by SYBT in their study of the distribution of Lα lines.

The selection of the quasars and lines has been quite rigorous. Only objects which have been observed at a resolution better than 7 A have been included and then the resolution has been degraded to 7 A, to provide uniformity of data. A further constraint has been placed upon the amount of spectrum observed shortward of Lα emission, in order to give a reasonable data base in each object. Consequently, a lower limit to β_{max} was set to $c/20$, and z_{em} had to be >2.05.

Further, in order to ensure that quasars in the same luminosity range were being compared irrespective of the type of line system, the Mann–Whitney U Test was applied to those objects making up the C IV and Lα samples. The result was that there was no difference between the two F_{opt} distributions at a confidence level greater than 1.2 σ.

The quasars comprising this sample are listed in Table I, together with the number of lines in each, at the degraded resolution and the quasar luminosity. In all, there were 462 acceptable Lα lines in the 26 objects.

To estimate the absolute luminosity of the quasars the approximate relation

$$\log (F_{opt}) = A \log (z_{em}) - 0.4 m_v + \text{const} \qquad (2)$$

was employed, where A is dependent upon the value of q_0. It has been shown that

TABLE I

Sample of quasars for Lyα analysis

Q	F_{opt}	N	$N(\beta < c/20)$	Ref.
0000 − 398	0.241	10	7	10
0049 − 393	0.511	4	2	10
0100 + 130	1.704	35	5	12
0122 − 380	1.195	17	6	5
0130 − 403	0.097	15	10	10
0138 − 381	0.753	6	6	10
0207 − 398	0.787	4	4	10
0226 − 038	0.701	22	7	4
0237 − 233	1.101	4	4	1
0324 − 407	0.852	18	5	10
0424 − 131	0.469	8	7	8
0453 − 423	0.851	10	7	4, 9
0457 + 024	0.359	12	6	8
0528 − 250	0.636	27	6	7
0642 + 449	0.465	22	4	2
0805 + 046	0.451	65	11	6
0820 + 296	0.223	24	9	4
0824 + 110	0.207	10	7	8
0830 + 115	0.352	41	10	8
1101 − 264	1.832	16	5	5
1225 + 31	2.232	17	4	11
1226 + 105	0.210	8	6	8
1331 + 170	1.724	7	1	3
2126 − 158	1.286	37	9	13
2251 + 244	0.411	14	6	4
2251 − 154	1.126	9	7	8

1. Boroson *et al.*: 1978, *Astrophys. J.* **220**, 772.
2. Carswell *et al.*: 1975a, *Astrophys. J.* **195**, 269.
3. Carswell *et al.*: 1975b, *Astrophys. J.* **196**, 351.
4. Carswell *et al.*: 1976. *Astron. Astrophys.* **53**, 275.
5. Carswell *et al.*: 1981, Preprint.
6. Jian-sheng *et al.*: 1980, AAO preprint.
7. Morton *et al.*: 1980, *Monthly Notices Roy. Astron. Soc.* **193**, 399.
8. Roberts *et al.*: 1978, *Astrophys. J.* **224**, 344.
9. Sargent *et al.*: 1979, *Astrophys. J.* **230**, 49.
10. Whelan *et al.*: *Monthly Notices Roy. Astron. Soc.* **189**, 363.
11. Wilkerson *et al.*: 1978, *Astrophys. J.* **223**, 364.
12. Wingert: 1975, *Astrophys. J.* **198**, 267.
13. Young *et al.*: 1979, *Astrophys. J.* **229**, 891.

the rankings of F_{opt} are insensitive to A for $1 \leq A \leq 3$ (approximately the limits for a $q_0 = 1{,}0$ universe respectively). Hence, $A = 2$ has been adopted as a reasonable compromise. The constant in Equation 3 has been arbitrarily set to 6, to give values of $F_{opt} \sim 1$.

For reasons of generality, and because there is no evidence that the variables

are normally distributed, it was decided to use a non-parametric technique rather than a straight correlation analysis. The advantage of the former is that a correlation can be sought without knowing the exact form of the relationship, provided that the variables used can be transformed to the variables in the relationship by monotonic functions, both of which vary in the same sense. A straight correlation technique, such as linear regression, would not allow this. Instead, one would have to transform the variables into a plane in which the expected relation was linear.

Therefore, through the premise has been made that the expected correlation is as given by Equation (1) it has been possible to test for any relationship in which β increases with increasing F_{opt}. Consequently, the Spearman Rank Correlation Coefficient, r_s, was calculated in order to test for any correlation (Siegel, 1956).

The significance of any correlation detected can then be estimated by computing, for $N > 30$, the student's t statistic.

3. Results

The results of the Spearman Rank Correlation tests are displayed in Table II. Here r_s, t are as described above, P is the resultant confidence level at which the null hypothesis, that is, that there is no correlation, can be rejected. In the calculation of P the number of degrees of freedom has been taken to be the number of lines minus 2.

On the basis of these tests, it was felt that there was little evidence to support the proposed correlation. However, this could be an unfair judgement because if all systems were considered regardless of β, then it is inevitable that some intervening systems will occur and the number of these will increase with larger values of β. Furthermore, it is theoretically very difficult to radiatively accelerate absorption line clouds beyond 0.1–0.2c (Beltrametti and Perry, 1980). Therefore the β/F_{opt} analysis has been repeated for all systems within a restricted range of β.

TABLE II

Results of analysis

Corr.	r_s	t	P
(a) C IV			
$(\beta/\beta_{max})/F_{opt}$	0.191	1.767	<9%
β/F_{opt}	0.213	1.970	<6%
β/F_{opt} ($\beta < c/10$)	0.197	1.421	<15%
(b) Lα			
$(\beta/\beta_{max})/F_{opt}$	0.094	2.032	<4%
β/F_{opt}	0.125	2.707	<1%
β/F_{opt} ($\beta < c/20$)	0.1204	1.529	<12%

In this case, it is only necessary to repeat any analysis once because now both β/F_{opt} and $(\beta/\beta_{max})/F_{opt}$ are equivalent. The restricted C IV sample comprises a total of 52 absorption systems in 32 quasars. For the Lα data there were 161 lines distributed amongst the 26 quasars. The results are also shown in Table II. Once again, the lack of a statistically significant correlation must lead to the conclusion that the effect is undetectable. A similar study for a slightly smaller sample of C IV lines appeared in press while this work was being undertaken (Peterson, 1981). Although that study used a linear regression technique the result was in good agreement with that found here.

4. Conclusions

In view of the null result found for the correlation between intrinsic quasar luminosity and the expulsion velocity of the line systems, regardless of type, it must be concluded that there is no evidence against the extrinsic model, at present. One proviso must be made: namely, that of necessity a broadband optical luminosity has been used in this work. However, models of radiative acceleration predict that it is the UV flux which does most of the driving (e.g., Beltrametti, 1980). Therefore if the range of spectral indicies is large enough, then a correlation between F_{UV} and β need not imply a detectable correlation between F_{opt} and β for an ensemble of quasars.

If it is assumed that the lack of an observed correlation does imply that the lines are produced extrinsic to the quasar, then the question arises as to their location. The problem is heightened by the results of SYBT which showed that the two point correlation function for the z_{abs} distribution of Lα lines is consistent with the line producing regions being random in distance. This is unlike the galaxy and metal line distributions (WWPT; WCS). Experiments with the two point correlation technique used by SYBT have shown that it is not very sensitive to small amounts of clustering. This is primarily due to the relatively small numbers of lines in even the richest Lα forest.

There is some indirect evidence from UV studies of stars in the Magellanic Clouds that there is a halo around the Galaxy which produces metal line systems very similar to the mixed ionization type of absorption system seen in quasars (Savage and Jeske, 1980). It is, however, more difficult to place the Lα only clouds, especially as they do not appear to be associated with galaxies. We propose that this can be understood in terms of superclustering, if it is assumed that these clouds are associated with the supercluster as a whole, rather than with the component galaxies. It is interesting therefore to note that one model of superclustering, which is supported by recent galaxy redshift observations (e.g., Joeveer *et al.*, 1978; Tarenghi *et al.*, 1979), predicts that approximately 30% of the mass of the supercluster cell is in the form of dark matter unassociated with the galaxies (Einasto *et al.*, 1979).

It is now known how much of this matter is presently in gaseous form, but

implicit in the model is that most of this matter condensed at a very early epoch to form short lived, high mass stars. The work of Wagoner *et al* (1967) showed that certain models for high mass stars, $M > 1000\, M_{\odot}$, produced metal abundances which were very much less than solar making the metal lines invisible. If correct, it is therefore possible to reconcile the clouds producing the Lα only systems with the residue from the earliest epoch of supercluster formation.

Acknowledgements

I would like to thank my supervisors Drs P. W. J. L. Brand and S. V. M. Clube for many useful discussions, and Dr M. G. Smith for making data available prior to publication. I gratefully acknowledge the receipt of a postgraduate research grant from DENI.

References

Beltrametti, M.: 1980 *Astron. Astrophys.* **86**, 169.
Beltrametti, M. and Perry, J. J.: 1980, *Astron. Astrophys.* **82**, 99.
Einasto, J., Joeveer, M., and Saar, E.: 1979, preprint.
Joeveer, M., Einasto, J., and Tago, E.: 1978, *Monthly Notices Roy. Astron. Soc.* **185**, 357.
Perry, J. J. and O'Dell, S.L.: 1978, *Astron. Astrophys.* **62**, 229.
Peterson, B. M.: 1981, *Astron. Astrophys.* **92**, 382.
Sargent, W. L. W., Young, P. J., Boksenberg, A., and Tytler, D.: 1980, *Astrophys. J. Suppl.* **42**, 41 (SYBT).
Savage, B. D. and Jeske, N. A.: 1980, Preprint.
Siegel, S. 1956. *Nonparametric Statistics for the Behavioural Sciences*, McGraw-Hill Kogakusha, Tokyo, p. 116.
Tarenghi, M., Tifft, W. G., Chincarni, G., Rood, H. J., and Thompson, L. A.: 1979, *Astrophys. J.* **234**, 793.
Wagoner, R. V., Fowler, W. A., and Hoyle, F.: 1967, *Astrophys. J.* **148**, 3.
Weymann, R. J., Carswell, R. F., and Smith, M. G.: 1981, Preprint (WCS).
Weymann, R. J., Williams, R. E., Peterson, B. M., and Turnshek, D. A.: 1979, *Astrophys. J.*, **234**, 33 (WWPT).

Mon. Not. R. astr. Soc. (1982) 200, 785–792

An assessment of the significance of quasar alignments

A. S. Trew *Department of Astronomy, University of Edinburgh, Blackford Hill, Edinburgh EH9 3HJ, Scotland*

S. V. M. Clube and A. Savage *Royal Observatory Edinburgh, Blackford Hill, Edinburgh EH9 3HJ, Scotland*

R. G. Clowes *Department of Physics, University of Durham, South Road, Durham OH1 3LE*

Received 1981 November 11; in original form 1981 October 5

Summary. We have undertaken a systematic search in two fields of quasar candidates for alignments similar to those reported by Arp & Hazard (1980) in order to test the statistical significance of these associations. Comparisons with control fields generated by a Monte Carlo technique showed that when appropriate allowance has been made for clustering there is only marginal evidence for a statistically significant excess of aligned triplets over that expected by chance. It has not, however, been possible to examine the significance of the redshift patterns found by Arp & Hazard (1980) as reliable redshifts do not exist for the majority of the quasar candidates.

Introduction

Four sets of well aligned quasar triplets have recently been identified by Arp & Hazard (1980). The physical significance of these associations is, however, not clear since alignments amongst random sets of data points can occur by chance. Indeed, the number of chance alignments increases very strongly with the surface density of objects and the maximum length of association considered. In this paper, therefore, we seek to apply objective criteria defining an alignment to two large sets of quasar candidates, one of which includes the above triplets. These quasar candidates were discovered in two separate investigations by Hazard (unpublished) and Clowes & Savage (Clowes 1980; Clowes & Savage in preparation) by visual inspection of UKST prism plates and each set covers ~ 25 square degrees of sky. Each contains ~ 200 members with $m_J \lesssim 20$ distributed across the whole plate, the majority showing strong line or UV excess spectra.

Techniques

We considered two procedures using selection criteria defining alignments of scale length less than some upper limit R.

(1) The first procedure constructs a straight line between all pairs of quasar candidates with separations $\leqslant R$. The resultant set of lines is searched for pairs of similar slopes and with a common (central) member. The maximum allowable difference between the slopes is a free parameter and dictates the quality of the alignment. If the triplet has a length greater than R it is neglected.

It should be noted, however, that for pairs of points that are relatively close, positional errors can produce an unacceptably large range of slopes. The propagation of such errors will therefore produce spurious alignments by this procedure.

The technique can be applied in either (X, Y) space, as on the plate, or in (α, δ) space, as on the sky, the latter being of greater physical significance. This approach resembles in some respects the use of a three-point correlation function to search for triples which have the shape parameter (V) on the order of unity (Groth & Peebles 1977, Section 4) but any effects due to clustering must be taken into account separately.

(2) The second procedure uses a linear acceptance window as opposed to an angular one. Each quasar is taken in turn to lie at the middle of the straight side of a semicircle, the radius of which is R. The reason for using a semicircle is to eliminate any duplicity in the detection of alignments.

This 'central' quasar defines one end of any possible alignment with other quasars falling within the semicircle. The procedure is to calculate the line joining this quasar to each other object within the area and to determine the minimum distance from this line of all quasars which lie at smaller radii. Any triplets in which the middle member is displaced by an amount less than the acceptance window are deemed to be alignments. This method unlike the first avoids the propagation of positional errors along the alignment. Notice, however, that no attempt is made to calculate the best fit line to the triplet. The alignment is completely determined by the end points and hence the window half-width, x, is an underestimate of the goodness of fit of the line to the points.

As before, the test can be applied in both (X, Y) and (α, δ) spaces. However, because the arc of a great circle does not differ greatly from a straight line, over scales of a degree, estimates of the expected number of alignments produced by a random distribution of points are the same for both coordinate systems, if $R \lesssim 1^\circ$.

It can be shown (Edmunds & George 1981) that for a distribution of n objects with a uniform surface density ρ, maximum alignment length R and window half-width x, the expected number of alignments is

$$E = \tfrac{2}{3} \times n\pi R^3 \rho^2. \qquad (1)$$

Note that there is a non-linear dependence of E upon ρ; so, for a non-uniform surface density the fluctuations about the mean result in an increased number of alignments.

A comparison of the two above techniques on the fields in question, as well as a number of control fields (see below), showed little difference in the numbers of detected alignments at comparable sizes of the acceptance window for $R \leqslant 1^\circ$ and $x \lesssim 1$ arcmin. However, the first method is less convenient in practice and is significantly more susceptible to propagating errors. We consider only the second procedure hereafter.

The samples

The two samples of quasar candidates examined were selected from UKST prism plates UJ 3682P ($00^h\,53^m - 28^\circ\,03'$ (1950), South Galactic Pole, SGP) and UJ 4054P ($11^h\,40^m + 10^\circ$ (1950)); the plates are of 70 and 60 min exposure respectively on unfiltered IIIa-J emulsions and with a plate scale of 67.14 arcsec mm^{-1}. The SGP plate was searched by two of us (RGC & AS). A number of examinations of quasar candidates have been carried out at higher

dispersion on large telescopes (e.g. Clowes 1980; Arp & Hazard 1980) and these show that ~ 80–90 per cent of the probable candidates are quasars. The data on the $11^h40^m + 10°$ field was kindly supplied by Dr C. Hazard and is obviously of great importance as it contains the four previously known alignments.

The method for determining the positions of the objects was the same for both fields. The unvignetted portion of the corresponding direct plates (J3721 (SGP) and J4288 ($11^h40^m + 10°$)) were scanned by COSMOS at the Royal Observatory, Edinburgh (Pratt 1977), in thresholded mapping (TM) mode with an 8 μm increment and a 32 μm spot size. The plates were measured with a 7 per cent threshold cut above the local sky background intensity. It has been shown that for objects in the range 18–20 mag the rms error of the position of the intensity weighted image centroids is ~ 1.5–2 μm (Stobie *et al.* 1979).

The transformation from (X, Y) to (α, δ) is performed via a grid of SAO stars across the plate. Unfortunately, the intensity weighted centroids of these images can be severely affected by the off-centre haloes which surround them. To combat this the TM data were re-analysed with a threshold cut of 125 per cent, though this value is not critical, providing it is sufficiently large to remove the haloes. The positions of the objects so determined compared well with those found from profile fitting COSMOS mapping mode (MM) data. The transformation was carried out using a standard Gauss–Jordan polynomial fitting routine. In both fields ~ 60 SAO stars defined the transformation which using a quadratic function gave ~ 1.2 arcsec rms errors in the fits. Most of this is presumably due to unknown magnitude effects on the plate or induced by the COSMOS measuring process but uncertainties in the catalogue positions of the SAO stars may also be present due to accumulated errors in their proper motions.

The final samples taken from the unvignetted field consisted of 146 probable quasar candidates in the SGP within a central area of 245 x 240 mm and 189 probable candidates within 280 x 270 mm in the $11^h40^m + 10°$ field. This gives a surface density in both fields, fortuitously, of 7.2 per square degree. The $11^h40^m + 10°$ sample contains a number of objects originally identified as radio sources (Arp & Hazard 1980). The positions of six of the seven Parkes sources within the measured SGP field do not correspond uniquely to images visible on the direct plate. These were not considered as quasar candidates. The seventh object has recently been identified as a quasar (Savage & Wright 1981) which had been discovered in the prism searches.

In addition to the real data 10 fields of random points were constructed mimicking each real data set, to act as control samples. The random fields were distributed across the same area and contained the same number of objects as their real counterparts. In choosing the number of control fields a compromise must be sought between the amount of computer time available and the reliability of statistics produced by the analyses. Comparisons between the means and standard deviations derived from a few analyses with particular values of (R, x) on 10 and 100 fields, which agreed to within 10 per cent, showed that 10 control fields achieved a satisfactory balance.

The results

Care must be exercised in the choice of the maximum search radius, R. According to sampling theory, an upper limit of one half the length of the smaller side of the area containing the sample has to be placed upon R. To preserve uniformity between the fields this requires $R \lesssim 2°$. At the maximum level, however, the fraction of alignments lost due to edge effects is large being also dependent upon the shape of the area considered; at the limit $R = 1°$ the fraction missed is on the order of 10–20 per cent. Although allowance can be made for this effect, by constructing control fields larger than the data set and discounting

Table 1. Number of alignments found in α, δ space: random data. Figures for X, Y space are given in parentheses.

Field: SGP x arcsec	N	M	σ	$(N-M)/\sigma$	E^*
1	4 (4)	3.2 (3.0)	2.04 (2.05)	0.39 (0.49)	3.5
2	12 (12)	5.6 (7.0)	2.42 (2.58)	2.64 (1.94)	7.0
4	23 (23)	11.5 (13.4)	3.81 (4.43)	3.02 (2.17)	14.1
6.7	29 (30)	21.2 (21.2)	6.43 (5.71)	1.21 (1.69)	23.6
10	39 (40)	31.0 (31.0)	9.23 (9.32)	0.87 (0.97)	35.2
20	91 (91)	64.5 (65.7)	17.63 (17.85)	1.50 (1.42)	70.5
34	154 (154)	106.8 (107.9)	19.82 (19.70)	2.38 (2.34)	119.8
67	277 (274)	213.1 (214.9)	28.84 (28.43)	2.22 (2.32)	236.0
Field: $11^h\,40^m + 10°$					
1	5 (4)	3.9 (4.2)	1.20 (1.14)	0.92 (−0.18)	4.6
2	10 (10)	8.9 (9.2)	1.97 (1.87)	0.56 (0.43)	9.1
4	35 (35)	17.5 (17.7)	4.93 (521)	3.55 (3.32)	18.2
6.7	46 (47)	28.8 (29.0)	7.13 (6.99)	2.41 (2.58)	30.6
10	77 (77)	44.6 (45.2)	9.51 (9.73)	3.41 (3.27)	45.6
20	139 (139)	88.4 (89.8)	13.09 (13.63)	3.87 (3.61)	91.2
34	226 (226)	147.3 (149.3)	23.19 (24.38)	3.39 (3.12)	155.1
67	423 (423)	299.9 (305.2)	43.79 (46.94)	2.81 (2.51)	305.5

* A 20 per cent reduction has been applied to E to allow for the loss of alignments at the edge of the field.

alignments that cross the plate edge, it is desirable to limit the uncertainty, so we have restricted the search to a maximum possible radius of 1°. In order to ensure that this limit does not conceal any significant effects operating at smaller alignment lengths the analysis has been performed with four different values of R: 0.5°, 0.71°, 0.87° and 1°. The results for these values of R are consistent one with another and with equation (1), so we present only those for $R = 1°$.

Table 1 shows the numbers of alignments with lengths $\leqslant 1°$ found and expected as a function of the half-width of the acceptance window, x. N is the number of alignments detected in the real quasar samples, M is the mean number produced by the control fields, σ being the standard deviation and E is the number expected on the basis of equation (1). Examination of these tables shows that E agrees well with the mean number found by experiment in the control fields when a reduction of 20 per cent has been made to E to correct, approximately, for edge effects. It may also be noted that, as expected, the numbers of alignments detected in (X, Y) and (α, δ) space are very similar. The comparison between the real and expected detection rates is, however, not as good. This is especially apparent in the $11^h\,40^m + 10°$ field where the numbers diverge significantly at large window half-widths. A similar effect in the SGP field is rather weaker, though there is evidence for a marginally significant excess at small window sizes, $x \sim 4$ arcsec. At first sight, the discrepancy might be taken as evidence of real alignments in excess of those attributable to chance; there are two possible reasons for a divergence.

First, it is possible that if the alignments are real structures there is a degree of variability in the production mechanism which gives two trajectories differing by several degrees; though simple conservation of momentum considerations might lead one to expect perfect alignments. Secondly, any clustering present in the data will increase the number of detected alignments. This is apparent from equation (1) where we see that $E \propto \rho^2$ and those areas with an excess of objects are not completely compensated by those which are deficient. A comparison of clustered real data with unclustered control fields thus gives an excess. Without a precise theory it is not possible to quantify the first effect, but the second, *a priori*, is likely

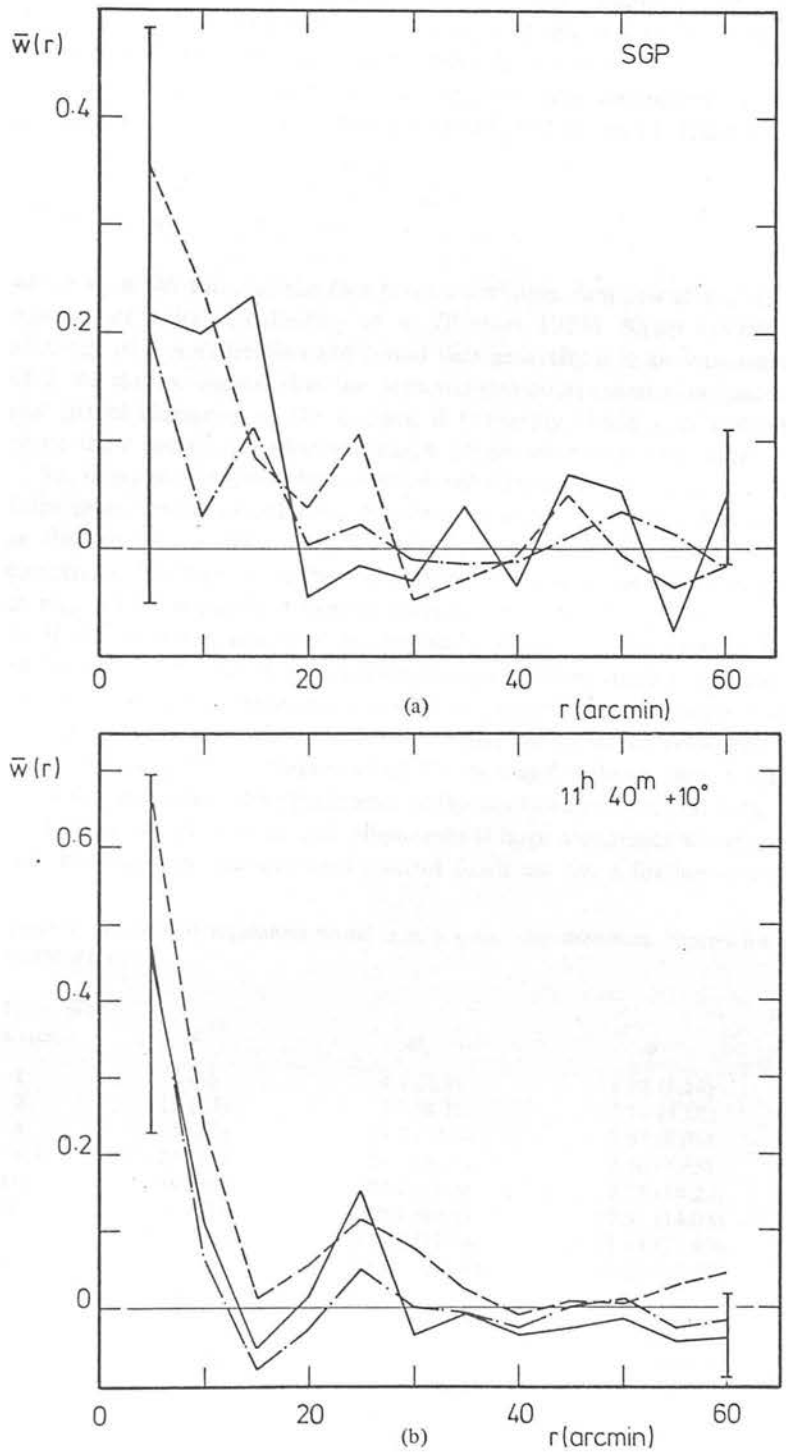

Figure 1. (a) Comparison of the real and imposed two-point correlation functions for the SGP. The solid line is the observed correlation function, the dotted line is the mean correlation function of the 10 control fields approximating that of the real data. The dashed line is the mean correlation function which gives the best fit to the observed number of alignments. (b) Comparison of the real and imposed two point correlation functions for the $11^h\,40^m + 10°$ field. The line symbols are the same as for (a).

to occur. We therefore assume in the first instance that physically real 'exact' alignments (i.e. small x) are of greater potential interest than 'loose' alignments (i.e. large x): and it could be that in applying a correction for clustering that causes N and m to agree at large x-values, an excess of alignments at small x-values will still be revealed.

In an attempt to allow for clustering we have determined the two-point correlation function for each field, the results can be seen in Fig. 1(a, b). The error bars are given by

$$(\Delta w_i)^2 = \frac{(1 + w_i)}{N_i} \tag{2}$$

where w_i is the value of the two point correlation function at that separation and N_i is the number of pairs contributing to w_i (Peebles 1973). Sharp (1979) has investigated the accuracy of this expression and found that generally it is an overestimate by about a factor of 2. We do not suggest that the observed two-point correlation functions necessarily imply real spatial clustering of the quasars, it is equally if not more probable that the observed clustering is caused, for whatever reason, by an uneven detection rate.

So, using an approximation in which the distribution of points was biased by the distance from their nearest neighbours, the observed two-point correlation functions were imposed on the sets of otherwise random control fields. The comparison of the observed two-point correlation functions with the mean of that for the clustered control fields can also be seen in Fig. 1(a, b). Agreement in both cases is within the statisitical errors. The determinations of M etc. were then repeated and the results are displayed in Table 2. The format is the same as Table 1 except that in this case no attempt has been made to estimate E. Exact agreement between real and control data is not to be expected since because of statistical fluctuations and the existence of higher order moments, the observed two-point correlation function may be biased, but a comparison of Tables 1 and 2 shows that, as expected, the effect of clustering is to lower the significance of the alignments in the real data.

Because the number of 'real' alignments at large acceptance windows continued to exceed that produced by the clustered control fields we ran a further series of simulations in an

Table 2. Number of alignments found in α, δ space: clustered data. Figures for X, Y space are given in parentheses.

Field: SGP x arcsec	N	M	σ	$(N-M)/\sigma$
1	4 (4)	4.1 (4.3)	1.73 (1.14)	−0.06 (−0.26)
2	12 (12)	7.9 (8.3)	3.75 (3.50)	1.09 (1.06)
4	23 (23)	14.6 (14.5)	5.87 (6.06)	1.43 (1.40)
6.7	29 (30)	24.1 (24.7)	7.40 (7.45)	0.66 (0.71)
10	39 (40)	37.2 (36.8)	9.75 (10.24)	0.18 (0.31)
20	91 (91)	73.5 (69.5)	12.95 (14.06)	1.35 (1.53)
34	154 (154)	126.1 (121.4)	21.58 (22.83)	1.29 (1.43)
67	277 (274)	247.6 (245.6)	32.26 (28.87)	0.91 (0.98)
Field: $11^h\,40^m + 10°$				
1	5 (4)	7.3 (5.2)	3.83 (3.39)	−1.53 (−0.35)
2	10 (10)	13.3 (10.8)	4.88 (5.31)	−0.68 (−0.15)
4	35 (35)	25.5 (22.8)	7.01 (7.24)	1.36 (1.69)
6.7	46 (47)	36.7 (35.6)	7.44 (12.22)	1.25 (0.93)
10	77 (77)	53.9 (53.9)	10.47 (14.39)	2.21 (1.60)
20	139 (139)	113.1 (103.7)	20.73 (24.39)	1.25 (1.45)
34	226 (226)	183.1 (176.6)	35.11 (35.28)	1.22 (1.40)
67	423 (423)	355.0 (357.6)	57.39 (60.71)	1.18 (1.18)

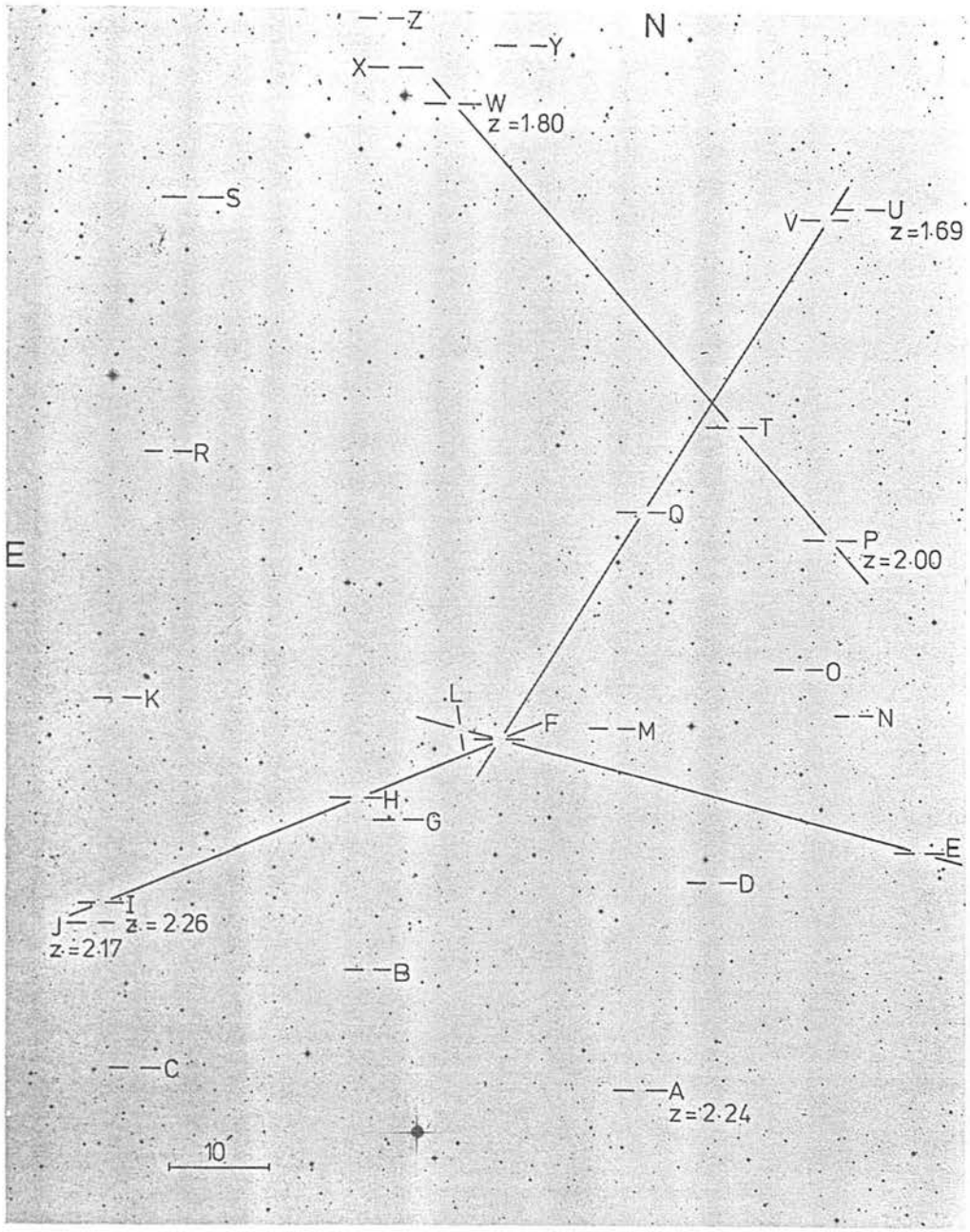

Plate 1. Photograph of a region of the SGP containing four alignments. The plate is B 3499, an unhypersensitized IIa-O of 60 min exposure. All probable quasar candidates are marked, redshifts are given when known. (Photograph courtesy of Photolabs, Royal Observatory Edinburgh.)

[*facing page* 790]

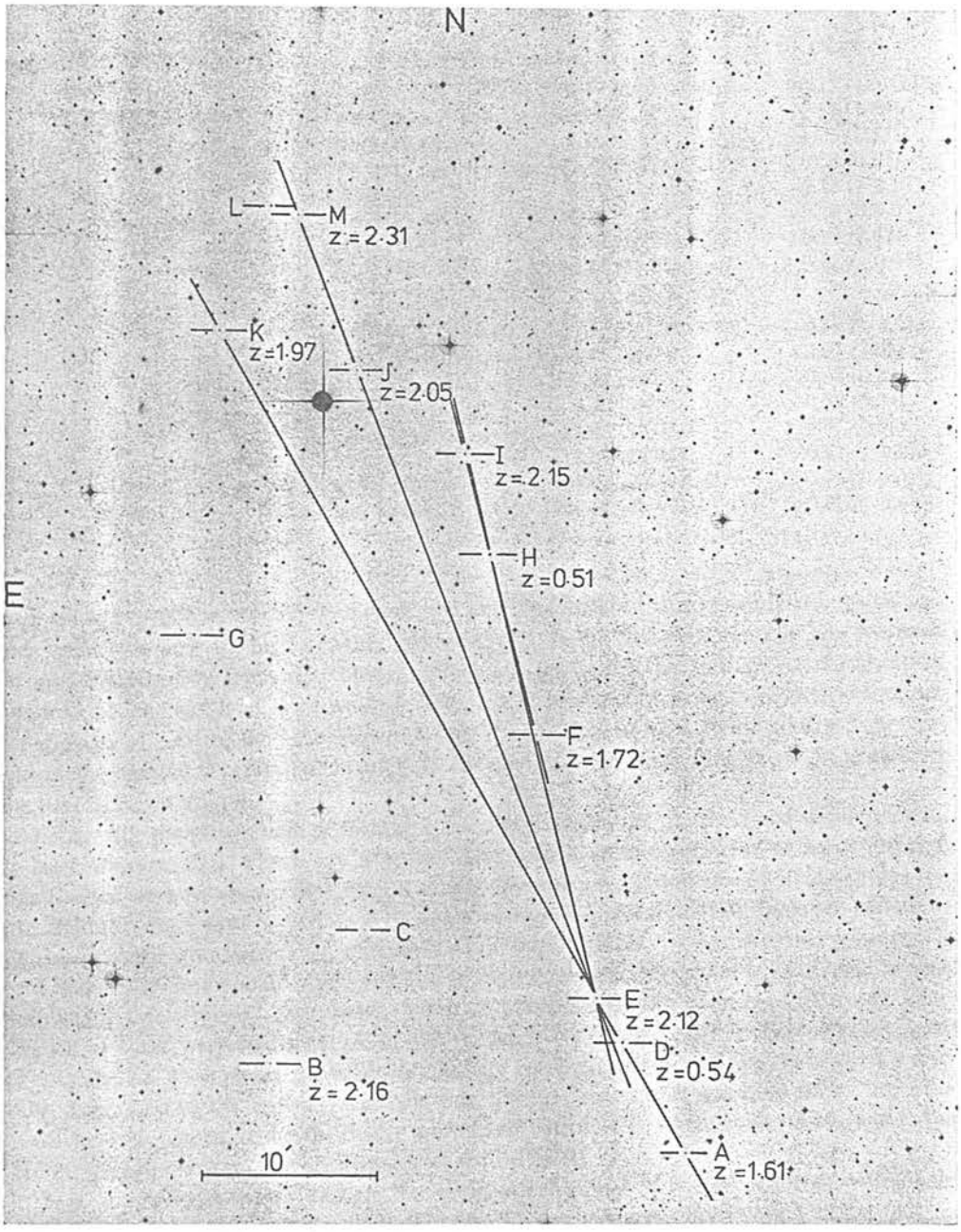

Plate 2. Photograph of a region of the $11^h\ 40^m + 10^o$ field from plate J 4288 surrounding the Arp & Hazard $11^h\ 30^m + 106^o$ group. All probable quasar candidates are marked with redshifts when these are known. (Photograph courtesy of Photolabs, Royal Observatory Edinburgh.)

Table 3. Number of alignments found in α, δ space: 'best fit' clustering data. Figures for X, Y space are given in parentheses.

Field: SGP x arcsec	N	M	σ	$(N-M)/\sigma$
1	4 (4)	4.5 (4.4)	2.13 (2.17)	−0.23 (−0.18)
2	12 (12)	8.7 (8.7)	3.25 (3.16)	1.02 (1.03)
4	23 (23)	16.7 (16.8)	4.96 (4.97)	1.27 (1.25)
6.7	29 (30)	27.0 (27.0)	5.32 (5.27)	0.38 (0.57)
10	39 (40)	40.9 (40.7)	8.40 (8.40)	−0.23 (−0.17)
20	91 (91)	83.9 (83.4)	9.54 (9.54)	0.74 (0.80)
34	154 (154)	144.5 (144.0)	16.12 (16.12)	0.59 (0.62)
67	277 (274)	293.2 (293.7)	36.83 (36.82)	−0.45 (−0.45)
Field: $11^h\,40^m + 10°$				
1	5 (4)	7.0 (7.0)	2.98 (2.71)	−0.67 (−1.11)
2	10 (10)	14.1 (14.6)	4.72 (4.53)	−0.87 (1.02)
4	35 (35)	28.1 (29.2)	7.02 (6.68)	0.98 (0.87)
6.7	46 (47)	42.4 (44.1)	9.49 (8.46)	0.38 (0.34)
10	77 (77)	66.1 (68.3)	11.43 (10.08)	0.95 (0.86)
20	139 (139)	129.4 (139.3)	18.00 (17.76)	0.53 (−0.02)
34	226 (226)	218.6 (225.7)	28.86 (26.44)	0.26 (0.01)
67	423 (423)	432.4 (442.7)	48.08 (45.07)	−0.20 (−0.44)

attempt to reproduce, by trial and error, the observed number of alignments at large acceptance windows and to test whether the resultant mean two-point correlation function differed significantly from that observed. Table 3 illustrates the 'best fit' to the observed numbers of alignments at large window sizes, $x \geqslant 10$ arcsec. The mean correlation functions for the sets of control field are shown in Fig. 1(a, b). They agree with the observed curve to within the statistical errors but it must be stressed that the correlation function producing the best fit is not unique.

Thus, with the general aim of forcing agreement between the observed and simulated data at large window sizes where any observed 'alignments' are not expected to be of physical significance we have shown that there is no pronounced over-abundance of alignments in the real fields at small window sizes $x < 10$ arcsec when $R \leqslant 1°$. Nevertheless, there are persistent signs of a slight over-abundance of alignments in both fields at $x \sim 4$ arcsec; this corresponds to a linear displacement of ~ 25 kpc ($q_0 = 0$, $H_0 = 100\,\mathrm{km\,s^{-1}\,Mpc^{-1}}$) at $z \sim 2.2$. The sample numbers are statistically inadequate, but it is possible that this peak is of increased significance at some preferred value R in the range $0.5° \leqslant R \leqslant 1°$. As it is present in both the (X, Y) and (α, δ) analyses the effect is unlikely to be an artefact of the astrometric reduction. According to the analyses with the four limiting values of R specified above, there are ~ 60 triplets aligned to better than 4 arcsec and with $R \leqslant 1°$ when ~ 40 are expected. The effect, though marginal, has significance at the $2\,\sigma$ level.

It is interesting, however, to note that unusual collections of triplets can exist without the overall statistics being necessarily significant. This is illustrated by Plates 1 and 2. All the triplets marked are aligned in (α, δ) space to better than ~ 2.5 arcsec. Plate 1 is an extension of two separate quasar triplets found by Arp & Hazard, except now a fan-like structure becomes apparent with one of the original triplets changing into a quadruplet. The original triplets are quasars A, D, E and F, H, I. Quasar E actually contributes to two other triplets in addition to the quadruplet. Redshifts, where these have been determined from spectroscopic observations on a large telescope or can be uniquely found from the prism spectra, are shown alongside the objects.

Conclusions

It may be concluded from these fields that there is no strong evidence for an excess of aligned quasar triplets over that expected in a random or clustered distribution of points where the imposed two-point correlation function agrees with that observed to within the statistical errors. However, as a comparison of Tables 1 and 2 shows any such statement is crucially dependent upon the degree of clustering present in the data. Table 1 may be taken as representing an upper limit to the significance of any real effect since a random distribution gives the lowest expected number of alignments, but it should be kept in mind that any estimate of alignments in the real data depends upon the availability of a complete sample. In particular, if there is any bias in the detection technique (e.g. which excludes low redshift quasars), it could work in the direction of underestimating the number of alignments. Similarly, any inclusion of non-quasars for which physical alignments are improbable will lead to an underestimation. Such imponderables are outside the scope of this investigation and we can only point to one marginal effect for structures of dimensions $R \leqslant 1^{\circ}$, $x \sim 4$ arcsec. Confirmation of the reality of this will require similar studies in additional fields of quasar candidates. In the meantime, we conclude that, if real, there is a ~ 30 per cent probability that any single alignment of the kind selected by Arp & Hazard is physically significant. This probability of course improves if the actual redshift values are of importance.

It has not been possible to establish whether any redshift patterns, similar to those reported by Arp & Hazard (1980) exist along a significant proportion of the alignments discovered here as most of the quasar candidates do not have reliable redshifts. In any case it is difficult to quantify the significance of the redshift trends as both radio loud objects and those selected from prism surveys contributed to the Arp & Hazard alignments and these two types have different redshift distributions (*cf.* Wills & Lynds 1978; Hewitt & Burbidge 1980).

Further progress will only be possible when more high quality data sets become available. To improve the statistics these should cover an at least comparable area to that considered here and perhaps use a more objective method for selecting the quasar candidates to try and improve the uniformity of detection.

Acknowledgments

We would like to thank Dr C. Hazard for releasing his data prior to publication; also Dr E. J. Zuiderwijk and Mr P. C. Hewett for several helpful suggestions improving the analysis and the COSMOS and Image and Date Processing groups at the Royal Observatory Edinburgh for their assistance in measuring the plates.

AST gratefully acknowledges the receipt of a postgraduate research grant from DENI.

References

Arp, H. C. & Hazard, C., 1980. *Astrophys. J.*, 240, 726.
Clowes, R. G., 1980. *PhD thesis*, University of Edinburgh.
Edmunds, M. & George, G. H., 1981. *Nature*, 290, 481.
Groth, E. J. & Peebles, P. J. E., 1977. *Astrophys. J.*, 217, 385.
Hewitt, A. & Burbidge, G. R., 1980. *Astrophys. J. Suppl.*, 43, 57.
Peebles, P. J. E., 1973. *Astrophys. J.*, 185, 413.
Pratt, N. M., 1977. *Vistas in Astronomy*, 21, 1.
Savage, A. & Wright, A. E., 1981. *Mon. Not. R. astr. Soc.*, 196, 927.
Sharp, N. A., 1979. *Astr. Astrophys.*, 74, 308.
Stobie, R. S., Smith, G. M., Lutz, R. K. & Martin, R., 1979. *International Workshop on Image Processing in Astronomy*, p. 48, eds Sedmak, M., Capaccioli, M. & Allen, R. J., Osservatorio Astronomico di Trieste.
Wills, D. & Lynds, R., 1978. *Astrophys. J. Suppl.*, 36, 317.

ACKNOWLEDGMENTS

I should like to express my sincere gratitude to those people without whom this thesis would never have been written, nor the work so enjoyable. To my supervisors, Drs. Peter Brand and Victor Clube, who gave their time unstintingly and guidance on those occasions when the way ahead was unclear. To all my colleagues at the Royal Observatory and the University of Edinburgh who provided much assistance, most notably Steve Heathcote and Paul Hewett.

Finally, I should like to thank my family for their constant interest and encouragement, especially Dr. Lesley Smart, who in gaining much amusement from my English grammar helped make this thesis readable.

Many thanks to you all.

BIBLIOGRAPHY

Aaronson M., McKee C. F. & Weisheit J. C. 1975 ApJ 198, 13

Abell G. 1958 ApJ Supp. 3, 211

Anderson J. 1971 A&A 13, 40

Arp H. C. 1970 AJ 75, 1

1971 Astrophys. Lett 9, 1

1977 CNRS No 37 "Declages vers le Rouge et Expansion de L' Univers", p377

1981 ApJ 250, 31

Arp H. C. & Hazard C. 1980 ApJ 240, 726

Arp H. C. & Surdej J. 1982 A&A 101, 109

Arp H. C., Pratt N. M. & Sulentic J. W. 1975 ApJ 199, 565

Atkinson R. d'E. 1962 Proc. Roy. Soc. 272, 60

Bahcall J. N. 1968 ApJ 153, 679

1971 AJ 76, 283

Bahcall J. N. & Wolf R. A. 1968 ApJ 152, 701

Bahcall N. A. 1977 Ann. Rev. Astr. & Astrophys. 15, 505

Bailey M. E. 1978 PhD. Thesis, University of Edinburgh

Bailey M. E. & Clube S. V. M. 1978 Nature 275, 278

Barnothy J. 1974 Bull. A. A. S. 6, 212

Beltrametti M. 1980 A & A 86, 169

Beltrametti M. & Perry J. J. 1980 A & A 82, 99

Bevington P. R. 1969 "Data Reduction and Error Analysis for the Physical Sciences", McGraw - Hill, New York

Blades J. C., Hunstead R. W. & Murdoch H. S. 1981 MNRAS 194, 669

Blair M. & Gilmore G. F. 1982 PASP 94, 742

Boksenberg A. 1972 Auxiliary Instrumentation for Large Telescopes, eds. Lausten N. & Reiz A., p295

Boksenberg A. & Burgess D. E. 1973 Astronomical Observations with Television Type Sensors, eds. Glaspy J. & Walker A., p21

Boksenberg A. & Sargent W. L. W. 1978 ApJ 220, 42

Boksenberg A., Danziger I. J., Fosbury R. A. E. & Goss W. M. 1980 ApJ 242, L145

Bolton J. G. 1976 IAU Symposium No. 76, "Radio Astronomy and Cosmology", ed. D. L. Jauncey, D. Reidel, Holland, p85

Bregman J. N. 1978 ApJ 224, 768

Broadbent S. R. 1980 J. R. Statist. Soc. A143, 109

Browne I. W. A. 1982 ApJ 263, L7

Browne I. W. A. & Cohen A. M. 1978 MNRAS 182, 181

Bruzual G. 1981 PhD. Thesis, University of California, Berkeley

Burbidge E. M. & Burbidge G. R. 1975 ApJ 202, 287

Burbidge G. R., O'Dell S. L., Roberts D. H. & Smith H. E. 1977 ApJ 218, 33

Caldwell J. A. R. & Ostriker J. P. 1981 ApJ 251, 61

Campbell A. W. 1981 MSc. Dissertation, University of Edinburgh

Canizaries C. 1982 Private Communication

Carswell R. F. 1982 Private Communication

Carswell R. F., Whelan J. A. J., Smith M. G., Boksenberg A. & Tytler D. 1982a MNRAS 198, 91

Carswell R. F., Morton D. C., Smith M. G., Turnshek D. A. & Weymann R. J. 1982 MNRAS Submitted

Cheney J. E. & Rowan-Robinson M. 1981 MNRAS 195, 831

Clowes R. G. 1980 PhD. Thesis, University of Edinburgh

Clube S. V. M. 1977 ApSS 50, 425

1978 Vistas Astr. 22, 77

1980 MNRAS 193, 385

1982 Proc. International Colloq. on the Scientific Aspects of Hipparcos, p187

Davis M. & Huchra J. P. 1982 ApJ 254, 437

Dawe J. A. 1981 "The Vignetting of the UK. Schmidt Telechscope

and Photographic Plate Non-Uniformity", Internal Report of the Royal Observatory, Edinburgh.

Dicke R. H. 1961 "Evidence for Gravitation Theories", Academic Press, London

Drew J. E. 1978 A&A 66, 343

Edmunds M. & George G. H. 1981 Nature 290, 481

Ellis R. & Phillips S. 1979 Private Communication

Field G. P., Arp H. C. & Bahcall J. N. 1973 "The Redshift Controversy", Benjamin, Reading, Mass.

Gilmore G. F. 1982 Private Communication

Ginzburg V. L. & Ozernoy L. M. 1977 ApSS 50, 23

Godwin J. G. & Peach J. V. 1977 MNRAS 181, 323

Goldstein H. 1974 "Classical Mechanics", Addison - Wesley, Reading, Mass.

Greenstein J. L. & Schmidt M. 1974 ApJ 140, 1

Greenstein J. L., Boksenberg A., Carswell R. F. & Shortridge K. 1977 ApJ 212, 186

Groth E. J. & Peebles P. J. E. 1977 ApJ 217, 385

Hawkins M. R. S. 1982 Private Communication

Hazard C. 1981 Private Communication

He X. T. 1982 Private Communication

He X. T., Smith M. G. & Trew A. S. 1982 In Preparation

Hewett P. C. 1982 Private Communication

Hewitt A. & Burbidge G. R. 1980 ApJ Supp. 43, 577

Hoag A. & Smith M. G. 1977 217, 362

Hodge P. W. 1965 ApJ 142, 1390

Hoyle F. 1981 "The Quasar Controversy Resolved", Cardiff

Hoyle F. & Narlikar J. V. 1974 "Action at a Distance in Physics and Cosmology", Freeman

Impey C. D. 1982 Private Communication

Kendall D. G. & Kendall W. S. 1980 Adv. Appl. Prob. 12, 380

Kippenhahn R. 1978 Physica Scripta 17, 201

Kunkel W. E. & Demers S. 1977 ApJ 214, 362

Longair M. S. & Seldner M. 1979 MNRAS 189, 433

Mattig W. 1958 Astr. Nach. 284, 109

Misner C. W., Thorne K. S. & Wheeler J. A. 1970 "Gravitation", Freeman

Narlikar J. V. 1977a Annals of Physics 107, 325

1977b CNRS No 37 "Declages vers le Rouge et Expansion de L' Univers", p347

1980 Private Communication

Oke J. B. 1974 ApJ Supp. 27, 21

Oort J. H. 1977 Ann. Rev. Ast. Astrophys 15, 295

Osmer P. S. 1980 ApJ 42, 333

Osmer P. S. & Smith M. G. 1980 ApJ 42, 333

Pecker J - C. 1977 CNRS No 37 "Declages vers le Rouge et Expansion de L' Univers", p451

Peebles P. J. E. 1973 ApJ 185, 413

Perry J. J. & O'Dell S. L. 1978 A & A 62, 229

Peterson B. A. 1978 IAU Symp. No. 79, "The Large Scale Structure of the Universe", P389

Peterson B. M. 1981 A & A 92, 382

Reid I. N. & Gilmore G. F. 1982 MNRAS 201, 51

Richstone D. O. & Schmidt M. 1980 ApJ. 235, 361

Sargent W. L. W. & Boroson T. 1977 ApJ 212, 383

Sargent W. L. W., Young P. J. & Schneider D. P. 1982 ApJ 256, 354

Sargent W. L. W., Young P. J., Boksenberg A. & Tytler D. 1980 ApJ. Supp. 42, 41 (SYBT)

Saslaw W. C., Valtonen M. J. & Aarseth M. J. 1974 ApJ 190, 253

Savage A. & Bolton 1979 MNRAS 188, 599

Savage A. & Wright A. 1981 MNRAS 196, 927

Savage A., Trew A. S., Chen J. & Weston T. 1982 To Be Submitted

Savage B. D. & Jeske N. A. 1980 ApJ 244, 768

Schaefer B. E. 1981 PASP 93, 253

Schneider D. P. & Young P. 1980 ApJ 238, 946

Schoenberg I. J. & Whitney A. 1953 Trans. A. Maths. Soc. 74, 246

Sharp N. A. 1979 A&A 74, 308

Shaver P. A., Boksenberg A. & Robertson J. W. 1982 Preprint

Siegel S. 1956 "Nonparametric Statistics for the Behaviourial Sciences", McGraw - Hill, New York

Smith H. E. 1978 Mercury 7, 27

Smith M. G. 1975 202, 591

Songaila A. 1981 ApJ 248, 945

Stobie R. S., Smith G. M., Lutz R. K. & Martin R. 1979 International Workshop on Image Processing in Astronomy, eds. Sedmak M., Capaccioli M. & Allen R. J., Osservatorio Astronomico di Trieste, p48

Stockton A. 1978 ApJ 223, 747

Strittmatter P. A. 1979 "Extra Galactic High Energy Astrophysics", eds. Blecha A. & Maeder S., Geneva Observatory.

Trew A. S. 1982 ApSS 82, 223

Trew A. S., Clube S. V. M., Savage A. & Clowes 1982a MNRAS 200, 785

Trew A. S., Clube S. V. M. & Savage A. 1982b Nature Submitted

Veron P. & Veron M. P. 1982 A & A 105, 405

Wall J. V. 1982 Preprint

Walsh D., Carswell R. F. & Weymann R. J. 1979 Nature 279, 381

Wampler E. J., Baldwin J. A., Burke W. L., Robinson L. B. & Hazard C. 1973 Nature 246, 204

Webster A. S. 1982a MNRAS 200, 47P

1982b MNRAS 201, 179

1982c Private Communication

Weymann R. J. 1980 Proc. IAU Symp. No. 92, "Objects of High Redshift", P107

Weymann R. J., Carswell R. F. & Smith M. G. 1981 Ann. Rev. Astr. & Astrophys. 19, 41 (WCS)

Weymann R. J., Boroson T., Peterson B. M., Butcher H. R. 1978 ApJ 234, 33

Weymann R. J., Williams R. E., Peterson B. M. & Turnshek D. A. 1979 ApJ. 234, 33 (WWPT)

Weymann R. J., Latham D., Angel J. R. P., Green R. F., Liebert J.,

Turnshek D. A., Turnshek D. E. & Tyson J. A. 1980 Nature 285, 641

Williams R. E. & Weymann R. J. 1976 ApJ 207, L143

Wright A. E., Morton D. C., Peterson B. A. & Jauncey D. L. 1982 MNRAS 199, 81

Young P. J., Sargent W. L. W. & Boksenberg A. 1982a ApJ Supp 48, 455 (YSB)

1982b ApJ 252, 10

Young P. J., Sargent W. L. W., Boksenberg A., Carswell R. F. & Whelan J. A. J. 1979 ApJ 229, 891

Zuiderwijk E 1982 Nature 295, 577

Zuiderwijk E. & de Ruiter H. R. 1982 Preprint